Characterising dopaminergic plasticity in the mouse olfactory bulb

Byrne, Darren John

Awarding institution:
King's College London

Characterising dopaminergic plasticity in the mouse olfactory bulb

Darren Byrne

Thesis submitted for the Degree of Doctor of Philosophy

September 2018

Centre for Developmental Neurobiology

Institute of Psychiatry, Psychology and Neuroscience

King's College London

Abstract

Experience can shape the brain through multiple interacting forms of neuronal plasticity. In the mouse olfactory bulb, a heterogenous population of dopaminergic neurons is known to be particularly plastic, regulating their gene expression and lifelong generation in an activity-dependent manner. However, how their electrophysiological function can change is not well understood. This thesis aimed to understand how olfactory bulb dopaminergic neurons respond functionally following perturbation of odour experience.

I live labelled olfactory bulb dopaminergic neurons using the $DAT^{IRES\mathit{cre}}$ transgenic mouse. I characterised the labelled population at postnatal day (P)28, showing that the majority of neurons are dopaminergic. Approximately 22% of the labelled population is calretinin-positive, which can be distinguished from the dopaminergic population by immunohistochemistry and electrophysiology. I used an odour deprivation manipulation, unilateral naris occlusion, for 1 and 3 days to study experience-dependent plasticity in the labelled neurons. I show with immunohistochemistry that the activity of these neurons is reduced and there is downregulation of the dopamine-synthesising enzyme, tyrosine hydroxylase, as quickly as 1 day after occlusion. To investigate electrophysiological functional plasticity, I used acute slice electrophysiology to study a subpopulation of olfactory bulb dopaminergic neurons that lack an axon. I demonstrate that the firing properties of these neurons are not affected by these durations of occlusion. However, I show that after 3 days of occlusion there is a significant increase in the sag potential, medium afterhyperpolarisation and amplitude and charge of mini excitatory postsynaptic currents in anaxonic olfactory bulb dopaminergic neurons.

I investigated $GABA_A$-mediated auto-inhibition in both subpopulations of olfactory bulb dopaminergic neurons – axonic and anaxonic. I show that, unlike presumed anaxonic cells, presumed axonic dopaminergic neurons do not have auto-inhibition, except following pharmacological enhancement of L-type calcium channels. Whilst studying auto-inhibition, I found a calcium-dependent current that was present in the majority of presumed axonic dopaminergic neurons and only a minority of the presumed anaxonic subpopulation. This work provides further insight into experience-dependent plasticity of olfactory bulb dopaminergic neurons and reveals important functional differences between subtypes of this population.

Acknowledgements

I would first like to give a massive thank you to my supervisor Matthew Grubb for the opportunity to undertake this PhD. From the beginning to the completion of this thesis, he has been incredibly supportive through every twist and turn. Without his enthusiasm and dedication this project would not have gotten to where it got to.

Grazie Elisa Galliano for being there on my first day in the lab, getting me to patch my first cell in slices and all her help during the years. Gracias Marcela Lipovsek for her support and for the times I wasn't patching to go to Pap's/Shrigley's and do the Guardian crossword. Gracias Andres Crespo for keeping the lab running smoothly and doing so, so much genotyping. Go raibh míle maith agat Lorcan Browne for all his help over the last few months and always answering my electrophysiology questions. I am also grateful for all the support that I have received from the other past (Adna Dumitrescu, Annisa Chand) and present (Menghon Cheah, Candida Tufo) members of the Grubb Lab and the many students that have come and gone.

Thank you to everyone I have met and helped me during my time at the CDN! In particular the past and current members of the Burrone and Andreae labs and all the people in the slice and ephys rooms for all the discussions and explanations and sharing of reagents. I would also like to thank the BSU staff for looking after the mice.

I would particularly like to acknowledge my fellow Grubb Lab PhD student Christiane Hahn for going through this entire process with me. This PhD would have been a very different experience without having her there in the office, the slice room, the ephys room, the lab, the BSU and Facebook Messenger.

Thank you to Dale Bryant for always being there for me. I cannot imagine what it would have been like to not have him there at home and helping me manage through the last few years. Finally, I would like to give a big thank you to my parents, Patricia and John, for their love and endless support with everything I do!

Declaration

The work presented in this thesis were entirely my own work, apart from those described below.

Matlab coding for analysing electrophysiological recordings was written by **Matthew Grubb**. The Matlab code to analyse the sag index was written by **Christiane Hahn** and **Matthew Grubb**. These scripts were modified by myself and I wrote the Matlab code to analyse the afterhyperpolarisation.

Figures 3.6 – 3.9: Immunohistochemistry, imaging and image analysis for timepoints 7, 14 and 21 days post-BrdU injection were performed by a master's student, **Krishna Kothandapani**, who I trained and supervised**.**

Table of Contents

List of Figures and Tables

List of Tables

Chapter One – Introduction

The ability to interact with the external world is one of the most basic features of the nervous system and is key for adaptation and survival. One of the fundamental questions in neuroscience is how changes in the external environment affect the sensory systems that process these experiences. For rodents, olfaction is one of the most important senses and is essential for feeding, social interactions, mating and survival. The olfactory bulb (see **Figure 1.1**) is the first brain region that processes odour information and demonstrates a range of plasticity mechanisms to respond to changes in the environment.

1.1 Olfactory bulb

1.1.1 Olfactory sensory neurons

Most odours are composed of a complex mixture of multiple odour molecules and the detection of odorants is mediated by G protein-coupled odorant receptors, with approximately 1,000 different odorant receptors identified in mice (Zhang and Firestein, 2002). Signalling of odour information to the olfactory bulb is initiated in the main olfactory epithelium that lines part of the highly intricate and bony plates known as turbinates located in the nasal cavity (Negus, 1959). Here, cilia of the olfactory sensory neurons (OSNs) detect chemical information by the binding of odorant molecules to their odorant receptors and mechanical stimulation from airflow (Buck and Axel, 1991; Grosmaitre et al., 2007). Upon binding an odorant, a transduction cascade follows. The activated odorant receptors activate a G-protein, which stimulates adenylyl cylase III to produce cAMP (Bakalyar and Reed, 1990). cAMP in turn activates ion channels, which results in depolarisation and calcium influx (Dhallan et al., 1990; Nakamura and Gold, 1987). Calcium-activated chloride channels enhance depolarisation through chloride efflux, increasing the likelihood of an action potential being generated (Kaneko et al., 2004).

Each OSN expresses a single odorant receptor with the other odorant receptor genes repressed by epigenetic factors (Clowney et al., 2012; Lyons et al., 2013). Though each OSN expresses only a single odorant receptor, each receptor can usually bind multiple odorant molecules with a wide range of affinities (Malnic et al., 1999). As such, an odorant will be encoded by the complex ensemble activity of multiple OSNs. This combinatorial activity allows a broad range of odorants to be encoded.

OSNs connect with the olfactory bulb, by projecting their unmyelinated axon through the cribriform plate. OSNs expressing the same type of odorant receptor have massive convergence

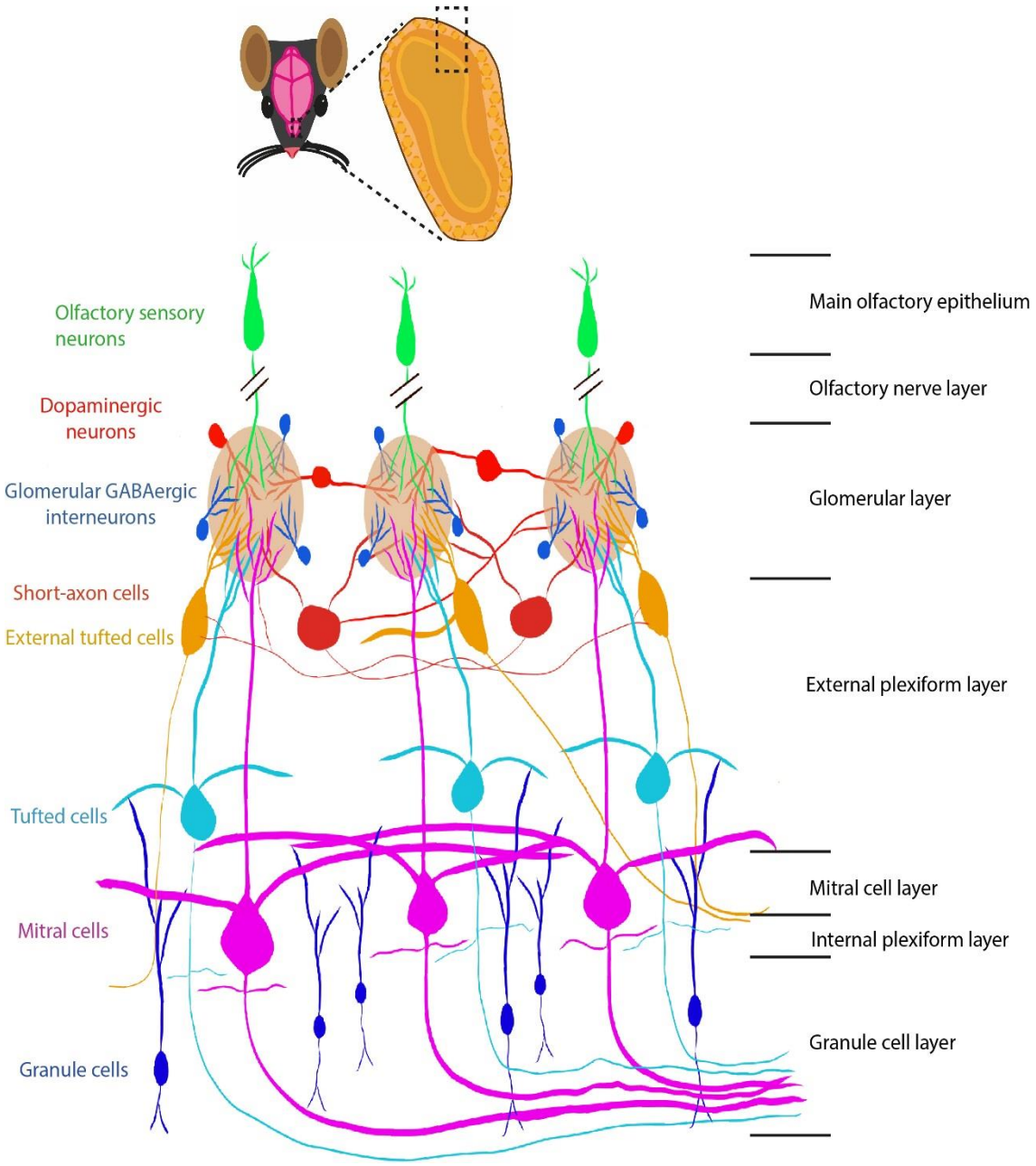

Figure 1.1: Schematic of the mouse olfactory bulb

of their axons at fixed sites in the olfactory bulb called glomeruli, located in the glomerular layer. Each glomerulus represents an anatomical and functionally distinct information processing module and receives input from 5,000 – 10,000 OSN axons expressing the same odorant receptor (Chen and Shepherd, 2005). There are approximately 1,800 glomeruli in each olfactory bulb, corresponding to each OSN subtype projecting to around two glomeruli, one lateral and one medial in each bulb (Mombaerts et al., 1996; Royet et al., 1988). Glomeruli associated with the same odorant receptor are referred to as isofunctional glomeruli (Lodovichi et al., 2003). Within each glomerulus, OSN terminals release glutamate onto postsynaptic neurons, including the projection neurons and heterogeneous populations of glomerular layer interneurons. The release probability of OSNs has been reported to be one of the highest of any presynaptic terminal and does not differ between postsynaptic targets (Grubb et al., 2008; Murphy et al., 2005).

OSNs are one of the few regenerating populations of neurons, with the population as a whole having a mean half-life of 26 days, although some neurons may survive as long as one year (Holl, 2018). A newborn OSN must extend its axon to the olfactory bulb and converge on its target glomerulus. Odorant receptor expression in immature OSNs precedes the innervation of glomeruli and is required for the highly precise targeting of glomeruli resulting in very few errors (Rodriguez-Gil et al., 2015; Treloar et al., 2002). Due to the turnover and regeneration of OSNs, there is constant rewiring of connections in glomeruli. Work by Cheetham et al. (2016) found that there is a rapid and continuous turnover of OSN presynaptic terminals, particularly in OSNs expressing immature markers. This turnover was found to be activity-dependent and was strongly downregulated in immature and mature OSNs axons following long-term odour deprivation. OSNs are, therefore, responsible for a high level of structural and synaptic plasticity that is constantly occurring within glomeruli.

1.1.2 Glomerular layer neurons

The glomeruli of the olfactory bulb glomerular layer are anatomically distinct regions that are adapted to process the distributed odour representations conveyed by OSNs. Each glomerulus is considered a functional unit because it receives inputs from OSNs expressing the same odorant receptor (Treloar et al., 2002). The dendrites of local interneurons extend their processes into glomeruli, with as many as 1,500 – 2,000 glomerular layer interneurons per glomerulus (Shipley et al., 1996). The organisation of processes within each glomerulus has been portioned into domains containing axodendritic synapses between OSNs and their target neurons (OSN zone) and domains predominately composed of dendrodendritic synapses between olfactory bulb neurons, including the projection neurons and glomerular interneurons

(non-OSN zone) (Kasowski et al., 1999; Kosaka et al., 1997). However, these interneurons and their function within the olfactory bulb are highly heterogenous.

Early work classifying these neurons described three types of interneurons within the glomerular layer of the rat olfactory bulb based on their morphology: external tufted cells; periglomerular neurons; and the short-axon cell (Pinching and Powell, 1971a, 1971b, 1971c). This work formed an important basis for further studies investigating the population of neurons in the glomerular layer.

1.1.2.1 External tufted cells

The population of excitatory interneurons in the glomerular layer are the external tufted cells. External tufted cells are a heterogenous population of glomerular layer interneuron, with differences in morphology, neurotransmitter release and molecular diversity. Work by Pinching and Powell (1971a) identified these neurons as having a large oval shaped soma and located at the border of the glomerular layer and the external plexiform layer. They were originally described as having a large primary, tufted, apical dendrite that arborises in a single glomerulus. Despite being described as rarely having secondary dendrites (Pinching and Powell, 1971a), it has since been found that approximately one-third of external tufted cells possess basal dendrites that extend to the external plexiform layer or only project a short distance from the soma into the glomerular layer (Hayar et al., 2004a). The dendritic tuft receives extensive input from OSN terminals (Hayar et al., 2004a). External tufted cells also connect with the dendrites of other neurons that innervate a glomerulus, including bulbar projection neurons and GABAergic glomerular layer interneurons (Hayar et al., 2004b). However, there is diversity in the types of neurons that subpopulations of external tufted cells connect with, for example, one subpopulation does not connect with the principle projection cells in the olfactory bulb (Tatti et al., 2014).

External tufted cells were considered to be exclusively glutamatergic; however, it has been found that these neurons can express GABAergic markers (Tatti et al., 2014). Subpopulations of external tufted cells also release peptide hormones: cholecystokinin (Liu and Shipley, 1994); and vasopressin (Tobin et al., 2010). The majority of external tufted cells fire bursts of action potentials; however, those with basal dendrites may not have this burst firing (Antal et al., 2006). External tufted cells fire spontaneously, which excites the glomerular layer GABAergic interneurons that they connect with, resulting in tonic GABA release (Shao et al., 2012). External tufted cells associated with the same glomerulus exhibit synchronous activity through coordinated synaptic transmission, gap junction coupling and glutamate spillover (Hayar et al.,

2005). External tufted cells also possess an axon that projects into the internal plexiform layer and synapses with granule cells that are associated with an isofunctional glomerulus. External tufted cells are, therefore, an important source of interglomerular connectivity between glomeruli that are innervated by OSNs expressing the same odorant receptor.

A primary role for external tufted cells in the glomerular microcircuit is the amplification of the monosynaptic input they receive from OSNs. Input amplification is mediated by recurrent excitation produced by the release of glutamate exciting neighbouring excitatory synapses, including other external tufted cells, bulbar projection neurons and GABAergic interneurons. Recurrent excitation produces a long-lasting excitatory current, which amplifies the OSN input and promotes mitral cell spiking (Najac et al., 2011; Vaaga and Westbrook, 2016). This long-lasting current is modulated by GABAergic input onto mitral and external tufted cells, shaping the strength and temporal structure of glomerular output (Shao et al., 2012).

1.1.2.2 Glomerular layer GABAergic interneurons

The most abundant neurons in the glomerular layer are GABAergic interneurons. The original description of these neurons classified them as a population known as periglomerular neurons (Pinching and Powell, 1971a). Morphologically, these neurons have a small soma and project their dendrites into a small area of a single glomerulus, or occasionally to multiple glomeruli. The soma and dendrites of periglomerular neurons have many spines and vesicles were observed in all parts of the cell. The majority of these neurons were originally believed to possess an axon (Pinching and Powell, 1971a); however, evidence from later work revealed that the majority of these neurons lack an axon and release neurotransmitters from their dendrites (Crespo et al., 2013; Smith and Jahr, 2002).

These glomerular layer interneurons were identified as GABAergic interneurons based on the expression of GABA-synthesising enzyme glutamic acid decarboxylase (GAD), with a subpopulation of this GABAergic population also identified as dopaminergic by the co-expression of tyrosine hydroxylase (Kosaka et al., 1985). Further molecular studies investigating the diversity of these interneurons revealed the expression of two GAD enzymes, GAD65 and GAD67, and the mutually exclusive expression of calretinin (CR), calbindin (CB) and tyrosine hydroxylase (TH) suggested that these markers correspond to specific subtypes, at least in mouse (Kosaka et al., 1995; Parrish-Aungst et al., 2007). Additional markers of other distinct subpopulations have also been identified, including neurocalcin, parvalbumin and $GABA_A$ receptor α5; however, these have not received the investigation that CR, CB and TH neurons have received (Panzanelli et al., 2007; Parrish-Aungst et al., 2007; Whitman and Greer, 2007).

Early classifications of glomerular layer GABAergic interneurons proposed that they could be separated into two populations based on their connectivity: type 1, which project their intraglomerular dendrites into OSN and non-OSN zones; and type 2, which project only into non-OSN zones (Kosaka et al., 1997). Electrophysiology and electron microscopy (EM) work have described the TH population as being type 1, receiving glutamatergic input from OSN terminals and local glutamatergic neurons (Kiyokage et al., 2010, 2017; Toida et al., 2000). In contrast the majority of CR and CB neurons are described as type 2, which receive sensory-driven input via external tufted cells (Kosaka and Kosaka, 2007; Kosaka et al., 1997; Shao et al., 2009; Toida et al., 1998).

Neuronal reconstructions of the subpopulations of glomerular layer GABAergic interneurons have revealed distinct morphologies that go beyond the initial description by Pinching and Powell (1971a) as neurons that mainly ramify dendrites in a small area of one glomerulus. Different populations can contact multiple glomeruli and/or ramify in a large area of a glomerulus (Tavakoli et al., 2018). Analysis using GAD67-GFP and GAD65-GFP mice by Kiyokage et al. (2010) determined that these two transgenic mice mostly label different glomerular layer populations. GAD65 neurons are mostly uniglomerular, extending processes to 1 to 3 glomeruli. In contrast, the majority of GAD67 neurons are oligoglomerular, innervating several glomeruli (5-8), while some GAD67 neurons are polyglomerular, contacting approximately 40 glomeruli.

CR neurons are the most numerous subtype of glomerular layer GABAergic interneuron; however, their function within the glomerular layer is largely unknown. EM work indicates that CR neurons primarily connect with mitral/tufted cell dendrites and receive feedforward excitatory input from OSNs via external tufted cells (Kosaka et al., 1997). In response to excitatory input, CR neurons can only respond with a single action potential, followed by an inactivation of the main voltage-dependent conductances until the input is terminated (Fogli Iseppe et al., 2016). Some CR neurons do not generate an action potential but can still be depolarised. It has been suggested that CR neurons could function to improve the signal-to-noise ratio by signalling and inhibiting projection neurons in response to weak or random excitatory inputs (Fogli Iseppe et al., 2016). However, odour detection normally consists of high frequency trains of action potentials, which would silence CR neurons and their inhibitory output.

The function of the CB subpopulation is even less understood than CR neurons. They have been shown to synapse with mitral/tufted cell dendrites and other glomerular interneurons (Kosaka et al., 1997). Their electrophysiological properties have not been directly investigated; however, they are believed to be able to fire multiple action potentials (Tavakoli et al., 2018). The majority

of calbindin neurons express the potassium channel Kv3.1 (Najac et al., 2015). Kv3.1-positive neurons in a transgenic mouse line, of which 50% are calbindin, receive OSN input indirectly via bulbar glutamatergic neurons. These neurons are involved in intraglomerular lateral inhibition between projection neurons that are associated with the same glomerulus (Najac et al., 2015).

In a later section (Chapter 1.2), I will discuss a subpopulation of glomerular layer GABAergic interneuron that also release dopamine and can be identified by the expression of TH.

Glomerular layer GABAergic interneurons are involved in intraglomerular inhibition through dendrodendritic release of neurotransmitters (Murphy et al., 2005). GABAergic interneurons receive spontaneous excitatory input, primarily from external tufted cells, that results in tonic neurotransmitter release into glomeruli that modulates the sensitivity of OSN input and glomerular output (Pirez and Wachowiak, 2008; Shao et al., 2009, 2012). In addition to tonic inhibition, glomeruli receive phasic inhibitory release in response to OSN input, further modulating glomerular excitation. The release of GABA has been found to have a bidirectional effect on the activity of GABAergic glomerular neurons, inhibiting when the neurons are firing and exciting when they are silent (Parsa et al., 2015). Intraglomerular inhibition may act to supress weakly activated glomeruli, while strong, high-frequency OSN input can silence GABAergic neurons and reduce intraglomerular inhibition, strengthening glomerular output.

1.1.2.3 Short-axon cells

The original description of glomerular layer neurons included a minor population of neuron that possessed an axon. These neurons were described as having a large cell body, with dendrites that spread around, and avoided, innervating glomeruli (Pinching and Powell, 1971a). Their dendrites had very few spines and rarely contained vesicles. As the name suggests, these neurons were described as having a short axon, which only extended for 1 or 2 glomeruli. However, the short-axon cell classification has since been found to be a misnomer – the axon can extend for ~1 mm and the original description was likely due to the poor penetration of the thin process during the staining protocol (Aungst et al., 2003; Kiyokage et al., 2010). Short-axon cells have been found to be involved in interglomerular connectivity, connecting with external tufted cells, mitral cells and glomerular layer GABAergic interneurons in distant glomeruli (Aungst et al., 2003; Banerjee et al., 2015; Liu et al., 2013, 2016; Whitesell et al., 2013).

It was suggested that short-axon cells are glutamatergic neurons that send excitatory connections between glomeruli (Aungst et al., 2003). This work was based on short-axon cells not being labelled by a GAD65 mouse, and by stimulating a glomerulus and recording excitatory

postsynaptic potentials (EPSPs) in glomerular layer interneurons 3 or 4 glomeruli away. However, GAD65 expression in the glomerular layer has been shown to be restricted to neurons that only contact one or a few glomeruli, and the neurons that contact multiple glomeruli, for example, short-axon cells, express GAD67 (Kiyokage et al., 2010). Specifically stimulating these short-axon cells also inhibits the activity of distant glomeruli (Whitesell et al., 2013). Therefore, short-axon cells are now widely accepted to be a population of GABAergic neurons that are involved in interglomerular inhibition. However, these neurons have been shown to extend dendritic processes into glomeruli, while Pinching and Powell (1971a) described short-axon cells as avoiding innervation of glomeruli. Therefore, short-axon cells may be a heterogenous population of axon-bearing interneurons in the superficial layers of the olfactory bulb.

1.1.3 Projection neurons

The neuronal populations that I have described so far do not extend processes outside of the olfactory bulb. There are two types of projection neurons that have been described within the olfactory bulb that transmit olfactory information through the lateral olfactory tract to higher brain regions for further processing: mitral cells; and tufted cells.

Mitral cells are the principle projection neuron in the olfactory bulb and send axonal projections throughout the entire olfactory cortex. These cells extend a primary apical dendrite, usually to a single glomerulus. Mitral cells have lateral dendrites that project horizontally in deeper regions of the external plexiform layer. There are conflicting reports whether mitral cells receive monosynaptic input from OSNs. It has been proposed that mitral cells mainly receive input indirectly via external tufted cells (Gire et al., 2012). However, it has been found that whether the response in a mitral cell is monosynaptic, polysynaptic or both, depends on the strength of odour stimulation (Najac et al., 2011; Vaaga and Westbrook, 2016). Weak stimulation of the olfactory nerve layer produces a slow current in mitral cells from the external tufted cells, whereas stronger stimulation produces a biphasic excitatory postsynaptic current (EPSC) with fast (OSN-input) and slow (external tufted cell-input) components. Gap junction coupling between distal tufts of mitral cells' primary dendrites function to synchronise the activity of mitral cells associated with the same glomerulus (Christie et al., 2005).

Along with mitral cells, tufted cells also extend a primary apical dendrite to a single glomerulus. However, their cell bodies are located in the external plexiform layer and they project their secondary dendrites in superficial parts of this layer. Tufted cells only project to rostromedial regions of the olfactory cortex. Tufted cells receive stronger OSN input than mitral cells and are functionally more excitable than mitral cells and have a higher firing frequency (Burton and

Urban, 2014; Nagayama et al., 2004). These cells, therefore, respond more to lower concentrations of odours. The response of mitral cells is delayed compared to tufted cells due to glomerular layer inhibition of mitral cells (Fukunaga et al., 2012).

Mitral/tufted cells are involved in recurrent excitation within a glomerulus through the dendritic release of glutamate (Carlson et al., 2000). This occurs along with external tufted cells, and as discussed, creates a long-lasting current that functions to amplify OSN input. In the mammalian olfactory bulb, the odour environment is explored with 2 – 12 Hz repetitive sniffing (Kay et al., 2009). The activity of projection neurons are locked to distinct phases of the sniff cycle, established by larger feedforward inhibition from GABAergic input onto mitral cells (Fukunaga et al., 2012). It has been posited that this allows the tufted cells to send an initial snapshot of the odour environment, while mitral cells send more processed information later (Fukunaga et al., 2012).

1.1.4 Granule cell layer interneurons

The most numerous population of neuron in the olfactory bulb is the granule cell population located in the granule cell layer. These are anaxonic GABAergic neurons that have a small soma and extend an apical dendrite into the external plexiform layer where it ramifies and forms synapses with the secondary dendrites of mitral and tufted cells. Granule cells are also a heterogeneous population, with morphologically distinct subpopulations that ramify their apical dendrite in particular depths of the external plexiform layer, therefore, preferentially targeting dendrites of bulbar projection neurons in these regions (Greer, 1987). Granule cells receive excitatory input from the dendrites of the projection neurons onto their distal dendrites that extend into the external plexiform layer (Rall et al., 1966). These interneurons inhibit the projection neurons via dendrodendritic synapses and play an important role in the processing of odour information by regulating the activity of the bulbar output neurons. Granule cells also have basal dendrites that extend to deeper regions of the granule cell layer and these proximal dendrites are primarily targeted by inputs from cortical regions (Laaris et al., 2007).

Granule cells primarily target the secondary dendrites of bulbar projection neurons via reciprocal dendrodendritic interactions. The lateral dendrites of mitral cells are involved in action potential backpropagation, which is believed to result in the lateral inhibition of other mitral cells mediated by granule cells (Margrie et al., 2001). Despite tufted cells having synaptic connections with granule cells, they receive very weak or no lateral inhibition (Nagayama et al., 2004). Therefore, odour input that activates mitral cells associated with the input glomerulus results in the inhibition of weakly activated neighbouring mitral cells, improving signal-to-noise.

Besides granule cells there is another heterogeneous population of GABAergic interneurons in the granule cell layer referred to as deep short-axon cells (Eyre et al., 2008). Three subpopulations of these neurons have been identified by the distribution pattern of their axon. One subtype extensively ramifies in the glomerular layer and mediates inhibition of glomerular layer GABAergic interneurons and tufted cells (Burton et al., 2017). These cells also branch in the external plexiform and granule cell layers synapsing with granule cells. The other populations also target granule cells, either their distal dendrites in the external plexiform layer or proximal dendrites and soma in the granule cell layer (Eyre et al., 2008).

1.1.5 Centrifugal inputs

The olfactory bulb receives input from a number of cortical regions. Olfactory cortex pyramidal cells receive sensory input from mitral and tufted cells and project axons back to the bulb (Boyd et al., 2012). In particular, granule cells are a target of this excitatory input from centrifugal inputs onto their proximal dendrites located deeper in the granule cell layer (Laaris et al., 2007). This excitatory input onto granule cells is proposed to enhance inhibition of mitral/tufted cells (Balu et al., 2007; Shipley and Adamek, 1984). Therefore, the activity of bulbar projection neurons is being regulated by a cortical feedback loop. The glomerular layer also receives some monosynaptic input from the olfactory cortex, with stronger excitation of short-axon cells over the other populations (Boyd et al., 2012). GABAergic input from the basal forebrain innervates the olfactory bulb, particular GABAergic interneurons in the glomerular and granule cell layers (Gracia-Llanes et al., 2010).

The olfactory bulb also receives extensive input from neuromodulatory transmitters. Cholinergic input arises from the basal forebrain and activates nicotinic receptors on glomerular layer interneurons and mitral cells causing an excitatory effect, while activation of muscarinic receptors on granule cells inhibits firing and enhances their GABA release (Castillo et al., 1999). The noradrenergic input to the olfactory bulb originates from the locus coeruleus and primarily innervates the granule cell layer and inhibits granule cells (Linster et al., 2011). Noradrenergic terminals are also present in the glomerular layer and participates in supressing OSN input (Eckmeier and Shea, 2014). Serotonergic input from the dorsal and median raphe nuclei densely innervate the glomerular layer and produces membrane depolarisation and increased activity of neurons in these layers (Brill et al., 2016; Schmidt and Strowbridge, 2014). There is, therefore, modulation of olfactory bulb activity and odour processing by resident bulbar neurons and input from cortical and subcortical regions.

1.1.6 Odour processing in the olfactory bulb

The role of the olfactory bulb is to receive and transform odour information before sending it to higher cortical regions. The diversity of neurons and their function makes the olfactory bulb an important player in the initial processing of odour information. Odour identity is largely encoded by a spatial map of activated glomeruli in response to an odour (Wachowiak and Cohen, 2001). Glomeruli that respond to stimuli that share molecular features tend to loosely cluster and form a spatial map of odour stimulus features referred to as a chemotopic map (Mori et al., 2006). However, some research suggests that while a map is formed by the activation of different glomeruli in response to different odours, there is no chemotopic organisation (Ma et al., 2012a). An initial map is formed shortly after response onset and is then reorganised in a few hundred milliseconds to form more informative spatial maps of odour identity (Yaksi et al., 2007). This spatial segregation increases the contrast between odour-evoked activity in the olfactory bulb. However, similar odour stimuli evoke overlapping maps of activated glomeruli. Despite this, similar odours are still discriminable, indicating that spatial maps are not the sole process for odour identification. Olfaction is an active sense and odorant sampling is achieved through inhalation and sniffing, resulting in a temporal pattern of activity that shapes the formation of the spatial map after inhalation (Wesson et al., 2008). Overlapping glomerular representations of odorant identities can be dynamically reformatted into ensembles of temporally separated mitral/tufted cell activity within a single breath, mediated at least in part by the activity of granule cells (Gschwend et al., 2015). Therefore, odours are not only encoded by which neurons respond to an odour input, but also when these neurons respond.

The spatiotemporal formation of activity maps is confounded by odorant identity and concentration. Increasing odour concentration not only increases response amplitudes in glomeruli, but also leads to the activation and suppression of new glomeruli, altering the glomerular activity map (Wachowiak and Cohen, 2001). This creates a computational challenge for the encoding of odorant identity. The spatial patterns of activated glomeruli and the sequence of activation of individual glomeruli are conserved across different concentrations (Spors and Grinvald, 2002). Mitral cells, but not tufted cells, show long latency responses to weak stimulation, with increasing odour concentration this latency shortens and may be a mechanism to allow mitral cells to encode odorant concentration (Fukunaga et al., 2012; Geramita and Urban, 2017). Higher odour concentration monotonically increases OSN activity and input to glomeruli; however, mitral cells do not display this monotonic increase, except for the strongest responding cells (Banerjee et al., 2015; Davison and Katz, 2007). This can be mediated by lateral inhibition of mitral/tufted cells via reciprocal dendrodendritic synapses with granule cells. This is believed to sharpen the tuning of mitral cells and facilitate discrimination

by decorrelating neural responses (Geramita et al., 2016; Gschwend et al., 2015). This process acts to normalise mitral/tufted cell responses and decorrelate odour representations to aid odour identification. Lateral inhibition is stronger onto mitral cells in response to increased odour concentration (Geramita et al., 2016; Nagayama et al., 2004). In the piriform cortex it has been found that there is an odour representation that selectively attends to the earliest (strongest) olfactory bulb inputs, which is stable despite changing odour concentrations (Bolding and Franks, 2018).

There are also processes within the glomerular layer that act to normalise glomerular output. However, additional glomeruli are also activated by increased odour concentration. Therefore, there needs to be a gain control mechanism in the olfactory bulb to encode odorant identity despite dynamic glomerular responses. Lateral inhibition between glomeruli and intraglomerular inhibition has been posited as mechanisms that can filter out weakly activated glomeruli and sharpen the signal-to-noise ratio (Banerjee et al., 2015; Shao et al., 2012). One population of glomerular layer interneuron that has been particularly implicated in this process is the dopaminergic population. In the next section I will discuss in detail olfactory bulb dopaminergic neurons.

1.2 Olfactory bulb dopaminergic neurons

1.2.1 Dopaminergic neurons

There are a number of distinct brain regions in the mammalian central nervous system that possess dopaminergic neurons. These neurons are distributed as groups of cells in the ventral midbrain, diencephalon, retina and olfactory bulb (Björklund and Dunnett, 2007). Dopaminergic neurons can be readily identified by the expression of the enzyme tyrosine hydroxylase (TH). TH is the first enzyme in the dopamine biosynthesis pathway and catalyses the conversion of tyrosine to L-DOPA, the rate-limiting step in the production of dopamine. L-DOPA is then converted to dopamine by the enzyme DOPA decarboxylase (DDC). As dopamine is a catecholamine, TH and DDC are also markers for other catecholaminergic neurons. Other known dopaminergic markers include vesicular monoamine transporter 2 (VMAT2), which is required for transporting dopamine into vesicles, and dopamine transporter (DAT), which is responsible for the reuptake of dopamine from the synaptic cleft.

Dopaminergic neurons in the brain share some common features. Many dopaminergic populations have been shown to have pacemaker activity, an intrinsic ability to fire rhythmic action potentials, which produces a tonic release of neurotransmitter in the midbrain, retina and olfactory bulb (Feigenspan et al., 1998; Grace and Onn, 1989; Pignatelli et al., 2005). There is evidence that in addition to the synthesis of dopamine, many dopaminergic neurons can also synthesise and release another neurotransmitter. This dual transmitter phenotype has demonstrated the heterogeneity within and between populations of dopaminergic neurons. In the ventral tegmental area, dopaminergic neurons that target the nucleus accumbens have been shown to co-release glutamate, while dopaminergic neurons that target striatal spiny neurons and retinal dopaminergic neurons co-release GABA (Hirasawa et al., 2012; Tecuapetla et al., 2010; Tritsch et al., 2012). Co-transmission by dual transmitter dopaminergic neurons have temporal differences in release, with dopamine acting in a modulatory role with slow release and the other neurotransmitter such as glutamate having faster neurotransmission, which allows for timing-precise signalling (Chuhma et al., 2004). Different populations of dopaminergic neuron can release neurotransmitters from their dendrites, soma and axon and release transmitter by synaptic transmission or volume transmission (Björklund and Lindvall, 1975; Cragg et al., 2001; Hirasawa et al., 2012; Jaffe et al., 1998). In contrast to synaptic release, volume transmission is the non-synaptic release of neurotransmitter that diffuses through the extracellular space. Released dopamine can be taken back into the neuron through transporters, including DAT and norepinephrine transporter (NET) or enzymatically broken down by catechol-O-methyltransferase (COMT) (Wayment et al., 2001).

Within the olfactory bulb, dopaminergic neurons are primarily located in the glomerular layer, positioned around glomeruli, with a small proportion also located in the superficial external plexiform layer and occasionally deeper in this layer. Being placed at the entry level of the bulbar circuitry along with the presence of dopamine receptors on the terminals of OSNs and on bulbar neurons indicates that dopaminergic neurons play a significant role in odour processing. The dopaminergic population comprise approximately 10% of the neurons in the glomerular layer of the olfactory bulb (Parrish-Aungst et al., 2011).

1.2.2 Making an olfactory bulb dopaminergic neuron

During mid-embryonic development, olfactory bulb interneurons are predominately generated from progenitor cells in the subventricular zone of the dorsal lateral ganglionic eminence (dLGE) (Hinds, 1968). These immature interneurons then migrate to the developing olfactory bulb and position themselves in their destined layers (Pencea and Luskin, 2003). While this is the primary source of embryonic olfactory bulb dopaminergic neurons, it has also been suggested that local precursor cells within the olfactory bulb and progenitors in the medial septum also give rise to dopaminergic neurons during embryonic development (Inoue et al., 2007; Vergaño-Vera et al., 2006). Olfactory bulb interneurons, including dopaminergic neurons, continue to be generated in late-embryonic development and postnatal periods. Neural stem cells located in the subventricular zone (SVZ) of the lateral ventricle give rise to neuroblasts that migrate along the rostral migratory stream (RMS) to the olfactory bulb and differentiate into neurons (Luskin, 1993; Young et al., 2007). However, there is also evidence that there is a niche of precursors in the RMS itself that preferentially gives rise to dopaminergic neurons (Hack et al., 2005). Therefore, there does not appear to be a single spatial and temporal origin that is specific to olfactory bulb dopaminergic neurons. In addition, it has not been discovered whether there is a single gene or combinatorial code that is specific for determining olfactory bulb dopaminergic cell fate.

Despite the heterogeneity in the origin of these neurons, a number of transcription factors have been identified that are important for the correct differentiation of olfactory bulb dopaminergic neurons. However, these are not restricted to this population and are also expressed by some non-dopaminergic olfactory bulb neurons (Cave and Baker, 2009). The dopaminergic identity for olfactory bulb dopaminergic neurons has been shown to particularly rely on Pax6, Dlx2 and Meis2. Loss of just one of these transcription factors reduces the proportion of dopaminergic neurons generated, while appearing to increase the number of calretinin interneurons in the olfactory bulb (Agoston et al., 2014; Brill et al., 2008). In contrast, overexpression of Dlx2 increases the proportion of dopaminergic neurons, while decreasing the calretinin population

(Brill et al., 2008). ER81 is expressed in progenitor cells in the embryonic dLGE and postnatal SVZ and is co-expressed with differentiated dopaminergic neurons in the olfactory bulb (Cave et al., 2010; Stenman et al., 2003). ER81 is important for regulating the expression of *Th*; however, it is also expressed by a subpopulation of glomerular layer calretinin neurons (Allen et al., 2007). Therefore, expression of these (and other) transcription factors is important for specifying a dopaminergic identity.

Olfactory bulb dopaminergic neurons show expression of *Th* mRNA during neuronal migration through the RMS; however, there is not significant translation of TH until the neuron integrates into the glomerular layer circuitry and starts receiving sensory input (Baker et al., 2001; Saino-Saito et al., 2004). There is some evidence that immature dopaminergic neurons position themselves in the deeper bulbar layers and await a signal to fully differentiate and migrate into the glomerular layer (Pignatelli et al., 2009). The expression dynamics of other dopaminergic markers are less well-understood. Dopaminergic neurons in the olfactory bulb express another gene required for the synthesis of dopamine (*Ddc*) as well as genes required for its storage (*Vmat2*) and its uptake (*Dat*) (Cave et al., 2010). However, these neurons are not reported to express *Gtpch* (Cave et al., 2010), which is required for the synthesis of TH co-factor BH4 (Habecker et al., 2002).

1.2.3 Co-transmission of dopamine and GABA

Studies that have directly recorded dopaminergic release from olfactory bulb dopaminergic neurons in both *ex vivo* slices and dissociated cell cultures show that the dopamine signal recorded by amperometry is very small compared to dopaminergic neurons in other brain regions (Borisovska et al., 2013; Vaaga et al., 2017). The dynamics of neurotransmitter clearance following release shapes the amplitude and duration of the postsynaptic response. The most common method of clearing dopamine is by transporters, such as DAT, or via enzymatic breakdown by COMT. The expression of DAT in the olfactory bulb is reported to be low with conflicting reports on whether DAT protein is present (Cockerham et al., 2016; Mitsumoto et al., 2005). Though there is *Dat* gene promotor activity shown by DAT-Cre mouse models that label dopaminergic neurons in the olfactory bulb (Banerjee et al., 2015; Galliano et al., 2018). COMT activity has been posited as the primary mechanism for the clearance of dopamine in the olfactory bulb due to the high expression of this enzyme in the olfactory bulb and enhancement of dopamine signals following inhibition of COMT activity (Cockerham et al., 2016). In response to odour preference training, neonatal rats show a significant increase in the release of dopamine in the glomerular layer, in addition, dopamine metabolites produced by COMT are

significantly increased (Coopersmith et al., 1991). Further supporting a role for COMT in dopamine clearance in the olfactory bulb.

Dopaminergic neurons in the olfactory bulb are a subpopulation of glomerular layer GABAergic interneuron. The majority of TH neurons have also been shown to express the GABAergic marker GAD67, with a subset additionally expressing GAD65 (Kiyokage et al., 2010; Parrish-Aungst et al., 2007). GABA release from olfactory bulb dopaminergic neurons has been shown to be fast, whereas dopamine has an extended time course of release (Borisovska et al., 2013; Vaaga et al., 2017). Olfactory bulb dopaminergic neurons are, therefore, dual transmitter neurons releasing dopamine and GABA. GABA release onto postsynaptic neurons in the glomerular layer has been demonstrated by the presence of GABAergic inhibitory postsynaptic currents following the activation of olfactory bulb dopaminergic neurons (Banerjee et al., 2015; Vaaga et al., 2017). These neurons also show a $GABA_A$-mediated auto-inhibition current evoked by the dendritic release of GABA activating their own $GABA_A$ receptors (Borisovska et al., 2013; Maher and Westbrook, 2008).

1.2.4 Not all dopaminergic neurons are the same in the olfactory bulb

The presence of different subpopulations of dopaminergic neurons in the olfactory bulb has long been known. Work by Halász et al. (1981) found that TH-positive neurons could be classified based on the size of their soma, with one subpopulation having a large soma and another having a small soma. Since then several studies have attempted to address the heterogeneity in the dopaminergic population by putting forward different classifications. This has led to these neurons being described as periglomerular neurons, short axon cells, external tufted cells, a mixture of different populations and various other subclassifications within those descriptions (Bywalez et al., 2016; Halász et al., 1981; Vaaga et al., 2017). However, a growing body of work supports treating olfactory bulb dopaminergic neurons as two separate subpopulations. Morphological investigations have revealed that dopaminergic neurons in the olfactory bulb can also be classified by their processes. The majority of these neurons contact a small number of glomeruli within a relatively small region of the glomerular layer with their dendritic processes (**Figure 1.2A**). However, there is another subpopulation that show more extensive projections and contact many glomeruli and establish long-range interglomerular connections with an axon (Kiyokage et al., 2010; Kosaka and Kosaka, 2008) (**Figure 1.2B**).

The “large” soma size subpopulation was originally considered as a population of external tufted cells as their cell bodies were located at the boundary of the glomerular layer and external plexiform layer (Halász et al., 1981). However, morphometric analysis revealed that

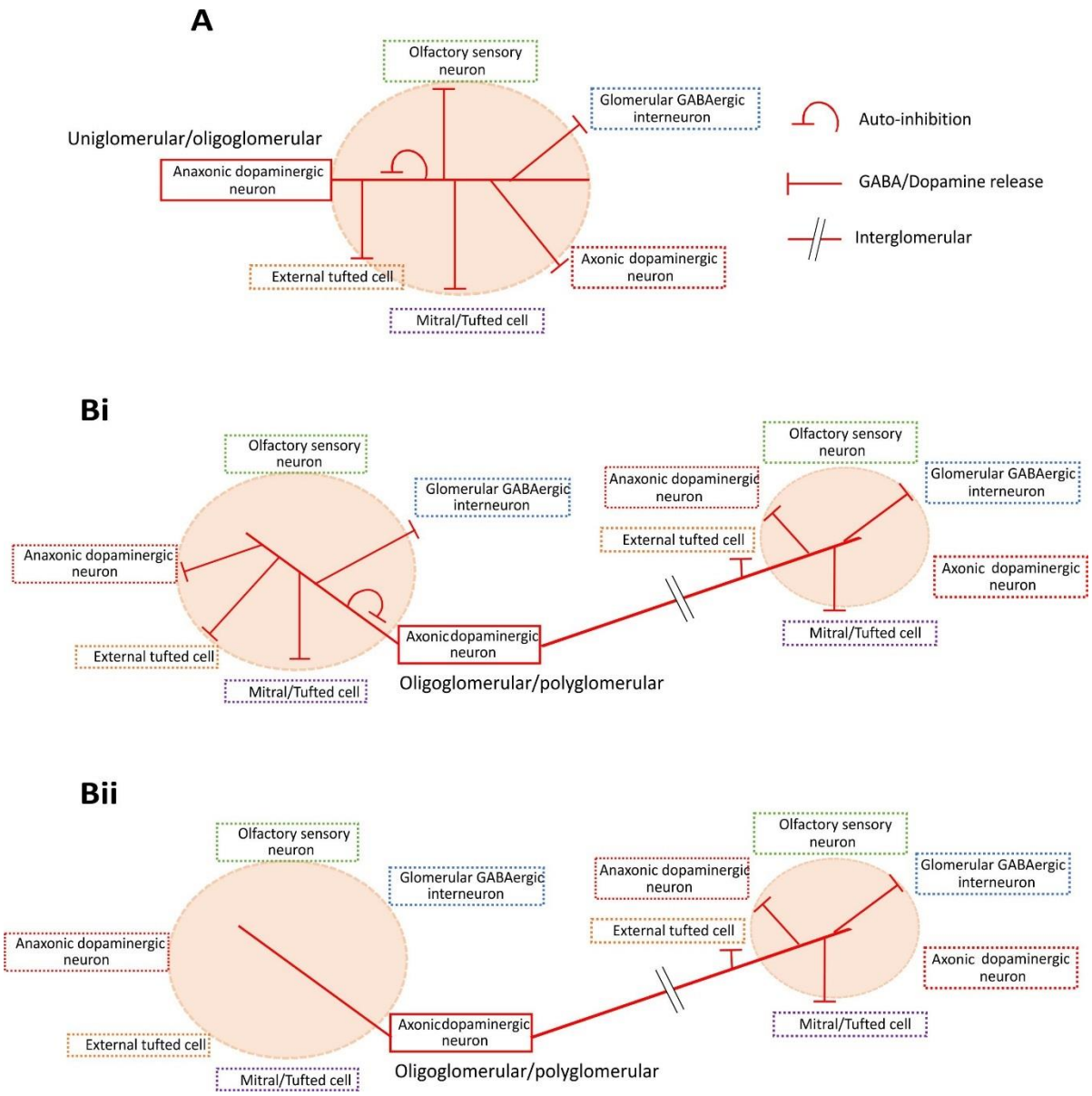

Figure 1.2 Schematic of the connectivity of olfactory bulb dopaminergic neurons

A: The release of GABA/dopamine from anaxonic dopaminergic neurons is involved in intraglomerular connectivity and signals to the neurons that project into glomeruli. The release of neurotransmitter also results in auto-inhibition. These neurons connect to one or a few glomeruli (uniglomerular/oligoglomerular).

B: It is unknown whether axonic dopaminergic neurons are (i) or are not (ii) involved in intraglomerular connectivity. These neurons possess an axon and connect to a few or many glomeruli (oligoglomerular/polyglomerular).

dopaminergic neurons did not have tufted dendrites and these neurons have a broad spread of dendrites, contacting many glomeruli and possess an axon (Galliano et al., 2018; Kiyokage et al., 2010). Therefore, this subpopulation may represent the short-axon cell (Kiyokage et al., 2010). However, these dopaminergic neurons extend processes into glomeruli, which is not reported to be a feature of short-axon cells (Pinching and Powell, 1971a). Developmentally, these neurons are generated exclusively during embryonic development, peaking around embryonic days 11-12 (Galliano et al., 2018; McLean and Shipley, 1988). It is not clear whether these neurons originate from precursor cells in the lateral ganglionic eminence or whether they are produced from local precursors within the nascent olfactory bulb (Stenman et al., 2003; Vergaño-Vera et al., 2006).

The “small” soma size subpopulation are located around glomeruli and only contact one or a few local glomeruli through dendritic process and do not possess an axon (Galliano et al., 2018). These neurons more closely resemble the periglomerular population of interneurons. However, dendritic arborisations of these neurons have been observed to be outside glomeruli, while others can innervate several glomeruli (Bywalez et al., 2016; Kiyokage et al., 2010). Therefore, they would appear to be a separate population from the classic definition of periglomerular neurons (Pinching and Powell, 1971a). Birthdating studies have found that this subpopulation are continuously generated throughout postnatal life (Galliano et al., 2018; Kosaka and Kosaka, 2009).

While these “large” and “small” categories may obscure further subpopulations, for example, dendritic arborisation patterns (Bywalez et al., 2016), these simplified descriptors classify these neurons by their major differences identified so far. Molecular identification of the specific dopaminergic subpopulations is complicated by the fact that there are currently no known markers specific to either subpopulation. This is further complicated as the transcription factors that have been identified for olfactory bulb dopaminergic cells have also been shown to be expressed by other bulbar neurons. To understand the processes that determine the dopaminergic fate would require an investigation into the gene expression of these neurons throughout their developmental process.

1.2.5 Functional properties

A characteristic feature of dopaminergic neurons is their pacemaker activity. This has been shown to be present in other dopaminergic neurons (Grace and Bunney, 1983). The dopaminergic population in the olfactory bulb have also been demonstrated to have autorhythmic firing in *ex vivo* slices and *in vitro* isolated cells (Pignatelli et al., 2005; Puopolo et

al., 2005). This pacemaker activity would be predicted to result in the tonic release of neurotransmitter from these neurons. In other pacemaker dopaminergic neurons, a hyperpolarisation-activated current (I_h) carried by HCN channels is important for the regulation of this activity (Neuhoff et al., 2002). However, in olfactory bulb dopaminergic neurons I_h does not regulate pacemaker firing, but it does influence the resting membrane potential and excitability of the neuron (Pignatelli et al., 2013). The potassium inward rectifier (KIR) current is another hyperpolarisation-activated current that is also involved in regulating their excitability (Borin et al., 2014). There is pharmacological evidence that several neurotransmitters are capable of modulating the excitability of these neurons. Application of noradrenaline, serotonin, histamine and the activation of acetylcholine receptors reduces the KIR current, while it is increased by the application of dopamine (Borin et al., 2014). Noradrenaline also decreases the amplitude of the I_h current (Pignatelli et al., 2013). However, it is unclear whether these effects are due to direct activation of receptors on the cells or indirectly through the neurons that contact bulbar dopaminergic neurons. As the olfactory bulb is densely innervated by neuromodulatory transmitters from cortical regions that terminates in the glomerular and granule cell layers (see Chapter 1.1.5) and the dopaminergic subpopulations appear to express receptors for these transmitters, these inputs are likely to affect the activity of dopaminergic neurons in the olfactory bulb.

The only study to investigate the functional differences between the two olfactory bulb dopaminergic subpopulations found that the anaxonic subpopulation was less excitable compared to the axonic subpopulation, initiating action potentials slower and unable to maintain a linear increase in repetitive firing (Galliano et al., 2018). *In vivo* there are differences in how these two subpopulations respond to odour input. The “large” dopaminergic neurons were found to be more broadly tuned to odour stimuli and despite their increased excitability measured *ex vivo*, they show weaker responses compared to the “small” neurons, as measured by GCaMP activity (Galliano et al., 2018). Functionally the anaxonic subpopulation are likely to be the dopaminergic neurons involved in intraglomerular inhibition (Vaaga et al., 2017). In contrast, the axonic subpopulation can extend their axons to signal glomeruli located a distance away and are likely to be involved in interglomerular inhibition (Banerjee et al., 2015). However, it is unclear whether the axonic subpopulation is involved in intraglomerular inhibition.

Given their strategic position surrounding glomeruli and their ability to form intraglomerular or interglomerular synaptic connections, what is the role of dopaminergic neurons in the olfactory bulb? Research exploring the distinct roles of the two subpopulations has only started to be addressed (Galliano et al., 2018). However, we can glean information about their role from

studies that have examined the function of dopamine and GABA in the olfactory bulb and evidence of interglomerular connectivity.

1.2.6 Intraglomerular connectivity

It has been reported that the majority (~75%) of dopaminergic neurons receive monosynaptic glutamatergic input following OSN stimulation (Pignatelli et al., 2009). However, Kiyokage et al. (2010) found that only around 30% of dopaminergic neurons receive direct input from OSN and the majority of OSN input is indirect through external tufted cells. EM work found that the vast majority of excitatory synaptic inputs to TH-positive neurons were from OSN terminals, with a proportion from dendrites of presumed mitral/tufted cells and also GABAergic neurons (Toida et al., 2000). These discrepancies between physiological and ultrastructural work were addressed by Kiyokage et al. (2017) who reported that OSN inputs preferentially targeted distal dendrites, while non-OSN inputs targeted proximal dendrites, which could generate more effective inputs.

EM work has suggested that the majority of olfactory bulb dopaminergic neuron output synapses are with presumed mitral/tufted cell dendrites and not OSN terminals (Kiyokage et al., 2017; Toida et al., 2000). This finding is surprising considering the presence of D_2 receptors on OSN terminals and suggests that these receptors are sensitive to the local concentration of dopamine within glomeruli rather than direct activation by synaptic contacts. The expression of D_2 receptors in glomeruli has revealed that this receptor is also expressed by mitral and tufted cells as well as inhibitory interneurons, including the dopaminergic population itself (Gutièrrez-Mecinas et al., 2005). GABAergic glomerular interneurons can also signal to other GABAergic interneurons, although this has not been definitively shown for the dopaminergic populations (Murphy et al., 2005; Smith and Jahr, 2002). Unlike other glomerular layer GABAergic interneurons and granule cells, dopaminergic neurons do not make reciprocal dendrodendritic synapses (Isaacson and Strowbridge, 1998; Kiyokage et al., 2017; Murphy et al., 2005; Toida et al., 2000). Dopaminergic neurons form serial synapses, receiving excitatory input from OSN terminals or mitral/tufted processes and form output synapses with mitral/tufted cells (Kiyokage et al., 2017).

Paired-pulse stimulation of the rat olfactory nerve layer and recording the synaptic response in mitral cells showed that the application of dopamine or the D_2 agonist, quinpirole, significantly suppressed the evoked EPSC response, which was completely reversed by the application of the D_2 antagonist, sulpiride (Ennis et al., 2001; Hsia et al., 1999). Despite the low expression of DAT and the dominant role of COMT (Cockerham et al., 2016), increasing extracellular dopamine

levels by application of the DAT blocker, cocaine, reduces the amplitude of OSN-evoked EPSCs, which can be reversed by the application of the D_2 receptor antagonist, sulpiride (Maher and Westbrook, 2008). However, this is not evidence for endogenous release of dopamine. Activation of $GABA_B$ receptors with the agonist, baclofen, produces a similar effect on OSN-evoked EPSCs, which is reversed by the $GABA_B$ antagonist, CGP55845 (Maher and Westbrook, 2008). Given their ability to release dopamine and GABA, olfactory bulb dopaminergic neurons can, therefore, play an important role in modulating olfactory input. However, in a TH-GFP mouse, depolarisation of individual TH-positive neurons was insufficient to observe dopaminergic or GABAergic presynaptic inhibition of OSN terminals (Maher and Westbrook, 2008). However, activation of a single periglomerular neuron can inhibit OSN release (Murphy et al., 2005). This suggest that there needs to be activation of multiple olfactory bulb dopaminergic neurons to produce an effect on OSN terminals.

Optogenetic stimulation of dopaminergic neurons expressing channelrhodopsin in the $DAT^{IREScre}$ mouse followed by OSN stimulation was sufficient to reduce the evoked EPSC recorded in mitral and external tufted cells (Vaaga et al., 2017). In mitral cells, this suppression of OSN-evoked EPSC was blocked by the presence of both $GABA_B$ and D_2 receptor antagonists. When these antagonists were used individually, the evoked-EPSC was still partially suppressed following optogenetic stimulation of the dopaminergic neurons. This provides evidence that the release of dopamine and GABA by the activation of dopaminergic neurons directly affects OSN terminals. Varying the time between the optogenetic stimulation of dopaminergic neurons and electrical stimulation of OSN afferents revealed that the attenuation of the evoked EPSC continued for hundreds of milliseconds. This is likely to be due to activation of metabotropic receptors having a longer lasting effect than ionotropic receptors and also the longer time course of dopamine release in these neurons. This extended presynaptic inhibition reduces OSN-evoked spiking in mitral and external tufted cells, affecting the output of the olfactory bulb (Vaaga et al., 2017). However, it is still unclear whether these effects come from physiological activation of olfactory bulb dopaminergic neurons.

These neurons and the majority of other anaxonic glomerular GABAergic interneurons can only release neurotransmitter via their dendrites. This can be demonstrated by depolarising these neurons to release GABA, which then bind to $GABA_A$ receptors present on their dendrites evoking a GABA-mediated self-inhibition response (Maher and Westbrook, 2008; Murphy et al., 2005; Smith and Jahr, 2002). There is also evidence from dissociated cultures of dopaminergic neurons that they can release neurotransmitter from their soma (Borisovska et al., 2013). Midbrain dopaminergic neurons are known to release neurotransmitter from their axon,

dendrites and soma (Björklund and Lindvall, 1975; Iravani et al., 1996). Dopaminergic neurons lacking an axon are likely to be involved in intraglomerular inhibition in the olfactory bulb. However, it is not clear whether axonic dopaminergic neurons can also release neurotransmitter via their dendrites or soma.

Dopamine receptors are not only present on OSN terminals, with external tufted cells expressing D_1 receptors. These neurons also express $GABA_A$ receptors and receive monosynaptic GABA input from olfactory bulb dopaminergic neurons (Vaaga et al., 2017). Optogenetic activation of dopaminergic neurons produces an intraglomerular fast, $GABA_A$ receptor-mediated inhibitory response in external tufted cells (Vaaga et al., 2017). The presence of gap junctions between dopaminergic neurons and external tufted cells has also been reported (Banerjee et al., 2015). Gap junctions between diverse types of dendritic processes in glomeruli has been shown (Kosaka and Kosaka, 2005). However, expression of a major gap junction forming protein, connexin 36, was found to be rarely expressed in TH-positive neurons (Kosaka et al., 2005). It is, therefore, not clear whether both subpopulations of dopaminergic neurons form gap junctions or the extent of these connections. It is unclear whether dopaminergic neurons act directly on mitral cells, despite reported presence of D_2 receptors in the latter cell type (Gutièrrez-Mecinas et al., 2005). Vaaga et al. (2017) found that optogenetically stimulating dopaminergic neurons rarely evoked GABAergic currents in mitral cells. However, one possibility could be that olfactory bulb dopaminergic neurons rarely make GABAergic synapses with mitral cells that activate $GABA_A$ receptors.

Signalling between dopaminergic neurons and other inhibitory glomerular layer interneurons has not been well described; however, dopaminergic neurons do have $GABA_A$ receptors (Maher and Westbrook, 2008). Parsa et al. (2015) described how GABA has a dual role in inhibitory glomerular interneurons depending on the activity of these neurons. The activation of $GABA_A$ receptors on quiescent neurons can induce the cells to fire, whereas GABA inhibits neurons that are firing. This bidirectional role for GABA on the firing of GABAergic interneurons could act to inhibit glomerular output in response to low sensory input and conversely auto-disinhibit inhibitory activity at high frequency. Olfactory bulb dopaminergic neurons, therefore, have the ability to affect the spatiotemporal pattern of glomerular output by modulating sensory input and intraglomerular activity. In addition, dopaminergic neurons have been found to signal to distant glomeruli.

1.2.7 Interglomerular inhibition

One of the most striking morphological differences between the two subpopulations of olfactory bulb dopaminergic neurons is the presence or absence of an axon. It has been posited that these neurons are involved in inhibition between glomeruli, i.e. interglomerular inhibition (Galliano et al., 2018). Optogenetic activation of dopaminergic neurons produces an interglomerular fast, $GABA_A$ receptor-mediated inhibitory response in external tufted cells (Banerjee et al., 2015; Liu et al., 2013). This inhibition activates the hyperpolarisation-activated current (I_h), which acts to repolarise the membrane potential towards the threshold for spiking. This repolarisation is potentiated by an excitatory response mediated by dopamine acting on D_1 receptors, which enhances rebound spiking (Liu et al., 2013). If mitral cells can receive direct stimulation from OSNs, the GABAergic inhibition of external tufted cells would reduce their excitatory drive of inhibitory interneurons, increasing the sensitivity of mitral cells to direct OSN inputs. The rebound excitation would then drive external tufted cell input to mitral cells, while also signalling to inhibitory interneurons. However, if activation of mitral cells is through external tufted cells (Gire et al., 2012), interglomerular connections can delay glomerular excitation through inhibition followed by excitation. Olfactory bulb dopaminergic neurons can, therefore, modulate sensory input through a direct pathway by presynaptic inhibition of OSN terminals or indirectly through the inhibition-excitation of external tufted cells. These actions may be partitioned between anaxonic and axonic dopaminergic neurons, respectively.

The presence of an interglomerular response in external tufted cells upon stimulation of olfactory bulb dopaminergic neurons would suggest a distinct role for the large, embryonic generated population. Only this population of GABAergic neurons in the glomerular layer appear to possess an axon permitting long distance signalling between glomeruli. Lateral inhibition between glomeruli has been posited as a mechanism to aid odour identification and/or discrimination (Banerjee et al., 2015). As odour identity is formed by the distribution of odorant information across glomeruli, lateral inhibition could aid in contrast enhancement and odour discrimination through the suppression of weakly activated glomeruli by strongly activated ones. Whitesell et al. (2013) found that an OSN-evoked long-lasting depolarisation and spiking in mitral cells were reduced when preceded by the stimulation of a glomerulus further away (≥200 µm), driven by GABAergic input onto external tufted cells.

Increasing odour concentration is associated with a concomitant increase in the amplitude and spatial spread of dopaminergic neuron activity in the olfactory bulb leading to suppression of mitral cell firing, mediated through external tufted cells, and implementing gain control of olfactory bulb output (Banerjee et al., 2015). This increase in dopaminergic activity is likely to

enhance both intraglomerular and interglomerular inhibition. The increased activity was also associated with sparser activation of mitral cells, resulting in decorrelated odour representations, i.e. the activity produced by individual odours becomes more distinct. This decorrelation of responses has been posited as a mechanism to aid the separation of stimuli (Vinje and Gallant, 2000).

It is unclear whether olfactory bulb dopaminergic neurons that mediate interglomerular inhibition also take part in intraglomerular inhibition. An EM study in the rat olfactory bulb did not find any evidence for the dendrites of axonic TH-positive neurons forming presynaptic connections, though vesicles were present in their dendrites (Liberia et al., 2012). However, this study only focussed on axonic dopaminergic neurons that are occasionally located in the deep regions of the external plexiform, while these neurons are primarily located in more superficial regions (Galliano et al., 2018). The original description of short-axon cells reported that vesicles were generally absent from dendrites and cell body of these neurons and these neurons did not synapse with OSNs (Pinching and Powell, 1971a). However, axonic dopaminergic neurons may not conform to the classical description of short-axon cells (see Chapter 1.2.4). However, if they do indeed lack the capability to release transmitter from their dendrites, it suggests that axonic olfactory bulb dopaminergic neurons are exclusively involved in interglomerular inhibition, though further work is needed to substantiate this. Whether the axon-lacking subpopulation are also involved in interglomerular inhibition is unclear. These neurons have been shown to extend dendrites into multiple glomeruli and, therefore, may mediate a form of more local interglomerular inhibition – interglomerular centre-surround inhibition. Strongly activated glomeruli have been shown to suppress OSN release in surrounding glomeruli (Vučinić et al., 2006). It, therefore, appears that anaxonic dopaminergic neurons are involved in intraglomerular and local interglomerular inhibition, while axonic dopaminergic are involved in long distance interglomerular inhibition.

1.2.8 Role of dopamine in olfactory behaviour

Despite clear evidence that dopaminergic neurons are involved in the circuitry of the olfactory bulb, the specific role of dopamine in olfactory behaviour is still unclear. Activating bulbar dopamine receptors via pharmacological application to the olfactory bulb, particularly D_2 agonists, has been reported to worsen odour discrimination, while D_2 antagonists improve odour discrimination (Escanilla et al., 2009). However, odour detection and discrimination are unaffected in knockout D_2 receptor mice, although, more complex odour tasks requiring cognitive flexibility and higher cortical processing are impaired (Kruzich and Grandy, 2004). Endogenous dopamine release in the olfactory bulb may aid learning. Measuring dopamine

levels in the olfactory bulb of neonatal rats revealed that odour preference training (pairing an odour with tactile stimulation) produced a large and prolonged increase in dopamine levels, while presenting the odour or tactile stimulation separately produced a smaller dopamine response (Coopersmith et al., 1991). Mice lacking DAT show very specific deficits in olfactory discrimination; however, these defects could stem from a lack of DAT in other brain regions. After showing normal habituation and sensitivity to an odour, $DAT^{-/-}$ mice do not change their behaviour upon presentation of a novel odour compared to wildtype controls (Tillerson et al., 2006). In Parkinson's disease, which is associated with loss of dopaminergic neurons in midbrain, the olfactory bulb dopaminergic population is spared and its number may even increase, though this latter effect has been reported to be gender specific (Huisman et al., 2004, 2008; Mundiñano et al., 2011). Loss of the sense of smell is one of the earliest symptoms of Parkinson's disease and one possible explanation may be that there is enhanced inhibition in the olfactory bulb mediated by increased activity of dopaminergic neurons.

It is unclear what role the different subpopulations of olfactory bulb dopaminergic neurons play in olfactory behaviour. Current tests do not have the specificity or complexity to address the multiple potential roles each subtype may have in the circuit. There needs to be more targeted manipulations with very specific, tailored behaviour to start to understand their roles. However, there also needs to be more information of their role in the network.

1.3 Neuronal Plasticity

The ability of a neuron to respond to changes in the environment by changing how it receives or transmits information is known as neuronal plasticity. Numerous forms of plasticity have been described that can drive short to long-term alterations in the properties of neurons. These activity-dependent changes have been postulated to underlie learning and the formation of memories and also to maintain neuronal and network output. This section will introduce the olfactory bulb as a model for studying neuronal plasticity, different forms of plasticity and how they have been described in the olfactory bulb.

1.3.1 Olfactory bulb as a model system for studying plasticity

The olfactory bulb has several features that make it an attractive model system for studying experience-dependent plasticity. Unlike other sensory systems that require sensory signals to be sent through a thalamic relay, odour information is transmitted directly to the olfactory bulb where initial odour processing occurs (Kay and Sherman, 2007). Therefore, this brain region is unique, having a direct connection between a primary sensory neuron and the forebrain. The activity of the olfactory bulb can also be readily manipulated and controlled by sensory manipulations due to the direct connection between OSNs and olfactory bulb. The circuitry of the olfactory bulb is well-described and has some genetically tractable populations. Therefore, it is possible to study specific olfactory bulb populations and understand their role and function in bulbar circuitry.

Multiple different examples of plasticity in various neuronal populations have been described within the olfactory bulb. The olfactory bulb is one of the few brains regions where there is continuous generation of neurons throughout life. This includes OSNs and a number of GABAergic bulbar interneurons. The olfactory bulb, especially the glomerular layer, therefore, has a unique feature in the brain where both the presynaptic and postsynaptic neurons in the circuitry can be replaced.

1.3.2 Manipulating activity in the olfactory bulb *in vivo*

As the olfactory bulb is one synapse away from the sensory periphery, its activity can be readily controlled *in vivo* by manipulations to odour experience. Activity levels in the olfactory bulb can be elevated by olfactory enrichment and lowered by odour deprivation. Increasing activity across the entire bulb is a less reliable sensory manipulation due to the differing affinity of individual OSNs for odorants and odour concentration. Odour deprivation by removing sensory input is a more controllable manipulation. This can be achieved by removing OSNs by axotomy

or chemical deafferentation (Mandairon et al., 2003; Nadi et al., 1981). However, these can be invasive and damaging manipulations. A routinely employed method to reduce sensory experience is by blocking one naris either by cauterisation or the insertion of a removable plug, i.e. unilateral naris occlusion (Cummings et al., 1997; Farbman et al., 1988).

Unilateral naris occlusion deprives the ipsilateral bulb of airflow and sensory experience. Unilateral naris occlusion of 1 or 2 day old mice inhibits the development of the deprived bulb and by P30 it is ~25% smaller than nondeprived bulbs (Benson et al., 1984). However, the effects of odour deprivation are reversible and the olfactory bulb recovers its size (Cummings et al., 1997). Reversing plug-induced unilateral naris occlusion is a simpler procedure than cauterisation, as the latter requires additional surgery to reopen the naris. A concern associated with unilateral naris occlusion is the correct control to be studied. The contralateral bulb to the deprived naris is often used as a control; however, this manipulation disrupts normal breathing and increases the airflow through the open naris, potentially producing compensatory or pathological effects (Maruniak et al., 1989). Therefore, naïve animals that had no manipulation or are given a sham manipulation, for example, the insertion and immediate removal of the plug, are more suitable controls (Kass et al., 2013). Although within-animal comparisons are lost using these controls.

Studies investigating the plasticity of the olfactory bulb have described activity-dependent changes including to OSN release, gene expression, connectivity and bulbar output. These plasticity changes have the potential to affect the processing of odour experiences by the olfactory bulb. Of particular interest is the continuous generation of newborn neurons that integrate into the bulbar circuitry and represent an extreme form of plasticity.

1.3.3 Adult neurogenesis

The olfactory bulb and the hippocampus are two regions of the rodent brain that integrate newborn neurons throughout life. The functional role of adult neurogenesis is unclear; however, it is believed that adult neurogenesis represents a distinct form of extreme plasticity as the circuit must change and adapt to this continuous integration of immature neurons, which bring new properties to the circuitry (Lledo et al., 2006).

Adult neurogenesis has long been believed to be a turnover process to replace older neurons with new neurons. Evidence for this mechanism comes from lineage tracing experiments using thymidine analogs to label the DNA of dividing cells, which have found that after maturation these newborn neurons start to die (Petreanu and Alvarez-Buylla, 2002). In the glomerular layer

of the olfactory bulb work has suggested that there is an increase in the volume of this layer and/or net increase in certain subpopulations (Adam and Mizrahi, 2011; Ninkovic et al., 2007), while other work suggests that there is no significant change in neuronal composition or overall amounts in the olfactory bulb (Mizrahi et al., 2006; Platel et al., 2018). A fate-mapping study of 3 month old mice labelled all newborn neurons generated and found that approximately 32% of glomerular layer interneurons in the olfactory bulb were generated during the 9 month study period and there was an overall addition of new neurons to the glomerular layer (Ninkovic et al., 2007). This suggests that adult neurogenesis in the mouse olfactory bulb glomerular layer is a continuous process, constantly increasing the number of adult-generated glomerular layer interneurons to the overall population. However, another *in vivo* imaging study found that while there was a turnover of ~3% of glomerular layer interneurons per month, there was no net addition to the glomerular layer (Mizrahi et al., 2006).

The majority of olfactory bulb neurons that are generated by adult neurogenesis are granule cells (Luskin, 1993). Fate-mapping studies have found that newborn granule cells are more likely to ramify their dendrites in deeper parts of the external plexiform layer, a region primarily containing the lateral dendrites of mitral cells (Kelsch et al., 2007). However, in the granule cell layer of the olfactory bulb and the dentate gyrus of the hippocampus, it has been reported that there is low contribution of adult-generated granule cells (~14%) to the total population over 9 months (from 3 months old to 1 year old) (Ninkovic et al., 2007).

Recent work has suggested that neuronal turnover in the olfactory bulb is, in fact, a rare event and cell loss of adult-born neurons is virtually absent (Platel et al., 2018). This study found that using standard doses of thymidine analogs to label neurons results in toxicity and cell death. The continuous integration of newborn neurons resulted in the olfactory bulb enlarging by approximately 40% from 2 to 12 months. This study raises important questions about previous work that has investigated adult neurogenesis using thymidine analogs such as BrdU and EdU. It is interesting that other long-term imaging studies identified cell loss and turnover of glomerular layer interneurons (Adam and Mizrahi, 2011; Mizrahi et al., 2006). However, Platel et al. (2018) did find that odour deprivation affects neuronal survival and perhaps the odour environment of mice between the different long-term imaging studies impacted neuronal turnover.

Newborn neurons may also have a critical period where survival or death is determined by sensory experience (Platel et al., 2018; Yamaguchi and Mori, 2005). The role of sensory activity on the survival of newborn neurons in the olfactory bulb suggests that adult neurogenesis is not

just a passive process but has an important role in the functioning of the olfactory bulb. Odour enrichment and olfactory learning increases the survival of newborn neurons in the olfactory bulb and has been associated with improved odour memory and discrimination (Alonso et al., 2006; Bonzano et al., 2014; Kato et al., 2012; Rochefort et al., 2002). In contrast, odour deprivation by unilateral naris occlusion or deafferentation decreases the survival of newborn granule cells and glomerular layer GABAergic interneurons (Bastien-Dionne et al., 2010; Mandairon et al., 2003; Sawada et al., 2011; Yamaguchi and Mori, 2005). Odour deprivation in neonatal mice causes a persistent suppression in the generation of calretinin neurons in the glomerular layer, which does not recover after restoring normal olfactory input, while other glomerular layer interneurons recover (Kato et al., 2012).

Immature neurons generated by adult neurogenesis have been found to be more plastic than the more mature, resident population of neurons. Immature granule cells show experience-dependent changes to their connectivity, while the mature population appears more stable. After olfactory learning, excitatory and inhibitory input to newborn granule cells from both mitral cells and cortical regions are increased (Huang et al., 2016; Lepousez et al., 2014). Quast et al. (2017) found that as immature granule cells develop they spread their inhibitory map by forming more connections and becoming more broadly tuned to odours. However, it has also been shown that most adult-born granule cells narrow their tuning with maturation, with a small proportion showing broader tuning (Wallace et al., 2017). Olfactory training increases or prolongs broader tuning, while the inhibitory map of mature granule cells remains stable (Quast et al., 2017; Wallace et al., 2017). While learning induces expansion of immature granule cell sensory maps, odour deprivation prevents expansion and reduces excitatory inputs to these neurons, without affecting the mature granule cells (Quast et al., 2017). As adult-born glomerular layer GABAergic interneurons mature they increase OSN-evoked AMPA responses and downregulate NMDA responses, suggesting decreased synaptic plasticity with maturation (Grubb et al., 2008). These studies suggest that mature and immature neurons can have distinct roles in the processing of odour information in the olfactory bulb.

The processing of odour information has been suggested to be different between mature and immature neurons in the olfactory bulb. Immature granule cells are more responsive to novel odours compared to mature neurons and this increased responsiveness is long-lasting (Belnoue et al., 2011; Magavi et al., 2005). However, when learning to discriminate odours, mature granule cells are preferentially recruited over the immature population (Belnoue et al., 2011). In the glomerular layer, immature inhibitory neurons are highly responsive to sensory stimuli, which reduces as the neurons mature (Livneh et al., 2014). Interestingly, this study also found

that immature glomerular layer interneurons that were exposed to sensory enrichment demonstrate further reduced odour responsiveness when they mature. The authors hypothesised that this reduces inhibition onto interglomerular neurons, resulting in increased lateral inhibition, which is known to fine-tune odour processing.

Despite evidence that newborn neurons have increased plasticity and may aid odour processing, studies that have inhibited adult neurogenesis have not reliably found impairments in odour discrimination or memory (Breton-Provencher et al., 2009; Imayoshi et al., 2008). However, there may be specific roles for adult neurogenesis that are only apparent in certain behavioural tests, for example, olfactory perceptual learning (Moreno et al., 2009) and odour-reward memories (Arruda-Carvalho et al., 2014). As such, the precise role of adult neurogenesis to the function of the olfactory bulb is not clear; however, it is clear that newborn neurons continually integrate into the circuitry and are modified in an experience-dependent manner.

1.3.4 Short-term synaptic plasticity

Short-term synaptic plasticity is a rapid, activity-dependent modification of synaptic strength (Zucker and Regehr, 2002). This form of use-dependent plasticity can be seen with pairs or trains of stimuli that can result in enhancement (facilitation) or weakening (depression) of the synapse, which can last for milliseconds to seconds. The probability of vesicle release is dependent on the molecular and cellular process that drives vesicle exocytosis, including the strength of depolarisation, voltage-gated calcium channels and availability of vesicles (Becherer and Rettig, 2006). Repeated stimulation can result in short-term facilitation by increasing the probability of release, due to residual calcium in the presynapse that persists following synaptic activation (Katz and Miledi, 1968). In contrast, short-term depression reduces release probability by depletion of the vesicle pool, or inactivation of release sites or presynaptic channels (Schneggenburger et al., 2002). Postsynaptic processes such as receptor saturation and desensitisation can also contribute to short-term depression (Foster et al., 2002).

1.3.5 Hebbian plasticity

Synaptic plasticity is often known as Hebbian plasticity after Donald Hebb who theorised the existence of a process whereby patterns of activity in neighbouring pre and postsynaptic zones would trigger the strengthening of this connection (Hebb, 1949). The first experimental description of Hebbian plasticity was by Bliss and Lømo (1973) who found that the repetitive stimulation of the perforant path fibres to the dentate gyrus of the hippocampus for several seconds (3-15 seconds) resulted in an increase in the amplitude of extracellularly recorded field potentials that lasted for 30 minutes to 10 hours, a mechanism referred to as long-term

potentiation (LTP). This was a landmark paper that formed the basis for the future study of neuronal plasticity. The induction of LTP depends on highly correlated pre and postsynaptic activity between neurons and has since been described in various cell types and at excitatory and inhibitory synapses. Following on from this work, a decrease or decorrelated activity between neurons results in the weakening of the strength of the synapse, a process known as long-term depression (LTD) (Dudek and Bear, 1992; Ito and Kano, 1982).

The strengthening of synapses at glutamatergic connections via LTP has been attributed to an increase in AMPA receptor-mediated currents that allows NMDA receptor activation and calcium entry, which then drives an increase in AMPA conductance or local insertion of more AMPA receptors into the postsynapse. The weakening of a synapse by LTD is the converse of this process. The induction of LTP or LTD has been associated with structural changes at the postsynapse. The size of dendritic spines have been found to increase in response to LTP, while LTD can lead to the elimination of synaptic structures (Van Harreveld and Fifkova, 1975; Shinoda et al., 2005). LTP and LTD can also be induced by changes in the presynapse that modify neurotransmitter release (Castillo, 2012).

The induction of LTP and LTD is heavily dependent on the temporal order of inputs in the modification of synapses. Levy and Steward (1983) found that when a weak input preceded a stronger input that LTP was produced; however, reversing the order led to depression. By considering the timing of inputs further work found that neurons show spike-timing-dependent plasticity (STDP). With STDP, inputs are potentiated if presynaptic firing precedes postsynaptic firing; however, when presynaptic input does not precede a postsynaptic neuron's activity, this input is depressed (Bi and Poo, 1998; Markram et al., 1997).

1.3.6 Short-term and Hebbian synaptic plasticity in the olfactory bulb

Multiple forms of short- and long-term synaptic plasticity have been observed in the olfactory bulb at a number of synaptic sites. The release probability of neurotransmitter from OSN terminals is reported to be one of the highest of any synapse in the brain and shows strong depression in response to repeated stimulation and recovers with a monotonic time course (Murphy et al., 2004). As discussed previously, OSN terminals are regulated by presynaptic inhibition from intraglomerular GABAergic interneurons. Strengthening or weakening this inhibition can decrease or increase OSN neurotransmitter release and short-term depression, respectively (Aroniadou-Anderjaska et al., 2000; Hsia et al., 1999). GABAergic synapses in the glomerular layer can display heterogeneous patterns of short-term plasticity, including depression and combined facilitation/depression (Nusser, 2002). Short-term depression also

occurs at the synapse from external tufted cells to mitral cells and also auto-excitatory responses in external tufted cells from released glutamate binding to their own glutamatergic receptors (De Saint Jan et al., 2009). Moderate short-term synaptic facilitation has been observed at the mitral-to-granule excitatory synapse, while the granule-to-mitral inhibitory synapse strongly depresses (Dietz and Murthy, 2005). These short-term plasticity mechanisms would have an important role for the activation of neurons in the olfactory bulb by adapting to the natural high-frequency OSN input and the subsequent processing of odour information.

Long-term Hebbian synaptic plasticity has also been investigated in the olfactory bulb. Ennis et al., (1998) observed LTP at the synapse of OSN terminals and mitral cell dendrites. Inducing LTP by tetanic stimulation of the olfactory nerve resulted in the potentiation of NMDA-receptor dependent spiking in mitral cells. The amplitude of glomerular field EPSPs can be increased for up to 30 minutes in response to the theta burst stimulation of OSN input. Recording of EPSCs in external tufted cells and GABAergic glomerular interneurons confirmed that there was a potentiation of the currents in these neurons, particularly external tufted cells (Yuan, 2009). LTD has also been described at the OSN to mitral cell synapse (Mutoh et al., 2005). This study found an LTD induction protocol resulted in a depression of the glomerular field EPSPs and OSN-to-mitral cell EPSPs, that was still present two hours later. Calcium imaging revealed that this LTD was driven by the downregulation of presynaptic calcium influx.

Hebbian plasticity has also been observed at non-OSN synapses in the bulb. Stimulating the proximal excitatory inputs to olfactory bulb granule cells, which are largely cortical feedback inputs, has been shown to induce LTP in rat acute slices (Gao and Strowbridge, 2009; Ma et al., 2012b). STDP was found to be required for the induction of this LTP, with EPSPs in granule cells potentiated when they were stimulated to fire action potentials after the stimulation of the synaptic inputs and depressed when firing preceded the stimulation. However, LTP at this synapse may be specific for newborn granule cells. As these neurons mature the expression of LTP at the synapse of centrifugal inputs to granule cells is lost (Nissant et al., 2009). Applying the same LTP induction protocol to excitatory inputs to granule cells originating from mitral cells, located on distal granule cell dendrites in the EPL, resulted in depression of the inputs. These synaptic plasticity processes resulted in granule cell inputs to mitral cells to be potentiated or depressed following stimulation of proximal or distal inputs to granule cells, respectively (Gao and Strowbridge, 2009; Ma et al., 2012b). *In vivo* work in the rat has supported this *ex vivo* work by demonstrating that high-frequency activation of centrifugal inputs from the piriform cortex to granule cells produces a long-lasting potentiation of local field potentials and extended mitral

cell inhibition (Cauthron and Stripling, 2014). Therefore, the recent history of excitatory input onto granule cells can affect the inhibition of mitral cells.

1.3.7 Homeostatic plasticity

A potential consequence of Hebbian plasticity is the risk of destabilising network activity by unrestrained potentiation or depression of neuronal connections, which could lead to issues such as epilepsy and neurodegenerative disease (Collingridge et al., 2010; Turrigiano and Nelson, 2000). Synaptic input is modulated by intrinsic properties of a neuron before being converted into output. Homeostatic plasticity has been proposed as a mechanism to regulate and stabilise the network in response to activity-dependent changes.

1.3.7.1 Homeostatic synaptic plasticity

The earliest description of homeostatic synaptic plasticity was the discovery of synaptic scaling in cultures of rat visual cortical pyramidal neurons (Turrigiano et al., 1998). The activity of these neurons was chronically manipulated by 48 hours treatment with either TTX to block action potentials and decrease activity or blocking $GABA_A$-mediated inhibition by bicuculline to increase activity. To understand how synaptic inputs had changed, whole-cell voltage-clamp recordings were performed to record miniature excitatory postsynaptic currents (mEPSCs). Activity blockade was associated with an overall increase in the amplitude of mEPSCs, while increased activity resulted in a decrease in mEPSC amplitudes. The authors discovered that these changes were multiplicative for all the excitatory synapses in a neuron and as such preserved the relative differences in synaptic weighting between conditions.

As synaptic scaling is typically measured as changes to AMPA-mediated mEPSCs, it would suggest that the number or kinetics of AMPA receptors are altered. The number of AMPA receptors is known to correlate with the size of dendritic spine size (Matsuzaki et al., 2001). Investigating mEPSCs and spines following binocular deprivation by bilateral retinal lesions found synaptic upscaling of mEPSCs in visual cortex neurons *ex* vivo and an associated increase in spine size *in vivo* (Keck et al., 2013). Homeostatic synaptic plasticity can also be driven by presynaptic mechanisms, chronic perturbations of activity in hippocampal cultures has been demonstrated to change calcium influx at the presynapse, resulting in altered release probability (Zhao et al., 2011).

TTX-induced monocular deprivation produced synaptic scaling in layer 2/3 and layer 4 visual cortex neurons, but only during their respective critical periods, demonstrating that synaptic scaling can be dependent on developmental age and cortical layer (Desai et al., 2002). Activity

blockade of CA1 pyramidal neurons *in vivo* by TTX revealed that only juvenile rats demonstrated homeostatic synaptic scaling of mEPSCs (Echegoyen et al., 2007). However, both adult and juvenile rats had an increase in the frequency of mEPSC events, indicating that there were probably presynaptic changes at all ages.

Synaptic scaling is not restricted to excitatory synapses, with evidence of homeostatic synaptic plasticity at inhibitory synapses, largely mediated by the number of $GABA_A$ receptors at the synapse (Rannals and Kapur, 2011). However, activity-dependent modification of chloride levels that produce a shift in the GABAergic reversal potential has also been identified as a potential mediator of homeostatic $GABA_A$ synaptic scaling (Karmarkar and Buonomano, 2006). Inhibitory synapses onto excitatory neurons have been found to scale in the opposite direction from excitatory synapses. Activity deprivation by TTX treatment decreases the amplitude and frequency of miniature inhibitory postsynaptic currents (mIPSCs) in dissociated rat cortical cultures as a result of reduced numbers of $GABA_A$ receptors (Kilman et al., 2002). A similar result was found in rat hippocampal cultures; however, changes to frequency and synapse density appeared to be restricted to more immature neurons and modifying the amount of GABA in individual vesicles reduced mIPSC amplitude (Hartman et al., 2006).

However, there is evidence that not all inhibitory synapses are scaled proportionally and that this depends on the identity of the presynaptic interneuron. Studying evoked IPSCs found that visual deprivation resulted in a weakening of feedback inhibition by GABAergic fast-spiking neurons onto pyramidal neurons, whereas feedforward inhibition by GABAergic regular-spiking non-pyramidal neurons was strengthened (Maffei et al., 2004). This input-dependent plasticity of GABAergic synapse has also been shown in hippocampal slice cultures (Kim and Alger, 2010).

1.3.7.2 Homeostatic intrinsic plasticity

Homeostatic plasticity is not only restricted to the synapse, with experience-dependent changes to intrinsic properties of neurons an important mechanism to adjust neuronal excitability. In response to a given input, the output of that neuron will be determined by an interplay between the composition, distribution and number of ion channels and their conductance. Changes in intrinsic excitability can, therefore, be achieved by modifications to the channels and currents that regulate the output properties of neurons.

Early research investigating homeostatic intrinsic plasticity utilised the same experimental paradigms that induced synaptic scaling. TTX treatment of cultured cortical neurons resulted in an overall increase in the intrinsic excitability of the neurons (Desai et al., 1999a). This was

achieved through an increase in depolarising sodium currents and a decrease in hyperpolarising potassium currents. Modifying the balance of these inward and outward currents resulted in a lower threshold for action potential firing. Increased excitability has also been observed following *in vivo* TTX treatment in hippocampal neurons (Echegoyen et al., 2007). Elevating activity by prolonged depolarisation of hippocampal cell cultures or fear conditioning in rats has the inverse effect of reducing the excitability of neurons (O'Leary et al., 2010; Santini et al., 2008). However, as with synaptic plasticity, intrinsic plasticity exhibits great diversity and how it is induced can depend on the cell type, developmental age and the underlying properties that have been modified (Nataraj et al., 2010).

The modification to channels that regulate the excitability of a neuron can include increasing/decreasing the density of a channel or altering the channel kinetics. Dendritic ion channels regulate dendritic excitability and integration of input signals. High density of HCN channels at dendrites has been described in a number of cell types, including hippocampal pyramidal neurons, where increased activity is associated with a decline in HCN channel subunits, reduced I_h and increased excitability (Shah et al., 2004). Reduced activity can change the expression of potassium channels at the axon initial segment (AIS) from fast activating Kv1.1 channel to the slower Kv7.2, increasing neuron excitability (Kuba et al., 2015).

The effect of homeostatic synaptic and intrinsic plasticity appears to be part of a compensatory mechanism to adjust synaptic strength and excitability to stabilise network activity around a set dynamic range (Turrigiano, 2008). However, it is unclear whether the set point is determined on the individual neuron level or the circuit as a whole. Slomowitz et al. (2015) demonstrated that activity-deprivation of hippocampal cell cultures induced an initial drop in population firing rate that returned to control levels after two days. However, the majority of individual neurons had not returned to their control firing rates, suggesting a population set point of activity rather than on the single neuron level. In contrast, neurons in the visual cortex were found to have returned to within 15% of their individual baseline firing rate following visual deprivation (Hengen et al., 2016).

1.3.8 Structural plasticity

Structural plasticity is the activity-dependent modification of neuron or circuit structure. At the extreme level, structural plasticity includes the addition of newborn neurons into established circuits (see Chapter 1.3.3), requiring remodelling of the circuitry. However, smaller scale changes can occur that modify the input and/or output of neurons. Neurons can undergo substantial changes in dendritic spines and dendritic branching in an activity-dependent

manner. *In vivo* imaging has shown that spine formation, turnover and morphology is highly dynamic in response to changes in the sensory environment (Keck et al., 2011; Trachtenberg et al., 2002). It is believed that these changes are the structural consequence of Hebbian and homeostatic plasticity on the synapse. The axon similarly displays dynamics in axonal boutons in response to changes in activity (De Paola et al., 2006). In addition to this, the AIS can also show plasticity. The AIS is a specialised structure found close to the soma of axon-bearing neurons. Its location, morphology and high density of voltage-gated ion channels make it the initiation site for action potential generation in neurons with an axon. It has been shown that this structure can change its location and size in an activity-dependent manner. In response to increased activity of several days *in vitro* the AIS of excitatory hippocampal neurons can move distally along the soma, which was associated with reduced excitability of the neuron (Grubb and Burrone, 2010). This form of plasticity has also been observed *in vivo*, with auditory deprivation associated with an increase in the length of the AIS and increased excitability of avian brainstem auditory neurons (Kuba et al., 2010).

1.3.9 Experience-dependent plasticity in the olfactory bulb

In the olfactory bulb changes to the odour environment can induce plasticity mechanisms to adapt the circuitry to altered sensory input. Odour deprivation can induce experience-dependent changes in the olfactory bulb, for example, through homeostatic synaptic changes that affect the strength of excitatory synapses in glomeruli (Tyler et al., 2007). Unilateral naris occlusion in P2 rats for two weeks affected the presynapse by increasing the release probability of OSNs without increasing the amount of glutamate released. Odour deprivation also increased recurrent excitation in external tufted cells and the amplitude of AMPA-mediated and NMDA-mediated mEPSCs in external tufted cells and glomerular layer GABAergic interneurons. The abundance of pre and postsynaptic glutamatergic proteins were also increased in glomeruli. Shorter-duration odour deprivation for 3 days also increased AMPA-mediated mEPSC amplitudes. However, the majority of glomerular layer GABAergic interneurons receive input from external tufted cells, suggesting that excitatory synaptic scaling is not dependent on the presynaptic neuron. Therefore, there are probably changes at OSN and external tufted cell synapses with glomerular layer GABAergic neurons.

The increase in OSN release probability and excitatory synaptic scaling on external tufted cells (Tyler et al., 2007) would be assumed to increase the transmission of OSN input. However, excitatory synapses on GABAergic neurons have also been strengthened, which would be predicted to increase their excitability and inhibitory output. This suggests that synaptic scaling can occur in the glomerular layer of the olfactory bulb; however, whether this is acting to

stabilise network activity around a physiological set point, i.e. homeostatic plasticity, is unknown. However, the firing rates of mitral cells increases after odour input has been restored following odour deprivation (Philpot et al., 1997; Rodriguez-Gil et al., 2015; Wilson and Sullivan, 1995). Neonatal unilateral naris occlusion increases odour responses of OSNs in the deprived naris (Barber and Coppola, 2015; He et al., 2012). This indicates that there is a compensatory mechanism in the olfactory bulb during odour deprivation to reduce inhibition and/or increase excitation to make the most of any remaining sensory input.

Structurally, the dendrites of immature and mature adult-born glomerular layer interneurons and granule cells show high-turnover of dendritic spines, with ~20% of spines being added and eliminated daily, regardless of maturational age (Mizrahi, 2007; Sailor et al., 2016). Dendritic dynamics can be affected by sensory input. Spines can also relocate along dendrites of mature granule cells within a few minutes of changes to activity (Breton-Provencher et al., 2016). Odour enrichment increases dendritic branching of immature glomerular layer interneurons, while odour deprivation had no obvious effects (Livneh et al., 2014; Mizrahi, 2007). However, odour deprivation can affect dendritic arborisation and decrease spine density of immature granule cells (Kelsch et al., 2009; Saghatelyan et al., 2005). Experience-dependent plasticity of dendrites in the olfactory bulb would be expected to reshape neuronal connections and affect odour processing. (**Table 1.1** summarises the connectivity between neurons in the olfactory bulb and the known or potential plasticity at these connections).

The olfactory bulb also needs odour experience to develop intrabulbar projections between isofunctional glomeruli, formed by the axons of external tufted cells. In mice, this connection is diffuse early postnatally and refines in the first 7 weeks of life (Marks et al., 2006). While the formation of this connection is developmentally regulated, its refinement requires continuous sensory activity. Loss of odour input results in a regression of this connection and the projections become broader (Marks et al., 2006). However, this is reversible and restoring sensory input following odour deprivation drives these connections to become refined (Cummings and Belluscio, 2010). Odour enrichment can accelerate the activity-dependent refinement of the projections (Marks et al., 2006). Cortical inputs that innervate the olfactory bulb also show experience-dependent plasticity. In response to odour deprivation during early development, the high innervation of cholinergic inputs to the glomerular layer is impaired and the number of inputs reduced (Salcedo et al., 2011). The distribution and density of noradrenergic and serotonergic inputs to the olfactory are increased following odour deprivation, particularly in the glomerular layer (Briñón et al., 2001; Gómez et al., 2006, 2007).

The olfactory bulb has also been observed to modify the synthesis of neurotransmitters in response to changes in the odour environment. Expression of the GABA synthesising enzyme, GAD67 has been found to be decreased in response to odour deprivation (Banerjee et al., 2013; Lau and Murthy, 2012; Parrish-Aungst et al., 2011; Wang et al., 2017). This could act to reduce the synthesis and availability of GABA. As signal transmission from OSNs to mitral cells is modulated by glomerular layer GABAergic interneurons changes in neurotransmitter synthesis would be expected to affect odour processing. The olfactory bulb may, therefore, be adapting to decreased sensory input by reducing GABA-mediated inhibition in order to increase bulbar excitability.

Neuron	Output	Plasticity	Example references
OSN	GL GABAergic interneuron, ETC, M/T cell	Short-term, LTP, LTD, adult neurogenesis, structural	Pinching and Powell, 1971a,b; Ennis et al., 1998; Aroniadou-Anderjaska et al., 2000; Mutoh et al., 2005; Cheetham et al., 2016; Holl, 2018
Glomerular layer GABAergic interneuron [incl. anaxonic dopaminergic neurons]	*Auto-inhibition*, OSN, GL GABAergic interneuron, SAC, ETC, M/T cell	Short-term, synaptic scaling, adult neurogenesis, structural	Pinching and Powell, 1971a,b; Toida et al., 1998; Nusser, 2002; Smith and Jahr, 2002; Kosaka and Kosaka, 2005; Murphy et al., 2005; Mizrahi , 2006; Mizrahi 2007; Tyler et al., 2007; Shao et al., 2009
External tufted cell	*Auto-excitation*, GL GABAergic interneuron, ETC, M/T cell, granule cell	Short-term, synaptic scaling	Pinching and Powell, 1971a,b; Lodovichi et al., 2003; Hayar et al., 2004b; Hayar, 2005; Tyler et al., 2007; De Saint Jan et al., 2009
Short-axon cell [incl. axonic dopaminergic neurons]	ETC, M/T cell, GL GABAergic interneuron	Structural	Pinching and Powell, 1971a,b; Aungst et al., 2003; Banerjee et al., 2015; Chand et al., 2015; Liu et al., 2016
Mitral/Tufted cell	*Auto-excitation*, GL GABAergic interneuron, ETC, M/T cell, granule cell, olfactory cortex	Short-term, LTP, LTD	Nicoll and Jahr, 1982; Ennis, et al., 1998; Dietz and Murthy, 2005; Hayar 2005; Kosaka and Kosaka, 2005; Mutoh et al., 2005
Granule cell	M/T cell	Short-term, LTP, adult neurogenesis, structural	Rall et al., 1966; Luskin, 1993; Dietz and Murthy, 2005; Mizrahi, 2007
Deep short-axon cell	GL GABAergic interneuron, granule cell, ETC, tufted cell	Short-term	Eyre et al., 2008; Burton et al., 2017

Table 1.1 Summary of connections and plasticity in the olfactory bulb

1.4 Plasticity of dopaminergic neurons in the olfactory bulb

A notable omission from the above description of neuronal plasticity in the olfactory bulb is an exploration of plasticity in the dopaminergic population. The next section will discuss the activity-dependent changes that have been described for olfactory bulb dopaminergic neurons.

1.4.1 Activity-dependent gene expression

Olfactory bulb dopaminergic neurons are known to be particularly susceptible to sensory input. It has long been recognised that these neurons regulate the expression of TH and consequently dopamine production according to sensory experience. Removing OSN input by chemical or surgical deafferentation results in the downregulation of TH and dopamine in the glomerular layer (Baker et al., 1983; Kawano and Margolis, 1982). Odour deprivation studies by unilateral naris occlusion have demonstrated that this process is activity-dependent and not due to the physical loss of OSNs (Baker et al., 1993; Cummings et al., 1997). Restoring activity by the rejuvenating OSNs reinnervating glomeruli or opening the closed naris reverses the downregulation of TH (Baker et al., 1983; Kosaka et al., 1987). Studying the expression of other dopaminergic markers, *Ddc*, *Vmat2* and *Dat*, revealed that *Ddc* and *Vmat2* were not regulated in an activity-dependent manner, while *Dat* showed a small decrease in expression after 1-3 months of deprivation from P42-56 mice (Cave et al., 2010). *In situ* hybridisation has revealed that *Th* mRNA in rats significantly reduces after 2 days of unilateral naris occlusion, with a smaller drop in TH protein expression, that continues decreasing until levelling out around 30 days after occlusion (Young Cho et al., 1996). Further work has shown that reduced TH expression can stabilise after 21 days of occlusion (Bastien-Dionne et al., 2010).

Studying the expression of DDC demonstrated that dopaminergic neurons were still present in the olfactory bulb, suggesting reduced expression of TH is not due to dopaminergic neurons dying (Baker, 1990). However, Sawada et al. (2011) found that olfactory bulb dopaminergic neurons have lower survival in response to deprivation and have increased expression of apoptotic markers, indicating that their survival may be affected by reduced activity. In addition, work by Grier et al. (2016) found that there is an increase of microglia density and dynamics following 7 days of odour deprivation. This study found an increase in interactions between microglia and dopaminergic neurons and evidence of microglia phagocytosing components of dopaminergic neurons in the olfactory bulb. Therefore, there is evidence that dopaminergic neurons are dying in response to prolonged odour deprivation.

Restoring sensory input induces TH recovery and return to control levels (Baker et al., 1983; Kosaka et al., 1987). Increased expression of TH above control levels has been demonstrated in response to increased activity *in vitro* as quickly as 1 day (Chand et al., 2015). Activity-dependent increase of TH results from the influx of calcium through NMDA receptors and L-type calcium channels (Chand et al., 2015; Cigola et al., 1998; Puche and Shipley, 1999). Unpublished work from my lab has found that olfactory enrichment for 1 day *in vivo* results in a significant increase in the expression of TH (Elisa Galliano).

The activity-dependent expression of TH suggests that dopamine levels play an important role in the initial processing of odour information. In the rat olfactory bulb, olfactory deprivation has been associated with an increase in the density of dopamine D_2 receptor, but not D_1, based on receptor autoradiography analysis (Guthrie et al., 1991). The D_2 receptor is known to be expressed on OSN terminals where it has an important role in presynaptic inhibition and may be expressed by other olfactory bulb neurons (Gutièrrez-Mecinas et al., 2005). As dopamine levels are reduced following odour deprivation (Kawano and Margolis, 1982), activation of dopaminergic receptors in the olfactory bulb would be affected, including OSN terminals, external tufted cells and potentially mitral cells. The expression levels of COMT, the enzyme identified as having a dominant role in the clearance of dopamine in the bulb, is unchanged in response to unilateral naris occlusion (Cockerham et al., 2016). This result coupled with the reduced expression of TH would supposedly act to further suppress of dopamine levels in the bulb. However, upregulation of D_2 receptors may be required to ensure dopaminergic activity under certain circumstances, for example, strong or repetitive input.

TH expression and an associated elevation in dopamine levels has been found to be increased in female mice following mating (Serguera et al., 2008). These mice were found to have impaired odour perception, showing a lack of social odour discrimination and reduced sensitivity to male urine. These phenotypes were rescued by the administration of the D_2 receptor antagonist, spiperone. In another experiment, reopening a naris following odour deprivation resulted in increased mitral cell sensitivity and decreased discrimination to odours, which was replicated in control mice that were given spiperone (Wilson and Sullivan, 1995). These studies demonstrate that the activity-dependent regulation of TH and dopamine levels affects odour processing in the olfactory bulb and the reported increased D_2 expression is not sufficient to compensate for these changes.

The regulation of TH expression has been associated with the expression of the transcription factor COUP-TFI, which is highly expressed in olfactory bulb dopaminergic neurons (Bovetti et

al., 2013). The expression of COUP-TFI is also downregulated in response to odour deprivation. Conditional knockout of COUP-TFI in progenitor cells that will give rise to olfactory bulb interneurons reduces the expression of TH in the olfactory bulb. The survival of newborn interneurons and the expression of transcription factors involved in generating the dopaminergic identity are not affected by this knockout. However, without dopaminergic markers, such as DDC, it is unclear whether these neurons are dopaminergic neurons with reduced TH expression or are another population of interneuron. Epigenetic mechanisms and DNA secondary structure have also been implicated in the expression of TH (Banerjee et al., 2013; Wang et al., 2017). During migration, *Th* promoter activity is suppressed by histone deacetylase (HDAC) activity and in mature dopaminergic neurons odour deprivation results in increased HDAC2 expression and HDAC-mediated modification to the *Th* promoter (Banerjee et al., 2013). Activity can also modify the secondary structure of proximal promoters of the *Th* gene, affecting the binding of transcription factors that facilitates the transcription of *Th* (Wang et al., 2017).

1.4.2 Structural plasticity

Experience-dependent changes to the structure of olfactory bulb dopaminergic neurons have not been widely investigated. Glomerular layer GABAergic interneurons have been shown to have dendritic plasticity in immature and mature cells (Livneh and Mizrahi, 2011; Mizrahi, 2007). While this work likely includes dopaminergic neurons, there is currently no description of dendritic plasticity in olfactory bulb dopaminergic neurons. *In vitro* work has investigated the plasticity of AIS in axonic bulbar dopaminergic neurons (Chand et al., 2015). In response to 1 day of increased activity *in vitro*, axonic olfactory bulb dopaminergic neurons have been shown to lengthen their axon and move it closer to the soma (Chand et al., 2015). The consequence of this structural change would be expected to increase excitability; however, intrinsic excitability was unaffected *in vitro* (Chand et al., 2015). It is possible that other functional changes in the neuron offset the structural plasticity of the AIS. 1 day of decreased activity by TTX treatment *in vitro* or unilateral naris occlusion *in vivo* shortens the AIS (Chand et al., 2015; Galliano et al., *in preparation*). The main form of (extreme) structural plasticity that has been associated with olfactory bulb dopaminergic neurons is adult neurogenesis.

1.4.3 Adult neurogenesis in the olfactory bulb dopaminergic neurons

The exclusive generation of axonic olfactory bulb dopaminergic neurons during embryonic development (Galliano et al., 2018), means that the anaxonic subpopulation are unique in their ability to be continuously generated throughout life and integrate into olfactory bulb circuitry. Postnatally born olfactory bulb dopaminergic neurons are generated from neural stem cells in

the SVZ of the lateral ventricle, where they migrate through the RMS to reach the olfactory bulb. A fate-mapping study labelled all newborn neurons generated in adult mice (3 months old) over 9 months and found that approximately 32% of dopaminergic neurons in the olfactory bulb were generated during this period and there was an overall addition of new neurons to the glomerular layer (Ninkovic et al., 2007). A long-term imaging study supported this, revealing that there was a net addition of dopaminergic neurons to the glomerular layer (Adam and Mizrahi, 2011). The continual generation and net increase of dopaminergic neurons suggests that these neurons have an important role in the circuitry and function of the olfactory bulb.

As previously discussed, sensory experience has been found to affect the survival of newborn interneurons in the glomerular layer in general and also granule cells. However, there are effects specific to dopaminergic neurons. Long-term olfactory enrichment (~9 weeks) selectively increases the population of newborn dopaminergic neurons in the glomerular layer (Bonzano et al., 2014), while short-term enrichment (~3-4 weeks) did not produce significant increases (Bonzano et al., 2014; Bovetti et al., 2009). This result is contrary to the argument put forward by Pignatelli et al. (2009) that there are immature dopaminergic in the granule cell layer that can differentiate and integrate into the bulbar circuitry faster than it takes to generate a new neuron. Perhaps terminal differentiation of these purported immature dopaminergic neurons is dependent on a specific signal and not just sensory experience. Ablation of olfactory bulb dopaminergic neurons by injecting 6-hydroxydopamine (6-OHDA) or MPTP results in an increase in the incorporation and survival of dopaminergic neurons in the glomerular layer, suggesting a compensatory mechanism to restore the lost dopaminergic activity in the circuit (Lazarini et al., 2014; Yamada et al., 2004). The restoration of the dopaminergic population was found to begin within two weeks of the ablation and was not be due to increased neurogenesis in the SVZ. This could indicate an increased survival of newborn neurons or terminal differentiation of the immature dopaminergic neurons.

Odour deprivation reduces the survival and integration of newborn neurons into the glomerular layer of the olfactory bulb. This includes the dopaminergic population. However, it is not clear whether the dopaminergic population may be particularly vulnerable to odour deprivation compared to the other glomerular layer interneurons. It has been shown the proportion of newborn neurons that express TH is reduced, which can be due to decreased survival of dopaminergic neurons and/or activity-dependent reduction of TH expression (Bastien-Dionne et al., 2010; Bovetti et al., 2009). Survival of dopaminergic neurons has been reported to depend on sensory input, suggesting that survival of newborn dopaminergic neurons may be more affected by odour deprivation (Grier et al., 2016; Sawada et al., 2011).

Overall, the activity-dependent modifications to olfactory bulb dopaminergic neurons and their functional role in odour processing makes these neurons an excellent neuronal population in which to study experience-dependent plasticity. Nevertheless, there is still a lot unknown about how these neurons can change.

1.5 Thesis overview

The current evidence demonstrates that there is experience-dependent plasticity in olfactory bulb dopaminergic neurons. *In vitro* manipulations of their activity have shown that plasticity changes can occur within 1 day, while *in vivo* work has identified changes after 2 days. However, a description is missing of whether the electrophysiological functional properties of these neurons demonstrate experience-dependent plasticity *in vivo*.

In this thesis I investigated how different durations of odour deprivation (1 and 3 days) affects olfactory bulb dopaminergic neurons, particularly the anaxonic subpopulation. To study these neurons functionally *in vivo* requires using a mouse line that accurately live-labels olfactory bulb dopaminergic neurons. I, therefore, employed a mouse line to label these neurons and characterised the labelled population using immunohistochemistry, electrophysiology and birthdating analysis (Chapter 3). I also confirmed that unilateral naris occlusion for 1 and 3 days can reduce the activity of the labelled neurons and that activity-dependent plasticity can be observed using immunohistochemistry (Chapter 3).

The functional plasticity of anaxonic olfactory bulb dopaminergic neurons is not currently well-understood. I, therefore, investigated the activity-dependent plasticity of intrinsic functional properties of these neurons in acute slice preparation (Chapter 4). As synaptic activity has been reported to be altered by odour deprivation, I next investigated how the excitatory and inhibitory synapses of these neurons are affected by unilateral naris occlusion (Chapter 5). Finally, I took advantage of the ability of these neurons to self-inhibit to address two outstanding questions: 1) is their GABA release affected by occlusion?; and 2) is self-inhibition a feature of both subpopulations of olfactory bulb dopaminergic neurons? (Chapter 5).

Chapter Two – Methods

2.1 Reagents

All reagents were purchased from Sigma-Aldrich (Merck, UK), unless otherwise stated.

2.2 Mice

All experiments were performed in accordance with the UK Home Office personal and project licences held by myself and my supervisor, Matthew Grubb. Mice of either gender were used and housed under a 12 hour light-dark cycle in an environmentally controlled room with access to water and food *ad libitum*. Day of birth was designated as P0. DAT$^{IRES\,cre}$ mice (B6.SJL-*Slc6a3*$^{tm1.1(cre)Bkmn/J}$, Jax stock 006660) were crossed with Rosa26-floxed stop tdTomato reporter mice (Gt(ROSA)26Sor$^{tm9(CAG\text{-}tdTomato)Hze}$, Jax stock 007909) to generate DAT-tdTomato mice. Wild-type C57/Bl6 mice (Charles River) were used to back-cross each generation of transgenic mice.

2.3 Unilateral naris occlusion

Olfactory sensory deprivation was induced by unilateral naris occlusion, using a custom-made plug (Cummings et al., 1997). Each plug was constructed by knotting suture (Ethicon Ethilon Monofilament Polyamide 6) around a piece of unscented dental floss and pulled through the lumen of PTFE-tubing with an outer-diameter of 0.6 mm and inner-diameter of 0.3 mm (VWR International, cat#: S1810-04). Mice were anaesthetised with isoflurane and the plug trimmed, coated in petroleum jelly and inserted into the right naris. Mice were returned to their home cage and left for 1 or 3 days before perfusion or slice electrophysiology. Presence of the nose plug was confirmed by examining the nasal cavity after olfactory bulb dissection. Sham controls had a nose plug inserted into the right naris and removed. Anaesthetised controls were anaesthetised briefly with isoflurane, but had no plug inserted into either naris.

2.4 Immunohistochemistry and imaging

2.4.1 Transcardial fixative perfusion

P28 and P30 DAT-tdTomato mice were anaesthetised with an intraperitoneal overdose of pentobarbital. Perfusions were begun after the mouse had stopped responding to the toe/tail pinch and ocular reflex test. The mouse was secured in the supine position. The thoracic cavity was exposed by gentle cutting and the ribcage was held open with clips. A syringe connected to a peristaltic pump was inserted into the left ventricle and the right atrium was cut. Immediately, 20 mL PBS with 20 U/mL of heparin was perfused throughout the mouse. The solution was

switched to 20 mL of 4% paraformaldehyde (PFA) in PIPES buffer (3% sucrose, 60 mM PIPES, 25 mM HEPES, 5 mM EGTA, and 1 mM $MgCl_2$). PFA was prepared in batches and frozen at -20°C and defrosted shortly before use. On completion of perfusion, the mouse was decapitated and the brain removed from the skull and post-fixed in 4% PFA overnight. The brain was then washed with PBS (3x5 minutes) and stored in phosphate buffered saline (PBS) and 0.05% sodium azide for up to 6 months. For sectioning, brains were embedded in 6% agarose and sliced either coronally or sagittally at 50 µm using a vibratome (Leica VT1000s) (Wetzlar, Germany). Slices were stored in PBS and 0.05% sodium azide at 4 °C before staining.

2.4.2 Immunohistochemistry

Free-floating slices were incubated at room temperature (RT°C) [18-24°C] for 2 hours in a blocking and permeabilising solution (10% normal goat serum in PBS containing 0.25% Triton-X and 0.02% sodium azide). They were then incubated in primary antibody diluted in the blocking solution at 4°C for between 18-24 hours (see **Table 2.1** for antibodies used and their working dilution). For immunofluorescence intensity analysis (see 2.4.5), slices were incubated for approximately 72 hours in primary antibody solution. Slices were then washed with PBS (3x5 minutes) and incubated in the species appropriate secondary antibody (Alexa Fluor® Life Technologies) diluted 1 : 1,000 in the blocking solution at RT°C for 2 hours. After 3x5 minutes washes in PBS, slices were mounted on glass slides with MOWIOL® (Millipore).

2.4.3 Birthdating neurons

To birthdate neurons, mice were injected with a saline-based solution containing 50 mM bromodeoxyuridine (BrdU). Mice were injected at specific ages (P1, P7, P9, P11, P14 and P21) and all BrdU injected mice were perfused at the same age, P28. The solution was prepared fresh and exposure to light was restricted. The pH was adjusted to 7.4 using NaOH. Due to their small size, P1 mice were given a single subcutaneous injection (0.075 mL / g) in the neck, all other mice were given a single intraperitoneal injection (0.075 mL / g). A DNA hydrolysis step was required to allow BrdU detection in fixed-tissue. Slices were incubated in 2 M HCl for 30 minutes at 37°C and washed 5x5 minutes with PBS before proceeding with the rest of the immunohistochemistry protocol as described above.

Antibody	Species	Dilution	Supplier (product code)
BrdU	Rat	1 : 1,000	BioRad (OBT0030)
Calbindin	Rabbit	1 : 5,000	Swant (CB38a)
Calretinin	Mouse	1 : 5,000	Millipore (MAB1568)
	Rabbit	1 : 5,000	Swant (7699/3H)
cFos	Mouse1	1 : 1,000	Santa Cruz (sc166940)
Dopamine transporter (DAT)	Rat	1 : 500	Abcam (ab5990)
Dopa decarboxylase (DDC)	Mouse2a	1 : 1,000	Santa Cruz (sc-293287)
Doublecortin (DCX)	Rabbit	1: 500	Abcam (ab18723)
GABA	Rabbit	1 : 1,000	Sigma (A2025)
Glutamate decarboxylase 67 (Gad67)	Mouse2a	1 : 500	Millipore (MAB351R)
Red fluorescent protein (tdTomato)	Rabbit	1 : 1,000	Clontech (632496)
	Rat	1 : 1,000	Chromotek (5F8)
Tyrosine hydroxylase (TH)	Mouse	1 : 1,000	Millipore (MAB318)
	Rabbit	1 : 1,000	Millipore (AB152)

Table 2.1: Primary antibodies

In preliminary analyses, the BrdU antibody was found to cross-react with all mouse primary antibodies. This was prevented by performing a sequential immunohistochemistry protocol. Following the DNA hydrolysis step, the standard immunohistochemistry protocol was performed with all primary antibodies (except BrdU) and left overnight at 4°C. The next day secondary antibodies were applied as normal for 2 hours, removed and slices washed. The BrdU primary antibody was then applied. Again, slices were left overnight at 4°C and secondary antibody and mounting were performed the following day.

2.4.4 Fixed-tissue imaging

All images were acquired with a laser scanning confocal microscope (Zeiss LSM 710 Axio Examiner Z1) using appropriate excitation and emission filters, a pinhole of 1 AU and a 40x oil immersion objection. Laser power, gain and offset were manually set to prevent fluorescence saturation and ensure optimum signal-to-noise. For analysing co-localisation of markers, multiple Z-stacks were taken around the entire olfactory bulb section.

Images for analysing co-localisation of DAT-tdTomato with dopaminergic markers and other olfactory bulb subpopulation markers were acquired at a resolution of 512 x 512 pixels (0.277 µm /pixel) and a Z step of 1 µm. For analysing BrdU expression, images were acquired at a resolution of 512 x 512 pixels (0.415 µm /pixel) and a Z step of 1 µm. BrdU labelled cells and

biocytin-filled neurons were imaged at 5x zoom with a resolution of 512 x 512 pixels (0.083 µm /pixel) and a Z step of 0.5 µm.

2.4.5 Immunofluorescence intensity analysis

This experiment was designed to minimise and control for potential between-section experimental variability that could affect the measure of immunofluorescence intensity. Three sets of four mice were used. To reduce the effect of the homecage environment, each set belonged to the same litter and were exposed to the same odour environment until unilateral naris occlusion at P27. Control mice were anaesthetised at P27. All mice were returned to the homecage and left for 1 or 3 days.

Perfusions and post-fixing were performed as described previously (see 2.4.1). When perfusing a set, the same PFA batch was used. Mice were perfused within 30 minutes of each other. Brains from the same set were cut to the same size and co-embedded in 6% agarose to ensure all brains would be sliced together. The agarose block was cut with landmarks to ensure each mouse could be reliably identified. Co-embedded slices were processed for immunohistochemistry as described previously (see 2.4.2), with primary antibodies applied for 72 hours. Therefore, all control and occluded sections on each slice were exposed to identical reagents at identical concentrations for identical periods of time. The olfactory bulb sections in a co-embedded slice were imaged on the same day using identical laser and detection settings that were optimised for that co-embedded slice. Z-stacks were taken from different parts of an olfactory bulb slice, setting the start and end Z-positions using the DAT-tdTomato fluorescence. The start position was step as the top of the section when fluorescence could be detected. Images were acquired at a resolution of 512 x 512 pixels (0.277 µm /pixel) and a Z step of 1 µm.

All immunohistochemistry, imaging and image analysis of tissue from mice that had been manipulated was performed blind to experimental group.

2.4.6 Image analysis

All image analysis was performed using ImageJ software (Fiji). Cells were counted manually using the cell counter plugin and only if their soma was entirely inside the image area. Soma size was measured at the neuron's widest area in the Z-stack, identified when the soma was larger than in the slice above and below. For measuring immunofluorescence intensity, neurons were identified for analysis solely by the expression of DAT-tdTomato. TH and GAD67 expression was located primarily outside the nucleus, therefore, average immunofluorescence intensity (mean grey value; MGV) was measured in the somatic cytoplasm only. For DDC and cFos, MGV was

measured in the entire soma. All tdTomato cells that had the entire cell body within the image area and the widest soma area could be confirmed were measured in each stack.

For migration of BrdU-labelled cells in the rostral migratory stream (RMS), multiple Z-stacks in sagittal sections were taken from the most caudal region of the olfactory bulb to the point where migrating neuroblasts begin to migrate radially. These Z-stacks were stitched manually to produce a continuous image of migrating neuroblasts in the RMS. Mean immunopositive cell densities were calculated as 1,000 cells per mm^3 ($x10^3 / mm^3$) from the Z-projection volumes (212.55 µm x 212.55 µm x stack depth).

For immunofluorescence intensity analysis, background MGV were taken from unlabelled regions of each Z-stack and subtracted from the MGV of each cell in that Z-stack. Data was normalised to the control average (1 and 3 day) in each slice.

2.5 Electrophysiology

2.5.1 Acute slice preparation

P21-35 DAT-tdTomato mice were deeply anaesthetised with isoflurane and decapitated. The olfactory bulb and frontal cortices were rapidly removed and transferred into ice-cold sucrose slicing medium (containing in mM: 240 sucrose, 5 KCl, 1.25 Na_2HPO_4, 2 $MgSO_4$, 1 $CaCl_2$, 26 $NaHCO_3$ and 10 D-glucose, bubbled with 95% O_2 and 5% CO_2). 300 µm horizontal sections of the olfactory bulb were cut using a Leica vibratome (VT1000S) (Wetzlar, Germany) and were transferred to standard artificial CSF (ACSF; containing in mM: 124 NaCl, 5 KCl, 1.25 Na_2HPO_4, 2 $MgSO_4$, 2 $CaCl_2$, 26 $NaHCO_3$ and 20 D-glucose, continuously bubbled with 95% O_2 and 5% CO_2, pH 7.4, ~310 mOsm). Slices were left to recover at RT°C for at least 45 minutes before experiments began. For auto-evoked inhibition recordings, slices were first placed in bubbled ACSF for 30 minutes in a warming bath at 34°C and then left to recover for at least 30 minutes at RT°C. It was found that this recovery phase increased survival of axonic dopaminergic neurons following acute slice preparation.

2.5.2 Slice electrophysiology

For whole-cell recordings, individual slices were placed in a chamber mounted either on a Zeiss LSM 710 Axio Examiner Z1 confocal or FN1, Nikon microscope and held in place with a slice anchor made of stainless steel and nylon thread. DAT-tdTomato neurons were visualised with a 40x water immersion objective and tdTomato fluorescence was revealed by a helium neon laser (confocal) or LED (CoolLED pE-100) (FN1 microscope) with appropriate excitation and emission

filters. Slices were continuously superfused with ACSF heated to physiologically-relevant temperature (34 ± 1°C) using an in-line solution heater (TC-344B, Warner Instruments). Recordings were carried out using a Heka EPC10/2 amplifier coupled to PatchMaster acquisition software. Signals were Bessel filtered at 10 kHz (filter 1) and 2.9 kHz (filter 2, active filters used in voltage-clamp only), digitised and sampled at 20 kHz (50 µs interval sample), unless otherwise stated. Recording electrodes were pulled from borosilicate glass [outer diameter (OD), 1.5mm; inner diameter (ID), 1.17mm] (GT100T-10, Harvard Apparatus) with a vertical puller (PC-10, Narishige) and the tip fire-polished with a microforge (MF-830, Narishige). Pipettes were filled with intracellular solution (see **Table 2.2** for intracellular solutions) and had resistance of 3-5 MΩ in K-gluconate and 2-4 MΩ in caesium internals. All internal solutions were pH ~7.3 and 280-290 mOsm and had 0.15 % biocytin added. Liquid junction potential was calculated for each intracellular solution and ACSF using pClamp (Molecular Devices) and was uncorrected for (see **Table 2.2** for liquid junction potential for each intracellular solution in standard ACSF). All drugs were added to ACSF and applied to the slice by perfusion (see **Table 2.3** for drugs). Fast capacitance was compensated as much as possible in the cell-attached configuration after a gigaseal was formed. After membrane rupture, slow capacitance was also compensated but kept inactive, unless otherwise stated.

In whole-cell voltage-clamp mode, the average current response to a double test pulse (5 ms steps, -10 and +10 mV) from the holding voltage of -60 mV was used to estimate series resistance (R_S; peak current), input resistance (R_I; steady-state holding current at new voltage) and membrane capacitance (C_M; area under the exponentially decaying current from peak to steady-state current). Recordings were discarded when a current ≥100 pA was required to hold the membrane potential at -60 mV. For auto-evoked inhibition recordings, membrane properties were calculated from a single 5 ms, -10 mV voltage step. Membrane tests were performed before and after each protocol. Recordings of intrinsic properties and mini postsynaptic currents were not included in analyses if R_S was > 30 MΩ or if it changed by more than ± 20% during the course of the experiment. Recordings of auto-evoked inhibition were not included in analyses if R_S was > 25 MΩ or if it changed by more than ± 30% during the course of the experiment.

K-Gluconate [Chapter 4]
in mM: 124 K-gluconate, 9 KCl, 10 KOH, 4 NaCl, 10 HEPES, 28.5 Sucrose, 4 Na_2ATP, 0.4 Na_3GTP (*pH with KOH*) [**liquid junction potential: ~11.5 mV**]
Caesium Methanesulfonate [Chapter 5 (mini E/IPSCs)]
in mM: 130 $CsMeSO_4$, 8 $MgCl_2$, 0.2 EGTA, 10 HEPES, 10 Na-Phosphocreatine, 4 Na_2ATP, 0.4 Na_3GTP (*pH with CsOH*) [**liquid junction potential: ~10.4 mV**]
Caesium Chloride [Chapter 5 (auto-evoked inhibition)]
in mM: 125 CsCl, 10 HEPES, 0.1 EGTA, 4 MgATP, 0.3 Na_3GTP, 10 phosphocreatine, 10 GABA (*pH with CsOH*) [**liquid junction potential: ~4.2 mV**]

Table 2.2: Intracellular solutions

Drug	Concentration	Supplier (product code)
APV	50 µM	Sigma (A5282)
BayK 8644	5 µM	Tocris (1544)
Gabazine	10 µM	Tocris (1262)
NBQX	10 µM	Sigma (N183)
TTX	1 µM	Alomone (T-550)

Table 2.3: Drugs

2.5.3 Recovering patched neurons

After completion of electrophysiology experiments, the pipette was gradually removed with a small amount of positive pressure applied to try and dislodge the patched neuron from the pipette. Once the pipette was separated from the cell, the acute slice was transferred to 4% PFA. The slice was fixed overnight at 4°C, washed with PBS (3x5 minutes) and stored in PBS and 0.05% sodium azide at 4°C, for up to 3 months. Standard immunohistochemistry protocols were used (see 2.4.2). As there was biocytin in the intracellular solution, Streptavidin 488 (Alexa Fluor® Life Technologies) diluted 1 : 1,000 was included with the secondary antibodies to bind the biocytin in the patched neuron.

2.5.4 Intrinsic recordings

All intrinsic recordings were performed using K-Gluconate intracellular solution and standard ACSF with synaptic blockers [10 µM NBQX, 50 µM APV, 10 µM SR-95531 (gabazine)]. Exported traces were analysed using custom-written routines in MATLAB (Mathworks; Matthew Grubb,

Christiane Hahn and myself). In current-clamp, neurons were held at -60 mV (V_{HOLD}) and analysis of sweeps were only performed if baseline V_{HOLD} was between -57 mV and -63 mV.

2.5.4.1 Resting membrane potential

Immediately after membrane rupture, the resting membrane potential was recorded at $I = 0$ in current clamp for 5 seconds and the mean voltage calculated. If there was at least 1 spontaneous action potential, the resting membrane potential was not calculated for that neuron.

2.5.4.2 Passive properties

The passive properties, R_S (MΩ), R_I (MΩ) and C_M (pF) were calculated from the first test series after membrane rupture, as described in 2.5.2.

2.5.4.3 Single action potential

For recording of single action potentials, neurons were held at -60 mV in current-clamp with 100% bridge balance. 10 or 500 ms somatic current injections of Δ+5 pA steps were applied until threshold was reached and an action potential occurred ($V_M > 0$ mV). If the 10 ms experiment was repeated several times in the same neuron, the experiment with the first spike that had V_{HOLD} closest to -60 mV was analysed. To categorise a neuron as monophasic or biphasic, the action potential did not have to be within this baseline.

10 ms duration current injections were sampled at high temporal resolution 200 kHz (5 µs sample interval) and the recordings were smoothed prior to differentiation using a 20 point (100 µs) sliding filter. 500 ms duration current injections were smoothed using a 2 point (100 µs) sliding filter. The first derivative of the smoothed trace was used for *dV/dt* and phase plane plot analyses. Voltage threshold was taken as the potential at which *dV/dt* first passed 10 V/s. Spike width was calculated at the midpoint between voltage threshold and maximum voltage (V_{MAX}). Rheobase was calculated from the 500 ms current injection as the minimum current value at which an action potential was first fired. Delay to first spike was the time between the start of the 500 ms current injection and the voltage maximum of the first action potential. The fast afterhyperpolarisation was calculated as the relative difference between the voltage threshold and the voltage minimum after the first spike fired during 500 ms current injection.

Neurons were visually determined as monophasic or biphasic from the phase plane plot of the 10 ms action potential. Monophasic neurons had a monotonic plot with continually increasing rate-of-rise and biphasic neurons had an inflection in rate-of-rise over the initial rising phase of the waveform. Each plot was independently identified by myself and Matthew Grubb with 100%

agreement. A quantitative measure of spike onset sharpness was also employed using a custom Matlab script written by Maxim Volgushev (Baranauskas et al., 2010; Volgushev et al., 2008), which returned the ratio of errors produced by linear and exponential fits to variable initial portions of the phase plane plot between voltage threshold and 40% of maximum *dV/dt*. A maximum fit error >3 was classified as "steep" and indicated a biphasic neuron. A maximum fit error <1 was classified as "smooth" and indicated a monophasic neuron, which agreed with the visual identification.

2.5.4.4 Multiple action potentials

To study multiple action potentials, 500 ms somatic current injections of Δ+5 pA were applied in current-clamp mode until the point where the neurons entered depolarisation block. If this experiment was repeated in the same neuron, the experiment that contained the maximum number of spikes was used for analysis of multiple action potentials and first action potential. Multiple spiking properties were analysed up to the point that the maximum number of spikes was reached. The inter-spike interval (ISI) was calculated as the time between each spike V_{MAX} and was calculated for each trace. Instantaneous frequency (IF) was calculated as the reciprocal of the first ISI (1/ISI) in each trace. Input-output curves were constructed by plotting the maximum number of spikes or the IF at each level of injected current density (pA/pF). A line was fitted to the linear portion of the spiking input-output curve (defined as the first four sweeps that contained action potentials) and its slope calculated.

Spike frequency adaptation (SFA) was investigated by studying the sweep that was +30 pA above the first sweep that contained an action potential. SFA was calculated based on Guan et al. (2015) as:

$$SFA = \left(\frac{frequency\ of\ first\ ISI - \ frequency\ of\ last\ ISI}{frequency\ of\ first\ ISI}\right) x\ 100$$

2.5.4.5 Sag potential

To study the sag potential, 500 ms somatic current injections of Δ-10 pA were applied in current-clamp mode until the point where the neuron's steady-state voltage passed -100 mV. The steady-state voltage (V_{SS}) was the average voltage of the last 10 ms of the current step. The sag potential (V_{SAG}) was identified as the minimum voltage response within the first 50 ms of the current step (the instantaneous voltage response). The rebound voltage was the maximum voltage at the current step offset. A rebound spike was counted where rebound voltage was > 0 mV. If the sag potential experiment was repeated several times in the same neuron, the first

experiment was analysed. The sag index was calculated for current injections corresponding to V_{SS} = -100 mV determined from polynomial fits to the sweeps (Chittajallu et al., 2013) using the equation:

$$sag\ index = \frac{V_{HOLD} - V_{SS}}{V_{HOLD} - V_{SAG}}$$

2.5.4.6 Afterhyperpolarisation

To study the afterhyperpolarisation (AHP) generated in response to multiple action potentials, 500 ms somatic current injections of Δ+5 pA were applied until the point where the neurons entered depolarisation block. Input-output curves were constructed by plotting the minimum voltage reached after the current step by the maximum number of spikes in each sweep.

To compare the AHP evoked by a set number of action potentials, I used a protocol with 10 suprathreshold current injections (350-600 pA; 2 ms), repeated at 50 Hz. AHP start was calculated as the point after the last spike when voltage was below baseline V_{HOLD} for that sweep. The protocol was repeated 10 times and AHP duration was calculated as the mean time it took to return to baseline V_{HOLD}. The medium AHP was analysed from AHP start to AHP start + 250 ms and an average response calculated. The peak medium AHP was the minimum voltage. Medium AHP area was the area under the curve. If the experiment was repeated several times in the same neuron, the first experiment was analysed.

2.5.5 Mini postsynaptic currents

All mini postsynaptic current recordings were performed in voltage-clamp mode using Caesium Methanesulfonate intracellular solution.

Mini excitatory postsynaptic currents (mEPSCs) were recorded in standard ACSF with 1 µM TTX, 50 µM APV and 10 µM SR-95531 (gabazine). mEPSCs were recorded as inward events at -70 mV in voltage-clamp for two minutes. Mini inhibitory postsynaptic currents (mIPSCs) were recorded in standard ACSF with 1 µM TTX, 10 µM NBQX and 50 µM APV. mIPSCs were recorded as outward events at +10 mV in voltage-clamp for two minutes. Minis were analysed using MiniAnalysis (Synaptosoft). The peak of events were manually detected, with a threshold of 5 pA. If the experiments were repeated, the experiment that had the smallest R_S was analysed. For each neuron an average event was created and either a single exponential (mEPSCs) or double exponential (mIPSCs) was fitted to calculate the decay. A weighted decay time constant (τ_W) was calculated from the double exponential fitted to average mIPSCs events where t_N is the

decay time constant for particular component of the curve and A_N is its peak amplitude (Luo et al., 2013):

$$\tau_W = \left(t_1 x \left[\frac{A_1}{A_1 + A_2} \right] \right) + \left(t_2 x \left[\frac{A_2}{A_1 + A_2} \right] \right)$$

2.5.6 Auto-evoked inhibition

All auto-evoked inhibition recordings were performed using Caesium Chloride intracellular solution and in standard ACSF with glutamatergic synaptic blockers [10 µM NBQX, 50 µM APV]. All auto-evoked inhibition recordings were sampled at 50 kHz (20 µs sample interval), with slow capacitance compensated. After membrane rupture, a test series was performed and a single action potential fired in current-clamp to classify a neuron as monophasic or biphasic (see 2.5.4.3). Spontaneous IPSCs were recorded as inward events at -80 mV for 1 minute while 1 µM TTX was added to the ACSF. Sodium channel block was confirmed by running an *IV* protocol and observing the block of the large, inward sodium current.

All auto-evoked inhibition protocols were performed in voltage-clamp from a holding potential of -80 mV, unless otherwise stated. Neurons were depolarised to 0 mV for 10 or 100 ms, before returning to -80 mV. Paired recordings were two 10 ms duration voltage steps with 50 ms inter-stimulus interval. All protocols were repeated 3 times, with 30 seconds in between each sweep, and an average response calculated. The block of $GABA_A$ receptors was by 10 µM SR-95531 (gabazine) and confirmed by the absence of IPSCs. Due to the presence of passive currents, sweeps were analysed from 10 ms after the end of the voltage step for 500 ms. Gabazine-sensitive currents were calculated as the difference between the pre-gabazine and post-gabazine protocols and the charge was the absolute area under the curve. Cadmium-sensitive currents were calculated using the same method, blocking calcium channels with 200 µM cadmium chloride ($CdCl_2$). The gabazine-insensitive current was the area under the curve of the post-gabazine response.

2.6 Statistical analysis

Statistical analysis was carried out using Prism (GraphPad), Matlab (Mathworks) or SPSS (IBM). All datasets were described as mean ± SEM, unless otherwise stated, *n* values reported in the text refers to number of cells and N values refer to number of mice. Details of all individual statistical tests are reported alongside the appropriate results. α values were set to 0.05 (except where a Bonferroni correction was carried out for multiple comparisons) and all comparisons were two-tailed.

For pairwise comparisons, sample distributions were tested for normality with the D'Agostino and Pearson omnibus test and parametric or non-parametric tests were carried out accordingly. For multiple group comparisons, if any group was not normally distributed, all groups were transformed by standard methods (logarithmic, square-root or reciprocal) and retested for normality. If data could not be rendered normal on the D'Agostino and Pearson test by any of these standard transformations, the data of each condition were analysed by fitting a normal distribution and calculating the percentage of variance explained by the fit (Matlab; script written by Matthew Grubb). A result ≥90% was considered as being normally distributed and analysed as such. If the result was <90%, data was analysed by ranks. If results were analysed using transformed data or ranks, this is indicated along with the results. If there was a significant result for multiple group comparisons, Sidak's post-hoc test was performed, unless otherwise stated. Fisher's exact test was performed when analysing proportions. Due to the design of this test, data had to be analysed twice, by combining groups based on manipulation and then duration of manipulation. A Bonferroni correction was therefore carried out for multiple comparisons in this instance ($\alpha = (0.05/2)$, therefore, $\alpha = 0.025$).

Chapter Three – Labelling and manipulating olfactory bulb dopaminergic neurons *in vivo*

3.1 Introduction

3.1.1 Mouse models to label olfactory bulb dopaminergic neurons

To be able to study dopaminergic neurons in the mouse olfactory bulb for immunohistochemistry and electrophysiology experiments, I need a live label that is clear, selective, comprehensive and benign for the mouse. Dopaminergic neurons are the only catecholaminergic neurons in the OB (Cave and Baker, 2009). This gives the opportunity to choose a number of markers to selectively label these cells using transgenic mice. Most work has centred on labelling dopaminergic neurons based on *Th* expression. In a TH$^{IRES\textit{cre}}$ line, the majority of labelled neurons in the mouse olfactory bulb were TH-positive and the majority of dopaminergic neurons were labelled (Adam and Mizrahi, 2011). As this mouse model is based on the Cre-lox system, the transcription of *Th* and *Cre* will irreversibly label the neuron with the reporter protein. While TH protein expression is restricted to the glomerular layer, *Th* transcription occurs in neurons located in the granule cell layer, which may be a reservoir of immature dopaminergic neurons (Banerjee et al., 2013; Pignatelli et al., 2009). During the maturation of olfactory bulb dopaminergic neurons there is transcription of the *Th* gene in immature neurons without significant translation (Baker et al., 2001). In TH-GFP mice, this early expression is enough to drive the expression of GFP in neurons located in the rostral migratory stream (RMS) and granule cell layer (Pignatelli et al., 2009; Saino-Saito et al., 2004). In this TH-GFP mouse, a transgene was constructed using the *Th* promoter and cDNA encoding GFP was randomly inserted into the genome. Other mice to label neurons include using the tet-system under the control of *Th* (TH-tTA) (Tillack et al., 2015). TH expression is also activity-dependent, which could affect the expression and intensity of the fluorescent protein in TH-GFP and TH-tTA mice. Therefore, labelling olfactory bulb dopaminergic neurons by a *Th* promoter risks labelling immature dopaminergic neurons or making sensory deprived neurons undetectable. In other brain regions, the specificity of TH-Cre mice to label dopaminergic neurons is reported to be low (Lammel et al., 2015).

Downstream of TH in the dopamine synthesis pathway is the enzyme, DOPA decarboxylase (DDC). Less is known about this protein in the olfactory bulb; however, its expression is not believed to be activity-dependent (Cave et al., 2010; Stone et al., 1990). Currently, there is no characterisation of a DDC-Cre mouse, although the mouse has been developed (Mutant Mouse

Resource and Research Center: #036641_UCD). Therefore, it is unclear how suitable DDC-mice would be to label olfactory bulb dopaminergic neurons.

Besides TH mice, the other main genetic means of labelling dopaminergic neurons in the olfactory bulb is through the *Dat* gene. Two Cre mice have been described that label dopaminergic neurons by the expression of *Dat*: a knock-in DAT-cre line, which is a heterozygous knockout of *Dat* (Zhuang et al., 2005); and a DAT$^{IRES cre}$ line that retains *Dat* expression from both alleles (Bäckman et al., 2006). DAT heterozygous knockout mice show behavioural deficits and reduced TH expression, dopamine release and reuptake (Giros et al., 1996). While there is an indication that the expression of *Dat* may be slightly activity-dependent (Cave et al., 2010), the expression of a fluorescent reporter protein would not be affected in these Cre mice. However, there is a DAT mouse that uses the tet-system (DAT-tTA) (Chen et al., 2015), which could be affected by this. In the midbrain, labelling dopaminergic neurons by the *Dat* promoter is far more selective for dopaminergic neurons and has fewer off-target mistakes (Lammel et al., 2015). Both DAT-Cre mice have been used in the olfactory bulb to label dopaminergic neurons, with high co-localisation with TH (Banerjee et al., 2015; Galliano et al., 2018; Ninkovic et al., 2010; Vaaga et al., 2017). Another mouse has been developed with GFP expressed under the control of the *Dat* promoter (Zhou et al., 2009). However, as *Dat* is not highly expressed in the olfactory bulb (Cockerham et al., 2016; Mitsumoto et al., 2005), the expression of GFP is weak (Zhou et al., 2009). As the DAT$^{IRES cre}$ mouse retains the function of both *Dat* alleles and the expression of reporter protein is not dependent on high *Dat* promoter activity, this mouse would be more suitable to permanently label dopaminergic neurons that does not affect the dopamine system in the mouse. However, the specificity of this mouse model to label dopaminergic neurons in the olfactory bulb is not fully known.

3.1.2 Heterogeneity in the maturational age of olfactory bulb dopaminergic neurons

The anaxonic olfactory bulb dopaminergic neurons are known to be continuously generated throughout life. Therefore, there would be heterogeneity in the age of these neurons labelled by transgenic mice. As discussed earlier, there is transcription of *Th* in immature dopaminergic neurons in the RMS and granule cell layer, despite TH protein only being detected in the glomerular layer (Baker et al., 2001; Saino-Saito et al., 2004). Therefore, very immature neurons would be labelled. There is currently no study examining the timeline of *Dat* expression in olfactory bulb dopaminergic neurons. However, there is evidence from dopaminergic neurons in the midbrain that expression of genes involved in the dopamine synthesis pathway precedes the expression of *Dat*. In the rat embryo, the expression of *Dat* in developing midbrain dopaminergic neurons is detectable around embryonic day 15 (E15), while *Th* expression is

already present at E12 (Perrone-Capano et al., 1994). Dopamine release also precedes reuptake mechanisms (Fiszman et al., 1991). If expression of *Th* and dopamine synthesis in the olfactory bulb also precedes the expression of *Dat*, the most immature olfactory bulb dopaminergic neuron labelled in the DAT^{IREScre} would be more mature than the equivalent in a transgenic mouse under the control of a *Th* or *Ddc* promoter. Therefore, there may be less heterogeneity in age range. This temporal heterogeneity has not been directly addressed. It has been found that there is net addition of dopaminergic neurons in the olfactory bulb and cell death may be largely absent in postnatally-generated neurons (Adam and Mizrahi, 2011; Platel et al., 2018). Therefore, there would be continued widening to the range of cell ages.

3.1.3 Unilateral naris occlusion affects olfactory bulb dopaminergic neurons

As discussed in Chapter 1, odour deprivation manipulations include unilateral naris occlusion or deafferentation. Unilateral naris occlusion by the insertion of a small plug is a reliable method for depriving one naris of sensory input (Cheetham et al., 2016; Cummings et al., 1997). This manipulation does not require painful or invasive surgery to seal or reopen the naris as is required with cauterisation (Guthrie et al., 1991). Inducing activity-dependent plasticity by odour deprivation is known to affect olfactory bulb dopaminergic neurons (Baker et al., 1983). In particular, the expression of TH is downregulated, which can be reversed by reopening the naris (Baker et al., 1983; Kosaka et al., 1987). Unilateral naris occlusion is, therefore, a simple and effective manipulation to induce experience-dependent plasticity in the olfactory bulb dopaminergic neurons. To date the earliest reported decrease in TH expression has been after 2 days of occlusion (Young Cho et al., 1996). However, chronic depolarisation of *in vitro* olfactory bulb dopaminergic neurons increases the expression of TH and changes the axon initial segment (AIS) after 1 day.

3.1.4 Chapter aims

For this project, I used the DAT^{IREScre} transgenic mouse crossed with a tdTomato reporter mouse to generate a DAT-tdTomato mouse to label olfactory bulb dopaminergic neurons for immunohistochemical and electrophysiological analysis. In this Chapter, I performed immunohistochemistry and acute slice electrophysiology to investigate the suitability of this mouse to label these neurons. I carried out BrdU injections at specific ages to describe the heterogeneity in the maturational age of the labelled neurons. I also used immunohistochemistry to characterise the effect of 1 and 3 days of unilateral naris occlusion on the activity of DAT-tdTomato neurons and their experience-dependent plasticity of neurotransmitter-synthesising enzyme expression.

3.2 Results

3.2.1 Labelling olfactory bulb dopaminergic neurons with the DAT^{IREScre} mouse

Initial experiments used immunohistochemistry to characterise the labelling of dopaminergic neurons in the olfactory bulb of DAT-tdTomato mice. Coronal slices from perfusion-fixed postnatal day (P) 28 DAT-tdTomato olfactory bulbs were stained with the dopaminergic marker, TH (**Figure 3.1A**). Overall, there appeared to be good co-localisation between the two markers and tdTomato expression was restricted to glomerular layer. It, therefore, appears that the dopaminergic neurons are being selectively labelled in the mouse. Quantifying the number of co-localised neurons revealed that the majority of DAT-tdTomato neurons expressed TH (71.5 ± 1.22%, n = 891, N = 3). The majority of TH-positive neurons were also DAT-tdTomato positive (66.6 ± 1.5%, n = 956, N = 3) (**Figure 3.1B**). It is known that there are at least two subpopulations of dopaminergic neurons in the olfactory bulb, which can be distinguished by the size of their somas. I, therefore, measured the soma area of all DAT-tdTomato and TH neurons. This revealed that large soma dopaminergic neurons are underrepresented, but not completely absent, in the DAT^{IREScre} olfactory bulb, in agreement with previous research (Galliano et al., 2018). However, it was interesting to note that in addition to large TH-positive neurons that were tdTomato-negative there were DAT-tdTomato neurons with a very small soma that were not TH-positive (soma area range; DAT-tdTomato neurons, 20 – 110 µm^2, n = 891, N = 3; TH neurons, 25 – 150 µm^2, n = 956, N = 3) (**Figure 3.1C**). Therefore, the DAT^{IREScre} mouse does not label all dopaminergic neurons, which is not a major concern as TH expression may precede *Dat* expression. However, there is a question of how selective the mouse is for dopaminergic neurons.

I further investigated the DAT-tdTomato neurons that did not express TH by comparing the soma area of this population against the DAT-tdTomato neurons that were TH-positive. This showed that the TH-negative neurons had a narrower soma area distribution (soma area range; TH-negative, 20 – 85 µm^2, n = 243, N = 3; TH-positive, 25 – 110 µm^2, n = 648, N = 3) (**Figure 3.1D**). I also observed that these neurons appeared to have weaker tdTomato fluorescence signal compared to the TH-positive population. Quantifying the fluorescence intensity of TH-negative DAT-tdTomato revealed that these neurons were significantly less bright (normalised tdTomato intensity ± SEM: TH-positive, 100 ± 1.31%, n = 648, N = 3; TH-negative, 70 ± 1.75%, n = 243, N = 3. Multi-level ANOVA controlling for mouse variance, $F_{(1,891)}$ = 158.77, $p < 0.0001$) (**Figure 3.1E**). These results show that in addition to the TH-positive population, the

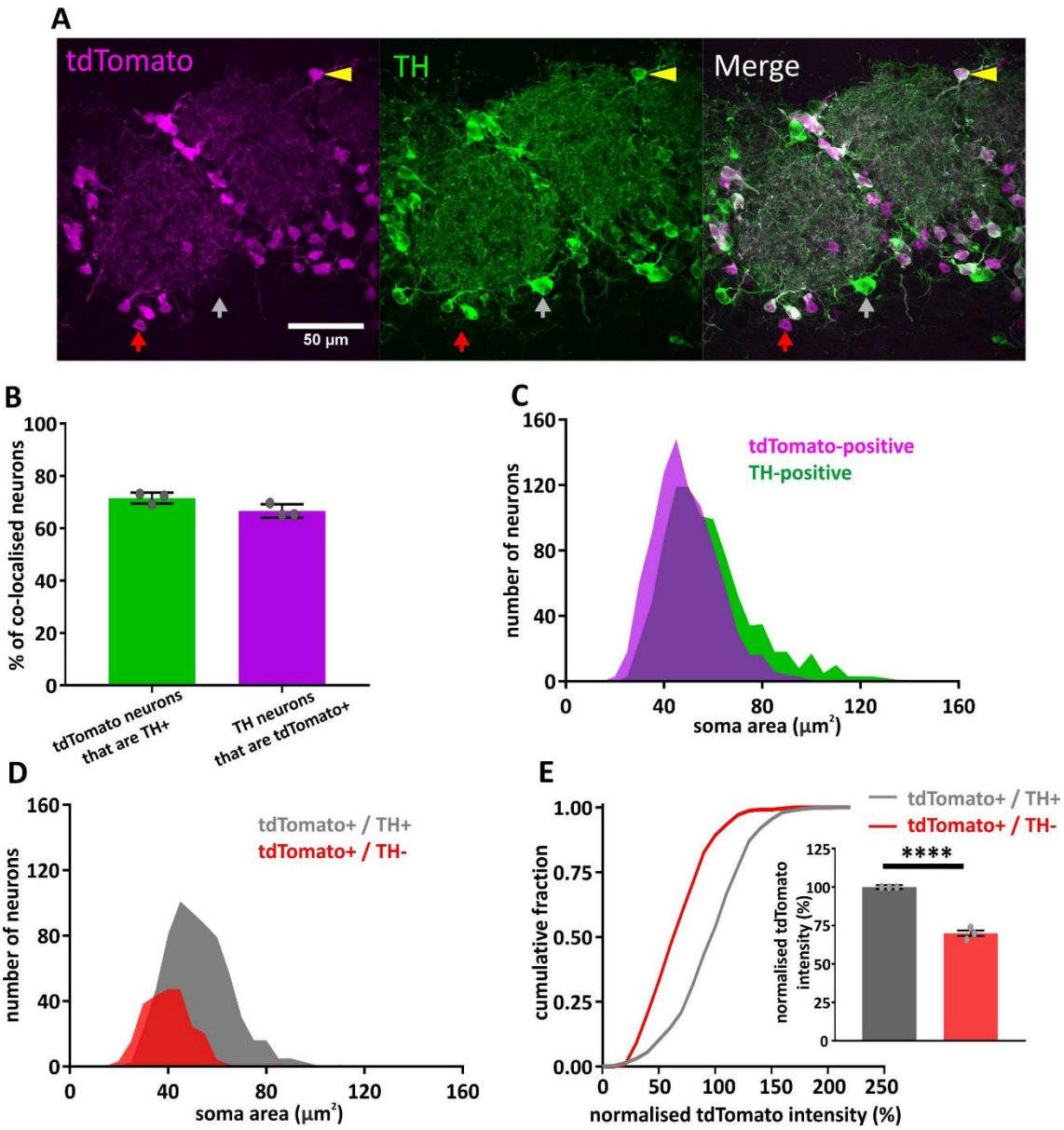

Figure 3.1: Co-localisation of DAT-tdTomato with tyrosine hydroxylase

A: Example maximum intensity projection images showing the expression of TH in the glomerular layer of the olfactory bulb in a DAT-tdTomato mouse. Yellow arrowhead indicates location of a neuron showing expression of both markers. Arrows indicate location of neurons expressing a single marker: red = DAT-tdTomato only; grey = TH only.

B: Bar plots showing the mean percentage ± SEM of tdTomato-positive neurons expressing TH (green) (n = 891) and TH-positive neurons expressing tdTomato (magenta) (n = 956). Grey circles indicate individual mice (N = 3).

C: Histograms showing the soma area distribution of tdTomato-positive and TH-positive neurons.

D: Histograms showing the soma area distribution of tdTomato neurons that are either positive (n = 648) or negative (n = 243) for TH.

E: Cumulative distribution of normalised tdTomato intensity (%) in TH-positive and TH-negative neurons. **Inset**: bar plot showing the mean ± SEM of normalised tdTomato intensity (%). Multi-level ANOVA controlling for mouse variance; effect of TH expression **** $p < 0.0001$. Grey circles indicate individual mice.

DAT-tdTomato mouse is faintly labelling a distinct subpopulation of small-soma glomerular layer neuron.

The expression of TH in the olfactory bulb is known to be activity-dependent (Baker et al., 1983). Therefore, DAT-tdTomato neurons that are TH-negative could still be dopaminergic neurons; however, low expression of TH could make their identification by immunohistochemistry difficult. To further characterise the dopaminergic identity of the DAT-tdTomato population, an additional dopaminergic marker, DOPA decarboxylase (DDC), was studied (**Figure 3.2A**). Previous work has found that the expression of this dopaminergic marker is not activity-dependent (Cave et al., 2010; Stone et al., 1990). Co-localisation analysis showed that the expression of DDC was highly co-expressed with TH; however, there was a subpopulation of neurons that only appeared to express DDC (% of DDC-positive neurons ± SEM: TH+/tdTomato+, 56.72 ± 1.23%; TH+ only, 32.1 ± 0.49%; tdTomato+ only, 2.45 ± 1.39%; DDC+ only, 8.73 ± 0.54%; *n* = 774, N = 3) (**Figure 3.2B**). Therefore, the DDC antibody appears to be a good candidate for labelling dopaminergic neurons in the olfactory bulb glomerular layer. The DDC-only neurons could indicate dopaminergic neurons with (potentially activity-dependent) low expression of TH.

Investigating TH-positive neurons revealed that virtually all of these neurons were also DDC-positive (% of TH-positive neurons ± SEM: DDC+/tdTomato+, 63.33 ± 0.41%; DDC+ only, 35.85 ± 0.35%; tdTomato+ only, 0.42 ± 0.24%; TH+ only, 0.4 ± 0.4%; *n* = 692, N = 3) (**Figure 3.2C**). Therefore, if TH expression can be detected in a neuron in the glomerular layer by immunohistochemistry, it will almost always have detectable DDC expression.

Studying DAT-tdTomato neurons revealed that only a minor population of DAT-tdTomato cells that were TH-negative were found to be DDC-positive. However, there were still DAT-tdTomato neurons that were neither TH or DDC-positive (% of tdTomato-positive neurons ± SEM: TH+/DDC+, 73.87 ± 3.97%; TH+ only, 0.46 ± 0.26; DDC+ only, 3.07 ± 7.7%; tdTomato+ only, 22.6 ± 2.02%; *n* = 598, N = 3) (**Figure 3.2D**). Therefore, there is a population of DAT-tdTomato neurons that do not show expression of either of these two dopaminergic markers. It is unlikely that the activity-dependent TH hypothesis explains the lack of specificity of the mouse line.

Since this mouse line labels dopaminergic neurons using the *Dat* gene, I investigated the expression of DAT with immunohistochemistry. However, expression of DAT in the olfactory bulb is known to be low (Cockerham et al., 2016; Mitsumoto et al., 2005) and I did not see any somatic label convincingly co-localised with DAT-tdTomato neurons (**Figure 3.3A**). This result

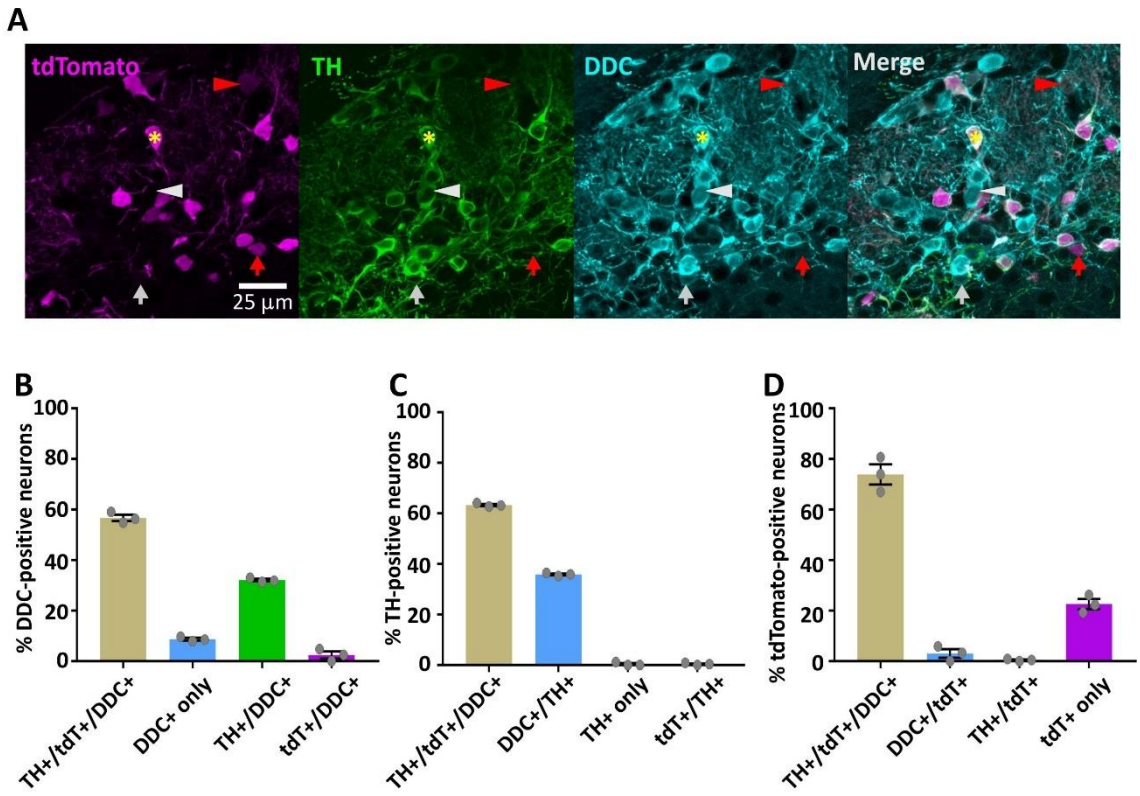

Figure 3.2: Co-localisation of DDC with TH and DAT-tdTomato

A: Example maximum intensity projection images showing the expression of DDC and TH in the glomerular layer of the olfactory bulb in a DAT-tdTomato mouse. Yellow star indicates location of a neuron showing expression of all three markers. Arrowheads indicate location of neurons expressing two markers: red = DAT-tdTomato and DDC; white = TH and DDC. Arrows indicate location of neurons expressing a single marker: red = DAT-tdTomato; white = DDC.

B-D: bar plots showing the mean percentage ± SEM of tdTomato, TH and DDC (co-)expression in (B) DDC-positive neurons (n = 774), (C) TH-positive neurons (n = 692) and (D) tdTomato-positive neurons (n = 598). Grey circles indicate individual mice (N = 3).

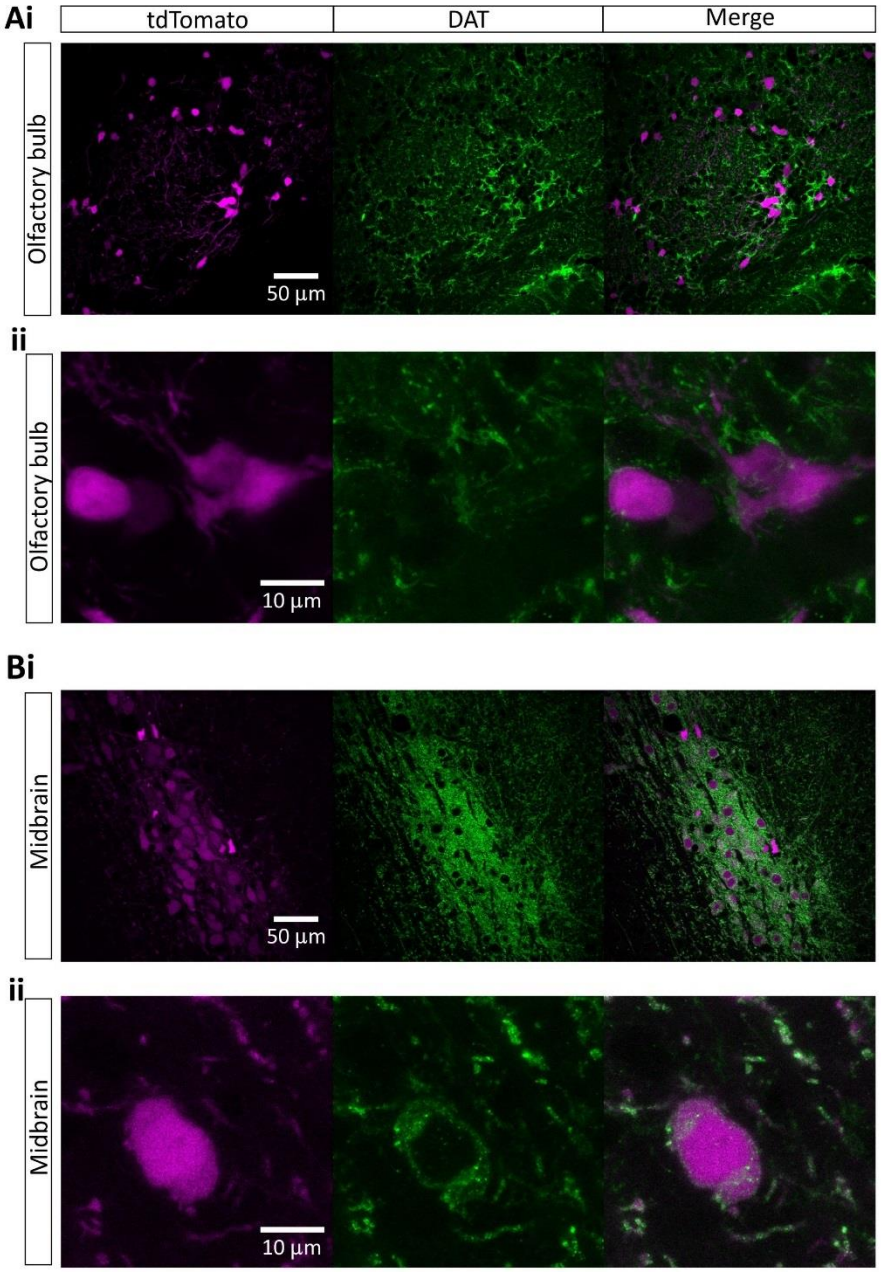

Figure 3.3: DAT antibody labels DAT-tdTomato neurons in the midbrain but not the olfactory bulb

A-B: Example maximum intensity projection images showing (i) zoomed out and (ii) zoomed in expression of DAT in (A) the glomerular layer of the olfactory bulb and (B) the midbrain of a DAT-tdTomato mouse.

could be due to an issue with the DAT antibody. Therefore, as a positive control, I labelled sagittal sections from the DAT-tdTomato mouse with the DAT antibody. This showed that DAT-tdTomato neurons outside the olfactory bulb in the midbrain had a predominately punctate expression of DAT in non-nuclear cytoplasmic regions (**Figure 3.3B)**. However, even here the staining was not very clear or specific. Therefore, I cannot identify dopaminergic neurons in the olfactory bulb by the expression of DAT via immunohistochemistry with this antibody.

3.2.2 Identifying DAT-tdTomato neurons that are not dopaminergic

Based on these results there appears to be a reasonably large proportion of DAT-tdTomato neurons that are not dopaminergic. Olfactory bulb dopaminergic neurons are one of the GABAergic neuronal populations that are present in the glomerular layer. Expression of GABA in the DAT-tdTomato mouse confirmed that these neurons were also GABAergic (**Figure 3.4A**). Other GABAergic populations in the glomerular layer can be identified by the mutually exclusive expression of calretinin or calbindin (Kosaka and Kosaka, 2007). Immunostaining for these markers in the DAT-tdTomato mouse revealed that there was no co-localisation of calbindin with the tdTomato label (**Figure 3.4B**). However, there were DAT-tdTomato neurons that were positive for calretinin (**Figure 3.4C**).

To characterise the labelling of calretinin in the DAT-tdTomato mouse, coronal sections of the olfactory bulb were stained for the expression of calretinin and TH (**Figure 3.5A**). This revealed that the majority of DAT-tdTomato neurons that were TH-negative were calretinin-positive (% of tdTomato-positive neurons ± SEM: TH+ only, 74.1 ± 2.24%; calretinin+ only, 21.71 ± 0.9; tdTomato+ only, 4.2 ± 1.4%; n = 1404, N = 3) (**Figure 3.5B**). There was a small population that was negative for both markers, likely corresponding to the minority of DDC-positive DAT-tdTomato neurons shown in Figure 3.3D, which could be low-activity TH-downregulated dopaminergic neurons. Based on the previous results, it appears that the DAT-tdTomato mouse labels a non-dopaminergic subpopulation of calretinin neurons that have a smaller soma size and weaker expression of tdTomato than the dopaminergic population.

The labelling of a sizeable non-dopaminergic population could affect the use of this animal model for targeted electrophysiological recordings. Research into the functional properties of glomerular layer dopaminergic and calretinin neurons has found distinct differences in their ability to fire action potentials. In response to long duration depolarisation, dopaminergic neurons fire repetitively (Galliano et al., 2018). In contrast, calretinin neurons can only fire

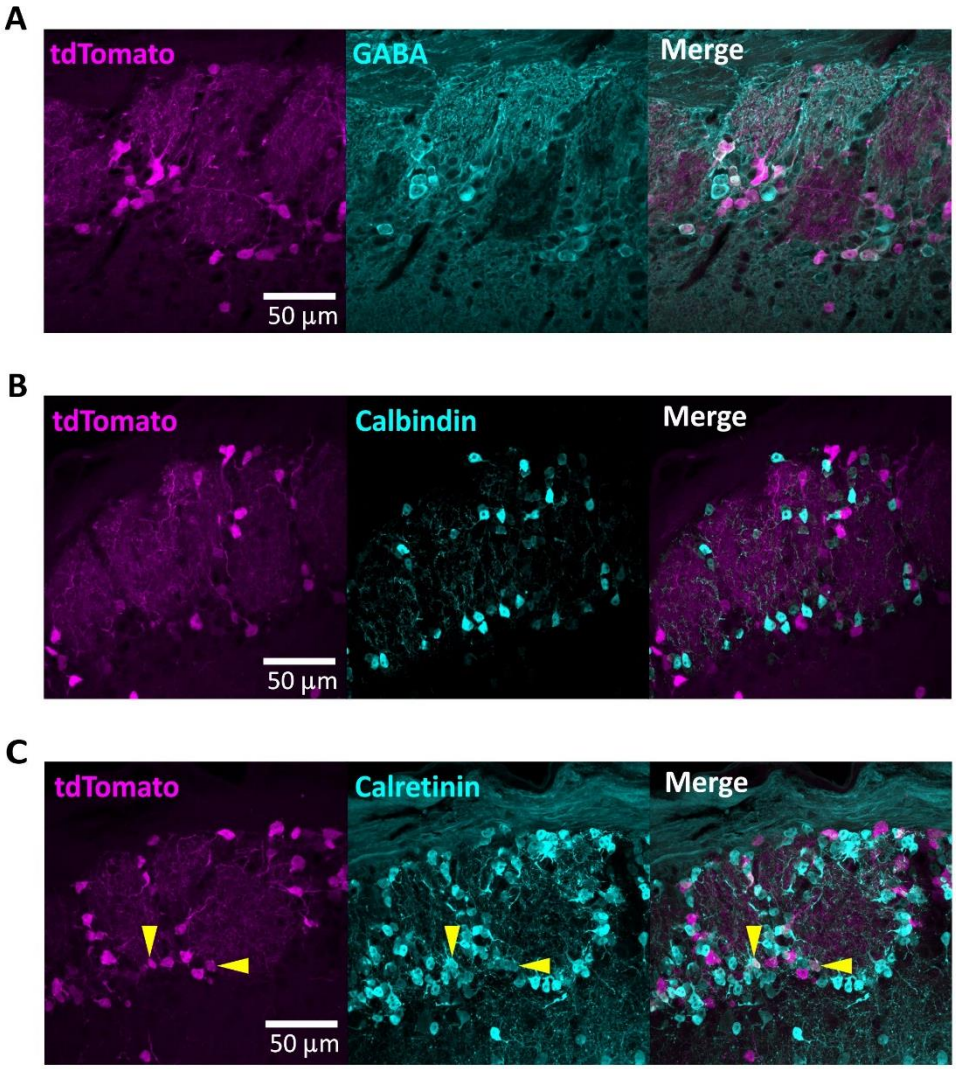

Figure 3.4: Expression of GABAergic markers in the DAT-tdTomato mouse

A-B: Example maximum intensity projection images of (A) GABA, (B) calbindin and (C) calretinin neurons in the glomerular layer of the olfactory bulb of a DAT-tdTomato mouse. Yellow arrowheads indicate example calretinin neurons that were co-localised with tdTomato expression.

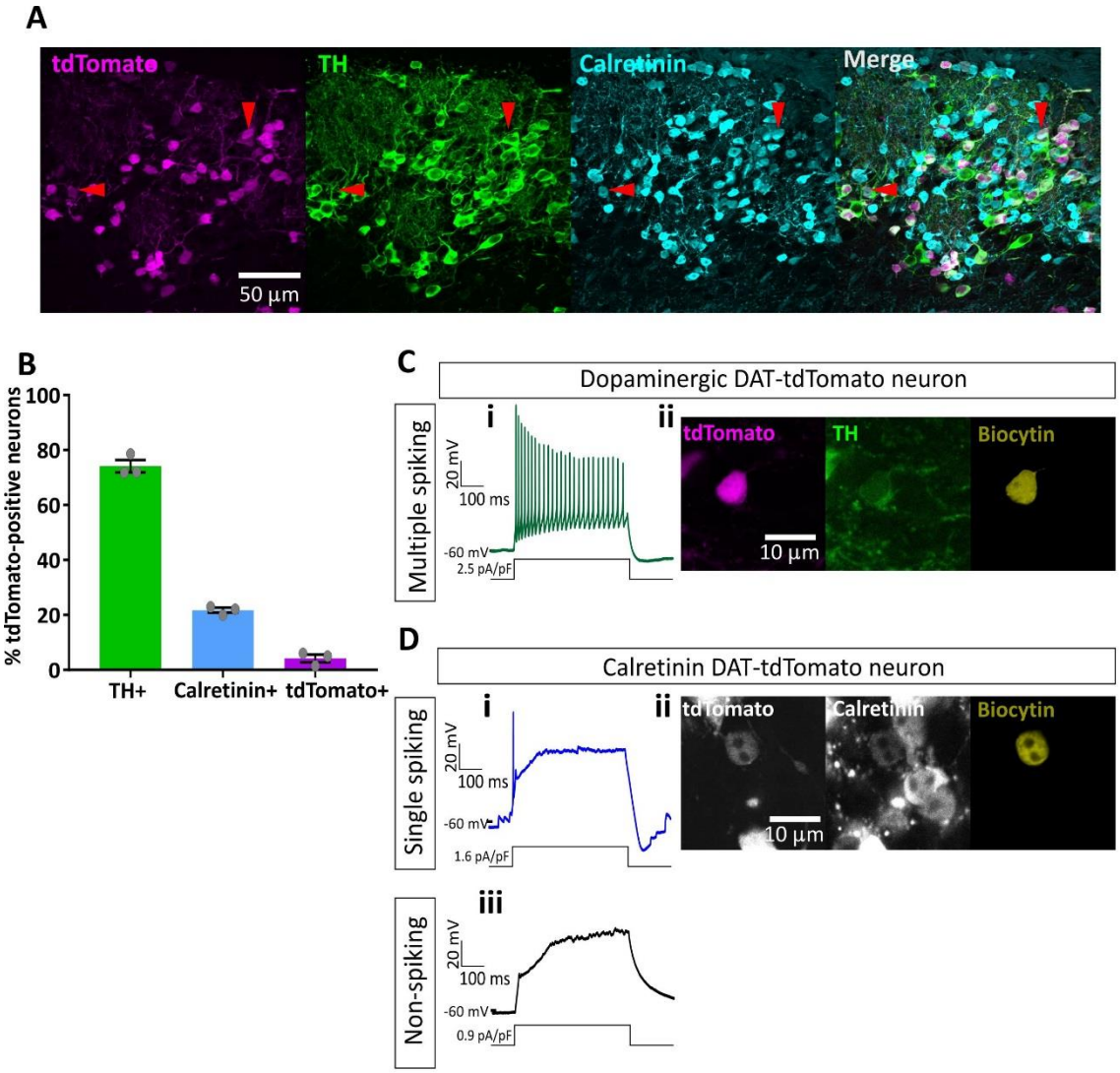

Figure 3.5: Non-dopaminergic DAT-tdTomato neurons are calretinin neurons

A: Example maximum intensity projection images showing the expression of TH and calretinin in the glomerular layer of the olfactory bulb in a DAT-tdTomato mouse. Red arrowheads indicate locations of example neurons expressing DAT-tdTomato and calretinin.

B: Bar plots showing the mean percentage ± SEM of tdTomato, TH and calretinin expression in tdTomato-positive neurons (n = 1404). Grey circles indicate individual mice (N = 3).

C-D: (i) Example traces of (C) multiple and (D) single spiking fired by DAT-tdTomato neurons in response to depolarising steps of 500 ms duration. (ii) Images of neurons presented in (i) that were filled with biocytin and immunostained for (C) TH and (D) calretinin. (iii) Example trace of DAT-tdTomato neuron that did not spike in response to depolarisation.

single action potential at the start of the depolarisation followed by a plateau. There is also a proportion (~18%) of these neurons that are unable to generate an action potential (Fogli Iseppe et al., 2016).

To investigate whether this characteristic firing behaviour was present in the subpopulation of calretinin-positive DAT-tdTomato neurons, I targeted DAT-tdTomato neurons in acute slices for whole-cell electrophysiology recordings using fluorescence intensity and soma size as a guide. Repetitive firing was induced by injecting increasing current steps for 500 ms (**Figure 3.5Ci**). With biocytin in the intracellular solution, I then tried to recover the patched cells and perform immunohistochemistry. However, post-recording recovery of olfactory bulb dopaminergic neurons for immunohistochemical analysis is low (Galliano et al., 2018), therefore, the majority of neurons were not recovered. However, I did recover one neuron that fired multiple action potentials and was positive for biocytin and TH (**Figure 3.5Cii**).

I specifically targeted DAT-tdTomato neurons that had a small soma and very weak tdTomato fluorescence. Some of these were found to only fire a single or no action potential (**Figure 3.5Di,iii**). Post-recording immunohistochemistry revealed that a single-spiking neuron was indeed positive for calretinin (**Figure 3.5Dii**). Unfortunately, the non-spiking DAT-tdTomato neuron did not survive post-recording. However, based on the characteristic plateau that was observed and data from previous work (Fogli Iseppe et al., 2016), this is likely to be a calretinin-positive neuron.

Overall, these results show that while the DAT^{IREScre} line does not perfectly label olfactory bulb dopaminergic neurons, the subpopulation of calretinin-positive DAT-tdTomato neurons can be identified and avoided by immunohistochemistry, live-label features and electrophysiology.

3.2.3 Birthdating postnatally generated DAT-tdTomato neurons

The majority of neurons labelled in the DAT^{IREScre} mouse belong to the subpopulation of dopaminergic neurons with a small soma size that are known to lack an axon (Galliano et al., 2018). These neurons are continually generated postnatally, therefore, there would likely be heterogeneity in the age of tdTomato-positive neurons. To investigate the maturity of DAT-tdTomato neurons, BrdU was injected at different postnatal timepoints and studied when the mice had reached P28. BrdU labels dividing cells that are in S-phase, which in the mouse subventricular zone (SVZ) can last up to 17 hours for neural stem cells, 9 hours for intermediate progenitors and 4 hours for neuroblasts (Ponti et al., 2013). The bioavailability of BrdU is approximately 2 hours (Matiašová et al., 2014), therefore, DAT-tdTomato progenitors that are

in or enter S phase during this period will be labelled. By assessing the latest age at which BrdU injection could produce co-label with tdTomato-positive neurons in the glomerular layer, this would give an indication of what was the minimum age of DAT-tdTomato neurons at P28 and the range of cell maturity in the population. Initial experiments were performed by myself and my student, Krishna Kothandapani, studying the BrdU label 7, 14 and 21 days post-BrdU injection (dpi), with follow-up work done by myself at 17, 19 and 27 dpi. All BrdU injected mice were perfused at P28.

Postnatally born glomerular layer interneurons originate from the SVZ and must migrate along the RMS to enter the olfactory bulb. Using sagittal sections of the olfactory bulb and frontal cortices from 7, 14 and 21 dpi mice (**Figure 3.6A**), we stained for BrdU and an immature neuronal marker, doublecortin (DCX), in order to identify the RMS as it enters the olfactory bulb (**Figure 3.6B**). A high density of BrdU cells could be identified in the RMS at 7 dpi. With increasing dpi, there was a decline in the number of BrdU cells as they cleared the RMS. By 21 dpi, very few BrdU cells were still present in the RMS, with the majority presumably migrating towards or positioned in the layers of the olfactory bulb. Some BrdU cells may also have undergone cell death.

In the glomerular layer, very few BrdU cells could be identified 7 dpi. A number of BrdU cells were positioned within the glomerular layer 14 dpi. By 21 dpi we could identify DAT-tdTomato neurons that were also BrdU-positive (**Figure 3.6C**). The mean density of BrdU cells within the glomerular layer was quantified. This showed a linear increase in the density of BrdU cells in the glomerular layer at P28 with increasing dpi (mean ± SEM: 7 dpi, $0.74 \pm 0.04 \times 10^3$ cells/mm^3, N = 2; 14 dpi $11.73 \pm 2.06 \times 10^3$ cells/mm^3, N = 2; 21 dpi, $25.98 \pm 2.26 \times 10^3$ cells/mm^3, N = 2) (**Figure 3.6D**). Therefore, most postnatally born cells from the labelled cohort have cleared from the RMS by 21 dpi and are migrating and positioning into the overlying layers of the olfactory bulb.

Based on initial results, additional BrdU injections were performed at P1, P9 and P11 (**Figure 3.7A**) to characterise the maturation of DAT-tdTomato neurons. We investigated the proportion of DAT-tdTomato neurons that were labelled with BrdU (**Figure 3.7B**). The largest cohort of BrdU-positive DAT-tdTomato neurons were labelled at P1 and this size decreased with later timepoints, until P14 when BrdU-positive DAT-tdTomato neurons were almost undetectable (**Figure 3.7C**) (**Table 3.1**). Therefore, the minimum age of DAT-tdTomato neurons at P28 is ~14 days old; however, the majority of the population is older. The co-label of tdTomato and BrdU

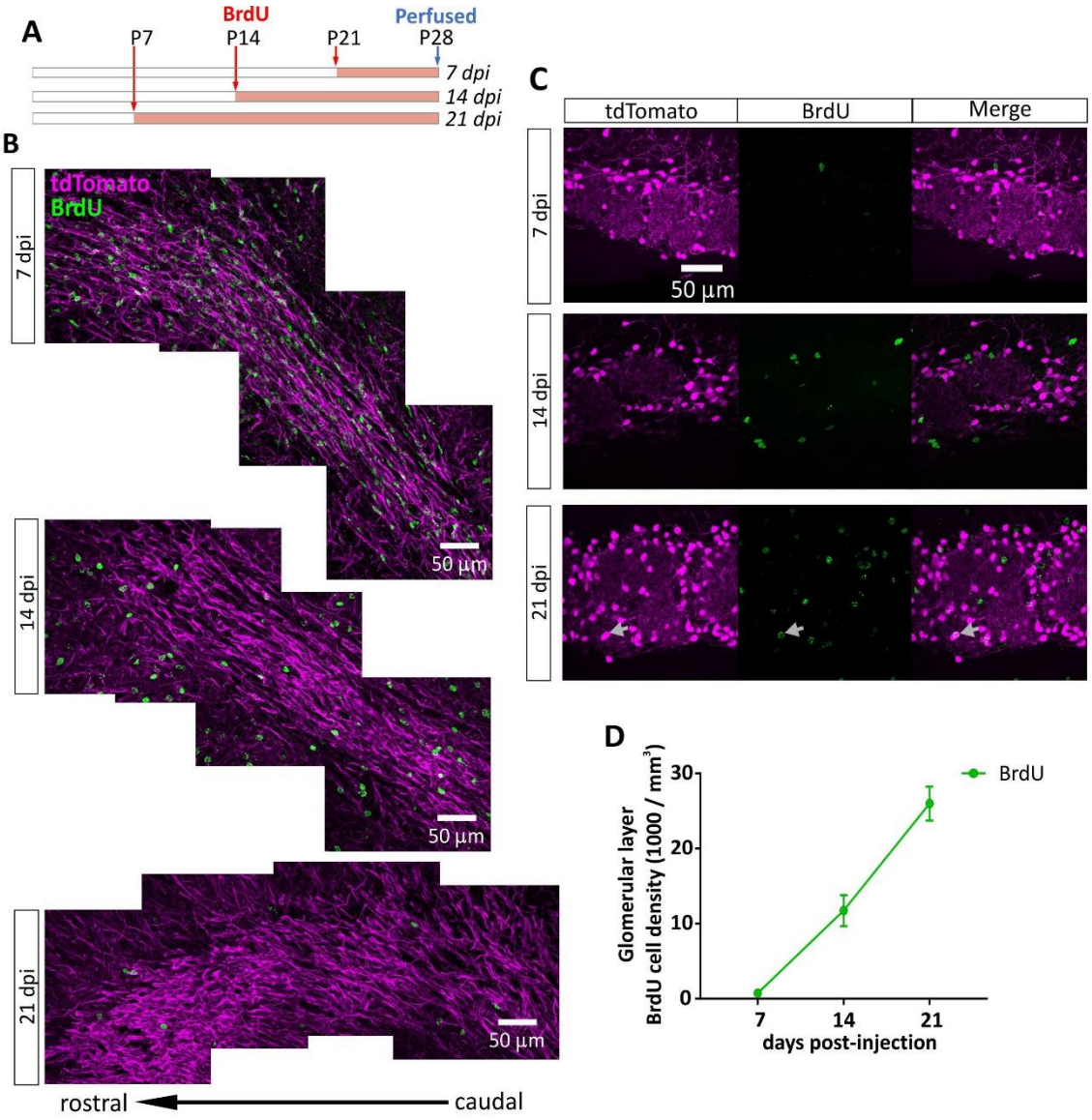

Figure 3.6: BrdU labelling in the DAT-tdTomato mouse

A: Timeline of BrdU injections.

B-C: Example maximum intensity projection images showing the expression of BrdU-positive cells in (A) the rostral migratory stream as it enters the olfactory bulb and (B) the glomerular layer from P28 DAT-tdTomato mice 7, 14 and 21 days post-BrdU injection (dpi). Grey arrows indicate the location of a BrdU labelled DAT-tdTomato neuron.

D: Line plot showing the mean ± SEM of BrdU cell density (1000 / mm^3) in the glomerular layer of the olfactory bulb, 7, 14 and 21 dpi.

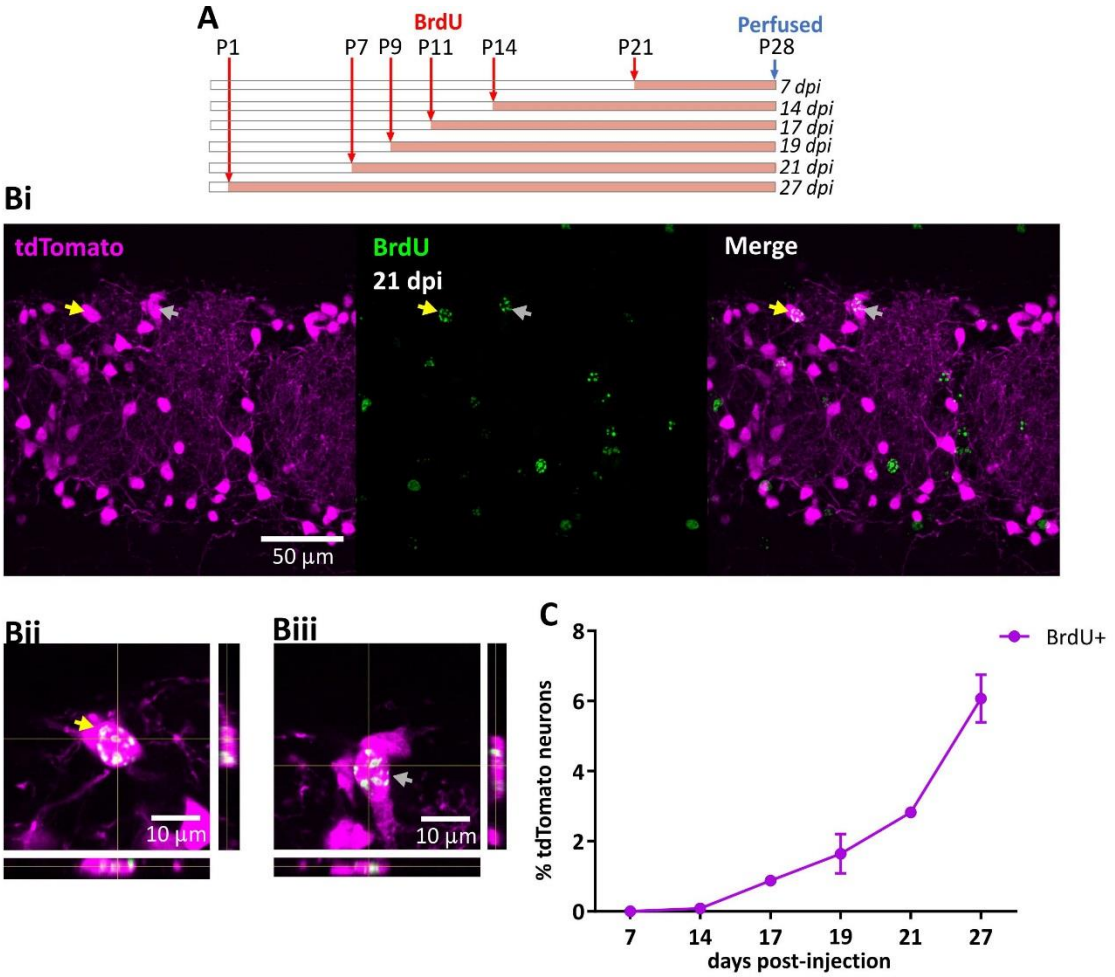

Figure 3.7: Birthdating analysis of DAT-tdTomato neurons

A: Timeline of BrdU injections.

B: (i) Example maximum intensity projection images showing the expression of BrdU in the glomerular layer of the olfactory bulb in a P28 DAT-tdTomato mouse 21 days post-BrdU injection (dpi). Arrows indicate the locations of example BrdU-positive neurons. (ii-iii) Zoomed in and orthogonal view of example cells indicated in Ai.

C: Line plot showing the mean percentage ± SEM of tdTomato neurons expressing BrdU, at specific days post-BrdU injection. [SEM bars were not inserted if they were shorter than the height of the symbol.]

at the different timepoints indicates that a sizeable proportion of DAT-tdTomato neurons at P28 are generated postnatally.

	7 dpi	14 dpi	17 dpi	19 dpi	21 dpi	27 dpi
Mean ± SEM	0	0.08 ± 0.02	0.87 ± 0.13	1.65 ± 0.56	2.82 ± 0.02	6.07 ± 0.68
***n* (N)**	*2504* (2)	*2635* (2)	*1931* (2)	*2142* (2)	*2694* (2)	*2136* (2)

Table 3.1: % DAT-tdTomato neurons labelled with BrdU

3.2.4 Dopaminergic markers in postnatally born neurons

The expression of dopaminergic markers in early postnatally generated glomerular layer interneurons is not well described. We, therefore, investigated the expression of dopaminergic markers in BrdU-labelled cells. Coronal olfactory bulb sections from mice injected with BrdU (7, 14 and 21 dpi) (**Figure 3.8A**) were stained for TH (**Figure 3.8B**) and DDC (**Figure 3.8C**). We investigated the expression of TH, DDC and DAT-tdTomato in BrdU-positive cells (**Figure 3.8D**) (**Table 3.2**). The most recently BrdU-labelled cells (7 dpi) did not express any dopaminergic markers. At the other two timepoints (14 dpi and 21 dpi) a higher proportion of BrdU-positive cells expressed DDC compared to TH. There were consistently fewer BrdU-positive DAT-tdTomato neurons at 14 and 21 dpi compared to DDC and TH. Based on the characterisation of the DAT-tdTomato label, ~22% of these neurons would not be dopaminergic (see Figure 3.2D). As virtually all TH-positive neurons are also DDC-positive, (see Figure 3.2C), we studied the proportion of BrdU-labelled cells that were positive for DAT-tdTomato, but negative for DDC. At 14 dpi, the very few BrdU-labelled DAT-tdTomato neurons were all positive for DDC, indicating that only dopaminergic DAT-tdTomato neurons were generated at this timepoint. Despite 21 dpi DAT-tdTomato neurons comprising ~8% of BrdU-positive cells, non-dopaminergic DAT-tdTomato neurons were only ~1% of BrdU-positive cells. Therefore, the majority of BrdU-positive DAT-tdTomato neurons at 21 dpi (~85%) are dopaminergic. Compared with the proportion of dopaminergic neurons in the general tdTomato population at P28 (~78%), this suggests that postnatally generated DAT-tdTomato are more likely to be dopaminergic than the overall tdTomato-positive population at P28. Therefore, tdTomato neurons are more likely to be dopaminergic at these timepoints.

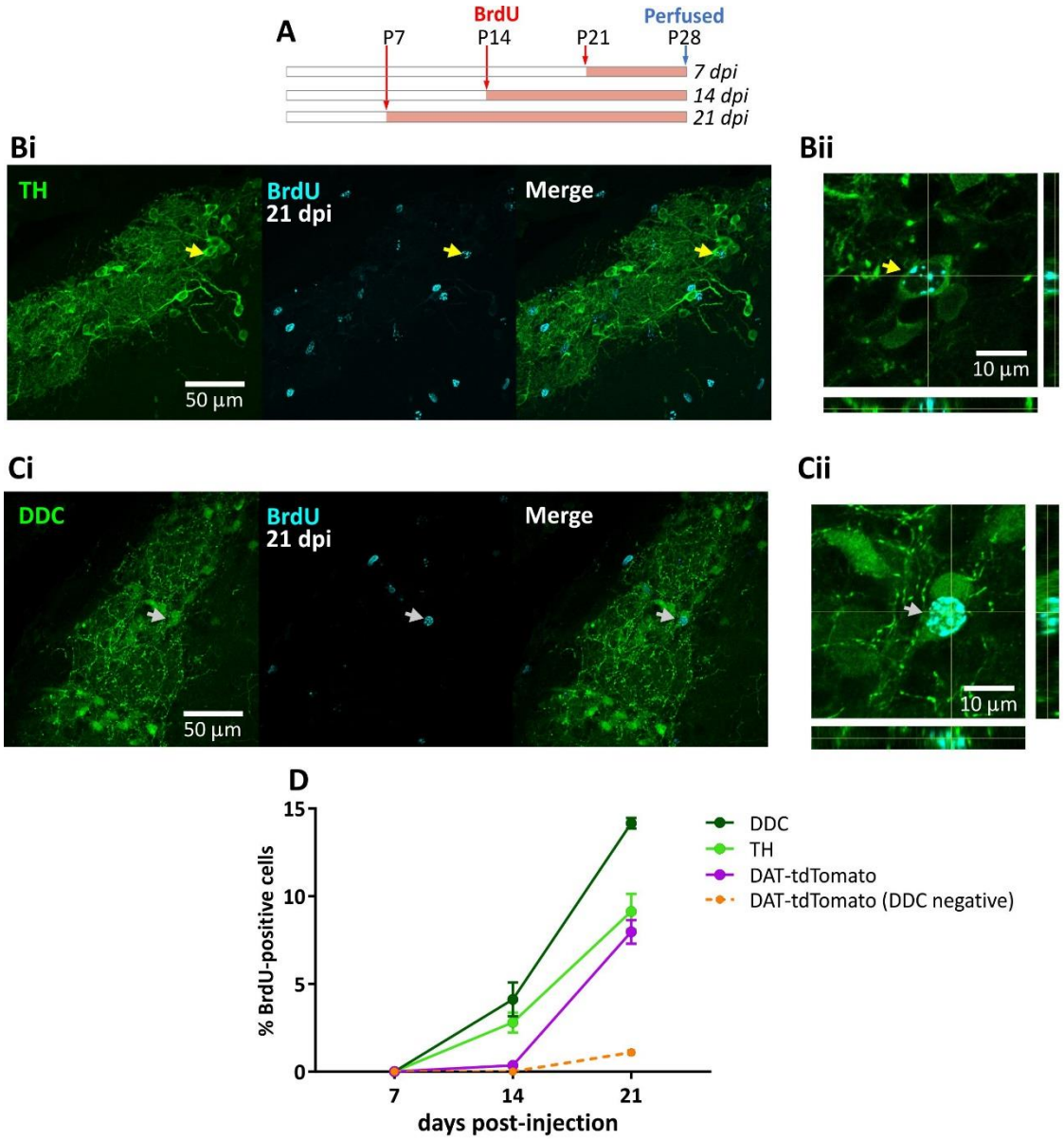

Figure 3.8: Birthdating analysis of dopamine markers in DAT-tdTomato neurons

A: Timeline of BrdU injections.

B-C: (i) Example maximum intensity projection images showing the expression of (A) TH and (B) DDC in the glomerular layer of the olfactory bulb in a P28 DAT-tdTomato mouse 21 days post-BrdU injection (dpi). Arrows indicate the locations of example BrdU-positive neurons; yellow = TH-positive neuron; grey = DDC-positive neuron. (ii) Zoomed in and orthogonal view of example cells.

D: Line plots showing the mean percentage ± SEM of BrdU-positive cells in the glomerular layer expressing DDC, TH, DAT-tdTomato and DAT-tdTomato (DDC-negative) at specific days post-BrdU injection.

	7 dpi	14 dpi	21 dpi
DDC	0	4.12 ± 0.96	14.16 ± 0.3
TH	0	2.8 ± 0.57	9.12 ± 1.01
DAT-tdTomato	0	0.35 ± 0.07	7.97 ± 0.69
DAT-tdTomato (DDC negative)	*0*	*0*	*1.1 ± .012*
n (N)	*39* (2)	*570* (2)	*949* (2)

Table 3.2: % BrdU-positive cells expressing dopaminergic markers

3.2.5 Postnatal generation of calretinin DAT-tdTomato neurons

As there were very few BrdU-positive non-dopaminergic DAT-tdTomato neurons at 21 dpi, we studied different timepoints to better understand the postnatal generation of non-dopaminergic DAT-tdTomato cells (**Figure 3.9A**). The characterisation of the mouse line demonstrated that these neurons belong to the calretinin population of glomerular layer interneurons. Therefore, we next investigated BrdU labelling in calretinin-positive DAT-tdTomato neurons (**Figure 3.9B**). We found that ~5% of these neurons were labelled with BrdU when injected at P1; however, this proportion sharply declined at the later timepoints (**Figure 3.9C**) (**Table 3.3**). One explanation could be that postnatally generated calretinin neurons are slower to develop than the dopaminergic population. However, studying the percentage of BrdU cells in the glomerular layer that were calretinin-positive revealed that over 1/3 of BrdU cells were expressing calretinin after only 14 dpi (mean ± SEM: 7 dpi, 0 %, *n* = 10, N = 2; 14 dpi, 36.1 ± 0.81 %, *n* = 186, N = 2; 21 dpi, 35.24 ± 0.11 %, *n* = 383, N = 2) (**Figure 3.9D**). It, therefore, appears that calretinin-positive DAT-tdTomato neurons are generated early postnatally or, possibly, embryonically.

Overall, it appears that the minimum age of DAT-tdTomato neurons at P28 is ~14 days old; however, only a small number of cells from the total population will be this age. However, a sizeable proportion of DAT-tdTomato neurons are generated postnatally, which are more likely to be dopaminergic than calretinin-positive.

	7 dpi	14 dpi	17 dpi	19 dpi	21 dpi	27 dpi
Mean ± SEM	0	0	0	0	0.41 ± 0.41	4.68 ± 0.54
n (N)	293 (2)	275 (2)	190 (2)	177 (2)	261 (2)	248 (2)

Table 3.3: % calretinin DAT-tdTomato neurons BrdU-positive

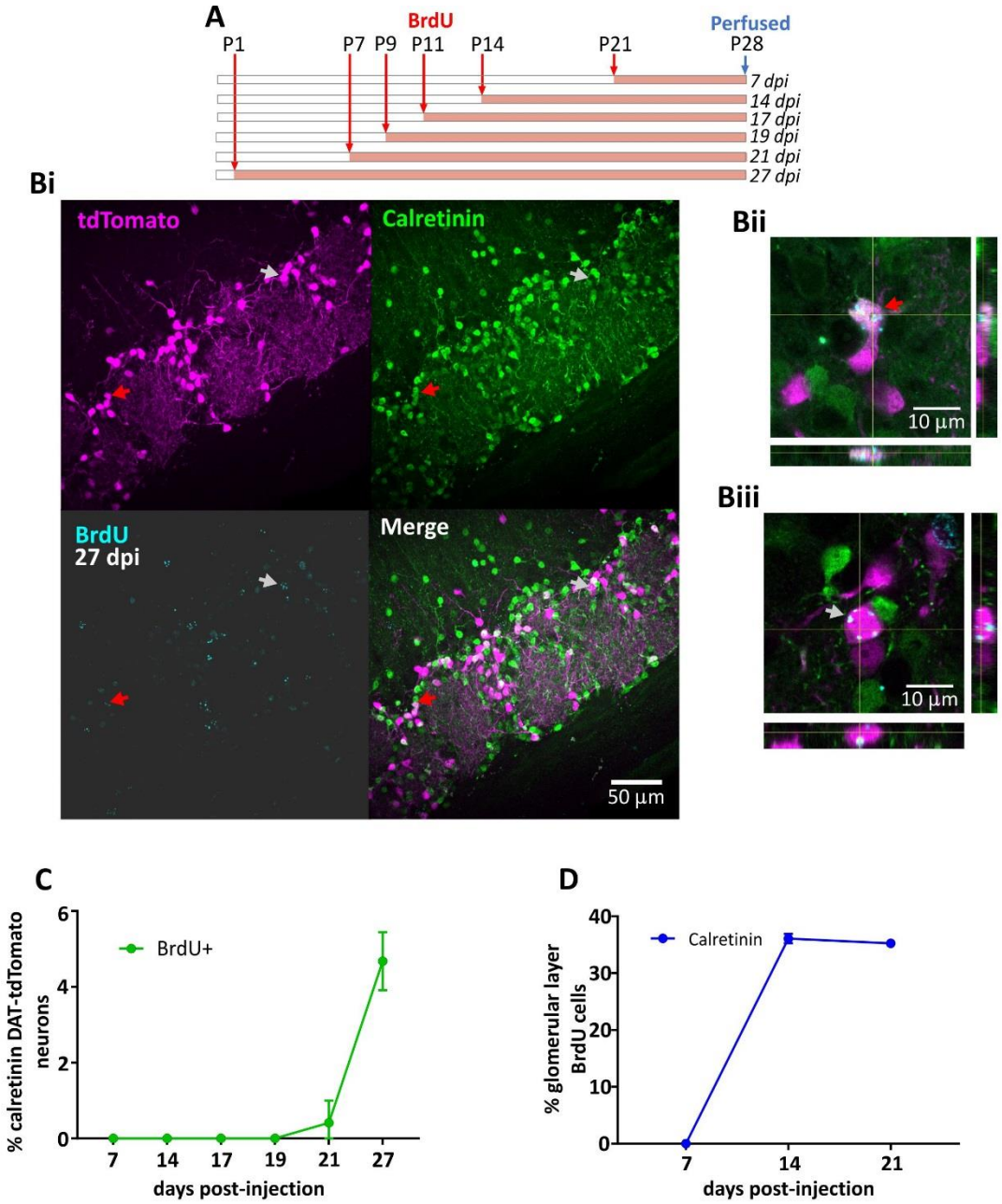

Figure 3.9: Birthdating analysis of calretinin DAT-tdTomato neurons

A: Timeline of BrdU injections.

B: (i) Example maximum intensity projection images showing the expression of calretinin and BrdU in the glomerular layer of the olfactory bulb in a P28 DAT-tdTomato mouse 27 days post-BrdU injection (dpi). Arrows indicate the locations of example BrdU-positive neurons; red = DAT-tdTomato and calretinin-positive neuron; grey = DAT-tdTomato-positive neurons. (ii-iii) Zoomed in and orthogonal view of example cells indicated in Ai.

C-D: Line plots showing the mean percentage ± SEM of (B) calretinin DAT-tdTomato neurons expressing BrdU and (C) BrdU-positive glomerular layer cells expressing calretinin, at specific days post-BrdU injection.

3.2.6 Reducing the activity of DAT-tdTomato neurons with unilateral naris occlusion

The results so far have thoroughly described the population of neurons that are labelled by the $DAT^{IREScre}$ mouse, which have been found to be continuously generated postnatally. These neurons are also likely to be active and receiving input as they are expressing the activity-dependent enzyme, TH. Unilateral naris occlusion has been described as a reliable manipulation to reduce the activity of the olfactory bulb ipsilateral to the occluded naris (Coppola, 2012). However, these studies have only investigated occlusion on a relatively long timescale. I, therefore, investigated whether the activity of DAT-tdTomato neurons had been affected by unilateral naris occlusion after 1 or 3 days.

The immediate early gene, cFos, is a well-known marker of recent neuronal activity. It has previously been shown that there is differential expression of immediate early genes in the olfactory bulb depending on cell type; however, cFos has been reported to label glomerular layer neurons (Bepari et al., 2012). I, therefore, studied the immunofluorescence intensity of cFos in DAT-tdTomato neurons as a measure of activity in these neurons after 1 or 3 days of unilateral naris occlusion or time-matched anaesthetised controls (**Figure 3.10A**). In control mice there was clear co-localisation of cFos with DAT-tdTomato neurons. Occluded mice were found to have significantly lower expression of cFos after both 1 and 3 days of occlusion (normalised immunofluorescence intensity (%) mean ± SEM: 1 day control, 102.5 ± 3.83%, n = 316, N = 2; 1 day occluded, 56.85 ± 2.1%, n = 358, N = 2; 3 day control, 97.53 ± 3.3%, n = 317, N = 2; 3 day occluded, 62.87 ± 2.63%, n = 309, N = 3. Multi-level ANOVA controlling for set variance, effect of manipulation, $F_{(1,1298.36)} = 60.73$, $p < 0.0001$; effect of time, $F_{(1,1298.36)} = 1.4$, $p = 0.24$; effect of manipulation x time interaction, $F_{(1,1299.37)} = 3.4$, $p = 0.07$. Bonferroni post-hoc test comparing control versus occluded (significance at $p < 0.025$): 1 day, $F_{(1,673.45)} = 115.76$, $p < 0.00005$; 3 day, $F_{(1,626)} = 68.56$, $p < 0.00005$) (**Figure 3.10C**). It can be concluded that the activity of DAT-tdTomato neurons is reduced by unilateral naris occlusion and this manipulation can be used to study activity-dependent plasticity in these neurons.

3.2.7 Activity-dependent plasticity of TH in response to odour deprivation

A well-known feature of olfactory bulb dopaminergic neurons is their ability to regulate their expression of TH in an activity-dependent manner, including after unilateral naris occlusion by plug insertion (Baker et al., 1983; Cummings et al., 1997). As I have shown, 1 and 3 days of unilateral naris occlusion is sufficient to reduce the activity of DAT-tdTomato neurons. I, therefore, investigated whether TH expression had started to be affected by the manipulation.

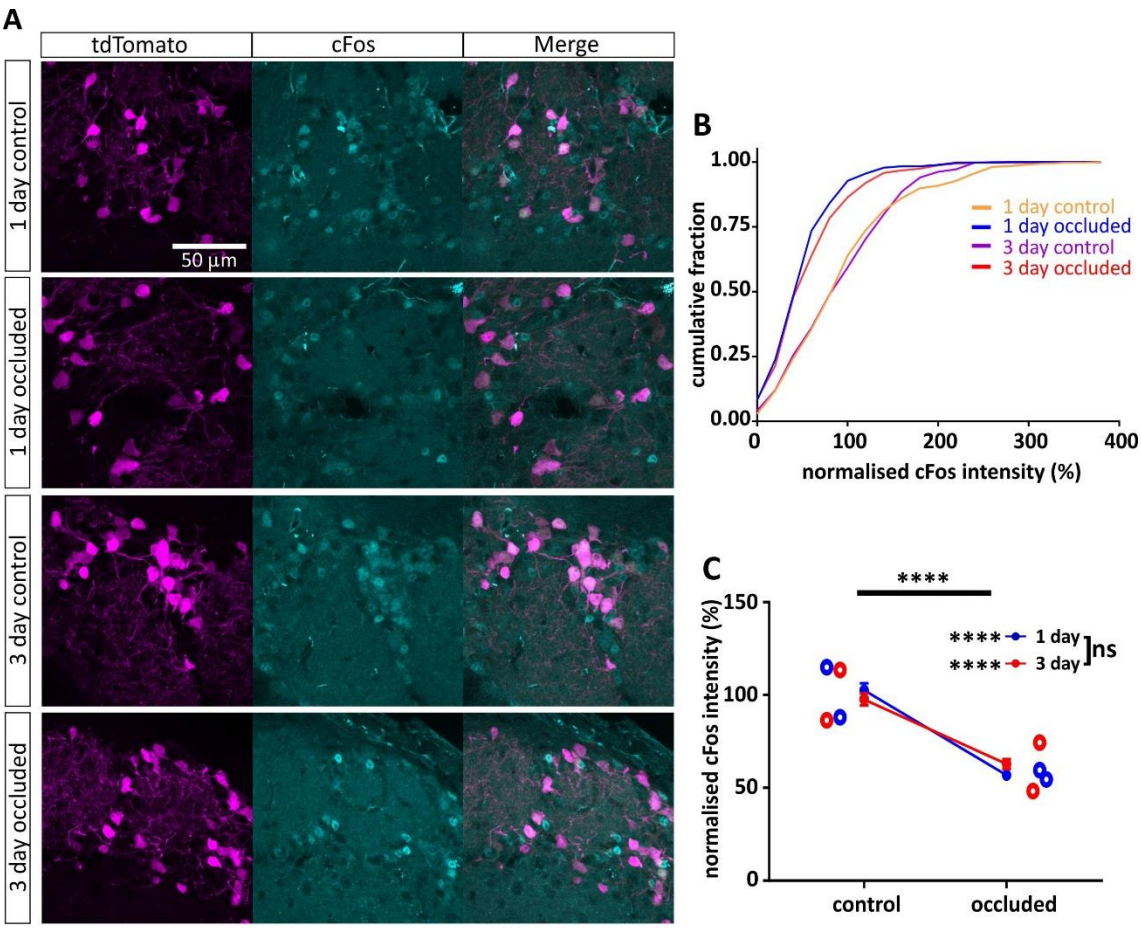

Figure 3.10: 1 and 3 day unilateral naris occlusion reduces cFos expression in DAT-tdTomato neurons

A: Example maximum intensity projection images showing the expression of cFos in the glomerular layer of the olfactory bulb in 1 and 3 day control and occluded DAT-tdTomato mice. All images are from the same set and were imaged with the same settings.

B: Cumulative distribution of normalised cFos intensity (%) in DAT-tdTomato neurons.

C: Line plots showing the mean ± SEM of normalised cFos intensity (%). Multi-level ANOVA controlling for set variance; effect of manipulation, **** $p < 0.0001$; effect of time, ns: non-significant. Bonferroni post-test (significance when $p < 0.025$); 1 day, effect of manipulation, **** $p < 0.00005$; 3 day effect, effect of manipulation, **** $p < 0.00005$. Open circles show the mean cFos intensity (%) for individual mice.

[B-C (n): 1 day control (316); 1 day occluded (358); 3 day control (317); 3 day occluded (309)].

The shortest published example of occlusion affecting TH is work by Young Cho et al. (1996) who reported that 2 days of odour deprivation induced a small, but significant, decrease in *Th* mRNA and a smaller decrease in protein expression. Work by Chand et al. (2015) studying olfactory bulb dopaminergic neurons *in vitro* reported an increase in TH immunofluorescence intensity after only 1 day of elevated activity. I, therefore, used changes in immunofluorescence intensity as a measure of activity-dependent plasticity in TH protein levels after 1 or 3 days of unilateral naris occlusion.

Occlusion was associated with a decrease in the immunofluorescence intensity of TH in DAT-tdTomato neurons after only 1 day, which reduced further after 3 days (**Figure 3.11A-B**). There was a significant interaction between the effects of the manipulation and the duration of the occlusion (normalised immunofluorescence intensity (%) mean ± SEM: 1 day control, 95.27 ± 3.35%, n = 460, N = 3; 1 day occluded, 70.96 ± 3.16%, n = 408, N = 3; 3 day control, 107.3 ± 4.64%, n = 298, N = 2; 3 day occluded, 57 ± 2.32%, n = 461, N = 3. Multi-level ANOVA controlling for set variance, effect of manipulation, $F_{(1,1546.1)} = 2.9$, $p = 0.09$; effect of time, $F_{(1,1625.67)} = 3.1$, $p = 0.08$; effect of manipulation x time interaction, $F_{(1,1612.99)} = 11.67$, $p = 0.001$. Bonferroni post-hoc test comparing control versus occluded (significance at $p < 0.025$): 1 day, $F_{(1,866.98)} = 27.41$, $p < 0.00005$; 3 day, $F_{(1,639.03)} = 76.36$, $p < 0.00005$) (**Figure 3.11C**). These results support the finding of Chand et al (2015) that the activity-dependent expression of TH can occur within 1 day of activity perturbations, but is the first time that downregulation of TH expression has been demonstrated this early *in vivo*. This result is also further evidence for the efficacy of unilateral naris occlusion to reduce the activity of DAT-tdTomato neurons.

TH changes could be underestimated or skewed by the complete disappearance of TH in some cells. However, this is mitigated by identifying cells by the expression of tdTomato. One possibility for reduced TH expression is an increase in the proportion of calretinin DAT-tdTomato neurons after occlusion, which would affect the mean immunofluorescence intensity of all DAT-tdTomato neurons. Accordingly, I calculated whether occlusion had affected the proportion of calretinin DAT-tdTomato neurons. This showed that there was not a significant difference in the proportion of calretinin-positive DAT-tdTomato neurons following occlusion (% of calretinin DAT-tdTomato neurons; 1 day control, 20.95%, n = 506, N = 3; 1 day occluded, 24.5%, n = 502, N = 2; 3 day control, 23.91%, n = 343, N = 2; 3 day occluded, 25%, n = 424, N = 3. Fisher's exact test, effect of manipulation, $p = 0.22$; effect of time, $p = 0.40$) (**Figure 3.11D**). Therefore, the decrease in TH expression is not due to a change in the proportion of DAT-tdTomato neurons that were calretinin-positive.

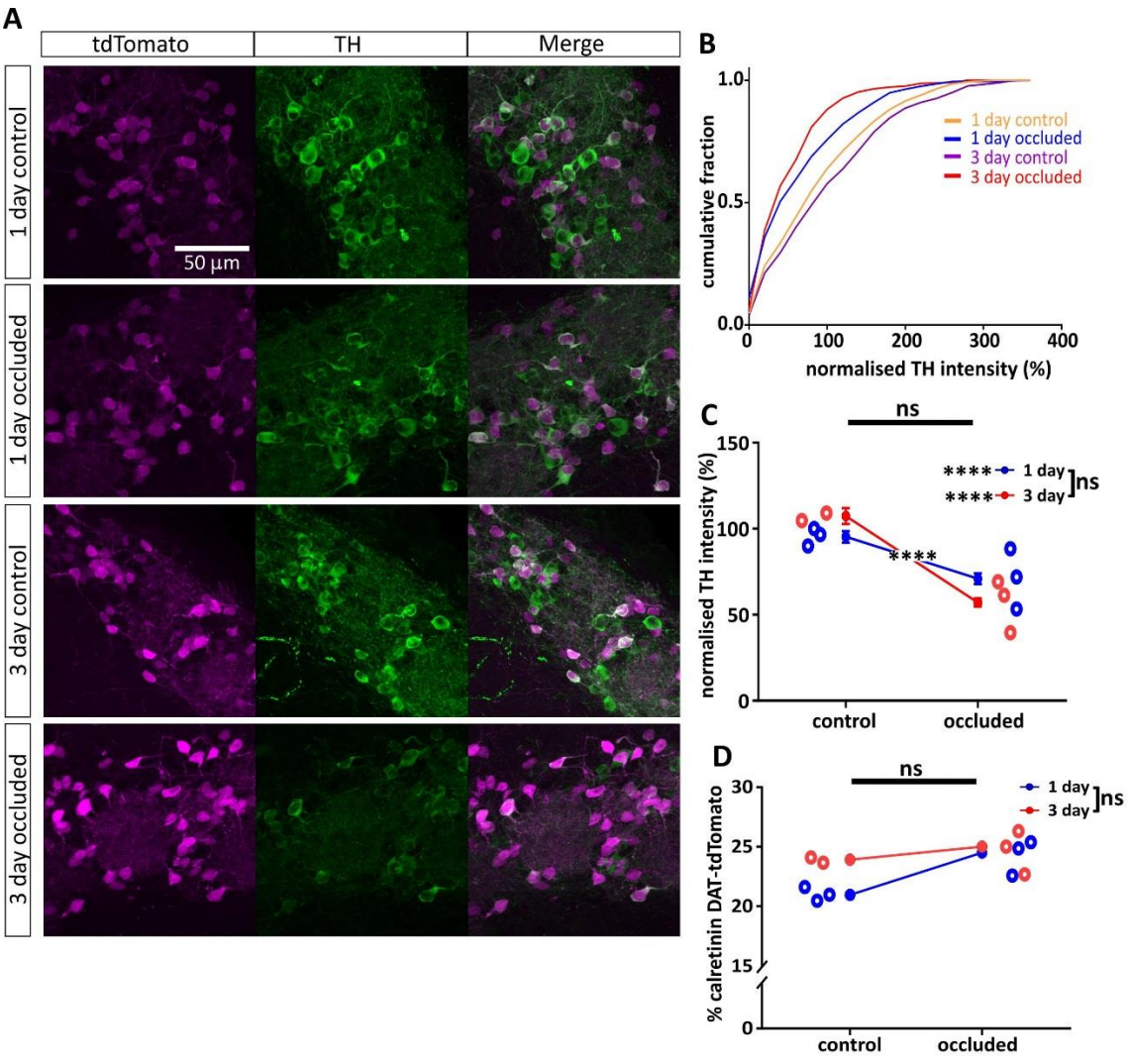

Figure 3.11: 1 and 3 day unilateral naris occlusion reduces TH expression in DAT-tdTomato neurons

A: Example maximum intensity projection images showing the expression of TH in the glomerular layer of the olfactory bulb in 1 and 3 day control and occluded DAT-tdTomato mice. All images are from the same set and were imaged with the same settings.

B: Cumulative distribution of normalised TH intensity (%) in DAT-tdTomato neurons.

C-D: Line plots showing the mean ± SEM of (C) normalised TH intensity (%) and (D) the percentage of calretinin DAT-tdTomato neurons. (C) Multi-level ANOVA controlling for set variance; effect of manipulation x time interaction, **** $p < 0.0001$; effect of manipulation and effect of time, ns: non-significant. Bonferroni post-test (significance when $p < 0.025$); 1 day, effect of manipulation, **** $p < 0.00005$; 3 day effect, effect of manipulation, **** $p < 0.00005$. (D) Fisher's exact test; effect of manipulation and effect of time, ns: non-significant. Open circles show the mean TH intensity (%) or mean % of calretinin DAT-tdTomato neurons for individual mice.

[B-C (n): 1 day control (460); 1 day occluded (408); 3 day control (298); 3 day occluded (461)].

[D (n): 1 day control (506); 1 occluded (502); 3 day control (343); 3 day occluded (424)].

3.2.8 Activity-dependent plasticity of DDC

As TH is the rate-limiting enzyme in the synthesis of dopamine, reduced expression of this protein would impact the ability of DAT-tdTomato neurons to produce L-DOPA. The enzyme DDC synthesises dopamine from L-DOPA, therefore, I investigated whether DDC was also affected by unilateral naris occlusion. Previous work did not find an effect of odour deprivation on *Ddc* mRNA levels in the rat olfactory bulb, 40 days after naris closure (Cave et al., 2010; Stone et al., 1990). Again, I analysed immunofluorescence intensity as a measure of DDC protein expression in DAT-tdTomato neurons after 1 and 3 days of unilateral naris occlusion (**Figure 3.12A-B**).

This analysis revealed that occlusion had a small but significant effect on the immunofluorescence intensity of DDC in DAT-tdTomato neurons. Interestingly, post-hoc tests demonstrated that this effect was being driven by a reduction only after 1 day of occlusion, with expression of DDC in 3 day occluded DAT-tdTomato neurons returning to control levels (immunofluorescence intensity (%) mean ± SEM: 1 day control, 97.99 ± 2.61%, n = 417, N = 2; 1 day occluded, 82.88 ± 2.47%, n = 425, N = 2; 3 day control, 104.2 ± 3.45%, n = 198, N = 1; 3 day occluded, 96.03 ± 2.61%, n = 412, N = 2. Multi-level ANOVA controlling for set variance, effect of manipulation, $F_{(1,452)} = 10.19$, $p = 0.001$; effect of time, $F_{(1,1452)} = 1.95$, $p = 0.16$; effect of manipulation x time interaction, $F_{(1,1452)} = 1.44$, $p = 0.22$. Bonferroni post-hoc test comparing control versus occluded (significance at $p < 0.025$): 1 day, $F_{(1,917)} = 10.3$, $p = 0.001$; 3 day, $F_{(1,535)} = 4.45$, $p = 0.04$) (**Figure 3.12C**). As the activity-dependent changes in DDC expression appear to be transient, it not surprising that Stone et al. (1990) did not see any changes after 40 days of occlusion.

3.2.9 Activity-dependent plasticity of GAD67

Brief unilateral naris occlusion appears to affect the synthesis of dopamine in the olfactory bulb. Olfactory bulb dopaminergic neurons also express GABA synthesising enzymes. Other work has investigated whether the enzyme glutamic acid decarboxylase (GAD), which is involved in the synthesis of GABA, was affected by deafferentation or unilateral naris occlusion (Banerjee et al., 2013; Lau and Murthy, 2012; Parrish-Aungst et al., 2011; Wang et al., 2017). It has been found that only one GAD isoform, GAD67, demonstrates activity-dependent changes in mRNA levels and protein expression by both Bradford protein assay and immunohistochemistry as soon as 7 days after sensory manipulation. The majority of olfactory bulb dopaminergic neurons are known to be positive for GAD67 (Kiyokage et al., 2010), therefore, I investigated whether levels

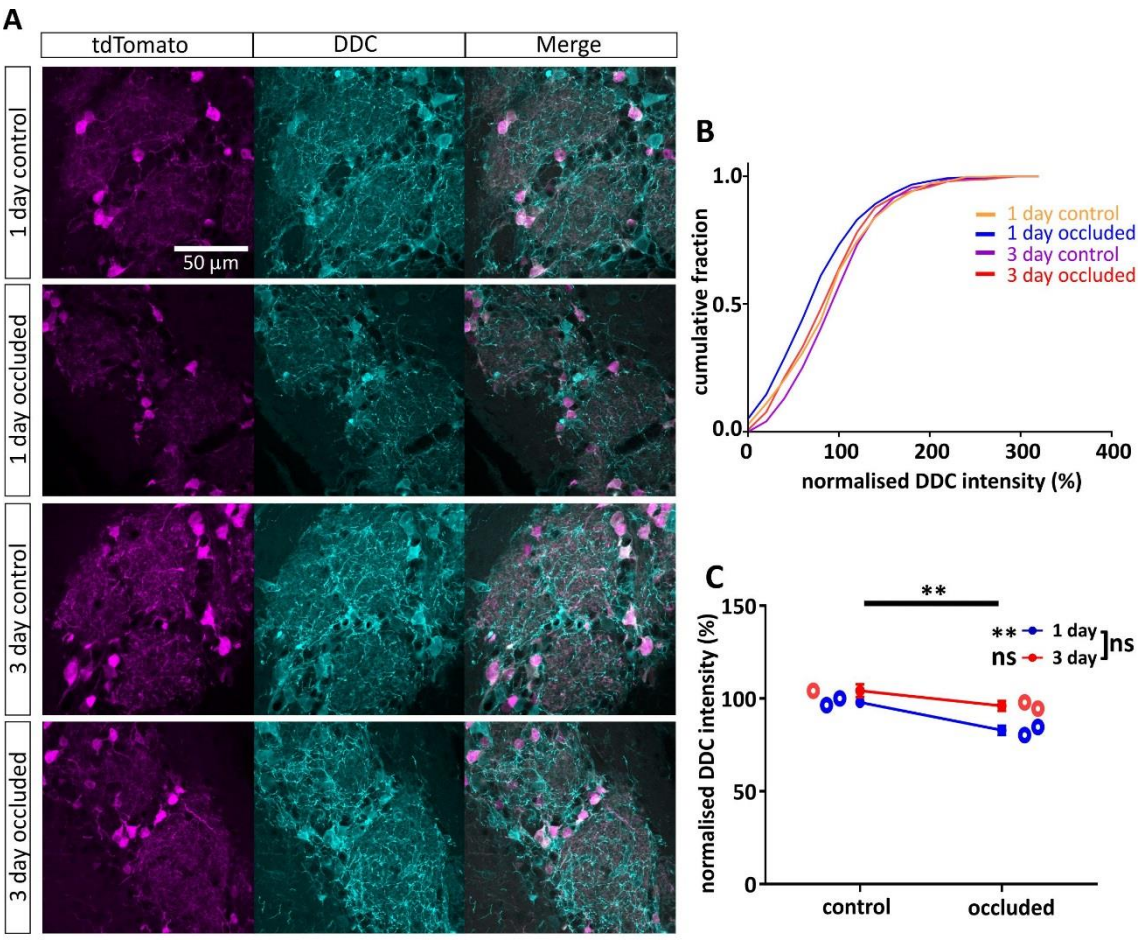

Figure 3.12: DDC expression in DAT-tdTomato neurons is reduced only after 1 day of unilateral naris occlusion

A: Example maximum intensity projection images showing the expression of DDC in the glomerular layer of the olfactory bulb in 1 and 3 day control and occluded DAT-tdTomato mice. All images are from the same set and were imaged with the same settings.

B: Cumulative distribution of normalised DDC intensity (%) in DAT-tdTomato neurons.

C: Line plots showing the mean ± SEM of DDC intensity (%). Multi-level ANOVA controlling for set variance; effect of manipulation, ** $p < 0.01$; effect of time, ns: non-significant. Bonferroni post-test (significance when $p < 0.025$); 1 day, effect of manipulation, ** $p < 0.005$; 3 day, effect of manipulation, ns: non-significant. Open circles show the mean DDC intensity (%) for individual mice.

[B-C (n): 1 day control (417); 1 day occluded (425); 3 day control (198); 3 day occluded (412)].

of this enzyme had been affected by 1 or 3 days of occlusion in DAT-tdTomato neurons by studying immunofluorescence intensity (**Figure 3.13A-B**).

No changes in immunofluorescence intensity of GAD67 in DAT-tdTomato neurons were found after 1 or 3 days of unilateral naris occlusion (immunofluorescence intensity (%) mean ± SEM: 1 day control, 97.43 ± 3.1%, *n* = 261, N = 3; 1 day occluded, 92.93 ± 2.9%, *n* = 314, N = 3; 3 day control, 103.5 ± 3.7%, *n* = 192, N = 2; 3 day occluded, 94.03 ± 2.88%, *n* = 304, N = 3. Multi-level ANOVA controlling for set variance, effect of manipulation, $F_{(1,1071)} = 1.6$, p = 0.21; effect of time, $F_{(1,1071)} = 0.09$, p = 0.77; effect of manipulation x time interaction, $F_{(1,1071)} = 0.62$, p = 0.43) (**Figure 3.13C**). This suggests that 1 and 3 days of unilateral naris occlusion do not change the expression of GAD67 protein in DAT-tdTomato olfactory bulb neurons as measured by immunofluorescence intensity.

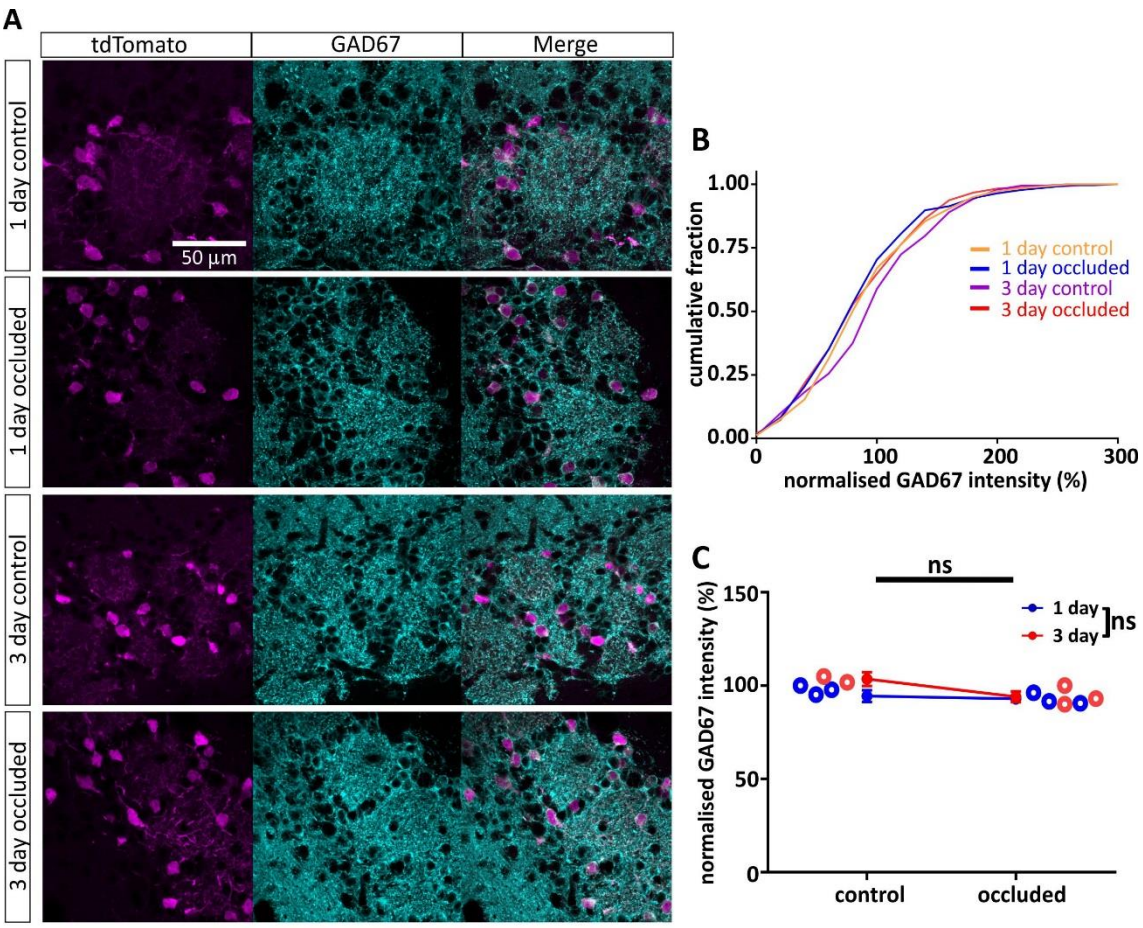

Figure 3.13: 1 and 3 day unilateral naris occlusion does not affect GAD67 expression in DAT-tdTomato neurons

A: Example maximum intensity projection images showing the expression of GAD67 in the glomerular layer of the olfactory bulb in 1 and 3 day control and occluded DAT-tdTomato mice. All images are from the same set and were imaged with the same settings.

B: Cumulative distribution of normalised GAD67 intensity (%) in DAT-tdTomato neurons.

C: Line plots showing the mean ± SEM of normalised GAD67 intensity (%). Multi-level ANOVA controlling for set variance; effect of manipulation and effect of time, ns: non-significant. Open circles show the mean GAD67 intensity (%) for individual mice.

[B-C (n): 1 day control (261); 1 day occluded (314); 3 day control (192); 3 day occluded (304)].

3.3 Discussion

The results in this chapter demonstrate that the majority of olfactory bulb cells labelled in the DAT^{IREScre} mouse are dopaminergic neurons. There is preferential labelling of the small soma size population of dopaminergic neurons that are known to undergo adult neurogenesis. Birthdating analysis revealed that postnatally generated DAT-tdTomato neurons are present at P28, with a minimum age of ~14 days. A subpopulation of non-dopaminergic (calretinin-positive) neurons are also labelled; however, this population can be identified by both immunohistochemistry and electrophysiology and only appear to be generated during early development. The activity of DAT-tdTomato neurons can be reduced by 1 and 3 days of unilateral naris occlusion, which induces activity-dependent changes in enzymes required for the synthesis of dopamine.

3.3.1 The DAT^{IREScre} as a mouse model to label olfactory bulb dopaminergic neurons

The work presented in this chapter has characterised the labelling and maturation of olfactory bulb dopaminergic neurons. The decision to use the DAT^{IREScre} mouse over a TH-Cre mouse was due to reported labelling of neurons outside of the glomerular layer raising issues with dopaminergic specificity in the TH-Cre line (Saino-Saito et al., 2004). In general, labelling dopaminergic neurons using a *Dat* gene driver is considered to be far more selective compared to those using *Th*. Lammel et al. (2015) found that in their DAT-Cre mouse only 4% of labelled neurons in the midbrain did not express TH, compared to 31-52% in different *Th* driver lines. However, this study did not describe the proportion of dopaminergic neurons that were labelled. It is acknowledged that there needs to be strong promoter activity and high Cre expression to get 100% recombination (Wilson and Kola, 2001) It is clear that not all dopaminergic neurons in the olfactory bulb are labelled in this mouse. I found that approximately 1/3 of TH-positive neurons are not tdTomato-positive. Fewer large soma TH-positive neurons are tdTomato-positive and the majority of large soma dopaminergic neurons belong to the axon-bearing subpopulation (Galliano et al., 2018). However, axonic olfactory bulb dopaminergic neurons are still labelled in this mouse line and there is no evidence that they are different to tdTomato-negative axonic olfactory bulb dopaminergic neurons (Galliano et al., 2018). DAT-Cre mice have been used in a number of studies to investigate both subpopulations of olfactory bulb dopaminergic neurons (Banerjee et al., 2015; Galliano et al., 2018).

It is unclear why axonic dopaminergic neurons are underrepresented in the mouse. Unfortunately, the DAT antibody could not be used to identify neurons in the olfactory bulb, therefore, it is not clear whether these neurons are tdTomato-negative because they do not

express (sufficient) *Dat* or recombination could not be achieved. Combining *in situ* hybridisation for *Dat* with immunohistochemistry for tdTomato could help explain the incomplete labelling of dopaminergic neurons in the olfactory bulb, particularly amongst the axonic subpopulation. Outside the olfactory bulb it has been reported that other monoamine transporters can clear dopamine in regions with low DAT expression (Chotibut et al., 2012; Morón et al., 2002). Enzymatic removal of dopamine by COMT has been reported to predominate over DAT activity in the olfactory bulb for clearing released dopamine (Cockerham et al., 2016). Therefore, DAT expression may not be a requirement for olfactory bulb dopaminergic neurons. However, there is sufficient *Dat* activity to drive Cre expression and recombination to permanently label these neurons in the olfactory bulb. Therefore, the DAT$^{IRES cre}$ line labels both subpopulations of olfactory bulb dopaminergic neuron and, despite not being entirely selective, it can be used for the purposes of this project.

3.3.2 Maturation heterogeneity in the dopaminergic population

As a subpopulation of olfactory bulb dopaminergic neurons are continually generated throughout life, it was important to understand the heterogeneity in the maturation of tdTomato-positive neurons in the olfactory bulb. This is particularly important as immature neurons are believed to be more plastic than mature neurons (Lledo et al., 2006). Investigating the maturation of newborn neurons normally involves the administration of cell division markers such as BrdU/EdU at a certain age and waiting for different periods of time before fixation (Bagley et al., 2007). However, I used a different approach and administered BrdU at a range of ages, then analysed the outcome of these different timed pulse injections at the same chase age (P28). Therefore, this gives an insight into the minimum age of DAT-tdTomato neurons at this age. Studying the expression of different dopaminergic markers also allowed me to provide an initial characterisation of the temporal expression of these proteins.

The expression of TH and other markers of glomerular layer interneurons in postnatally generated neurons has been demonstrated as quickly as 7 dpi in adult mice (approximately 8 weeks old) (Bagley et al., 2007). However, I did not find expression of dopaminergic markers or calretinin 7 dpi. Indeed, there were a very small number of BrdU cells in the glomerular layer at 7 dpi. By 14 dpi there was a dramatic increase in BrdU labelled neurons in the glomerular layer and ~1/3 of these neurons were expressing the marker, calretinin. TH and DDC neurons labelled with BrdU were also identifiable 14 dpi, although these account for <1% of their respective populations, with DAT-tdTomato neurons barely present. This suggests that at P28 the most immature DAT-tdTomato neuron will be 14 days old; however, the vast majority of the population will be older than that. Interestingly, the majority of DAT-tdTomato neurons labelled

with BrdU were expressing DDC (~85%), while in the general population ~22% of DAT-tdTomato neurons are not dopaminergic. If the majority of calretinin-positive tdTomato neurons are generated embryonically, this suggests that the DAT-tdTomato mouse becomes more selective for labelling dopaminergic neurons early during postnatal development.

Characterising the label of dopaminergic neurons with the DDC antibody in the general population at P28 showed that virtually every TH-positive neuron (~99%) expresses DDC. Therefore, the higher proportion of BrdU cells expressing DDC (14-21 dpi) likely represent the small population of neurons that only have detectable DDC. As TH expression is activity-dependent, it is possible that some immature dopaminergic neurons have detectable DDC prior to detectable TH or *Ddc* is expressed earlier than *Th*. It is unclear how long of a delay there is from *Dat* expression to tdTomato expression. There would need to be sufficient Cre expression to allow recombination, which can then allow tdTomato expression. A thorough investigation of *Th, Ddc* and *Dat* co-expression would be required in BrdU labelled mice to understand the sequence of expression of these dopaminergic genes. However, there are some assumptions that can be made based on these results:

- Postnatally generated DAT-tdTomato neurons are even more likely to be dopaminergic than calretinin-positive.

- At P28, the most immature DAT-tdTomato neuron is more mature than the most immature TH-positive or DDC-positive neuron.

- DDC expression may be detectable before TH expression and both are detectable before DAT-tdTomato expression. However, it is unclear whether this is due to the time it may take for Cre-lox recombination to drive tdTomato expression.

- The DDC-positive / TH-negative neurons that were identified when characterising the DDC antibody (~11% of the DDC-positive population) may represent immature dopaminergic neurons that have not yet expressed TH.

Overall, the immunohistochemistry results show that the $DAT^{IRES\mathit{cre}}$ mouse labels dopaminergic neurons in the olfactory bulb with reasonable selectivity. These are predominately the axon-lacking subpopulation that is generated throughout life. The birthdating analysis shows that, at P28, the DAT-tdTomato neurons will be more mature than TH and DDC labelled neurons. This suggests that dopaminergic neurons labelled in this mouse are less heterogenous with respect to neuronal identity and maturation than TH or DDC transgenic mice would be and to

the dopaminergic neurons identified by TH or DDC immunohistochemistry at P28. The biggest issue with the DAT-tdTomato label in the juvenile mouse olfactory bulb is the expression of tdTomato in a minority of calretinin-positive glomerular layer interneurons.

3.3.3 Why are a minority of calretinin neurons labelled?

The labelling of calretinin neurons does not appear to be unique to the DAT^{IREScre} mouse. The knock-in DAT-Cre mouse (Zhuang et al., 2005) has also been found to have a fraction of calretinin neurons labelled, though this was not quantified (Ninkovic et al., 2010). It is unclear whether there is transient expression of DAT during the development of calretinin-positive neurons resulting in the permanent effect of Cre-lox recombination or whether DAT expression is a feature of certain calretinin neurons, i.e. do mature calretinin DAT-tdTomato still express DAT? Unfortunately, studying the expression of DAT was not possible due to the DAT antibody not being able to label in the olfactory bulb. Future work could use *in situ* hybridisation to further investigate the expression of *Dat* in this subpopulation. In addition to this, work in my lab has been using single-cell RNA-seq to study the transcriptome of DAT-tdTomato neurons (Marcela Lipovsek). This work has been able to identify two clear populations, one dopaminergic and one calretinin. Preliminary work suggests that some of these calretinin neurons still express *Dat* at P28; however, it is at far lower levels than in the dopaminergic population.

Based on the birthdating experiments, BrdU expression seems to be restricted to calretinin DAT-tdTomato neurons that are generated early postnatally. This is a time period during which there is a peak in the production of olfactory bulb interneurons (Hinds, 1968). BrdU injections during pregnancy would be needed to determine whether these neurons are also generated embryonically. However, it has been found that the majority of calretinin neurons in the glomerular layer are generated postnatally, with very few generated embryonically (Batista-Brito et al., 2008). Therefore, if calretinin-positive tdTomato neurons are not generated after the first postnatal week and there is cell death, the tdTomato population in the adult might be more homogeneously dopaminergic. Recent work has demonstrated that neuronal death within the olfactory bulb is virtually absent (Platel et al., 2018). This suggests that these calretinin DAT-tdTomato neurons will remain in the olfactory bulb; however, their proportion within the total DAT-tdTomato population will be continually diluted over time, as more postnatally-generated and exclusively dopaminergic tdTomato-positive cells join the network.

However, why are calretinin neurons specifically labelled as DAT-tdTomato? Fate-mapping neuronal precursors that generate glomerular layer GABAergic interneurons has demonstrated that the decision to differentiate into a dopaminergic neuron over a calretinin neuron can be

made by just a few transcription factors. Loss of Pax6, Dlx2 or Meis2 reduces the proportion of postnatal dopaminergic neurons that are generated, while increasing the number of calretinin neurons (Agoston et al., 2014; Brill et al., 2008). Overexpression of Dlx2 increases the proportion of dopaminergic neurons and decreases the calretinin population (Brill et al., 2008). The transcription factor ER81 is also expressed in both calretinin and dopaminergic neurons in the glomerular layer and is important for regulating the expression of *Th* (Cave et al., 2010). Therefore, the molecular determinants to become dopaminergic or calretinin appear to be similar between both populations. Further work is needed to understand what factors are important for the expression of *Dat*. It is possible that there may be transcription factors shared between dopaminergic and calretinin neurons that can promote *Dat* expression.

Despite the presence of calretinin-positive DAT-tdTomato neurons, I have demonstrated that these neurons can be identified by immunohistochemistry, electrophysiology and, to an extent, morphology and tdTomato intensity. Therefore, research investigating olfactory bulb dopaminergic neurons should have careful consideration for using this mouse, based on the research question. For example, studying the transcriptome on a population-level would be affected by the presence of the non-dopaminergic population. Immunohistochemistry would also be affected unless staining for calretinin or other dopaminergic markers was used. However, as I have shown the proportion of calretinin-positive DAT-tdTomato neurons is not affected by 1 or 3 days of unilateral naris occlusion. Therefore, activity-dependent results are not due to changes in the proportion of this subpopulation.

3.3.4 The activity of olfactory bulb dopaminergic neurons can be readily manipulated

I found that the activity of DAT-tdTomato neurons could be reduced by 1 and 3 days of unilateral naris occlusion. The expression of cFos is a well-known marker for neuronal activity; however, it is not expressed by every neuron in the mouse olfactory bulb (Bepari et al., 2012). I have shown that DAT-tdTomato neurons express cFos under baseline conditions and this expression is downregulated by unilateral naris occlusion after 1 day and remains low after 3 days. Therefore, the ipsilateral olfactory bulb is being deprived of sensory input, supporting the use of unilateral naris occlusion as an odour deprivation manipulation for DAT-tdTomato neurons. This reduction in activity was further confirmed by the downregulation of TH, which is often used as a marker of occlusion effectiveness (Kass et al., 2013; Wilson and Sullivan, 1995).

Previous work has shown that TH expression is reduced as early as 2 days following odour deprivation (Young Cho et al., 1996). I have built on this work by demonstrating that this activity-dependent plasticity can be observed after only 1 day of occlusion, supporting work that

demonstrates an increase in TH expression after 1 day of increased activity *in vitro* (Chand et al., 2015). The further reduction in TH expression between 1 day and 3 days supports research showing that the downregulation of TH is progressive for approximately 3 weeks after odour deprivation and then stabilises (Bastien-Dionne et al., 2010). There are a number of different mechanisms that have been implicated in the activity-dependent plasticity of TH expression; however, whether all these processes are directly downregulating TH is unknown. There may be one primary mechanism affecting TH expression and the other changes are downstream or separate effects. Activity-dependent changes to DNA secondary structure and epigenetic factors are known to affect TH expression have been demonstrated in response to odour deprivation (Banerjee et al., 2013; Wang et al., 2017). The expression of the transcription factors ER81 and COUP-TFI are both decreased in the mouse olfactory bulb following odour deprivation and are involved in the regulation of TH expression (Bovetti et al., 2013; Cave et al., 2010). On-going work in my lab is to investigate gene expression in single DAT-tdTomato neurons following occlusion, giving important insight into experience-dependent genetic changes (Marcela Lipovsek).

The expression of DDC was also found to be downregulated in response to odour deprivation, but only after 1 day and returned to baseline levels by 3 days. This was a small decrease in expression and is the first reported indication that DDC can be regulated in an activity-dependent manner in the mouse olfactory bulb. Previous work has not identified changes in DDC after longer duration odour deprivation (Cave et al., 2010; Stone et al., 1990). Therefore, downregulation of DDC appears to be a transient process. Expression of DDC in the midbrain has been reported to be affected within a few hours of activation or blockade of dopamine receptors, suggesting that DDC can be modulated by changes in activity (Hadjiconstantinou et al., 1993; Zhu et al., 1993). Further work is needed to confirm whether downregulation of DDC after 1 day of occlusion is a consistent activity-dependent modification, for example, by using mRNA analysis (*in situ* hybridisation or qPCR/RNA-seq) or protein expression (Western blot).

It is interesting that long-term odour deprivation reduces TH expression and does not affect DDC. Both of these enzymes are required for the synthesis of dopamine; however, TH catalyses the rate limiting step. Therefore, regulating TH activity can significantly increase or decrease the production of dopamine most effectively. In other brain regions TH activity is regulated in an activity-dependent manner. *In vitro* cultures of mouse midbrain dopaminergic neurons has demonstrated that the expression of TH is downregulated within 20 hours of activity blockade and upregulated by increased activity (Aumann et al., 2011). This study also found that *in vivo*

manipulations using drugs affect TH activity, but only investigated after 2 weeks and did not report the expression of DDC. TH can also be rapidly (de)phosphorylated, affecting the activity of the enzyme within minutes (Dunkley et al., 2004). It, therefore, appears that the regulation of TH is an important mechanism used by dopaminergic neurons to regulate the synthesis of dopamine.

The expression of the GABA synthesising enzyme, GAD67, has also been reported to be regulated by activity in the olfactory bulb. However, I did not find changes in the expression of GAD67 in DAT-tdTomato neurons after occlusion. This supports work by Baker et al. (1993) and Stone et al. (1991) who did not find activity-dependent changes in GAD expression, from 20 days to 2 months following sensory deprivation; however, these studies did not distinguish between the different GAD isoforms. Parrish-Aungst et al. (2011) found reduced expression of GAD67, but not GAD65, after 7 days of unilateral naris occlusion and deafferentation measuring immunofluorescence intensity in the glomerular layer and protein expression in the entire bulb. Other studies also support this result, showing decreased expression in mRNA and protein expression and immunofluorescence intensity following chemical deafferentation (Lau and Murthy, 2012) and unilateral naris occlusion (Banerjee et al., 2013; Wang et al., 2017). However, these studies used longer duration manipulations and did not distinguish between different neuronal populations in the olfactory bulb. The decrease in GAD67 was also smaller than that in TH (Banerjee et al., 2013; Parrish-Aungst et al., 2011; Wang et al., 2017). Therefore, 1 or 3 days of unilateral naris occlusion may not be sufficient to induce activity-dependent changes in GAD67; measures based on immunofluorescence intensity may not be sensitive enough to always detect changes in GAD67; and/or these changes are driven in neurons not labelled by the DAT-tdTomato mouse. However, total GAD67 immunofluorescence in the olfactory bulb of 1 or 3 day occluded mice did not appear to be different based on a qualitative examination of the coronal sections. Other work in my lab using deafferentation of OSNs by administration of methimazole in adult mice (a process that leads to reduced olfactory bulb input over weeks) was also not found to affect GAD67 expression (Andres Crespo and Victoria Wong, *unpublished data*).

Studying changes in immunofluorescence intensity is not the optimal method for investigating activity-dependent plasticity in protein expression. Results can be confounded by variability in duration of immunohistochemistry steps, the concentration of antibodies and image acquisition settings. However, in this experiment every step was designed to control and normalise for between-section factors that could affect the immunofluorescence intensity. Further work could investigate changes in gene expression and protein levels by dissociating occluded and control

olfactory bulbs and fluorescently sorting DAT-tdTomato neurons. This allows these changes to be studied in a defined population, as opposed to studying the entire olfactory bulb (for example, Banerjee et al., 2013; Parrish-Aungst et al., 2011).

Nevertheless, the results presented in this chapter give an important first indication that the activity of DAT-tdTomato neurons is reduced by 1 and 3 days of unilateral naris occlusion and can show activity-dependent plasticity. How the intrinsic functional properties of these neurons are affected will be explored in the next chapter.

Chapter Four – Intrinsic plasticity of olfactory bulb dopaminergic neurons

4.1 Introduction

4.1.1 Intrinsic plasticity of interneurons in response to activity deprivation

The translation of synaptic input to neuronal output is determined by the functional intrinsic properties of neurons. There is a large body of evidence that a neuron's intrinsic excitability can be regulated in an activity-dependent manner. This is unsurprising given the array of functional processes involved in regulating the excitability of a neuron, ranging from the number, density and distribution of channels in the membrane, to the kinetics of these channels, which all have the potential to be modified by activity.

Work done *in vitro* has shown that chronic activity block by TTX decreased the threshold for action potential firing of pyramidal neurons from the visual cortex through increased inward sodium currents and reduced outwards currents (Desai et al., 1999a). This early work demonstrated that neurons can modify their excitability in an activity-dependent manner by regulating voltage-dependent conductances. However, these processes are slow and cumulative and require hours or days to produce observable changes (Desai et al., 1999a). Subsequent research has shown that a variety of neurons throughout the brain are capable of regulating their intrinsic excitability in response to changes in activity, including GABAergic neurons following activity deprivation.

Research studying intrinsic plasticity in GABAergic neurons has revealed a diversity of activity-dependent changes. Some GABAergic neurons show a decrease in excitability following manipulations that reduce activity *ex vivo* (TTX treatment) (Maffei and Turrigiano, 2008) or *in vivo* (monocular deprivation and whisker trimming) (Shim et al., 2016; Sun, 2009). This decrease in excitability can act to shift the excitation-inhibition balance in favour of network excitation, with some being mediated by specific changes to underlying channels including HCN and potassium channels (Maffei and Turrigiano, 2008; Shim et al., 2016; Sun, 2009). However, other inhibitory neurons can demonstrate an increase in excitability following activity block, which may be offset at the network level by changes in synaptic input or a concomitant increase in excitability in excitatory neurons (Bartley et al., 2008; Desai et al., 1999b; Gibson et al., 2006). Other work has shown that inhibitory neurons can have an initial drop in excitability that then recovers to baseline levels (Hengen et al., 2013; Kuhlman et al., 2013). Therefore,

activity-dependent responses to changes in activity in inhibitory neurons are complex and diverse and can vary over time.

4.1.2 Intrinsic properties of olfactory bulb dopaminergic neurons

Despite the acceptance of two main subtypes of dopaminergic neuron in the olfactory bulb (see Introduction 1.2.4), the majority of the work studying the electrophysiological properties of these neurons has treated them as a single population. This work has shown that these neurons have pacemaker activity that is driven by a persistent sodium current and a T-type calcium current and their resting membrane potential is regulated by the hyperpolarisation-activated current (I_h) and the inward-rectifier potassium (KIR) current (Borin et al., 2014; Pignatelli et al., 2005, 2013). Recent work by Galliano et al., (2018) has started to address the heterogeneity in this population. By studying the rising phase of the single action potential recorded somatically, it is possible to ascertain whether the spike has been generated at the soma or distal to the soma, in the latter case most often at the axon initial segment (AIS) (Chand et al., 2015; Galliano et al., 2018). Galliano et al. (2018) has demonstrated that dopaminergic neurons with an axon have greater intrinsic excitability than the anaxonic subpopulation, initiating action potentials faster and to lower amplitude somatic current injection and firing more action potentials in response to longer somatic current injections. The clear functional difference in the excitability of these neurons further supports the need to investigate these dopaminergic neurons as separate populations, especially when characterising activity-dependent alterations.

Increasing activity of both olfactory bulb dopaminergic neuron subpopulations *in vitro* does not produce significant activity-dependent changes in action potential properties, despite the same chronic depolarising stimulus producing structural plasticity of the AIS (Chand et al., 2015). However, preliminary work from my lab has found that after 1 day of unilateral naris occlusion *in vivo*, both populations of olfactory bulb dopaminergic neuron show decreased excitability, firing fewer action potentials to prolonged current injection, in particular the axonic population. The axonic subpopulation also shows structural plasticity, with the AIS shortening its length (Galliano et al., *in preparation*). Therefore, olfactory bulb dopaminergic neurons can show functional plasticity changes in response to activity deprivation, in addition to experience-dependent changes in gene expression (Chapter 3 and (Baker et al., 1983; Cummings et al., 1997; Young Cho et al., 1996)).

However, it is unknown what effect occlusion has on other intrinsic properties of olfactory bulb dopaminergic neurons that could be modulated in an activity-dependent manner, in particular I_h, which is known to be plastic. This current has been found to be modified in response to

decreased activity in other neuronal populations, affecting excitability (Breton and Stuart, 2009; Shim et al., 2016). It is also uncertain how longer duration activity deprivation affects the intrinsic properties of olfactory bulb dopaminergic neuron.

4.1.3 Chapter aims

In this chapter, I will investigate whether there is functional experience-dependent plasticity in olfactory bulb dopaminergic neurons after 1 or 3 days of unilateral naris occlusion. Using patch-clamp electrophysiology in acute slices of the DAT-tdTomato mouse, I will specifically target the main subpopulation of dopaminergic neurons labelled in this mouse, the small soma size population that lack an axon. I will record membrane properties, spike firing characteristics and sag potential (a current-clamp proxy for I_h) that will provide a broad and highly quantitative characterisation of the functional intrinsic plasticity of these neurons.

4.2 Results

4.2.1 Targeting DAT-tdTomato neurons in acute slices

Olfactory bulb dopaminergic neurons were targeted for electrophysiology in acute slices by the Cre-dependent expression of tdTomato under the DAT promoter (**Figure 4.1A**). As previously discussed, the dopaminergic subpopulation of DAT-tdTomato positive olfactory bulb neurons have a slightly larger soma area and brighter fluorescence than the subpopulation of calretinin neurons labelled in this mouse (see Figure 3.1). Therefore, neurons with a small soma and dim fluorescence were not targeted for patching. In addition, any calretinin cell that was accidently patched could be identified by their inability to fire multiple action potentials (see Figure 3.4). I also avoided targeting DAT-tdTomato neurons with a very large soma as these were more likely to belong to the subpopulation of axon-bearing dopaminergic neuron that are underrepresented in this mouse model (Galliano et al., 2018). Moreover, dopaminergic neurons with an axon could be identified and excluded from analysis by studying the rising phase of the action potential. By plotting the phase plane plot of action potential voltage versus its rate-of-rise, neurons can be classified as having an axon or not based on the presence or absence of a double-peaked waveform, respectively (**Figure 4.1B-C**). This biphasic waveform is a result of the action potential initiating distal to the soma, most often at the AIS where a dense concentration of sodium channels open. The monophasic waveform indicates initiation of an action potential at the recording site, indicating the absence of an AIS (Chand et al., 2015; Galliano et al., 2018).

4.2.2 Passive properties

To isolate the functional intrinsic properties of these neurons, all recordings were obtained in the presence of glutamatergic and GABAergic synaptic blockers (50 µM APV, 10 µM NBQX and 10 µM Gabazine). Pacemaker activity is a well-described feature of these neurons (Pignatelli et al., 2005) and at times, spontaneous spiking could be identified while forming a seal; however, this often slowed down or stopped when the seal was formed or when the voltage clamp was being brought to -60 mV. Due to the irregularity of this spontaneous activity and its sensitivity to seal conditions, I did not study this feature of these neurons.

Immediately following membrane rupture, the resting membrane potential was recorded at $I = 0$ in current-clamp. This was performed quickly to reduce the effect that dialysing the neuron with intracellular recording solution would have on resting membrane potential. As these

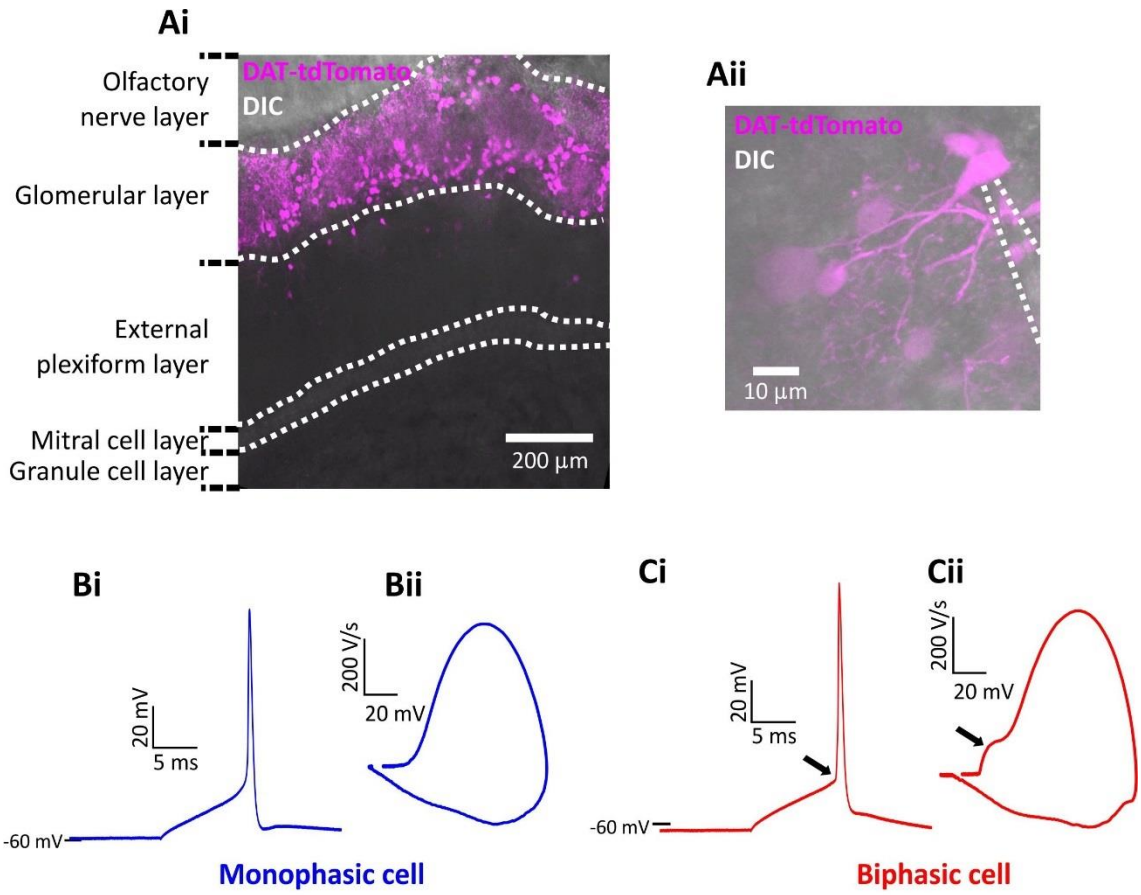

Figure 4.1: Targeting olfactory bulb dopaminergic neurons without an axon

Ai-ii: Example maximum intensity projection images of DAT-tdTomato expression. (i) Horizontal acute olfactory bulb slice showing expression highly restricted to the glomerular layer. (ii) DAT-tdTomato neuron targeted for electrophysiology, dashed white lines indicate location of pipette.

B-C: Example current-clamp traces of single action potentials fired by (B) monophasic and (C) biphasic cells. (i) Action potentials fired to threshold 10 ms somatic current injection. (ii) Phase plane plots of the spikes shown in (i). Arrow points to the AIS-dependent first action potential phase.

neurons could show spontaneous activity (**Figure 4.2A**), resting membrane potential was only recorded in neurons that were silent at $I = 0$. Though not significant, there was a trend for naris occlusion to be associated with an increase in spontaneous firing activity at $I = 0$ (% of neurons that fired at least one spontaneous action potential: 1 day control, 7.5% $n = 40$; 1 day occluded, 22.6% $n = 31$; 3 day control, 12% $n = 25$; 3 day occluded, 17.5% $n = 40$. Fisher's exact test, effect of manipulation, $p = 0.10$; effect of time, $p > 0.99$) (**Figure 4.2B**). This could suggest that occlusion depolarises the resting membrane potential of these neurons, bringing them closer to threshold. However, there was no effect of occlusion on resting membrane potential in silent neurons (mean ± SEM: 1 day control, -70.1 ± 1.23 mV, $n = 37$; 1 day occluded, -72.23 ± 1.43 mV, $n = 24$; 3 day control, -70.34 ± 1.46 mV, $n = 22$; 3 day occluded, -70.02 ± 1.3 mV, $n = 40$. Two-way ANOVA, effect of manipulation, $F_{(1,112)} = 0.44$, $p = 0.51$; effect of time, $F_{(1,112)} = 0.51$, $p = 0.48$; effect of manipulation x time interaction, $F_{(1,112)} = 0.79$, $p = 0.38$) (**Figure 4.2C**).

Passive membrane properties, specifically input resistance (R_I) and membrane capacitance (C_M), were measured by averaging responses to ± 10 mV voltage steps from the holding potential of -60 mV in voltage clamp. There was no difference in C_M following occlusion (mean ± SEM: 1 day control, 25.09 ± 1.23 pF, $n = 41$; 1 day occluded, 26.95 ± 1.57 pF, $n = 34$; 3 day control, 26.55 ± 1.54 pF, $n = 26$; 3 day occluded, 27.56 ± 1.21 pF, $n = 44$. Two-way ANOVA, effect of manipulation, $F_{(1,141)} = 1.06$, $p = 0.30$; effect of time, $F_{(1,141)} = 0.55$, $p = 0.46$; effect of manipulation x time interaction, $F_{(1,141)} = 0.09$, $p = 0.76$) (**Figure 4.2D**).

Activity-dependent changes in R_I have been shown *in vitro* and *in vivo* (Grubb and Burrone, 2010; Rosenkranz and Grace, 2002). However, in olfactory bulb dopaminergic neurons there was no effect of occlusion on R_I (median [with interquartile range]: 1 day control, 889.5 [512.8 – 1391] MΩ, $n = 41$; 1 day occluded, 708.3 [544.6 – 1287] MΩ, $n = 34$; 3 day control, 817.8 [610 – 1267] MΩ, $n = 26$; 3 day occluded, 1033 [690.4 – 1450] MΩ , $n = 44$. Two-way ANOVA on ranks, effect of manipulation, $F_{(1,141)} < 0.01$, $p = 0.98$; effect of time, $F_{(1,141)} = 1.62$, $p = 0.21$; effect of manipulation x time interaction, $F_{(1,141)} = 0.94$, $p = 0.34$) (**Figure 4.2E**). No changes in R_I were seen *in vitro* following 1 day of chronic depolarisation stimulation of olfactory bulb dopaminergic neurons (Chand et al., 2015).

No significant differences were found for series resistance (R_S) between any of the groups (mean ± SEM: 1 day control, 22.21 ± 0.57 MΩ, $n = 41$; 1 day occluded, 21.71 ± 0.55 MΩ, $n = 34$; 3 day control, 23.16 ± 0.66 MΩ, $n = 26$; 3 day occluded, 22.27 ± 0.45 MΩ , $n = 44$. Two-way

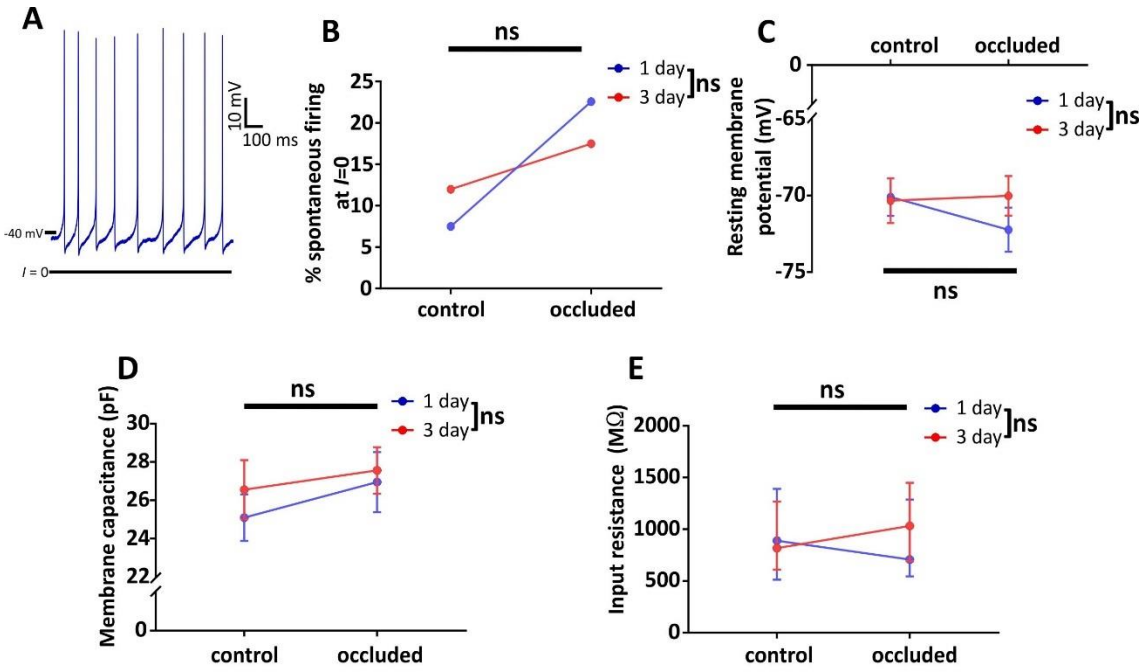

Figure 4.2: Passive properties are not affected by occlusion

A: Example trace of spontaneous firing at *I* = 0 in a 1 day occluded monophasic DAT-tdTomato neuron.

B: Line plots show the percentage of monophasic DAT-tdTomato neurons that were spontaneously active at I=0. Fisher's exact test; effect of manipulation, ns: non-significant; effect of time, ns: non-significant.

C-E: Line plots show the mean ± SEM of the (C) resting membrane potential (mV) and (D) membrane capacitance (pF) and (E) the median ± interquartile range of the input resistance (MΩ). (C- D) Two-way ANOVA; effect of manipulation, ns: non-significant; effect of time, ns: non-significant. (E) Two-way ANOVA on ranks; effect of manipulation, ns: non-significant; effect of time, ns: non-significant.

[B-E (n): 1 day control (41); 1 day occluded (34); 3 day control (26); 3 day occluded (44)].

ANOVA, effect of manipulation, $F_{(1,141)} = 1.56$, p = 0.21; effect of time, $F_{(1,141)} = 1.84$, p = 0.18; effect of manipulation x time interaction, $F_{(1,141)} = 0.11$, p = 0.74).

4.2.3 Single action potential

To study the properties of action potential firing following 1 or 3 days of unilateral naris occlusion, I used current-clamp protocols of both short (10 ms) and long (500 ms) duration, injecting current steps of increasing amplitude. An action potential was identified as a spike with maximum voltage greater than 0 mV. To study the properties of single action potentials, I first injected Δ+5 pA current steps of 10 ms duration until a single action potential was fired (**Figure 4.3A**).

A number of currents and associated channels control the precise waveform of a given cell's action potential. The opening of voltage-gated sodium channels is a major determinant of action potential initiation and upstroke. Voltage threshold was unchanged following occlusion (mean ± SEM: 1 day control, -32.74 ± 0.92 mV, $n = 20$; 1 day occluded, -32.76 ± 0.81 mV, $n = 17$; 3 day control, -33.36 ± 0.85 mV, $n = 10$; 3 day occluded, -33.16 ± 0.64 mV, $n = 15$. Two-way ANOVA, effect of manipulation, $F_{(1,58)} = 0.44$, p = 0.51; effect of time, $F_{(1,58)} = 0.51$, p = 0.48; effect of manipulation x time interaction, $F_{(1,58)} = 0.79$, p = 0.38) (**Figure 4.3B**). The steepest portion of the action potential upstroke is calculated as the maximum rate of rise and reflects maximal sodium ion flow. Again, this was not affected by naris occlusion (mean ± SEM: 1 day control, 591.6 ± 32.74 V/s, $n = 20$; 1 day occluded, 525.6 ± 27.24 V/s, $n = 17$; 3 day control, 550 ± 36.33 V/s, $n = 10$; 3 day occluded, 550 ± 28.97 V/s, $n = 15$. Two-way ANOVA, effect of manipulation, $F_{(1,58)} = 1.01$, p = 0.32; effect of time, $F_{(1,58)} = 1.01$, p = 0.32; effect of manipulation x time interaction, $F_{(1,58)} = 0.07$, p = 0.79) (**Figure 4.3C**).

As sodium channels begin to inactivate, the action potential reaches its peak and outward potassium ion flow is now the major conductance through potassium channels activated by the depolarisation. Changes to these channels affect the repolarisation phase of the action potential. I, therefore, studied the width at half-height, calculated as the width (ms) of the action potential half-way between the voltage threshold and the maximum voltage. No differences were found in this measure following occlusion (mean ± SEM: 1 day control, 0.35 ± 0.02 ms, $n = 20$; 1 day occluded, 0.39 ± 0.02 ms, $n = 17$; 3 day control, 0.4 ± 0.2 ms, $n = 10$; 3 day occluded, 0.38 ± 0.02 ms, $n = 15$. Two-way ANOVA, effect of manipulation, $F_{(1,58)} = 0.15$, p = 0.70; effect of

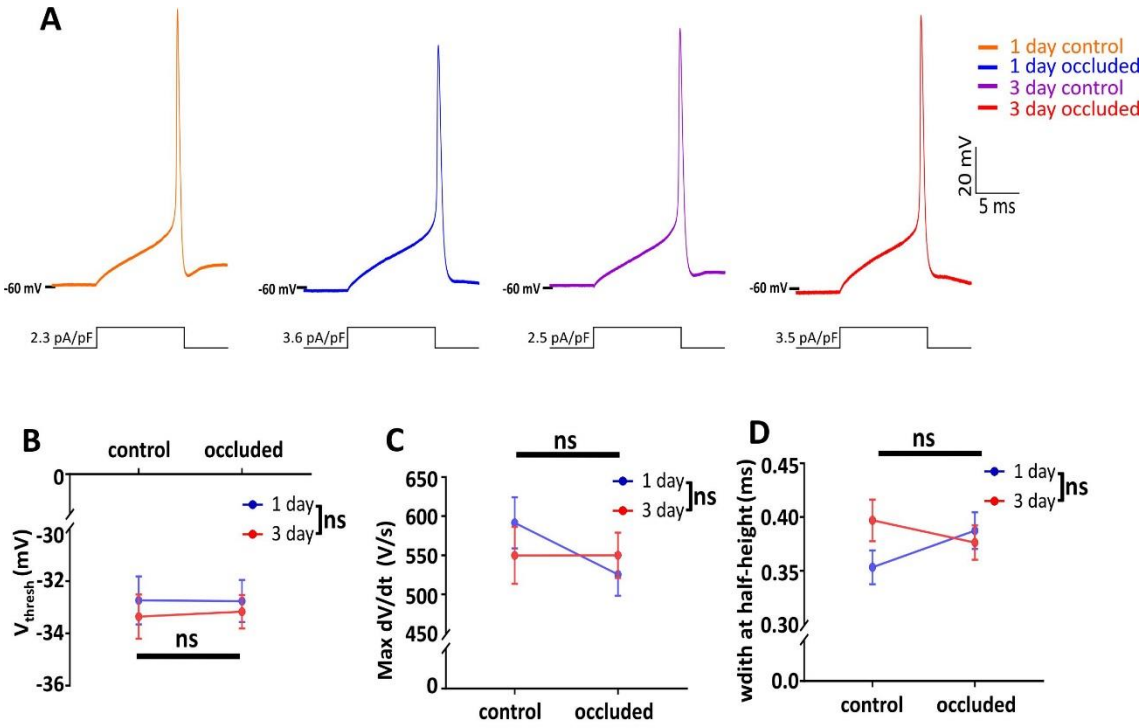

Figure 4.3: Single action potential properties are not affected by occlusion

A: Example traces of monophasic single action potentials fired to threshold 10 ms somatic current injection in 1 and 3 day control and occluded DAT-tdTomato neurons.

B-D: Mean ± SEM of (B) voltage threshold (V_{thresh}) (mV), (C) rate of rise (max *dV/dt*) (V/s) and (D) action potential width at half-height (ms). Two-way ANOVA; effect of manipulation, ns: non-significant; effect of time, ns: non-significant**.**

[B-D (n): 1 day control (20); 1 day occluded (17); 3 day control (10); 3 day occluded (15)].

time, $F_{(1,58)} = 0.86$, $p = 0.36$; effect of manipulation x time interaction, $F_{(1,58)} = 2.42$, $p = 0.13$) (**Figure 4.3D**).

I also studied the properties of the first action potential generated in response to Δ+5 pA current injection steps with a longer, 500 ms duration (**Figure 4.4A**). Rheobase was calculated as the minimal current amplitude required to generate an action potential in response to depolarisation steps lasting 500 ms. This was not different following occlusion (mean ± SEM: 1 day control, 22.45 ± 3.47 pA, $n = 20$; 1 day occluded, 21.56 ± 4.34 pA, $n = 18$; 3 day control, 15.42 ± 2.57 pA, $n = 12$; 3 day occluded, 13.52 ± 2.27 pA, $n = 21$. Two-way ANOVA on $\log_{10}$ transformed data, effect of manipulation, $F_{(1,67)} = 1.12$, $p = 0.29$; effect of time, $F_{(1,67)} = 2.52$, $p = 0.12$; effect of manipulation x time interaction, $F_{(1,67)} = 0.14$, $p = 0.71$) (**Figure 4.4B**).

I investigated whether there was a change in the delay from stimulus onset to the peak of the first action potential. It has been previously shown that the channel involved in regulating this delay (Kv1.1) can undergo activity-dependent changes in expression (Dehorter et al., 2015). When plotted there appeared to be a trend for a reduced delay following occlusion; however, this effect was not significant (mean ± SEM: 1 day control, 138.4 ± 20.24 ms, $n = 20$; 1 day occluded, 125.6 ± 14.7 ms, $n = 18$; 3 day control, 138.8 ± 16.78 ms, $n = 12$; 3 day occluded, 100.5 ± 8.34 ms, $n = 21$. Two-way ANOVA on $\log_{10}$ transformed data, effect of manipulation, $F_{(1,67)} = 1.76$, $p = 0.19$; effect of time, $F_{(1,67)} < 0.01$, $p = 0.99$; effect of manipulation x time interaction, $F_{(1,67)} = 1.21$, $p = 0.28$) (**Figure 4.4C**).

Based on the results obtained so far, there does not appear to be an effect of occlusion on the initiation or waveform of the action potential. During the repolarising phase of an action potential, the membrane potential of the neuron can be briefly taken to more hyperpolarised levels than the normal resting potential, before it recovers. This is known as the afterhyperpolarisation (AHP) and has been described as a feedback mechanism that plays an important modulatory role on consequent action potentials and the pattern of neuronal firing (Duménieu et al., 2015; Matthews et al., 2008). Different AHPs have been described, identified as fast, medium and slow. These vary based on their temporal dynamics, which in turn depend on the identity and kinetics of the currents regulating them (Kimm et al., 2015; Stackman et al., 2002; Tzingounis and Nicoll, 2008).

The AHP following a single action potential is mostly the fast AHP, which lasts up to 5 ms, and is generated by the calcium and voltage-dependent BK channel (Storm, 1987). The fast AHP was

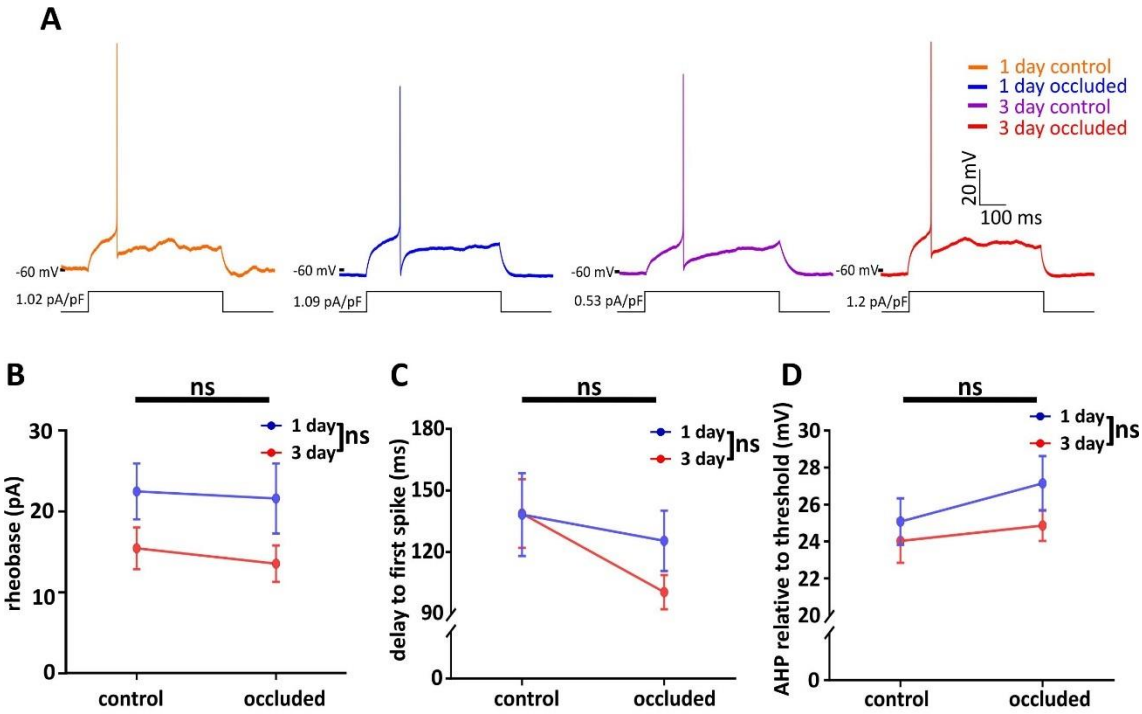

Figure 4.4: The first action potential during 500 ms current injection of increasing amplitude is not affected by occlusion

A: Example traces of the first action potential elicited during 500 ms current injections of increasing amplitude in 1 and 3 day control and occluded DAT-tdTomato monophasic neurons. **B-D:** Mean ± SEM of the (B) rheobase (pA), (C) delay to first spike (ms) and (D) amplitude of the afterhyperpolarisation relative to the action potential threshold (mV). (B-C) Two-way ANOVA on $\log_{10}$ transformed data; effect of manipulation and time, ns: non-significant. (D) Two-way ANOVA; effect of manipulation and time, ns: non-significant.

[B-D (n): 1 day control (20); 1 day occluded (18); 3 day control (12); 3 day occluded (21)].

calculated from the first action potential generated by the longer duration (500 ms) protocol as the difference between the voltage threshold and the most negative potential obtained during the repolarisation phase. There was no difference in the fast AHP following occlusion (mean ± SEM: 1 day control, 25.07 ± 1.27 mV, $n = 20$; 1 day occluded, 27.14 ± 1.48 mV, $n = 18$; 3 day control, 24.02 ± 1.18 mV, $n = 12$; 3 day occluded, 24.86 ± 0.83 mV, $n = 21$. Two-way ANOVA, effect of manipulation, $F_{(1,67)} = 1.37$, $p = 0.25$; effect of time, $F_{(1,67)} = 1.79$, $p = 0.19$; effect of manipulation x time interaction, $F_{(1,67)} = 0.24$, $p = 0.62$) (**Figure 4.4D**).

These results indicate that the single action potential is unchanged after 1 and 3 days of unilateral naris occlusion in monophasic olfactory bulb DAT-tdTomato neurons.

4.2.4 Multiple action potential firing

Despite no differences in the single action potential, occlusion could affect the ability of a neuron to fire multiple action potentials. Changes to the input-output of olfactory bulb dopaminergic neurons could potentially alter their release of GABA and dopamine, strongly affecting network behaviour in glomeruli. Repetitive spiking has been shown to be changed in an activity-dependent manner *in vitro* (Desai et al., 1999a; Grubb and Burrone, 2010) and *ex vivo* (Maffei and Turrigiano, 2008). To investigate this, repetitive firing was induced by injecting Δ+5 pA current steps for 500 ms (**Figure 4.5A**). This was continued until the neuron had reached maximal firing rate and depolarisation block had begun.

Comparing the maximum number of spikes fired following occlusion did not show any significant differences between treatment groups or times (mean ± SEM: 1 day control, 37 ± 3, $n = 24$; 1 day occluded, 32 ± 3, $n = 21$; 3 day control, 33 ± 3, $n = 13$; 3 day occluded, 31 ± 2, $n = 21$. Two-way ANOVA, effect of manipulation, $F_{(1,75)} = 1.81$, $p = 0.18$; effect of time, $F_{(1,75)} = 0.83$, $p = 0.37$; effect of manipulation x time interaction, $F_{(1,75)} = 0.48$, $p = 0.49$) (**Figure 4.5B**). However, this analysis does not identify whether there are more subtle changes in the spiking output of the neuron in response to input.

To investigate potential changes in the input-output relationship of these neurons in response to occlusion, the number of spikes evoked by a given injected current density (pA/pF) was plotted. As expected, the number of action potentials increased as the current density increased. When plotted, 1 day occluded neurons showed a slight trend to reduced excitability (**Figure 4.5C**). Analysis showed that the effect of manipulation and time were approaching

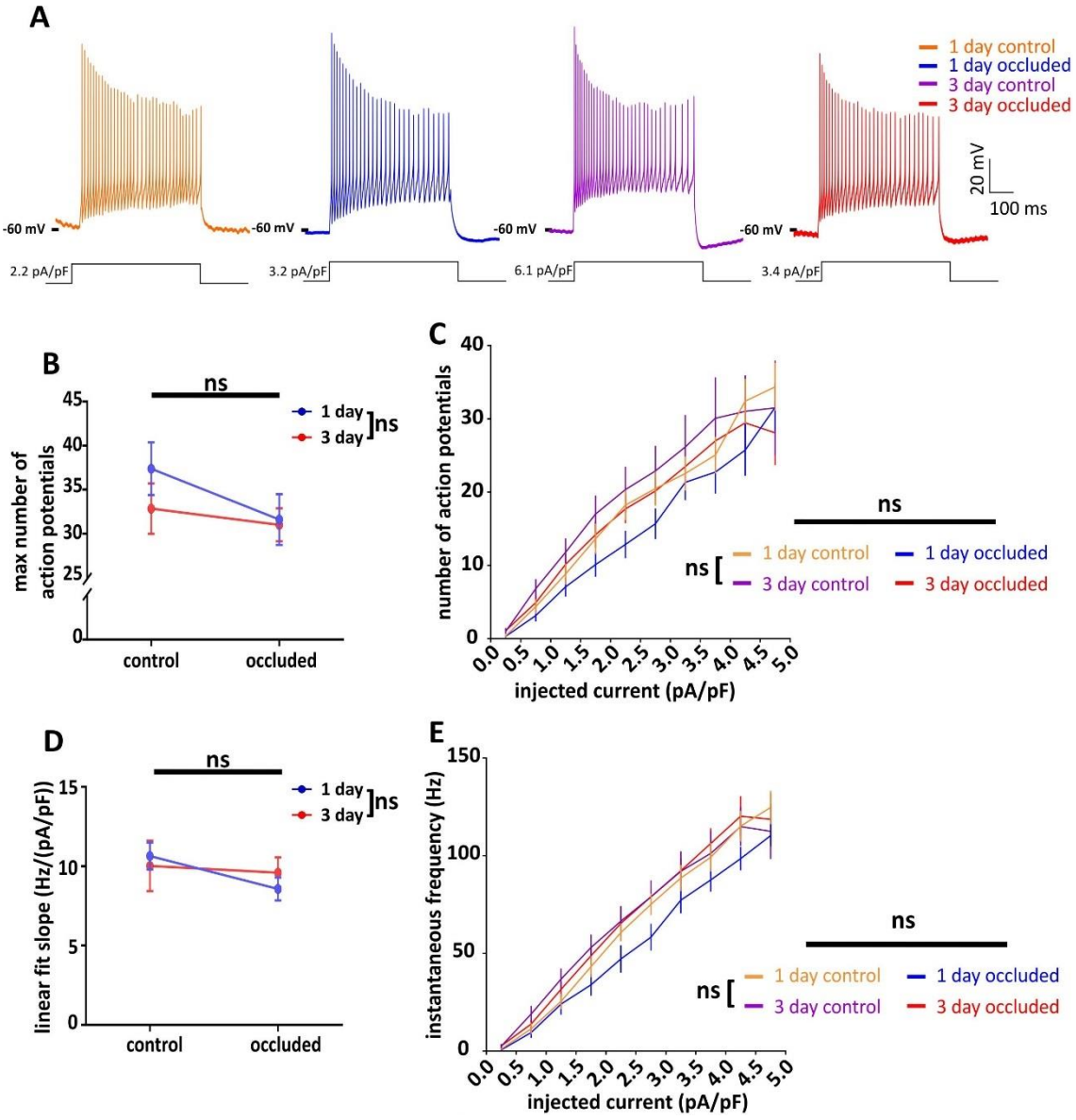

Figure 4.5: Multiple firing is not significantly different after unilateral naris occlusion

A: Example traces of the sweep with the maximum number of action potentials fired to 500 ms current injection in 1 and 3 day control and occluded DAT-tdTomato monophasic neurons.

B, D: Line plots showing the mean ± SEM of the (B) maximum number of potentials and (D) linear fit to the input-output slope (Hz/pA/pF). Two-way ANOVA; effect of manipulation, ns: non-significant; effect of time, ns: non-significant.

C, E: Input-output curves of injected current density (pA/pF) plotted against the mean ± SEM of (C) number of action potentials and (E) instantaneous frequency (Hz). Mixed model two-way ANOVA of input-output; effect of manipulation and effect of time; ns: non-significant.

[B-C, E (n): 1 day control (24); 1 day occluded (21); 3 day control (13); 3 day occluded (21)].

[D (n): 1 day control (23); 1 day occluded (19); 3 day control (12); 3 day occluded (19)].

significance (mixed model two-way ANOVA of input-output, effect of manipulation, $F_{(1,75)} = 3.017$, $p = 0.09$; effect of time, $F_{(1,75)} = 3.52$, $p = 0.06$; effect of manipulation x time interaction, $F_{(1,75)} = 0.14$, $p = 0.71$). None of the interactions involving input bin were found to be significant.

The slope of the initial, linear part of the input-output curve was calculated by fitting a line to the number of action potentials evoked in the first four sweeps with action potentials. This measure gives a single-value measure of the input-output relationship in a neuron as repeated-measures analysis of input-output curves can be insensitive to changes that depend on the ordered increase in injected current. Despite the trend towards shallower input-output curves seen for 1 day occluded cells, quantification of the input-output slope did not reveal any differences associated with occlusion (mean ± SEM: 1 day control, 10.65 ± 09 Hz/pA/pF, $n = 23$; 1 day occluded, 8.57 ± 0.73 Hz/pA/pF, $n = 19$; 3 day control, 10.02 ± 1.6 Hz/pA/pF, $n = 12$; 3 day occluded, 9.6 ± 0.97 Hz/pA/pF, $n = 19$. Two-way ANOVA on square-root transformed data, effect of manipulation, $F_{(1,69)} = 0.83$, $p = 0.37$; effect of time, $F_{(1,69)} = 0.02$, $p = 0.90$; effect of manipulation x time interaction, $F_{(1,69)} = 1.1$, $p = 0.30$) (**Figure 4.5D**).

Instantaneous frequency (IF) was calculated as the inverse of the period between the first two spikes in each sweep evoked by a given injected current density (pA/pF). Studying IF allows an investigation of repetitive spiking that is unaffected by spike patterning and depolarisation block that occurs later in the train. IF increased as the current density increased. Again, there was a slight shift in 1 day occluded neurons to having a lower instantaneous frequency versus current density, with the effect of time approaching significance (mixed model two-way ANOVA of input-output, effect of manipulation, $F_{(1,75)} = 1.42$, $p = 0.24$; effect of time, $F_{(1,75)} = 3.88$, $p = 0.052$; effect of manipulation x time interaction, $F_{(1,75)} = 0.57$, $p = 0.45$) (**Figure 4.5E**). None of the interactions involving input bin were found to be significant.

4.2.5 Afterhyperpolarisation following multiple action potentials

I have previously described the fast AHP that follows a single action potential. Following the firing of multiple action potentials other AHPs can be activated, these are the medium and slow AHPs. The medium AHP can also be activated by a single action potential and is mediated by the apamin-sensitive, small-conductance calcium-activated potassium (SK) channels (Bond et al., 2004; Stackman et al., 2002). It has also been shown to be regulated by voltage-gated potassium channels and hyperpolarisation-activated channels (Gu et al., 2005). The slow AHP has been described as a long-lasting current (>1 second), it is insensitive to apamin and is believed to be

due to calcium-dependent, voltage-independent potassium channels, though the exact channels responsible have not been definitively identified (Wang et al., 2016).

As an initial characterisation, I analysed the AHP generated following the end of 500 ms current steps that generated multiple action potentials (**Figure 4.6A**). The AHP was calculated as the difference between the holding voltage prior to the start of the current step and the minimum voltage following the current step. This AHP value was calculated for each current step and plotted against the number of action potentials generated for that step. In all groups the AHP increased along with the number of action potentials. There was also a significant effect of occlusion on the size of the AHP with it being larger in occluded neurons in comparison to the control groups (mixed model two-way ANOVA of input-output, effect of manipulation, $F_{(1,75)} = 5.8$, $p = 0.02$; effect of time, $F_{(1,75)} = 0.25$, $p = 0.62$; effect of manipulation x time interaction, $F_{(1,75)} = 0.21$, $p = 0.65$. Bonferroni post-hoc test comparing control versus occluded (significance at $p < 0.025$): 1 day, $F_{(1,49.16)} = 2.16$, $p = 0.15$; 3 day, $F_{(1,39.95)} = 3.68$, $p = 0.06$) (**Figure 4.6B**).

Following on from this finding, I designed a current-clamp protocol based on previous studies to specifically examine the AHP following multiple action potentials (Duménieu et al., 2015; Guan et al., 2015). A train of 10 action potentials at 50 Hz was evoked by injecting 2 ms-duration suprathreshold current steps (**Figure 4.7A-B**). The duration of the AHP was calculated as the time between the membrane potential falling below and then returning to the holding voltage. This increased with occlusion (mean ± SEM: 1 day control, 199.6 ± 35.7 ms, $n = 11$; 1 day occluded, 256.1 ± 41.46 ms, $n = 15$; 3 day control, 175.1 ± 28.41 ms, $n = 9$; 3 day occluded, 315.5 ± 45.15 ms, $n = 11$. Two-way ANOVA on $\log_{10}$ transformed data, effect of manipulation, $F_{(1,42)} = 6.78$, $p = 0.01$; effect of time, $F_{(1,42)} = 0.37$, $p = 0.55$; effect of manipulation x time interaction, $F_{(1,42)} = 0.61$, $p = 0.44$. Post-hoc Sidak's test between groups: 1 day, $t_{(42)} = 1.38$, $p = 0.32$; 3 day, $t_{(42)} = 2.26$, $p = 0.06$) (**Figure 4.7C**). These AHP duration values indicate that only the medium AHP was being activated by this protocol as the slow AHP has long duration decay, lasting >1 second (Andrade et al., 2012).

There was also a significant effect of occlusion on the peak amplitude of the AHP, particularly after 3 days (mean ± SEM: 1 day control, 2.7 ± 0.59 mV, $n = 11$; 1 day occluded, 3.4 ± 0.36 mV, $n = 15$; 3 day control, 3.1 ± 0.53 mV, $n = 9$; 3 day occluded, 5.4 ± 0.7 mV, $n = 11$. Two-way ANOVA, effect of manipulation, $F_{(1,42)} = 7.72$, $p = 0.008$; effect of time, $F_{(1,42)} = 4.7$, $p = 0.04$; effect of

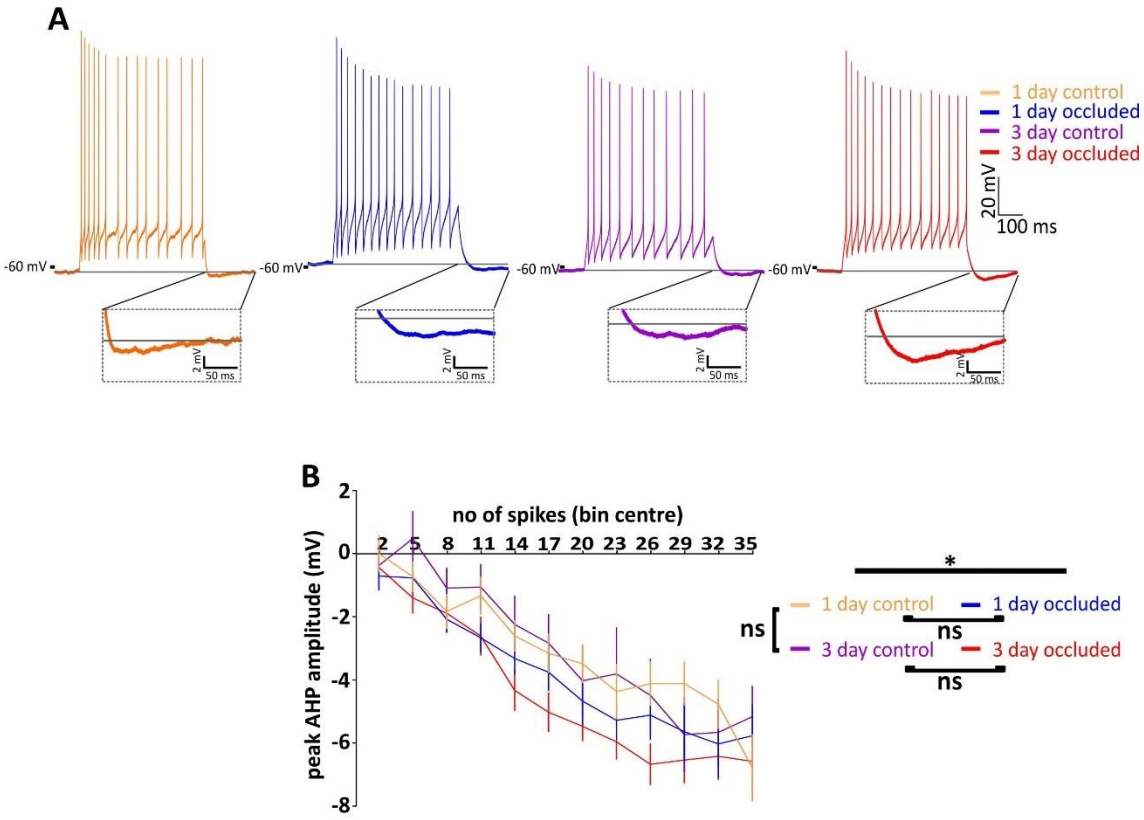

Figure 4.6: The afterhyperpolarisation after 500 ms current injection

A: Example traces of the afterhyperpolarisation (AHP) activated by multiple spiking during current injection steps of 500 ms in 1 and 3 day control and occluded DAT-tdTomato monophasic neurons. The solid line shows the baseline for that trace. **Insets**: expanded view of the AHP.

B: Mean ± SEM of the peak AHP amplitude (mV) plotted by binned spikes. Each bin corresponds to the bin centre ± 1 action potential. Mixed model two-way ANOVA of input-output; effect of manipulation, * $p < 0.05$; effect of time, ns: non-significant. Bonferroni post-test (significance when $p < 0.025$); 1 day, ns: non-significant; 3 day, ns: non-significant.

[B (n): 1 day control (24); 1 day occluded (21); 3 day control (13); 3 day occluded (21)].

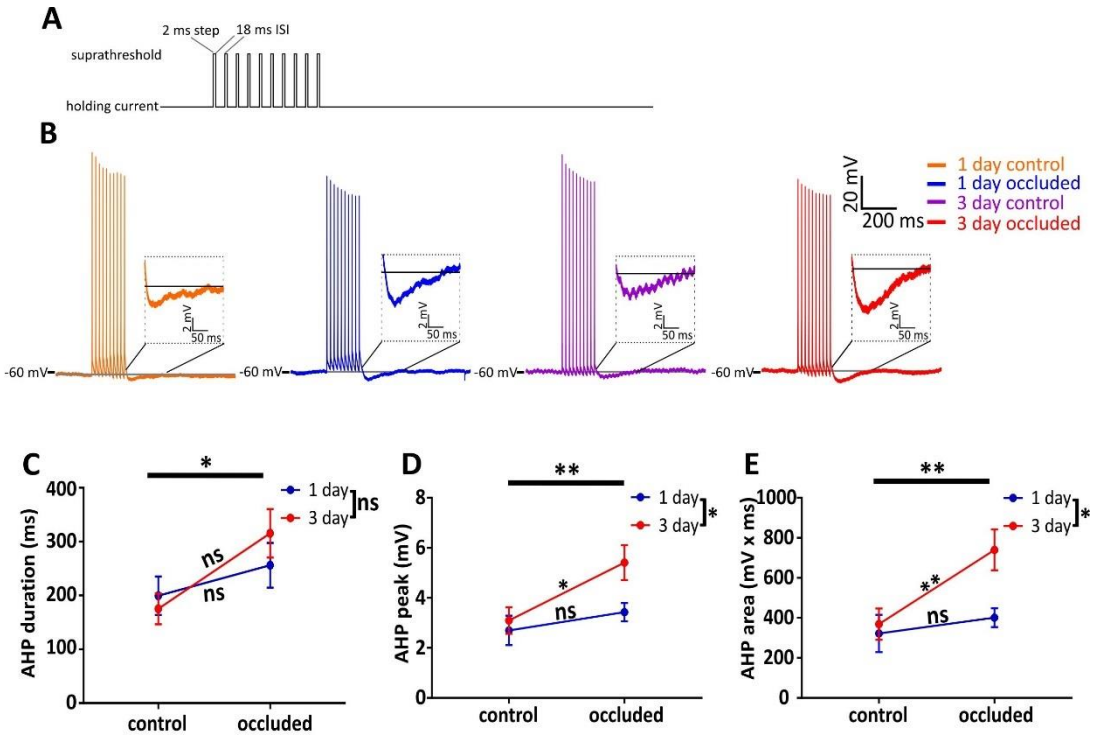

Figure 4.7: Occlusion increases the medium afterhyperpolarisation after a train of 10 action potentials

A: Current clamp protocol was ten 2 ms suprathreshold current injections at 50 Hz.

B: Example traces of the medium afterhyperpolarisation following ten action potentials at 50 Hz in 1 and 3 day control and occluded DAT-tdTomato monophasic neurons. **Insets**: expanded view of the medium afterhyperpolarisation. Solid horizontal lines indicate the baseline for that trace.

C-E: Mean ± SEM of the (C) AHP duration (ms), (D) peak amplitude (mV) and the (E) area (mV x ms) of the medium AHP. (C) Two-way ANOVA on $\log_{10}$ transformed data; effect of manipulation, * $p < 0.05$; effect of time, ns: non-significant. (D-E) Two-way ANOVA; effect of manipulation, ** $p < 0.01$; effect of time, * $p < 0.05$. (C-E) Sidak's multiple comparisons test, ** $p < 0.01$; * $p < 0.05$; ns: non-significant.

[C-E (n): 1 day control (11); 1 day occluded (15); 3 day control (9); 3 day occluded (11)].

manipulation x time interaction, $F_{(1,42)}$ = 2.09, p = 0.16. Post-hoc Sidak's test between groups: 1 day, $t_{(42)}$ = 1.01, p = 0.54; 3 day, $t_{(42)}$ = 2.82, p = 0.015) (**Figure 4.7D**). The area of the medium AHP was calculated by taking the area under the curve for 250 ms after the membrane potential went below the baseline holding voltage. The peak and duration of the AHP jointly determine its area, so it was to be expected that this measure was also found to be significantly larger in occluded neurons, again, with the greatest increase after 3 days (mean ± SEM: 1 day control, 322 ± 93.24 mV x ms, n = 11 ; 1 day occluded, 400.1 ± 47.31 mV x ms, n = 15; 3 day control, 368.8 ± 78.5 mV x ms, n = 9; 3 day occluded, 739.9 ± 102.1 mV x ms, n = 11. Two-way ANOVA, effect of manipulation, $F_{(1,42)}$ = 7.83, p = 0.008; effect of time, $F_{(1,42)}$ = 5.76, p = 0.02; effect of manipulation x time interaction, $F_{(1,42)}$ = 3.31, p = 0.08. Post-hoc Sidak's test between groups: 1 day, $t_{(42)}$ = 0.74, p = 0.71; 3 day, $t_{(42)}$ = 3.08, p = 0.007) (**Figure 4.7E**). The medium AHP appears to be specifically affected by activity deprivation in monophasic olfactory bulb DAT-tdTomato neurons, increasing with longer duration unilateral naris occlusion.

4.2.6 Sag potential

The hyperpolarisation-activated cation current (I_h) has previously been shown to be present in olfactory bulb dopaminergic neurons (Pignatelli et al., 2013). This current is generated through hyperpolarisation-activated cyclic nucleotide-gated (HCN) channels. This current has been associated with pacemaker activity in a number of autorhythmic cells. Work by Pignatelli et al. (2013) investigated the role of I_h in the pacemaker activity of olfactory bulb dopaminergic neurons by blocking the current with ZD7288. I_h was found not to have a direct role in the pacemaker mechanism; however, it did affect this activity by determining the resting membrane potential of the neurons.

Given the important role that I_h plays in olfactory bulb dopaminergic neurons, I investigated this current by recording the sag potential in current-clamp, a known proxy measure for I_h current magnitude (Angelo and Margrie, 2011). The sag potential was generated by holding the neuron at -60 mV and injecting Δ-10 pA current steps until the steady state response was beyond -100 mV (**Figure 4.8A**). There was no overall effect of occlusion or time on the sag index (see Methods 2.5.4.5), though the overall effect of occlusion was approaching significance. Post-hoc tests revealed that the sag potential was significantly larger after 3 days of occlusion (mean ± SEM: 1 day control, 0.91 ± 0.01, n = 33; 1 day occluded, 0.91 ± 0.02, n = 26; 3 day control, 0.91 ± 0.01, n = 18; 3 day occluded, 0.87 ± 0.01, n = 39. Two-way ANOVA, effect of manipulation, $F_{(1,112)}$ = 3.78, p = 0.054; effect of time, $F_{(1,112)}$ = 2.02, p = 0.16; effect of

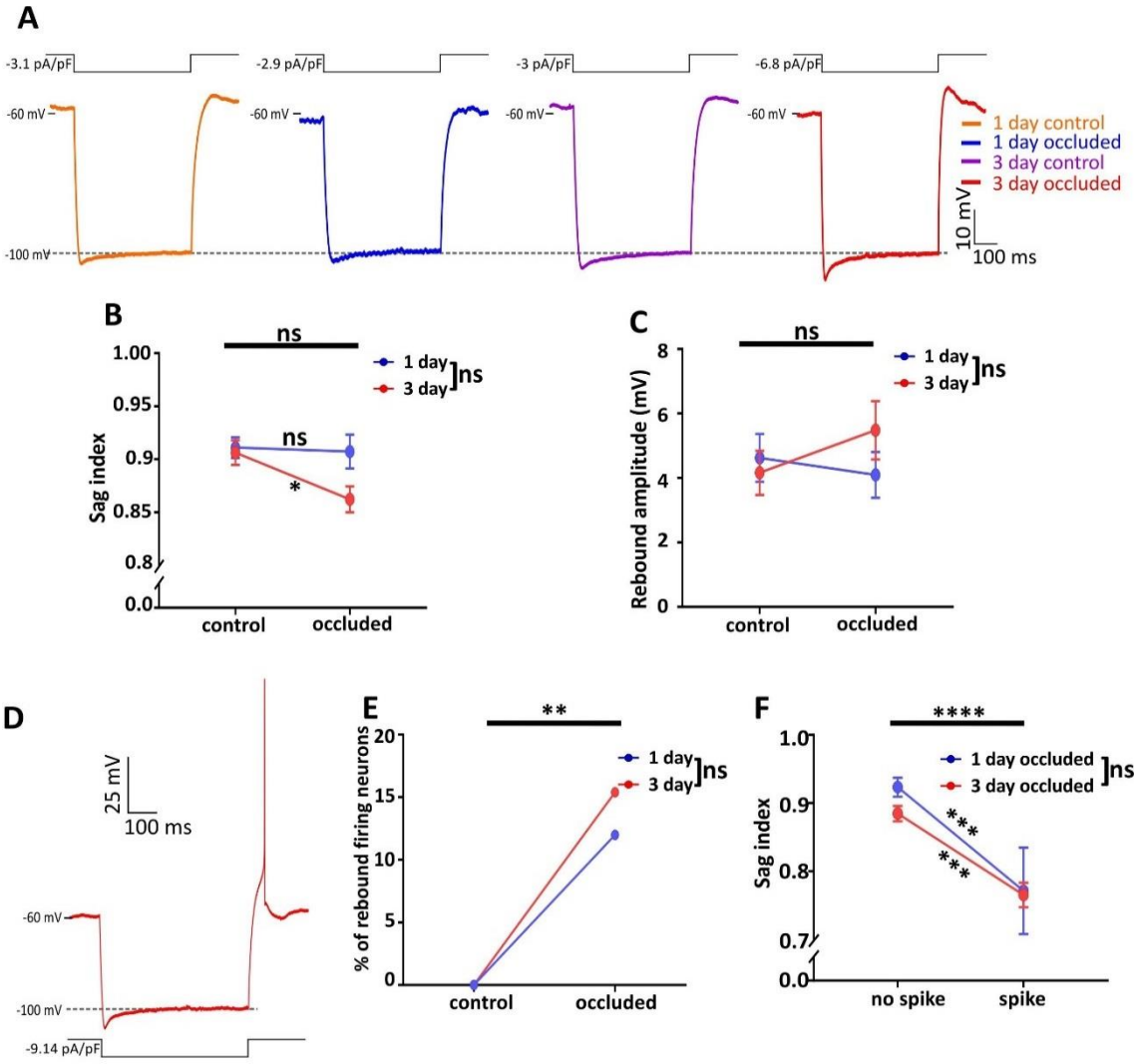

Figure 4.8: Longer duration occlusion increases the sag potential

A: Example traces of the voltage sag (proxy for the I_h current) activated by hyperpolarising current steps in 1 and 3 day control and occluded DAT-tdTomato monophasic neurons. The dashed grey line at -100 mV indicates the steady-state voltage response.

B-C, F: Line plots showing the mean ± SEM of the (B) sag index and (C) rebound amplitude (mV) in neurons that did not generate a rebound spike at current step offset and (F) sag index in occluded neurons that did or did not generate a rebound spike. Two-way ANOVA; effect of manipulation, **** $p < 0.0001$, ns: non-significant; effect of time, ns: non-significant; (B, F) Sidak's multiple comparisons test,*** $p < 0.001$; * $p < 0.05$; ns: non-significant.

D: Example trace from a 3 day occluded neuron showing a rebound spike at current step offset.

E: Plot showing the percentage of neurons that produced a rebound spike at current step offset. Fisher's exact test with Bonferroni correction (significance when $p < 0.025$); effect of manipulation **, $p < 0.005$; effect of time, ns: non-significant.

[B-C, E (n): 1 day control (33); 1 day occluded (26); 3 day control (18); 3 day occluded (39)].

[F (n): no spike 1 day occluded (23), 3 day occluded (33); spike 1 day occluded (3), 3 day occluded(6)].

manipulation x time interaction, $F_{(1,112)}$ = 2.9, p = 0.09. Post-hoc Sidak's test between groups: 1 day, $t_{(112)}$ = 0.18, p = 0.98; $t_{(112)}$ = 2.48, 3 day, p = 0.03) (**Figure 4.8B**).

The protocol to evoke the sag potential can result in a rebound depolarisation due to the closure of the HCN channels responsible for I_h. For some neurons the rebound depolarisation was enough to trigger an action potential (**Figure 4.8D**). I first analysed the rebound depolarisation in neurons that did not fire an action potential. There was no significant effect of occlusion on the amplitude of the rebound depolarisation (mean ± SEM: 1 day control, 4.6 ± 0.74 mV, *n* = 33; 1 day occluded, 4.1 ± 0.7 mV, *n* = 23; 3 day control, 3.63 ± 0.63 mV, *n* = 18; 3 day occluded, 5.58 ± 0.92 mV, *n* = 33. Two-way ANOVA, effect of manipulation, $F_{(1,104)}$ = 1.11, p = 0.29; effect of time, $F_{(1,104)}$ = 0.28, p = 0.60; effect of manipulation x time interaction, $F_{(1,104)}$ = 2.68, p = 0.10) (**Figure 4.8C**).

However, when analysing the proportion of neurons that fired an action potential when the steady state response had reached -100 mV there was a striking effect of occlusion. While no rebound action potential was observed in control neurons, approximately 10-15% of occluded neurons showed this behaviour (% of neurons that fired a rebound action potential: 1 day control, 0%, *n* = 33; 1 day occluded, 12%, *n* = 26; 3 day control, 0%, *n* =18; 3 day occluded, 15%, *n* = 39. Fisher's exact test with Bonferroni correction (significance at p < 0.025), effect of manipulation, p = 0.0046; effect of time, p = 0.32) (**Figure 4.8E**). Comparing the sag index in occluded neurons that generated a rebound spike revealed that their sag potential was significantly larger compared to neurons without a rebound spike (mean ± SEM: 1 day occluded no spike, 0.92 ± 0.01, *n* = 23; 1 day occluded spike, 0.77 ± 0.06, *n* = 3; 3 day control no spike, 0.88 ± 0.01, *n* = 33; 3 day occluded spike, 0.77 ± 0.02, *n* = 6. Two-way ANOVA, effect of rebound spike, $F_{(1,61)}$ = 31.88, p < 0.0001; effect of time, $F_{(1,61)}$ = 0.91, p = 0.34; effect of rebound spike x time interaction, $F_{(1,61)}$ = 0.5, p = 0.48. Post-hoc Sidak's test between groups: 1 day, $t_{(61)}$ = 3.92, p = 0.0005; $t_{(61)}$ = 4.22, 3 day, p = 0.0002) (**Figure 4.8F**). These results demonstrate that the sag potential is increased by longer duration occlusion. This increases the probability of a rebound spike, which is also observed to a lesser extent in response to shorter duration occlusion.

4.2.7 Spike frequency adaptation

Despite there being no striking changes in the ability to fire multiple action potentials (Figure 4.5), the results of the medium AHP and sag potential analyses above suggest that unilateral naris occlusion is producing experience-dependent changes in the intrinsic properties of monophasic olfactory bulb DAT-tdTomato neurons. I, therefore, investigated whether regularity of spiking was affected by sensory deprivation, by studying the adaptation of spiking frequency

during an extended period of excitation. This has been reported to be strongly modulated by the medium AHP (Vandecasteele et al., 2011). Spike frequency adaptation (SFA) refers to the frequency of action potentials progressively slowing following an initial high frequency of spikes and can be interpreted as a form of neuronal self-inhibition. I analysed the pattern of firing in a depolarising stimulation that was + 30 pA above spike threshold (**Figure 4.9A**). This approach was based on previous work studying SFA in substantia nigra *pars compacta* dopaminergic neurons (Vandecasteele et al., 2011).

At this stimulation, the majority of neurons had not yet reached their maximum firing rate and showed steady firing. Neurons that had reached their maximum firing rate <30 pA above spike threshold were not analysed. There was no significant difference between groups in the number of action potentials fired at this stimulation level (mean ± SEM: 1 day control, 17 ± 3, $n = 19$; 1 day occluded, 15 ± 2, $n = 19$; 3 day control, 16 ± 2, $n = 10$; 3 day occluded, 15 ± 2, $n = 16$. Two-way ANOVA on $\log_{10}$ transformed data, effect of manipulation, $F_{(1,60)} = 0.46$, $p = 0.50$; effect of time, $F_{(1,60)} = 0.03$, $p = 0.87$; effect of manipulation x time interaction, $F_{(1,60)} = 0.06$, $p = 0.81$) (**Figure 4.9B**).

To investigate the spiking pattern, SFA was calculated (see Methods 2.5.4.4), with a higher SFA indicating greater adaptation. All groups showed adaptation (SFA > 0), indicating higher initial instantaneous frequency. However, despite the activity-dependent changes observed in medium AHP and sag potential in monophasic olfactory bulb DAT-tdTomato neurons (Figures 4.7 and 4.8), there was no difference in SFA associated with occlusion (mean ± SEM: 1 day control, 49.68 ± 3.11, $n = 19$; 1 day occluded, 53.76 ± 4.14, $n = 19$; 3 day control, 46.01 ± 4.51, $n = 10$; 3 day occluded, 48.64 ± 3.1, $n = 16$. Two-way ANOVA, effect of manipulation, $F_{(1,60)} = 0.76$, $p = 0.39$; effect of time, $F_{(1,60)} = 1.3$, $p = 0.26$; effect of manipulation x time interaction, $F_{(1,60)} = 0.04$, $p = 0.85$) (**Figure 4.9C**).

4.2.8 Correlations between functional parameters

Given the lack of occlusion effect on any measure of spiking, it is unclear based on the current results what effect the changes in medium AHP and sag potential are having on intrinsic excitability of these neurons. To further explore these results, I investigated whether there were

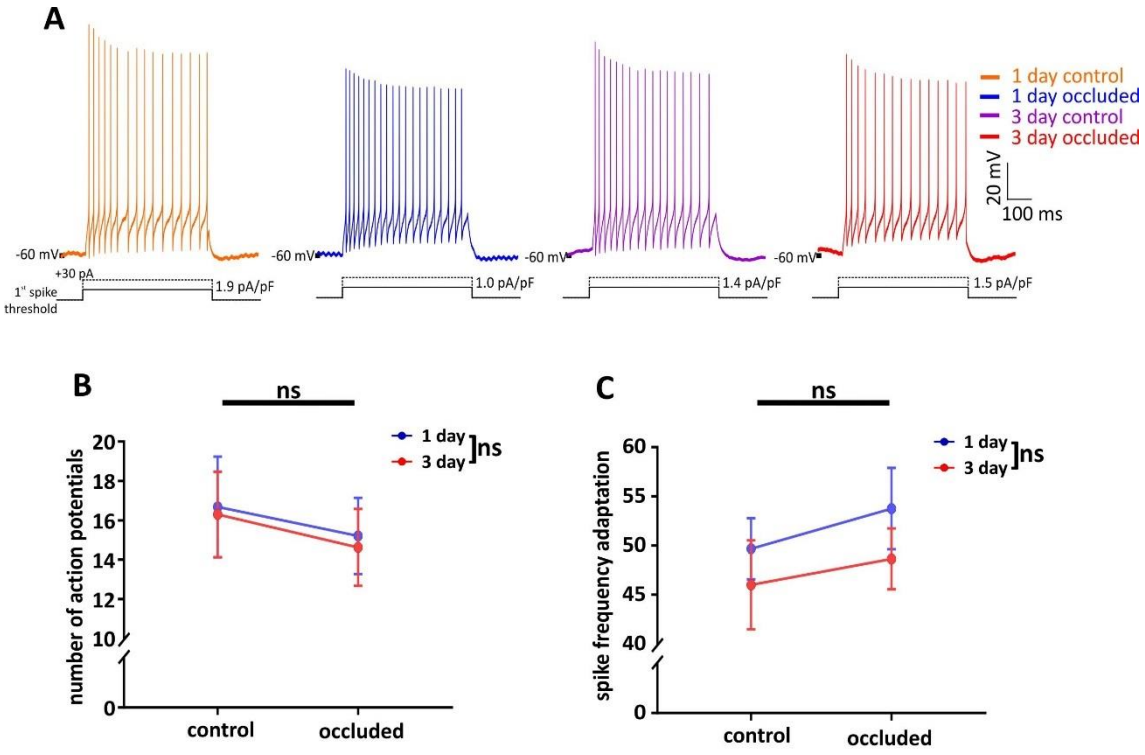

Figure 4.9: Spike frequency adaptation does not change with occlusion

A: Example traces of the sweep +30 pA above the spike threshold in 1 and 3 day control and occluded DAT-tdTomato monophasic neurons.

B-C: Line plots showing the mean ± SEM of the (B) number of action potentials fired at +30 pA above spike threshold and (C) spike frequency adaptation. (B) Two-way ANOVA of $\log_{10}$ transformed data and (C) two-way ANOVA; effect of manipulation, ns: non−significant; effect of time, ns: non-significant.

[B-C (n): 1 day control (19); 1 day occluded (19); 3 day control (10); 3 day occluded (16)].

associations between functional parameters within individual neurons that might not be evident in the group-level analyses carried out so far.

The HCN channels that generate I_h have been reported to contribute to the medium AHP; however, this only occurs at hyperpolarised membrane potentials. Since I found that occlusion, particularly after 3 days, affects medium AHP and sag potential, I analysed whether there was a correlation between these two properties. However, there was no significant association between them in any group except 3 day controls. This suggests that the change in medium AHP is not occurring as a consequence of an increase in the sag potential or vice versa (linear regression analysis: 1 day control, $R^2 = 0.07$, $F_{(1,7)} = 0.5$, $p = 0.50$, $n = 9$; 1 day occluded, $R^2 = 0.09$, $F_{(1,10)} = 1$, $p = 0.30$, $n = 12$; 3 day control, $R^2 = 0.71$, $F_{(1,4)} = 9.64$, $p = 0.04$, $n = 6$; 3 day occluded, $R^2 = 0.01$, $F_{(1,9)} = 0.12$, $p = 0.74$, $n = 11$) (**Figure 4.10**). Comparing the linear regressions revealed that there was a significant effect of manipulation, likely driven by 3 day control (two-way ANOVA, effect of manipulation, $F_{(1,34)} = 5.12$, $p = 0.03$; effect of time, $F_{(1,34)} = 1.1$, $p = 0.30$; effect of manipulation x time interaction, $F_{(1,34)} = 3.42$, $p = 0.07$. Post-hoc Sidak's test between groups: 1 day, $t_{(34)} = 0.32$, $p = 0.94$; 3 day, $t_{(34)} = 2.72$, $p = 0.02$).

I_h has been implicated in regulating neuronal firing, with a larger I_h shown to both increase and decrease intrinsic excitability (Angelo and Margrie, 2011; Shim et al., 2016; Van Welie et al., 2004). I have found that occlusion was associated with an increased likelihood of the rebound depolarisation firing an action potential. I, therefore, investigated whether sag index was associated with repetitive firing. Sag index showed a modest negative correlation with maximum firing rate that was significant in all groups except 1 day control, which was approaching significance (linear regression analysis; 1 day control, $R^2 = 0.17$, $F_{(1,17)} = 3.6$, $p = 0.08$, $n = 19$; 1 day occluded, $R^2 = 0.26$, $F_{(1,15)} = 5.31$, $p = 0.04$, $n = 17$; 3 day control, $R^2 = 0.65$, $F_{(1,6)} = 11.19$, $p = 0.02$, $n = 8$; 3 day occluded, $R^2 = 0.32$, $F_{(1,16)} = 7.61$, $p = 0.01$, $n = 18$) (**Figure 4.11A**). This strongly suggests that larger sag potential is associated with more firing. Comparing the linear regressions revealed that they were not significantly different (two-way ANOVA, effect of manipulation, $F_{(1,58)} = 2.79$, $p = 0.10$; effect of time, $F_{(1,58)} = 2.58$, $p = 0.11$; effect of manipulation x time interaction, $F_{(1,58)} = 1.29$, $p = 0.26$).

As medium AHP also regulates intrinsic excitability, I also investigated its association with maximum firing rate. However, there were no significant correlations for this measure (linear regression analysis: 1 day control, $R^2 = 0.003$, $F_{(1,7)} = 0.02$, $p = 0.80$, $n = 9$; 1 day occluded, $R^2 = 0.2$, $F_{(1,5)} = 1.2$, $p = 0.32$, $n = 7$; 3 day control, $R^2 = 0.83$, $F_{(1,1)} = 5$, $p = 0.27$, $n = 3$; 3 day occluded, $R^2 = 0.006$, $F_{(1,4)} = 0.02$, $p = 0.89$, $n = 6$) (**Figure 4.11B**).

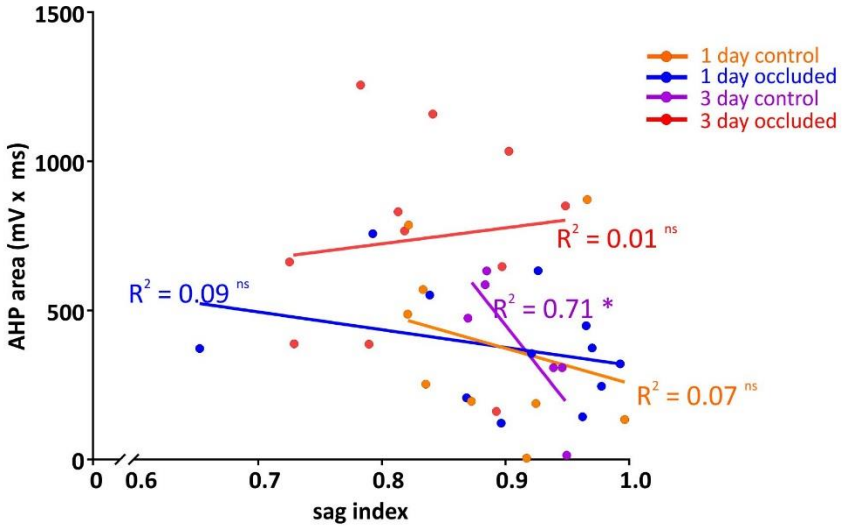

Figure 4.10: Correlation of sag index with medium AHP

Scatter plot of sag index versus AHP area (mV x ms) in 1 and 3 day control and occluded DAT-tdTomato monophasic neurons. Each dot represents a single cell. Lines show linear regression analysis for individual conditions and R^2 values. Deviation from zero; * $p < 0.05$; ns: non-significant.

[(n): 1 day control (9); 1 day occluded (12); 3 day control (6); 3 day occluded (11)].

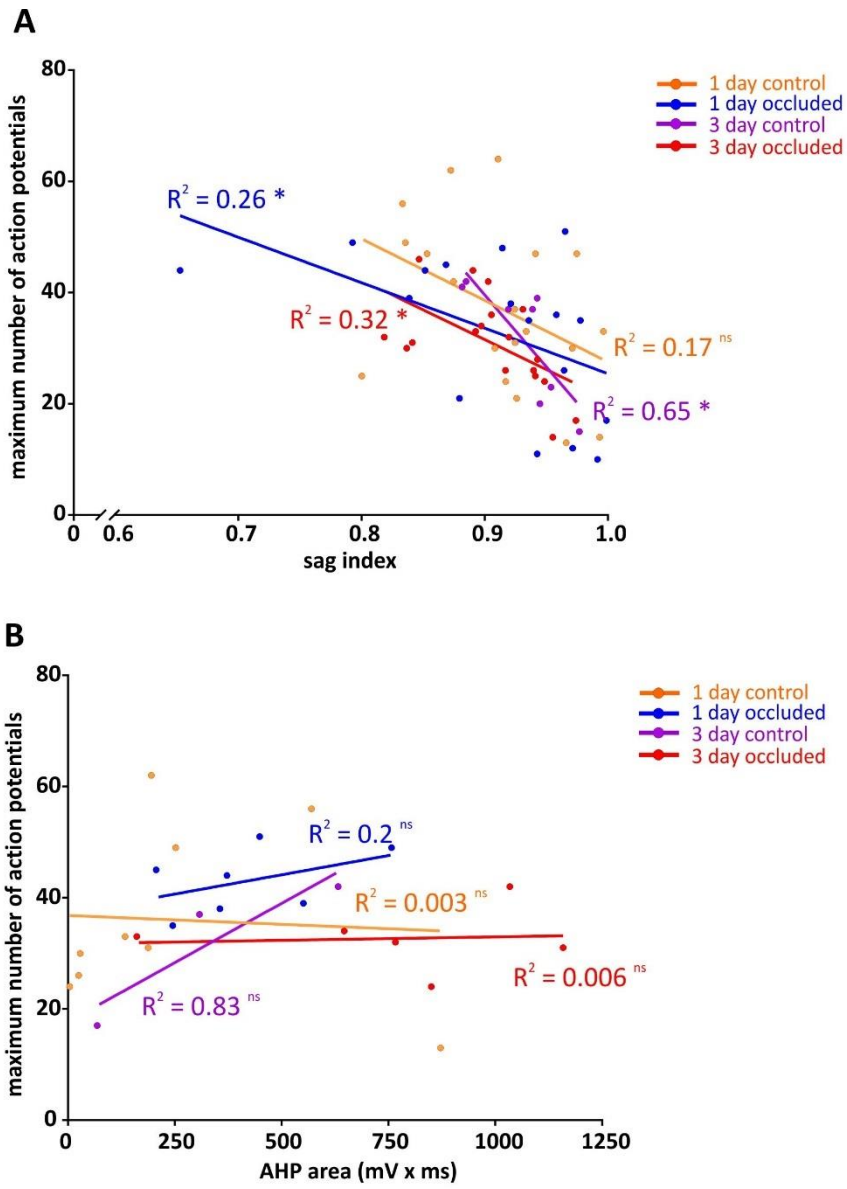

Figure 4.11 Correlation of sag index and AHP with maximum firing

A-B: Scatter plot of maximum number of actions potentials versus (A) sag index and (B) AHP area (mV x ms) in 1 and 3 day control and occluded DAT-tdTomato monophasic neurons. Each dot represents a single cell. Lines show linear regression analysis for individual conditions and R^2 values. Deviation from zero; * $p < 0.05$; ns: non-significant.

[A (n): 1 day control (19); 1 day occluded (17); 3 day control (8); 3 day occluded (18)].

[B (n): 1 day control (9); 1 day occluded (7); 3 day control (3); 3 day occluded (6)].

I_h has been particularly associated with the regulation of the resting membrane potential of olfactory bulb dopaminergic neurons by exerting a depolarising effect (Pignatelli et al., 2013). I investigated the correlation of resting membrane potential with sag index, which was significant in all groups except 3 day controls (linear regression analysis; 1 day control, $R^2 = 0.23$, $F_{(1,29)} = 8.61$, $p = 0.001$, $n = 31$; 1 day occluded, $R^2 = 0.66$, $F_{(1,17)} = 32.96$, $p < 0.0001$, $n = 19$; 3 day control, $R^2 = 0.003$, $F_{(1,13)} = 0.03$, $p = 0.85$, $n = 15$; 3 day occluded, $R^2 = 0.66$, $F_{(1,27)} = 53.23$, $p < 0.0001$, $n = 29$) (**Figure 4.12**). Comparing the linear regressions revealed that the effect of occlusion was approaching significance (two-way ANOVA, effect of manipulation, $F_{(1,86)} = 3.09$, $p = 0.08$; effect of time, $F_{(1,86)} = 1.83$, $p = 0.18$; effect of manipulation x time interaction, $F_{(1,86)} = 2.59$, $p = 0.11$). Therefore, the majority of groups show a correlation between the size of the sag potential and resting membrane potential.

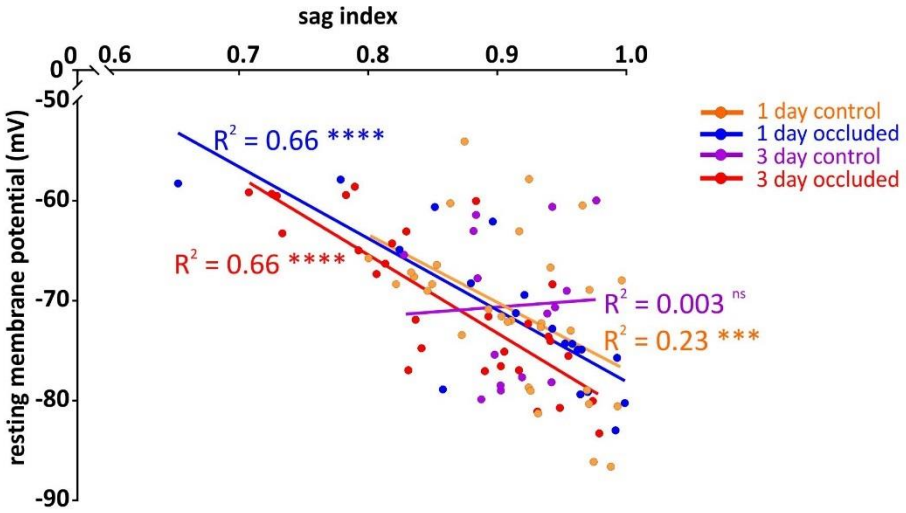

Figure 4.12: Correlation of sag index with resting membrane potential

Scatter plot of sag index versus resting membrane potential (mV) in 1 and 3 day control and occluded DAT-tdTomato monophasic neurons. Each dot represents a single cell. Lines show linear regression analysis for individual conditions and R2 values. Deviation from zero; **** $p < 0.0001$; *** $p < 0.001$; ns: non-significant.

[(n): 1 day control (31); 1 day occluded (19); 3 day control (15); 3 day occluded (29)].

4.3 Discussion

In this chapter, I investigated how the anaxonic subpopulation of dopaminergic neurons in the olfactory bulb change their intrinsic properties in response to sensory deprivation by unilateral naris occlusion. In the previous chapter, I showed that these neurons have reduced activity and alter their expression of TH in an experience-dependent manner after 1 and 3 days of occlusion. Here I build on this work by demonstrating that this manipulation also induces distinct forms of intrinsic plasticity changes, particularly after 3 days.

4.3.1 The effect of odour deprivation duration on functional properties

In Chapter 3 I found that 1 day of occlusion induced activity-dependent reductions in the expression of cFos and TH, with a small decrease in DDC. However, changes in functional properties were not significantly affected after 1 day. The role of intrinsic plasticity is proposed to be the maintenance of network stability by a balance between excitation and inhibition. This would suggest that in response to less activity there would be a need for less inhibition and, conversely, more activity would result in increased inhibition. Previous *in vitro* work did not find a significant effect of increased activity for 1 day on any intrinsic functional property in monophasic or biphasic olfactory bulb dopaminergic neurons (Chand et al., 2015). However, unpublished work from my lab studying multiple firing in monophasic and biphasic DAT-tdTomato neurons after 1 day of unilateral naris occlusion revealed that both subpopulations had a trend for less multiple firing, particularly the biphasic subpopulation (Elisa Galliano, *in preparation*).

I replicated this non-significant trend for less excitability in multiple spike firing in the monophasic dopaminergic subpopulation; however, this had resolved by 3 days. Previous work studying the excitability of inhibitory interneurons has found a diversity of responses following activity deprivation. This can include neurons that show a long-term reduction or increase in excitability, while other neurons have an initial change, which recovers to baseline (Desai et al., 1999b; Hengen et al., 2013). These changes can be mediated by regulating the expression or biophysical properties of voltage and/or calcium-gated ion channels. However, it is unclear what process may underlie the observed non-significant drop in excitability in monophasic olfactory bulb DAT-tdTomato neurons and whether other mechanisms are involved. Indeed, more data may reveal that this small effect is not a true phenotype. If there is a transient reduction in neuronal excitability, it is unclear what effect this could have on the function of these neurons in the glomerular layer. It can be speculated that the individual contribution will be small; however, a population-level decrease in excitability of these neurons could impact glomerular

processing. Despite a recovery in this small reduction in excitability, the output of these neurons is likely to be affected due to decreased expression of TH that would reduce the synthesis and availability of dopamine.

Sensory deprivation was associated with an activity-dependent increase in both sag potential and medium AHP. While the strongest effects on sag potential and medium AHP were observed at 3 days of occlusion, there were trends identified after 1 day. Therefore, functional changes may be starting to occur after 1 day of occlusion; however, longer durations may be required before inducing observable changes in these neurons. It is possible that the identified trends could be occurring in cells that had low activity prior to occlusion and are displaying effects of occlusion faster. Unfortunately, it is not possible to study these measures in individual neurons before and after occlusion. Intrinsic plasticity is often a cell-wide response that is driven by changes to gene expression and protein synthesis to modify the biophysical properties and/or abundance of ion channels on the membrane of neurons. This has been observed to be a slow and cumulative process that requires hours or days to produce measurable changes (Desai et al., 1999a). This slow mechanism may be important to allow the neuron to monitor and adapt to average activity in the network and adjust as required. However, intrinsic plasticity changes can also be rapid, occurring in minutes or hours, and mediated by post-translational modifications (Aizenman and Linden, 2000; Evans et al., 2015). It would be interesting for future research to investigate whether there are rapid (<1 day) changes in these neurons following odour deprivation.

It was important to include 1 and 3 day control mice to investigate whether there were functional effects associated with the manipulation procedure. There were no significant differences in the intrinsic properties of neurons in these two controls. However, it was interesting that the correlation of sag index to both resting membrane potential and medium AHP were found be different for 3 day control compared to the other groups. Sham unilateral naris occlusion has been reported to reduce neurotransmitter release from OSNs in the bulb ipsilateral to the sham naris compared to the unmanipulated bulb (Kass et al., 2013). In this published *in vivo* study, the plug was removed from occluded mice and a sham plug removal was performed on control mice a day before *in vivo* imagining recordings. It is unclear whether the effect of reduced neurotransmitter release is due to the sham insertion or the sham removal. However, it does indicate that even temporary insertion of an object into a naris can induce changes. It is interesting that Kass et al. (2013) found reduced neurotransmitter release and in my correlation analyses the 1 day control group resembled the occluded groups, possibly indicating a slight occlusion effect associated with sham occlusion. Work from my lab has

suggested that OSN-evoked monosynaptic paired-pulse ratio in external tufted cells is not different between sham and unperturbed groups (Christiane Hahn). However, further study of differences between sham and unmanipulated mice would be required to fully investigate the effect of sham occlusion.

4.3.2 The processes that could contribute to the observed plasticity changes

What could be the potential mechanisms responsible for the experience-dependent functional changes in these neurons? The sag potential is a proxy for I_h, which is driven by HCN channels. The gating, kinetics and expression of these channels are dependent on many intracellular mechanisms. It is unclear whether the increase in sag potential is due to enhanced channel density or changes in the kinetics or composition of the channels. Four HCN subunits have so far been identified and can form homomeric or heteromeric channels, with each subunit having different kinetics and voltage activation (Biel et al., 2009). The expression of these subunits and the complexes they form are affected by changes in activity (Zha et al., 2008). There could be an increased expression of HCN channels at the membrane due to increased trafficking by the chaperone protein, TRIPb (Lewis et al., 2009). Increased activity during seizures has been associated with disrupted interaction between HCN channels and TRIP8b, resulting in decreased HCN expression and I_h activity (Shin et al., 2008). TRIP8b can also cause a hyperpolarising shift in the voltage activation of HCN channels by blocking the activity of the second messenger, cAMP (Saponaro et al., 2014). Activation of HCN channels is facilitated by the activity of second messengers, including calcium and cAMP, shifting the activation of the HCN channels to more depolarised voltages and increasing the conductance and opening kinetics of the channels (Honnuraiah and Narayanan, 2013; Ludwig et al., 1998; Surges et al., 2006; Wilson and Garthwaite, 2010; Zong et al., 2012). The expression of HCN channels can also be mediated by the activity-dependent binding of the transcription factor NRSF, which can repress *Hcn* transcription during increased activity (McClelland et al., 2011). There would need to be further work to understand whether there has been an activity-dependent increase in the expression of HCN channels through increased protein trafficking or gene expression or whether the biophysical properties of the channels have been modulated. Work in my lab investigating gene expression in single DAT-tdTomato neurons following occlusion may give insight into the expression of *Hcn* genes or genes involved in regulating HCN channels (Marcela Lipovsek). It could also be possible to use immunohistochemistry to study the expression of different HCN channels following occlusion. Voltage-clamp experiments would be required to characterise changes in I_h conductance and kinetics following occlusion.

Several channels have been implicated in the regulation of the medium AHP. Certain channels have been suggested to be activated depending on the membrane potential, with a delayed rectifier potassium M-current, driven by Kv7 (KCNQ) channels, activated at more depolarised potentials and I_h activated at hyperpolarised potentials (Gu et al., 2005). I did not find a correlation between sag index and medium AHP for most of the groups, suggesting that increased medium AHP is not due to changes in I_h. There is also evidence that SK channels underlie this current (Bond et al., 2004; Stackman et al., 2002). Work characterising the currents present in olfactory bulb dopaminergic neurons identified a delayed rectifier potassium current (Pignatelli et al., 2005), which could represent the M-current. This study also reported the presence of a small potassium current that was calcium-dependent, potentially implicating SK channels. Therefore, a thorough pharmacological investigation would be required to identify the channels that are regulating this current in olfactory bulb dopaminergic neurons and whether any of these currents change after occlusion.

The AHP following repetitive firing has been studied in mitral cells; however, there was no distinction made between the medium and slow components, though the duration of the AHP was under 500 ms (Duménieu et al., 2015). This study found that this (probable) medium AHP is affected by synaptic input and increases when glutamatergic and GABAergic inputs are blocked. Therefore, either tonic or phasic intraglomerular glutamate and GABA release shapes the AHP. This suggests that the medium AHP could be increased following occlusion due to decreased synaptic inputs. However, as I was using synaptic blockers in my recording conditions, the increase in the medium AHP between groups indicates that there are intrinsic changes to the medium AHP in monophasic olfactory bulb dopaminergic neurons following occlusion.

Intracellular signalling pathways have been found to be implicated in the activity-dependent regulation of the AHP following a burst of action potentials. In particular, the activation of the transcription factor CREB following neuronal activity activates protein kinase A, leading to a suppression of postburst AHP (Haug and Storm, 2000; Oh, 2010). The activation of this pathway has been particularly implicated in the modulation of SK current (Haug and Storm, 2000). However, it has been found that Kv7 also demonstrates activity-dependent changes. Activation of glutamatergic receptors activates intracellular signalling pathways that decrease the M-current by reducing the expression of Kv7 (Li et al., 2015). It could, therefore, be possible that reduced excitatory input could facilitate the expression of Kv7 and/or SK channels through a reduction of intracellular signalling pathways. In order to fully characterise which channels are modified by occlusion and how I_h and medium AHP have been affected, follow up electrophysiology experiments under appropriate pharmacological conditions would be

required. I_h has been studied in olfactory bulb dopaminergic neurons by using a high potassium extracellular solution with blockers of sodium, calcium and KIR channels and glutamatergic and GABAergic receptors (Pignatelli et al., 2013). SK and Kv7 channels can be identified by the selective blockers apamin and XE991, respectively (Gu et al., 2005).

4.3.3 What could be the role of these changes on intrinsic properties?

Analysing firing properties in response to somatic current injections did not identify significant effects associated with occlusion in monophasic DAT-tdTomato olfactory bulb neurons. These are widely utilised measures to study and identify activity-dependent changes to neuronal excitability (Desai et al., 1999a; Grubb and Burrone, 2010). Based on the results I observed, these neurons do not appear to be changing their excitability after occlusion. However, as there are increases in sag potential and medium AHP, what could be the role of these changes?

Activity-deprivation has previously been found to increase the sag potential, resulting in reduced intrinsic excitability in Purkinje cells using rat organotypic cerebellar cultures (Shim et al., 2016). However, the activation of I_h affects neuronal excitability through opposing properties. Following an action potential, HCN channels are activated by post-spike repolarisation, which results in depolarisation due to I_h and promotes subsequent firing, making this current an important regulator of rhythmic firing (Pignatelli et al., 2013). I did find that there was a higher proportion of occluded neurons that were spontaneously active at $I = 0$ and an increase in rebound spiking following the sag protocol. In contrast to increased activity, I_h can decrease excitability by reducing input resistance as the channels are active at rest. Therefore, action potential initiation in response to depolarisation could be affected. Although there were no differences in firing after 3 days of occlusion, I found that larger sag potential was correlated with a higher maximum firing rate, which has previously been found for mitral cells (Angelo and Margrie, 2011). In mitral cells, I_h is highly variable across the population, which affects the functional properties of these neurons (Angelo and Margrie, 2011). This diversity is believed to be important for the integration of sensory input to mitral cells. It is unclear whether monophasic olfactory bulb dopaminergic neurons also have this diversity in I_h and whether occlusion could be affecting functional heterogeneity within this population.

It was interesting that sag index was correlated with multiple firing and resting membrane potential; however, on a group-level there were no significant changes in these measures. This is likely due to a high-level of variability between neurons within the population that is masking effects, which can only be observed on a cell-by-cell basis. Resting membrane potential and multiple firing are also regulated by other mechanisms besides I_h.

In olfactory bulb dopaminergic neurons at rest, there is a persistent, TTX-insensitive, sodium current driven by I_h (Pignatelli et al., 2005, 2013). HCN channels are voltage-gated ion channels that are permeable to sodium and potassium ions and at rest HCN channels are tonically active, producing a depolarising inward current (Hu et al., 2002). It would, therefore, be expected that if the voltage activation of HCN channels had been shifted to more depolarised potentials, resting membrane potential would also become more depolarised. However, in these neurons HCN channels are also acting against another current that regulates the resting membrane potential. The potassium inward rectifier (KIR) current is also active at rest, which exerts a hyperpolarising effect through an outward potassium current (Borin et al., 2014). It is unknown how the KIR current has been affected by naris occlusion and whether its activity has also been increased. If the medium AHP is being driven by the M-current in these neurons, the Kv7 channels are also known to be active at rest in other neurons and hyperpolarises the resting membrane potential (Halliwell and Adams, 1982). The activity of these currents would potentially counteract an increase in an I_h-mediated depolarisation. Previous work showing activity-dependent increase in I_h also did not find a change in resting membrane potential (Shim et al., 2016). Increased I_h due to a shift in its voltage-activation or increased channel density could act as a voltage-clamp to stabilise the membrane potential by opposing depolarisations or hyperpolarisations. However, I did not observe changes in rheobase, which would be expected if this was the case as more current would be required to fire an action potential.

There is currently no description of AHP currents in olfactory bulb dopaminergic neurons and what role they play in the function of the neurons. While the fast AHP has been implicated in sustained high-frequency firing, the medium and slow AHP decrease excitability (Buhl et al., 1994). The results presented in Figure 4.7 indicate that only medium AHP is being activated by the train of action potentials as the duration of the AHP is far shorter than what is known about the slow AHP (Wang et al., 2016). As the AHP following multiple spiking is affected by the number and frequency of action potentials (Duménieu et al., 2015), it is possible that this protocol was not sufficient to elicit the slow AHP. Protocols of varying frequency and number of action potentials would be needed to determine whether the slow AHP is indeed absent from this subpopulation of olfactory bulb dopaminergic neurons.

Medium AHP has been shown to be an important regulator of neuronal excitability. Pharmacologically enhancing the medium AHP decreases firing frequency and spike frequency adaptation, while blocking the current increases firing (Pedarzani et al., 2005; Savić et al., 2001; Wang et al., 2011). In mitral cells, a larger AHP (most likely medium AHP), reduced mitral cell firing and pattern of firing (Duménieu et al., 2015). However, I did not find any correlation

between the medium AHP and maximum number of spikes or a change in SFA. This raises the question of whether the repetitive firing protocols were sensitive enough to detect the effect of increased I_h and medium AHP on firing properties.

In pyramidal barrel cortex neurons, activity deprivation by whisker trimming was found not to affect somatic action potential properties, input-output firing to somatic current injections and resting membrane potential (Breton and Stuart, 2009). However, regular firing was affected with increased burst firing and reduced I_h at dendrites leading to increased dendritic excitability. Therefore, there is also the possibility that changes in excitability cannot be observed using somatic current injections and the observed functional changes may affect firing under more physiological conditions and/or dendritically localised synaptic input.

4.3.4 Potential effect on synaptic inputs

HCN channels in olfactory bulb dopaminergic neurons are suggested to play an important role in the dendrites of these neurons (Pignatelli et al., 2013). Initial work to identify I_h in olfactory bulb dopaminergic neurons did not find evidence of the current as they were studying acutely dissociated neurons (Pignatelli et al., 2005). Follow-up experiments in slices found that these neurons did have I_h and it was not previously identified due the loss of dendrites from the dissociation process (Pignatelli et al., 2013). In other neurons it has been shown that HCN density increases from proximal to distal dendrites, modulating synaptic input and neuronal excitability and normalising temporal summation of postsynaptic potentials at the soma (Angelo and Margrie, 2011; Berger et al., 2001; Magee, 1998). Therefore, increased I_h may be having a greater role at the dendrites rather than soma. This is suggestive of a role in the modulation of synaptic input. It would also suggest that I could be underestimating the sag potential due to dendritic filtering of I_h. However, monophasic DAT-tdTomato neurons have high R_I, indicating that they are electrotonically compact and any underestimation would likely be minimal.

As HCN channels are tonically active at rest, they reduce local membrane resistance and make dendrites “leaky”. Depolarisation by synaptic activity would inactivate HCN channels and their sodium flow, resulting in the hyperpolarisation of the membrane potential back to rest, reactivating HCN channels. Likewise, hyperpolarisation by synaptic activity would activate more HCN channels, depolarising the membrane potential. This activity of HCN channels in response to input reduces the amplitude and decay of synaptic events, leading to a reduction of synaptic-input excitability. Enhancing I_h conductance further reduces dendritic integration and neuronal excitability, while these are increased in response to blockade of I_h (Huang et al., 2009; Wang et al., 2007). Therefore, increased I_h following occlusion could be acting to reduce

excitatory and inhibitory responses following synaptic input, decreasing neuronal excitability. This effect would not be observable in response to somatic current injections.

The channels that may regulate medium AHP have also been found to have roles at dendrites and in modulating synaptic input. There is evidence that Kv7 channels that regulate the M-current are located at the soma and dendrites where they reduce the amplitude of excitatory inputs (Shah et al., 2011). SK channels are also present at dendrites and can affect synaptic input (Jones et al., 2017). These channels are activated by calcium, therefore, calcium influx through NMDA receptors and/or voltage-gated calcium channels will activate SK channels causing a hyperpolarisation and decreasing membrane resistance (Faber et al., 2005). As Kv7 channels are activated by depolarisation and SK channels are voltage-independent, it is unclear whether these channels would have an effect on inhibitory inputs. If these channels are active at rest, they may be inactivated, reducing their shunting effect on inhibitory inputs.

Therefore, the activity-dependent changes in sag potential and medium AHP may not directly affect firing properties. The increased biophysical properties or density of these channels may affect synaptic input, reducing excitation. Future work should investigate the distribution of these channels in monophasic olfactory bulb DAT-tdTomato neurons and combine this information with what is known about the spatial distribution of inputs onto these neurons (Kiyokage et al., 2017). By performing cell-attached recordings of these neurons in acute slices, while stimulating OSN inputs or monosynaptically connected bulbar neurons, it would be possible to investigate synaptic driven activity following occlusion. Whole-cell recordings could then be performed to correlate intrinsic properties with firing activity.

4.3.5 Implications for the function of monophasic dopaminergic neurons in the olfactory bulb

From what is known about the role of I_h and medium AHP in regulating intrinsic excitability we can hypothesise different explanations for what these results could mean for the activity of these neurons. If a dopaminergic neuron is spontaneously active, the increase in the sag potential could support this activity, by increasing the likelihood of subsequent action potentials. However, if the neuron is at rest, the result could be to inhibit firing by keeping the neuron around its resting membrane potential. As medium AHP is associated with reduced excitability, the repetitive firing of spontaneous action potentials could activate these channels, silencing the neuron and allowing I_h to stabilise the neuron at its resting membrane potential. This could help explain why there were no significant differences identified in the firing of multiple action

potentials as constant depolarisation was applied to the neuron, which would recruit I_h to support continued firing, mitigating the effect of activating medium AHP.

Comparing the firing properties of control and occluded neurons using selective blockers of medium AHP and I_h may give further insight into the role that these currents could play in regulating intrinsic excitability. For example, if the increase in medium AHP is reducing excitability, then blocking I_h would be expected to show less firing in occluded neurons and this would then be sensitive to medium AHP blockers. There may be a suggestion of this happening in 1 day occluded neurons. These neurons showed a trend to reduced firing and increased medium AHP, with the sag potential unaffected, though there was a higher probability of firing an action potential following the sag protocol. It would also be important to study more physiological firing, for example, recording pacemaker activity and cell-attached activity in response to OSN input might reveal differences in firing that cannot be observed using standard somatic current injection protocols.

These changes could have an important effect on the role of monophasic dopaminergic neurons in the olfactory bulb for intraglomerular activity. If the increase of I_h and the currents driving medium AHP are affecting synaptic inputs, this could make these neurons less responsive to inputs. Depending on how glutamatergic and GABAergic receptors are affected by occlusion, monophasic olfactory bulb dopaminergic neurons would likely require stronger excitatory input to fire. Conversely, they may also need greater inhibitory input to be silenced. They would also be less excitable if these currents are acting to clamp the neuron at the resting membrane potential. If firing was initiated, subsequent firing could be potentiated by I_h, which would then be suppressed by the activation of medium AHP. Under these scenarios, monophasic olfactory bulb dopaminergic neurons would be less active and contribute less to intraglomerular inhibition.

4.3.6 Impact of inhibition on excitability

It is interesting to note the differences in the repetitive firing of monophasic olfactory bulb dopaminergic neurons in this study compared to previous work. Focussing on the control groups, I found an average maximum firing of ~36 action potentials, whereas Galliano et al., (2018) reported an average of 10 action potentials fired. The main modification in the recording conditions is the presence of synaptic blockers in the results I have presented here, while Galliano et al. (2018) recorded in ACSF alone. Such a striking difference in the intrinsic excitability of these neurons across conditions strongly suggests that repetitive firing is regulated by synaptic activity. Tonic inhibition has been shown to reduce neuronal excitability and suppress

the ability to fire repetitive action potentials (Cope et al., 2005). It is known that there is tonic inhibition by GABA in glomeruli (Murphy et al., 2005; Shao et al., 2009). Repetitive firing could also evoke $GABA_A$-mediated auto-inhibition that has been shown to be present in olfactory bulb dopaminergic neurons (Maher and Westbrook, 2008). It is, therefore, important to understand how synaptic input to these neurons, especially auto-evoked inhibition, is affected by unilateral naris occlusion. This will be explored in the next chapter.

Chapter Five – Synaptic properties and experience-dependent plasticity of olfactory bulb dopaminergic neurons

5.1 Introduction

5.1.1 Synaptic plasticity of inhibitory neurons

The activity-dependent modification of synapses has been a long studied form of neuronal plasticity. The strengthening or weakening of connections between neurons in response to changes in activity affects the transmission of information at these synapses. The current research suggests that activity-dependent changes to the synapses of inhibitory neurons can be complex. Increasing levels of BDNF *in vitro*, as has been reported to occur with increased network activity, leads to an increase in miniature excitatory postsynaptic current (mEPSC) amplitudes in inhibitory visual cortical neurons, while activity suppression was found not to affect mEPSC amplitudes (Rutherford et al., 1998). In inhibitory hippocampal neurons activity deprivation is associated with a decrease in mEPSC amplitude (Chang et al., 2010). *In vivo* studies have shown that following monocular deprivation, inhibitory neurons can display increased spine size, with an increase in mEPSC amplitude (Barnes et al., 2017), while spines can also be lost with a decrease in the frequency of mini inhibitory postsynaptic current (mIPSC) events (Keck et al., 2011). These studies indicate that the synapses of inhibitory neurons can be affected in an experience-dependent manner

Olfactory learning has been associated with an increase in the density of excitatory and inhibitory synapses on granule cells; however, only an increase in the frequency of spontaneous IPSC events was observed (Lepousez et al., 2014). In the rat olfactory bulb, odour deprivation increases the amplitude of mEPSCs in external tufted cell and glomerular layer GABAergic interneurons (Tyler et al., 2007). This can occur after 3 days of occlusion. However, it is not known whether this can occur earlier or how specific populations of glomerular layer interneuron are affected.

5.1.2 Synaptic inputs to olfactory bulb dopaminergic neurons

The sources of glutamatergic and GABAergic inputs to olfactory bulb dopaminergic neurons have been described from physiology and electron microscopy (EM) work. In a TH-GFP mouse model, the majority of these neurons were found to respond monosynaptically to olfactory nerve stimulation (Pignatelli et al., 2009). Further work has shown that olfactory sensory neuron (OSN)

input to dopaminergic neurons is primarily targeted to distal dendrites (Kiyokage et al., 2017). Other glutamatergic inputs to dopaminergic neurons include those from external tufted cells and presumed mitral/tufted cells, which preferentially target the proximal dendrites (Kiyokage et al., 2017). Cortical feedback projections also release glutamate into the glomerular layer that activates glutamatergic receptors on GABAergic neurons (Boyd et al., 2012).

The GABAergic input to olfactory bulb dopaminergic neurons has been less described; however, EM work has shown that these neurons do receive GABAergic input from local interneurons in the glomerular layer (Toida et al., 2000). GABA release from GABAergic interneurons in the glomerular layer can signal to other GABAergic interneurons either through direct synaptic signalling or spillover (Murphy et al., 2005; Smith and Jahr, 2002). The glomerular layer also receives GABAergic cortical input (Gracia-Llanes et al., 2010) and input from deep short axon cells in the granule cell layer, which do target dopaminergic neurons (Eyre et al., 2008). Therefore, olfactory bulb dopaminergic neurons can receive glutamatergic and GABAergic inputs from a variety of neurons. However, whether any or all of these connections are modified in response to sensory experience is unknown.

5.1.3 Neurotransmitter release by olfactory bulb dopaminergic neurons

One known source of GABAergic input onto olfactory bulb dopaminergic neurons that has been demonstrated is from the neuron itself, i.e. auto-inhibition (Borisovska et al., 2013; Maher and Westbrook, 2008). This is produced by a GABAergic current that is generated by the release of GABA binding to a cell's own $GABA_A$ receptors. As the monophasic subpopulation of olfactory bulb dopaminergic neurons lack an axon, their release of neurotransmitter can only be somatodendritic (Borisovska et al., 2013; Maher and Westbrook, 2008). The ability to auto-inhibit suggests that these neurons have a feedback mechanism to regulate their own firing.

However, it is unclear whether this is also true for the subpopulation of dopaminergic neuron with an axon. These neurons are known to release GABA and dopamine from their axon and mediate interglomerular inhibition (Liu et al., 2013). EM work suggests that these neurons do not make dendrodendritic connections (Liberia et al., 2012) and, therefore, may not be involved in intraglomerular inhibition. This EM study found that their dendrites were exclusively the postsynaptic element when they formed synapses with GABAergic and non-GABAergic neurons. Their dendrites also did not form synapses with bulbar projection neurons, indeed when their dendrites were close to mitral/tufted cells, glial lamellae prevented contact. This study focussed on dopaminergic neurons in the rat olfactory bulb that were deep in the external plexiform,

while axonic dopaminergic neurons are often located more superficially around the border with the glomerular layer (Galliano et al., 2018). Other axon-bearing neurons in the olfactory bulb, including external tufted cells and the projection neurons, are known to release from their dendrites (Vaaga and Westbrook, 2017). However, it has been suggested that axon-bearing deep short axon cells do not form dendrodendritic synapses (Eyre et al., 2008). There, therefore, needs to be a functional investigation of whether axonic dopaminergic neurons have dendritic release of neurotransmitter.

5.1.4 Chapter aims

At present, there is no published work describing mE/IPSCs in olfactory bulb dopaminergic neurons, nor the plasticity of these events. Measuring AMPA receptor-mediated mEPSCs and $GABA_A$ receptor-mediated mIPSCs in DAT-tdTomato olfactory bulb neurons enables the assessment of experience-dependent plasticity of postsynaptic strength and presynaptic properties. In addition to this, I will build on previous work describing auto-inhibition currents in these neurons by investigating how they are affected by unilateral naris occlusion. Finally, I will also describe differences in auto-evoked inhibition between the two main subpopulations of olfactory bulb dopaminergic neurons and discuss their implications for connectivity and function in olfactory bulb circuitry.

5.2 Results

5.2.1 The effect of unilateral naris occlusion on mini excitatory postsynaptic currents

I first recorded AMPA mEPSCs in monophasic olfactory bulb DAT-tdTomato neurons after either 1 or 3 days of unilateral naris occlusion or sham occlusion. All mEPSC recordings were performed at -70 mV, using a caesium methanesulfonate internal solution. TTX, APV and gabazine were added to the standard ACSF to block sodium-mediated action potentials, NMDA and $GABA_A$ receptors, respectively. There were no differences in the passive properties of the neurons under these recording conditions (see **Table 5.1**). mEPSCs were recorded as fast inward currents at -70 mV (**Figure 5.1A-B**).

		R_I (MΩ) (†) (mean ± SEM)	C_M (pF) (mean ± SEM)	R_S (MΩ) (mean ± SEM)
1 day control (*n = 12*)		957.7 ± 178.6	24.2 ± 2.28	23.42 ± 1.06
1 day occluded (*n =14*)		1124 ± 181	24.48 ± 1.99	24.71 ± 1.01
3 day control (*n =10*)		805.7 ± 256.9	25.15 ± 2.06	22.17 ± 0.92
3 day occluded (*n = 15*)		884.1 ± 174.6	26.67 ± 1.76	22.83 ± 1.06
Two-Way ANOVA effect of	Manipulation	$F_{(1,47)} = 1.79$ p = 0.20	$F_{(1,47)} = 0.19$ p = 0.66	$F_{(1,47)} = 0.86$ p = 0.36
	Time	$F_{(1,47)} = 3.71$ p = 0.06	$F_{(1,47)} = 0.59$ p = 0.66	$F_{(1,47)} = 2.23$ p = 0.14
	Interaction	$F_{(1,47)} = 0.04$ p = 0.84	$F_{(1,47)} = 0.09$ p = 0.76	$F_{(1,47)} = 0.09$ p = 0.76

Table 5.1: Passive properties of mEPSC neurons

(†) = Two-way ANOVA on reciprocal transformed data

The frequency of mEPSCs is commonly used as an indicator of presynaptic release probability and number of release sites. After 1 and 3 days of occlusion this remained unchanged (mean ± SEM: 1 day control, 3.7 ± 0.61 Hz, *n* = 12; 1 day occluded, 3.51 ± 0.77 Hz, *n* = 14; 3 day control, 3.16 ± 0.57 Hz, *n* = 10; 3 day occluded, 3.38 ± 0.44 Hz, *n* = 15. Two-way ANOVA on $\log_{10}$ transformed data, effect of manipulation, $F_{(1,47)} = 0.002$, p = 0.96; effect of time, $F_{(1,47)} = 0.11$, p = 0.75; effect of manipulation x time interaction, $F_{(1,47)} = 0.46$, p = 0.50) (**Figure 5.1C**). The source of glutamatergic events in glomeruli could come from OSNs, external tufted cells, bulbar projection neurons and/or feedback from olfactory cortex. Given the potential heterogeneity of excitatory inputs to dopaminergic neurons this result only gives an indication of overall

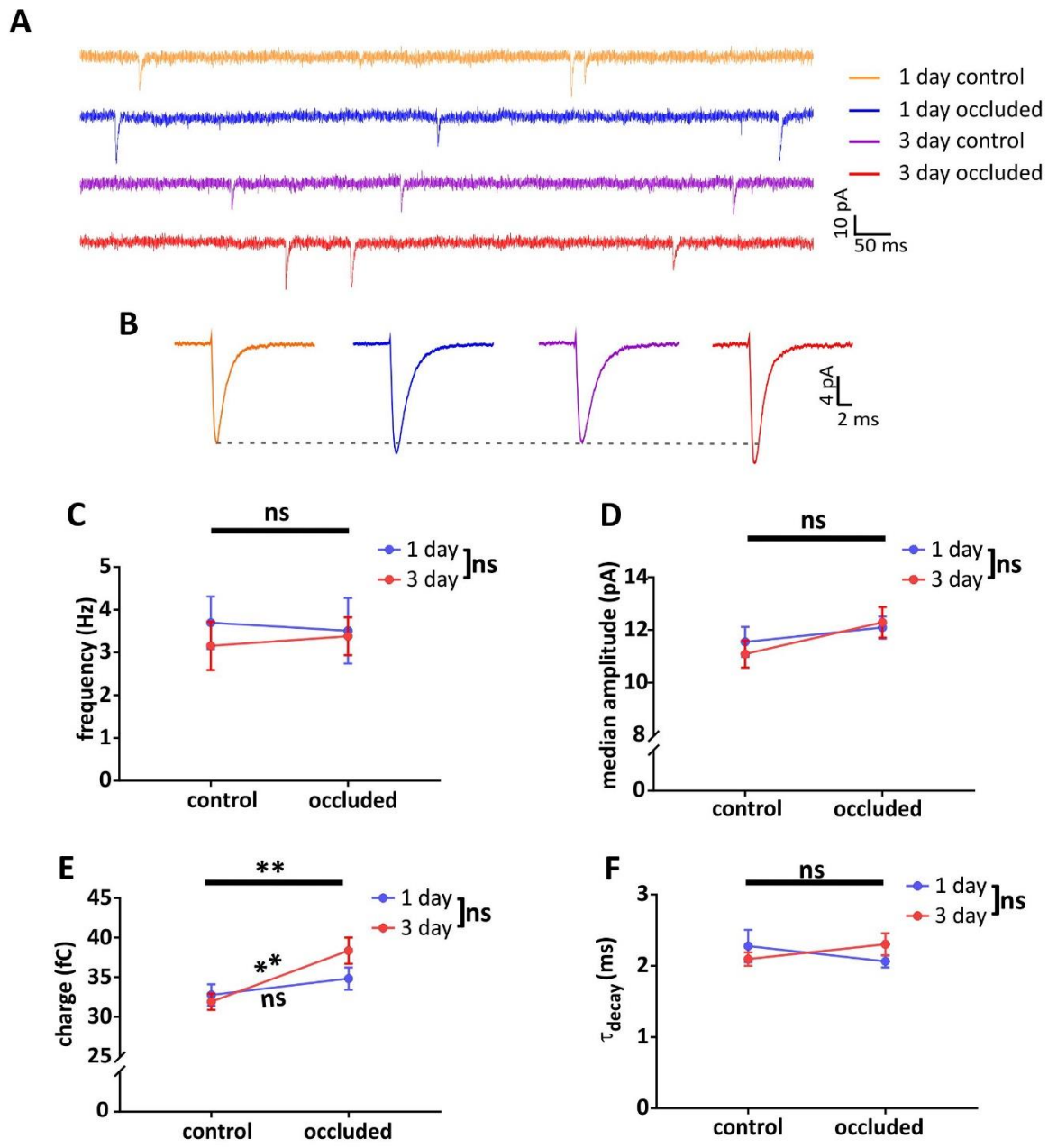

Figure 5.1: Occlusion affects the charge of mEPSCs

A: Example traces of mini excitatory postsynaptic currents recordings in 1 and 3 day control and occluded monophasic DAT-tdTomato neurons.

B: Example of an average mEPSC event from all mEPSC events recorded in a single neuron in each condition. Dashed line is aligned to the peak of the 1 day control trace.

C-F: Mean ± SEM of the (C) frequency (Hz), (D) median amplitude (pA), (E) charge (fC) of mEPSC events and (F) decay (ms) calculated by fitting a single exponential to an averaged mEPSC event generated by averaging all events in each cell. (C) Two-way ANOVA on the log10 transformed data, ns: non-significant. (D-F) Two-way ANOVA; effect of manipulation, ** $p < 0.01$; ns: non-significant; effect of time, ns: non-significant; Sidak's multiple comparisons test, ** $p < 0.01$; ns: non-significant.

[C-F (n): 1 day control (12); 1 day occluded (14); 3 day control (10); 3 day occluded (15)].

glutamatergic transmission onto these neurons, which appear to be unchanged following occlusion.

The amplitude of mEPSCs is used as a measure of quantal size and is mainly determined by the number of available AMPA receptors (Turrigiano et al., 1998). At sub-saturating levels it is also dependent on the amount of transmitter released in a single vesicle (Wu et al., 2007). However, in the glomerular layer, increased mEPSC amplitude following odour deprivation has been shown to be due to postsynaptic changes (Tyler et al., 2007). In response to occlusion, there was a small but non-significant increase in the median amplitude of mEPSC events experienced by monophasic DAT-tdTomato neurons (mean ± SEM: 1 day control, 11.54 ± 0.57 pA, n = 12; 1 day occluded, 12.09 ± 0.42 pA, n = 14; 3 day control, 11.08 ± 0.52 pA, n = 10; 3 day occluded, 12.28 ± 0.58 pA, n = 15. Two-way ANOVA, effect of manipulation, $F_{(1,47)}$ = 2.6, p = 0.11; effect of time, $F_{(1,47)}$ = 0.06, p = 0.80; effect of manipulation x time interaction, $F_{(1,47)}$ = 0.36, p = 0.55) (**Figure 5.1D**). AMPA amplitude is known to be affected by dendritic filtering as AMPA receptors are arrayed along the length of dendrites (Han and Stevens, 2009). This should be partially mitigated by the small size and electrotonic compactness of monophasic olfactory bulb dopaminergic neurons and unchanged passive properties between groups. Nevertheless, I also measured and compared the total charge transfer of mEPSC events, which has been reported to be less affected by filtering than amplitude (Han and Stevens, 2009). I found that there was a significant effect of occlusion on the charge of mEPSC events, particularly after 3 days of occlusion (mean ± SEM: 1 day control, 32.75 ± 1.36 fC, n = 12; 1 day occluded, 34.82 ± 1.4 fC, n = 14; 3 day control, 31.9 ± 1.03 fC, n = 10; 3 day occluded, 38.36 ± 1.67 fC, n = 15. Two-way ANOVA on $\log_{10}$ transformed data, effect of manipulation, $F_{(1,47)}$ = 8.6, p = 0.005; effect of time, $F_{(1,47)}$ = 0.8, p = 0.86; effect of manipulation x time interaction, $F_{(1,47)}$ = 2.03, p = 0.16. Post-hoc Sidak's test between conditions: 1 day, $t_{(47)}$ = 1.08, p = 0.49; 3 day, $t_{(47)}$ = 3.02, p = 0.008) (**Figure 5.1E**). This suggests that longer duration odour deprivation results in an increase in current through activated AMPA receptors in DAT-tdTomato neurons.

Increased charge could be the result of increased amplitude and/or slower kinetics of postsynaptic AMPA receptors. I next analysed the AMPA receptor kinetics by fitting a single exponential to the decay phase of an averaged mEPSC trace. Group comparisons did not reveal significant differences for the decay constant (τ), though 3 day occluded neurons had the longest decay (mean ± SEM: 1 day control, 2.28 ± 0.23 ms, n = 12; 1 day occluded, 2.06 ± 0.08 ms, n = 14; 3 day control, 2.1 ± 0.09 ms, n = 10; 3 day occluded, 2.31 ± 0.15 ms, n = 15. Two-way ANOVA, effect of manipulation, $F_{(1,47)}$ = 0.0005, p = 0.98; effect of time, $F_{(1,47)}$ = 0.034, p = 0.85; effect of manipulation x time interaction, $F_{(1,47)}$ = 0.191, p = 0.17) (**Figure 5.1F**). The slight trends for 3 day

occluded neurons to have the largest mEPSC amplitude together with the longest decay likely produce the significant effect on charge. Overall, there appears to be an effect of 3 day occlusion on mEPSCs in monophasic olfactory bulb dopaminergic neurons. These results also suggest that it is postsynaptic AMPA receptors that are being affected.

Multiplicative synaptic scaling has been proposed as a mechanism whereby all synapses would be proportionately adjusted to preserve the relative synaptic strengths within a neuron (Turrigiano et al., 1998). To compare multiplicative scaling in mEPSC amplitudes, 1 and 3 day events were analysed separately. 100 random events were selected from the 10^{th} to 90^{th} percentile of total events from each neuron, this was to ensure each neuron contributed equally and to avoid potential deviations of fit due to outliers (Kim et al., 2012). There were more occluded neurons at both timepoints and, therefore, a subset of these neurons was randomly selected to match the number in their respective controls (1 day = 1,100 events per group; 3 day = 900 events per group). The events were rank-ordered, plotted and fitted with a straight line ($y = ax$), giving a scaling factor of 1.063 and 1.147 for 1 and 3 day groups, respectively (**Figure 5.2A-B**).

The cumulative distribution of all mEPSC events were plotted and a two-sample Kolmogorov-Smirnov test was performed comparing control and occluded distributions (1 day control vs occluded, $p = 0.001$; 3 day control vs occluded, $p = 3.32 \times 10^{-9}$) (**Figure 5.2C-D**). The occluded events were scaled by the scaling factor and events that fell below the mEPSC amplitude threshold of 5 pA were not included in the analyses, as these could represent scaled-up subthreshold events (Kim et al., 2012). The cumulative distributions of these scaled events were plotted and compared to their controls. If there was multiplicative synaptic scaling, then the scaled distributions would not be statistically different from the controls. However, despite appearing almost indistinguishable by eye, the scaled distributions for both 1 day and 3 day groups remained significantly different (two-sample Kolmogorov-Smirnov; 1 day control vs scaled occluded, $p < 1 \times 10^{-37}$; 3 day control vs scaled occluded, $p = 3.76 \times 10^{-5}$) (**Figure 5.2.C-D**). This suggests that the Kolmogorov-Smirnov test is extremely sensitive to slight differences in distributions, especially with large *n*. In addition, the plots show that the biggest events appear to be most affected by occlusion and may explain the lack of global synaptic scaling.

Based on these results it appears that the increase in mEPSC amplitude after 3 day occlusion is not strictly multiplicative. To further characterise this, I also investigated whether lack of

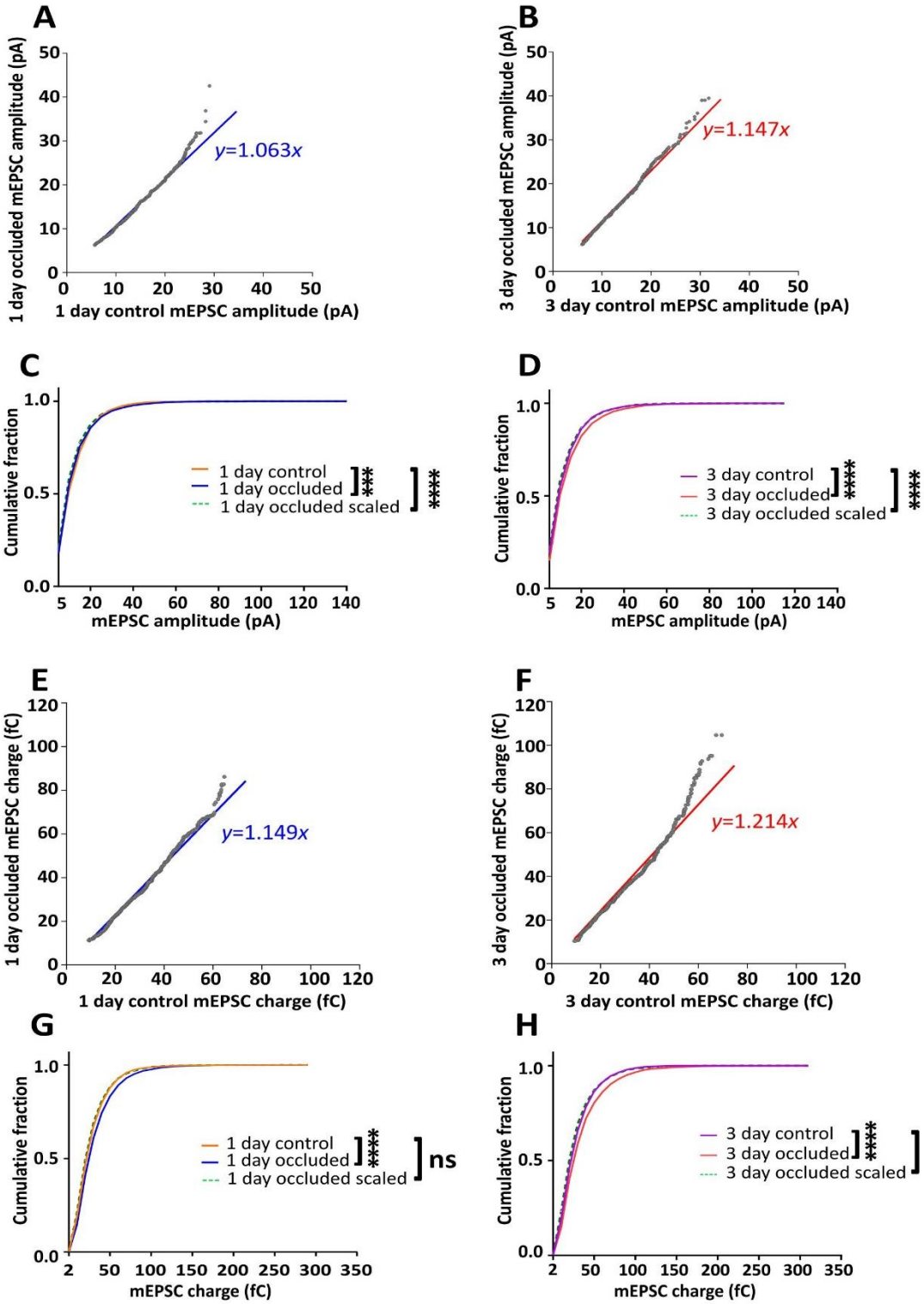

Figure 5.2: mEPSCs do not show strong evidence of multiplicative synaptic scaling

A-B, E-F: Rank-ordered (A-B) amplitudes and (E-F) charges of mEPSCs in 1 day and 3 day occluded monophasic DAT-tdTomato neurons plotted against their rank-ordered control mEPSCs . The straight line is a linear fit with a zero *y*-intercept and the equation $y = ax$.

C-D, G-H: Cumulative distribution of mEPSC (C-D) amplitudes and (G-H) charges of 1 day and 3 day control and occluded neurons. Individual mEPSC amplitudes and charges in 1 day occluded and 3 day occluded neurons were scaled by the calculated scaling function, $y = ax$. Two-sample Kolmogorov-Smirnov test, **** $p < 0.0001$, *** $p<0.001$, ns: non-significant.

multiplicative synaptic scaling was observed by analysing charge. Using the same approach as for mEPSC amplitudes, 1 and 3 day groups had scaling factors of 1.15 and 1.21, respectively (**Figure 5.2E-F**). The cumulative distributions showed that they were significantly different in both groups (two-sample Kolmogorov-Smirnov test; 1 day control vs occluded, $p < 1 \times 10^{-37}$; 3 day control vs occluded, $p < 1 \times 10^{-37}$) (**Figure 5.2G-H**). Scaling the occluded charges by their respective scaling factors produced a 1 day scaled distribution that was not significantly different from the control, while the 3 day scaled distribution still remained significantly different, despite appearing to be indistinguishable from the control distribution by eye (two-sample Kolmogorov-Smirnov; 1 day control vs scaled occluded, $p = 0.058$; 3 day control vs scaled occluded, $p = 3.1 \times 10^{-6}$) (**Figure 5.2G-H**). Therefore, there is an indication that mEPSC charge may show a slight increase in charge after 1 day occlusion that is maintained and increased by 3 days occlusion. However, the multiplicative nature of the change is not, likely due to the presence of larger events that are deviating from the linear fit.

The results investigating the amplitude and charge of mEPSCs suggests that strictly multiplicative synaptic scaling is not likely to be occurring after naris occlusion in this neuronal population. However, I had identified changes in mEPSC events. Previous research has shown that larger synapses may be preferentially enhanced by blocking activity (Thiagarajan et al., 2005), which is what my data is suggesting. To analyse this, I calculated the percentage of events that were greater than three standard deviations from the mean of total events from all groups (amplitude larger than 43.31 pA and charge large than 107.35 fC). There was a significant increase in the percentage of these very large events after occlusion, specifically the 3 day occluded group, as measured by amplitude (mean ± SEM: 1 day control, 1.23 ± 0.29 %, $n = 12$; 1 day occluded, 2.11 ± 0.76 %, $n = 14$; 3 day control, 1.28 ± 0.42 %, $n = 10$; 3 day occluded, 3.1 ± 0.61 %, $n = 15$. Two-way ANOVA on ranks, effect of manipulation, $F_{(1,47)} = 4.51$, $p = 0.04$; effect of time, $F_{(1,47)} = 1.69$, $p = 0.20$; effect of manipulation x time interaction, $F_{(1,47)} = 1.8$, $p = 0.19$. Post-hoc Sidak's test between groups: 1 day, $t_{(47)} = 0.56$, $p = 0.82$; 3 day, $t_{(47)} = 2.4$, $p = 0.04$) (**Figure 5.3A**). This result was also found when analysing very large events by charge (mean ± SEM: 1 day control, 1.27 ± 0.35 %, $n = 12$; 1 day occluded, 1.97 ± 0.47 %, $n = 14$; 3 day control, 0.87 ± 0.24 %, $n = 10$; 3 day occluded, 3.23 ± 0.67 %, $n = 15$. Two-way ANOVA on ranks, effect of manipulation, $F_{(1,47)} = 4.51$, $p = 0.04$; effect of time, $F_{(1,47)} = 1.699$, $p = 0.20$; effect of manipulation x time interaction, $F_{(1,47)} = 1.86$, $p = 0.19$. Post-hoc Sidak's test between groups: 1 day, $t_{(47)} = 0.56$, $p = 0.82$; 3 day, $t_{(47)} = 2.4$, $p = 0.04$) (**Figure 5.3B**). This suggests that large excitatory synapses may be preferentially potentiated following occlusion.

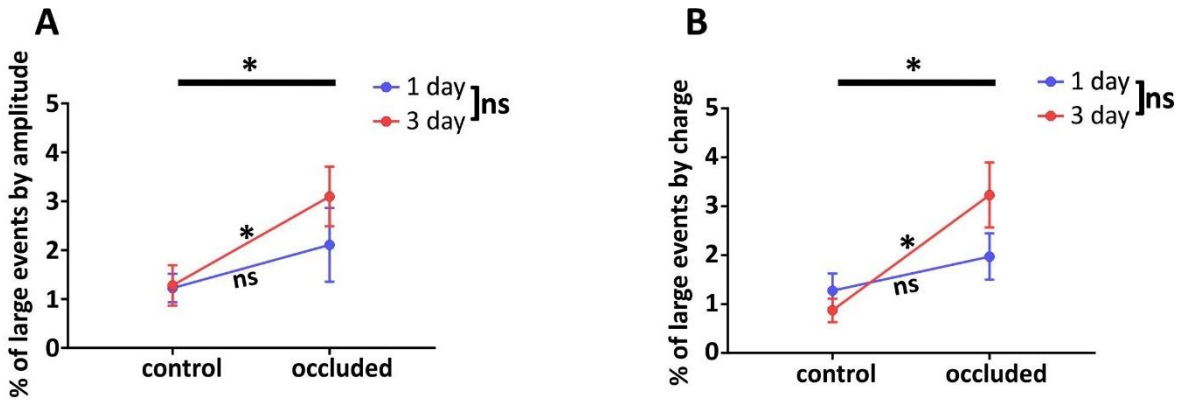

Figure 5.3: Occlusion increases the occurrence of large mEPSC events

A-B: Mean ± SEM of the % of very large events (defined as bigger than the mean of total events plus three standard deviations) by (A) amplitude and (B) charge. (A-B) Two-way ANOVA on ranks, effect of manipulation, * $p < 0.05$; effect of time, ns: non-significant. Sidak's multiple comparisons test, * $p < 0.05$; ns: non-significant.

5.2.2 The effect of unilateral naris occlusion on mini inhibitory postsynaptic currents

To test whether mIPSCs were modified by unilateral naris occlusion, 1 and 3 day control and occluded DAT-tdTomato neurons were targeted for whole-cell voltage-clamp recordings. All mIPSC recordings were performed at +10 mV, using a caesium methansulfonate internal solution and TTX, APV and NBQX added to the standard ACSF. There were no differences in the passive properties of the neurons between conditions (see **Table 5.2**). At +10 mV and with caesium methansulfonate internal solution, mIPSCs were recorded as outward events (**Figure 5.4A-B**).

		R_I (MΩ) (†) (mean ± SEM)	C_M (pF) (mean ± SEM)	R_S (MΩ) (mean ± SEM)
1 day control (*n = 11*)		1193 ± 376.4	27.37 ± 2.36	21.81 ± 1.16
1 day occluded (*n =17*)		1005 ± 94.22	27.66 ± 2.28	22.42 ± 1.15
3 day control (*n =10*)		908.5 ± 272.9	27.86 ± 2.47	22.88 ± 1.53
3 day occluded (*n = 12*)		985 ± 131.1	28.75 ± 1.91	20.67 ± 0.84
Two-Way ANOVA effect of	Manipulation	$F_{(1,46)} = 1.74$ p = 0.19	$F_{(1,46)} = 0.06$ p = 0.80	$F_{(1,46)} = 0.43$ p = 0.51
	Time	$F_{(1,46)} = 0.7$ p = 0.41	$F_{(1,46)} = 0.11$ p = 0.74	$F_{(1,46)} = 0.08$ p = 0.78
	Interaction	$F_{(1,46)} = 0.09$ p = 0.77	$F_{(1,46)} = 0.02$ p = 0.90	$F_{(1,46)} = 1.36$ p = 0.25

Table 5.2: Passive properties of mIPSC neurons

(†) = Two-way ANOVA on reciprocal transformed data

GABAergic release in glomeruli is likely to come from the GABAergic interneurons located in the glomerular layer, deep short-axon cells in the granule cell layer and some cortical input (Eyre et al., 2008; Gracia-Llanes et al., 2010; Murphy et al., 2005). Despite these numerous potential presynaptic input sources, the frequency of mIPSC events was very low, with no changes between the control and occluded groups (mean ± SEM: 1 day control, 0.28 ± 0.08 Hz, n = 11; 1 day occluded, 0.29 ± 0.04 Hz, n = 17; 3 day control, 0.37 ± 0.07 Hz, n = 10; 3 day occluded, 0.34 ± 0.05 Hz, n = 12. Two-way ANOVA on $\log_{10}$ transformed data, effect of manipulation, $F_{(1,46)} = 0.08$, p = 0.78; effect of time, $F_{(1,46)} = 2.82$, p = 0.10; effect of manipulation x time interaction, $F_{(1,46)} = 0.3$, p = 0.59) (**Figure 5.4C**). In addition, no significant differences were found for the mean amplitude of mIPSCs (mean ± SEM: 1 day control, 20.36 ± 1.53 pA, n = 11; 1 day occluded, 21.71 ± 1.19 pA, n = 17; 3 day control, 20.24 ± 1.05 pA, n = 10; 3 day occluded, 21.1 ± 1.35 pA, n = 12. Two-way ANOVA, effect of manipulation, $F_{(1,46)} = 0.68$, p = 0.41; effect of

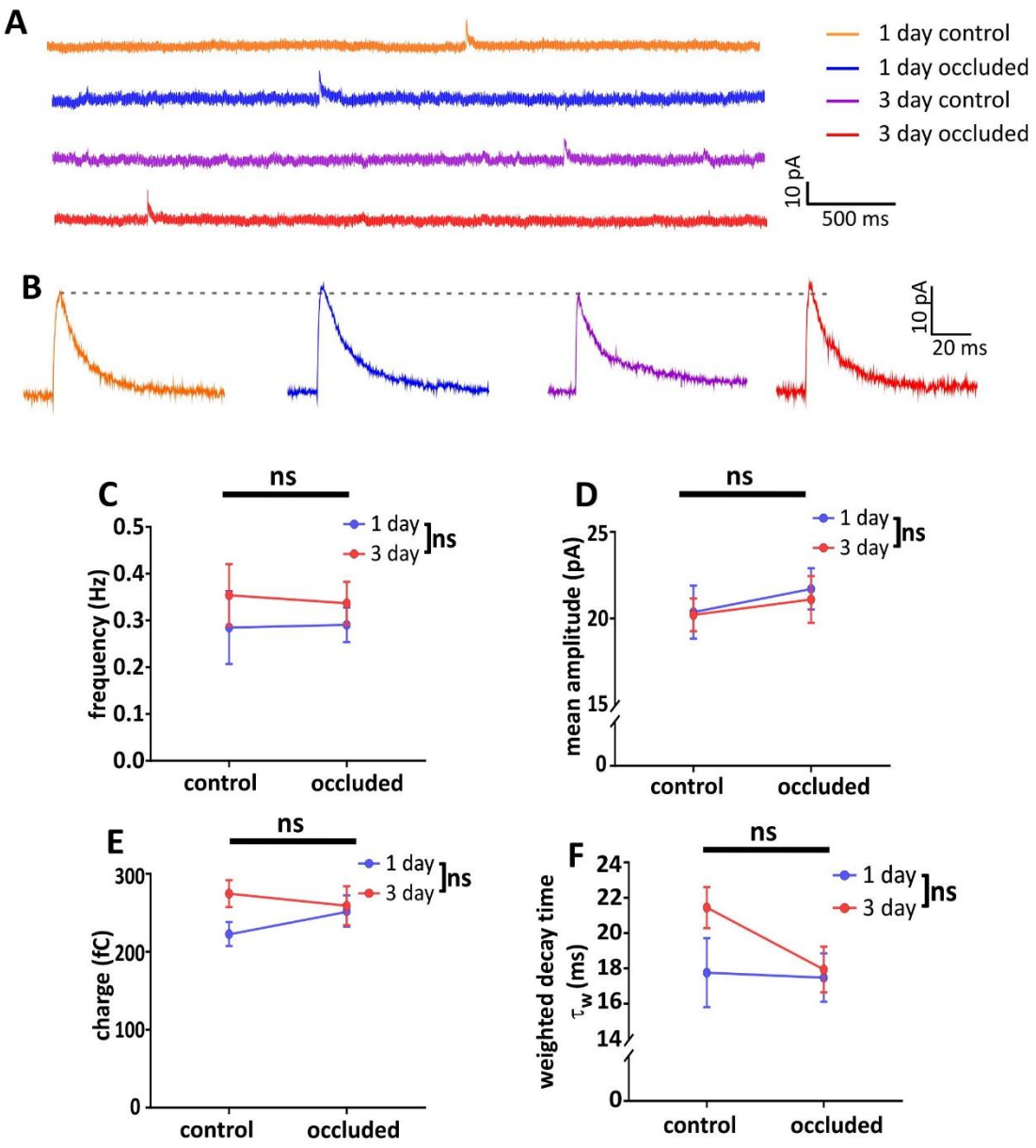

Figure 5.4: mIPSCs are not affected by occlusion

A: Example traces of mini inhibitory postsynaptic currents (mIPSCs) recordings in 1 and 3 day control and occluded monophasic DAT-tdTomato neurons.

B: Example averaged mIPSC events of the mean response from each condition. Dashed line is aligned to the peak of the 1 day control trace.

C-F: Mean ± SEM of the (C) frequency (Hz), (D) mean amplitude (pA), (E) charge (fC) of mIPSC events and (F) weighted decay time constant (τ_w) (ms) calculated by fitting a double exponential to an averaged mIPSC event generated by averaging all events in each cell. (C, F) Two-way ANOVA on the $\log_{10}$ transformed data, ns non-significant. (D-E) Two-way ANOVA, ns: non-significant.

[C-F (n): 1 day control (11); 1 day occluded (17); 3 day control (10); 3 day occluded (12)].

time, $F_{(1,46)} = 0.08$, p = 0.78; effect of manipulation x time interaction, $F_{(1,46)} = 0.03$, p = 0.86) (**Figure 5.4D**).

As with mEPSCs, mIPSC amplitude could be affected by dendritic filtering. Therefore, the charge of mIPSC events were also analysed. In agreement with the amplitude results, charge was not different between control and occluded conditions (mean ± SEM: 1 day control, 212.2 ± 15.41 fC, *n* = 11; 1 day occluded, 252.2 ± 20.21 fC, *n* = 17; 3 day control, 271.5 ± 18.78 fC, *n* = 10; 3 day occluded, 259.2 ± 25.05 fC, *n* = 12. Two-way ANOVA, effect of manipulation, $F_{(1,46)} = 0.42$, p = 0.52; effect of time, $F_{(1,46)} = 2.4$, p = 0.13; effect of manipulation x time interaction, $F_{(1,46)} = 1.5$, p = 0.23) (**Figure 5.4E**). To investigate the kinetics of $GABA_A$ receptors an averaged IPSC was generated for each cell. The IPSC decay was best fitted by a double exponential and a weighted mean decay time constant was calculated (τ_w) (Luo et al., 2013) (see Methods 2.5.5). There was no significant difference in this measure between the groups (mean ± SEM: 1 day control, 17.76 ± 1.94 ms, *n* = 11; 1 day occluded, 17.48 ± 1.37 ms, *n* = 17; 3 day control, 21.45 ± 1.17 ms, *n* = 10; 3 day occluded, 17.94 ± 1.3 ms, *n* = 12. Two-way ANOVA on $\log_{10}$ transformed data, effect of manipulation, $F_{(1,46)} = 1.54$, p = 0.22; effect of time, $F_{(1,46)} = 2.72$, p = 0.11; effect of manipulation x time interaction, $F_{(1,46)} = 1.32$, p = 0.26) (**Figure 5.4F**). These results suggest that unilateral naris occlusion does not affect basic spontaneous properties of ensemble $GABA_A$ synapses on monophasic DAT-tdTomato olfactory bulb neurons.

5.2.3 Auto-evoked inhibition in monophasic DAT-tdTomato neurons

As discussed previously, one source of GABAergic input to olfactory bulb dopaminergic neurons can be from the neurons themselves. Olfactory bulb dopaminergic neurons have been shown to release GABA that binds to their own $GABA_A$ receptors (Borisovska et al., 2013; Maher and Westbrook, 2008). Auto-inhibition by glomerular layer GABAergic interneurons is believed to be mediated by dendritic release of neurotransmitter (Murphy et al., 2005; Smith and Jahr, 2002). This auto-inhibition would be predicted to affect the activity of these neurons as GABA release in glomeruli can either induce firing in silent GABAergic interneurons or silence active neurons (Parsa et al., 2015).

To evoke auto-inhibition in olfactory bulb DAT-tdTomato neurons, I used whole-cell voltage clamp to hold neurons at -80 mV and stepped the membrane potential to 0 mV for 10 ms before returning to -80 mV to measure the auto-inhibition current. A high caesium chloride internal solution was used to allow chloride efflux through activated $GABA_A$ receptors. An inward current was observed at -80 mV after evoking transmitter release with transient depolarisation and this inward current was blocked by adding 10 µM of the $GABA_A$ antagonist, gabazine (**Figure 5.5A**).

The inward current did not have a smooth decay and had some noise likely reflecting asynchronous GABA release (Smith and Jahr, 2002). Due to the presence of passive changes associated with the voltage step, I analysed from 10 ms after the end of the voltage step to isolate the auto-evoked inhibition response. The charge of the response in control monophasic DAT-tdTomato neurons was calculated by subtracting the area under the curve of the pre-gabazine response from the post-gabazine response (mean ± SEM: control, 49.23 ± 11.6 pC, n = 12) (**Figure 5.5B**). The charge of these auto-evoked inhibition responses showed considerable variability from neuron to neuron (range: 8 to 143 pC), likely reflecting variation in passive membrane properties, the pool of available vesicles and number and location of release sites and $GABA_A$ receptors along the dendrites.

5.2.4 Rundown and somatic depolarisation do not affect the auto-evoked inhibition response

Analysing different auto-evoked inhibition protocols in a single neuron requires that the cell exhibits a stable response over the course of the experiment. In whole-cell recordings, neurotransmitter release can run down over time due to the neuron being dialysed with the intracellular solution in the recording pipette (Smith and Jahr, 2002). This would lead to a reduction in the size of the auto-inhibition response. To minimise this, all auto-evoked inhibition recordings were done with 10 mM GABA added to the internal solution. This has been shown to reduce the rundown of the response reported by others when GABA had been omitted, likely due to a lack of available GABA to fill synaptic vesicles (Bouhours et al., 2011; Smith and Jahr, 2002). To confirm that there was no change in the response over time, the 10 ms voltage step protocol was repeated three times, with five minutes in between each protocol (**Figure 5.6A**). This showed that there was no significant change in the charge of the auto-evoked inhibition response during the experiment, though there was a trend for the response to slightly increase (mean ± SEM: timepoint 1, 25 ± 7.99 pC; timepoint 2, 27.29 ± 9.57 pC; timepoint 3, 29.29 ± 11.22 pC; n = 5, one-way repeated measures ANOVA, $F_{(2,8)} = 0.93$, p = 0.44) (**Figure 5.6B**).

To further characterise the stability of the response during the experiment, I investigated the effect of somatic depolarisation on the response. Work by Bouhours et al. (2011) demonstrated that subthreshold somatic depolarisation enhanced GABA release and the charge of

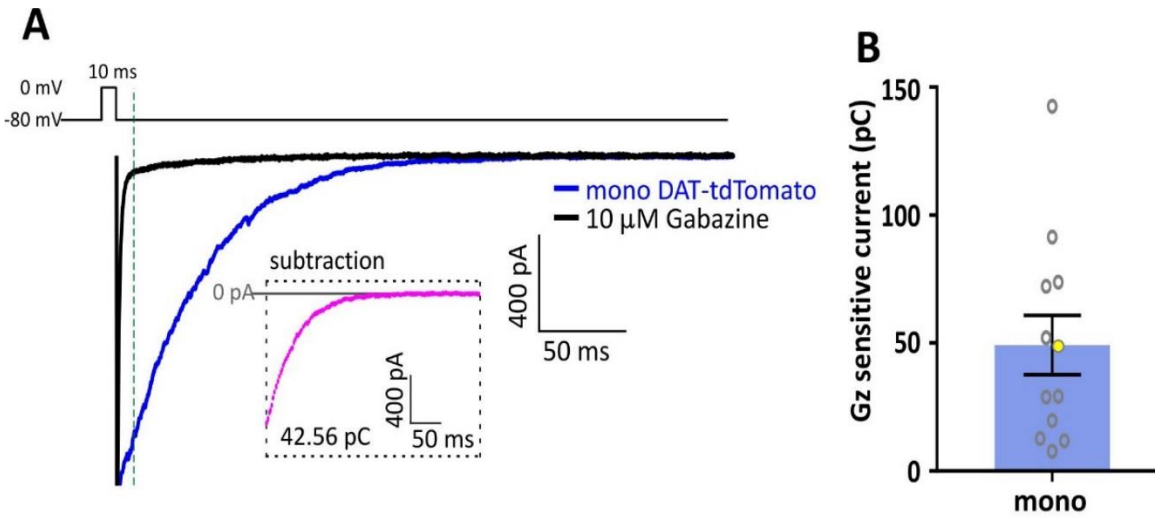

Figure 5.5: Auto-inhibition in monophasic DAT-tdTomato neurons

A: Example traces of auto-evoked inhibition following a 10 ms depolarisation from -80 mV to 0 mV in a monophasic DAT-tdTomato neuron before and after blocking with gabazine (Gz). Traces were analysed 10 ms after the end of the voltage step, indicated by the dashed line. **Inset**: gabazine-subtracted trace.

B: Scatter plot with bar shows the mean ± SEM charge (pC) of the gabazine-sensitive current. Open grey circles represent individual cells, yellow circle shows the value of the example cell in A.

[B (n): monophasic (12)].

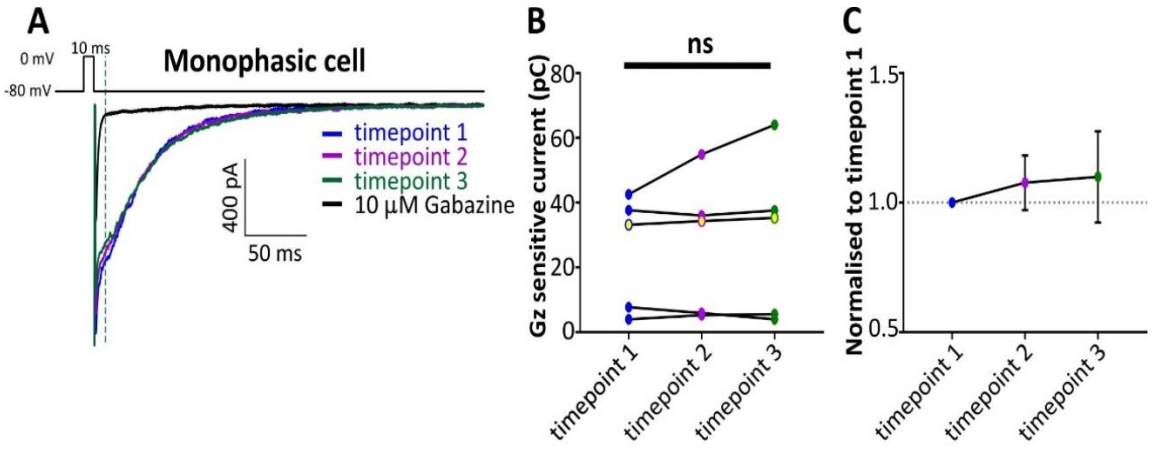

Figure 5.6: The auto-inhibition response does not rundown

A: Example traces of auto-evoked inhibition following a 10 ms depolarisation from -80 mV to 0 mV in a monophasic cell. The protocol was repeated at two more timepoints with 5 minutes between each repeat. Traces were analysed 10 ms after the end of the voltage step, indicated by the dashed line.

B: Comparison of the analysed auto-evoked inhibition charge (pC) after three repeats of the auto-evoked inhibition protocol. Circles represent individual cells and yellow circles show the values of the example traces shown in A. Repeated measures one-way ANOVA, ns: non-significant.

C: Auto-evoked responses normalised to auto-evoked response at timepoint 1. Circles show mean ± SEM.

[B-C (n): monophasic (5)].

auto-inhibition currents in cerebellar interneurons. This was due to an increase in baseline calcium concentration in presynaptic terminals, which enhanced the release probability of GABA. To study this in olfactory bulb dopaminergic neurons their somatic potential was held at either -50 mV or -80 mV for approximately 30 seconds before the start of the recordings. Neurons were then depolarised to 0 mV for 10 ms and then brought to -80 mV (**Figure 5.7A**). An auto-inhibition response was evoked after holding at both somatic potentials; however, there was no significant difference between holding at -50 mV or -80 mV (mean ± SEM: -50 mV response, 25.45 ± 4.53 pC; -80 mV response, 25.3 ± 7.3 pC; *n = 5,* paired t-test, $t_{(4)} = 0.052$, p = 0.96) (**Figure 5.7B**). Therefore, monophasic olfactory bulb dopaminergic neurons do not require extended periods of somatic depolarisation to facilitate GABA release, unlike cerebellar interneurons (Bouhours et al., 2011). Together these results suggest that the experimental design produces a reliable and stable response to study auto-evoked inhibition in this neuronal population.

5.2.5 The auto-evoked inhibitory response after 1 day of unilateral naris occlusion

The ability of olfactory bulb dopaminergic neurons to auto-inhibit gives the opportunity to study functional aspects of evoked GABA release in these neurons on both sides of the synapse. The mIPSC results indicated that there were no changes to pre or postsynaptic GABAergic input to monophasic olfactory bulb dopaminergic neurons after naris occlusion. However, there could be specific changes associated with GABA release and/or postsynaptic sites mediated by auto-inhibition. Changes in $GABA_A$-mediated auto-inhibition following occlusion would suggest that the release of GABA had been affected. As an initial characterisation I investigated the effect of 1 day of unilateral naris occlusion on the auto-inhibition response in monophasic olfactory bulb dopaminergic neurons.

Auto-inhibition was clearly present in both control and occluded groups, evidenced by large inward currents (**Figure 5.8A-B)**. Again, there was considerable variability in the auto-evoked response between the cells in each group. Overall, there was no significant difference between control and occluded neurons (mean ± SEM: control, 49.23 ± 11.6 pC, *n* = 12; occluded, 39.51 ± 9.9 pC, *n* = 9. t-test, $t_{(19)} = 0.61$, p = 0.55) (**Figure 5.8C**). Therefore, auto-evoked GABAergic responses appear to be largely unaffected by 1 day of occlusion.

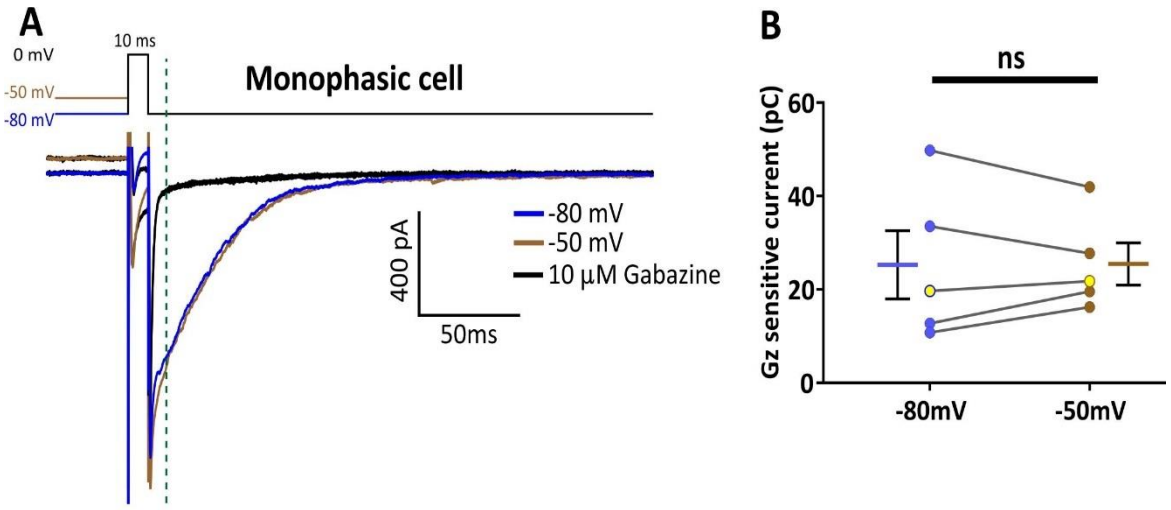

Figure 5.7: Somatic depolarisation does not increase the auto-evoked inhibition response

A: example traces of auto-evoked inhibition following a 10 ms depolarisation from either -80 mV or -50 mV to 0 mV in a DAT-tdTomato neuron before and after blocking with gabazine.

B: comparison of the auto-evoked inhibition charge (pC) from a holding potential of either -80 mV or -50 mV. Circles represent individual cells, line plots show mean ± SEM, and yellow circles show the values of the example cell in A. Paired t-test, ns: non-significant**.**

[B (n): monophasic (5)].

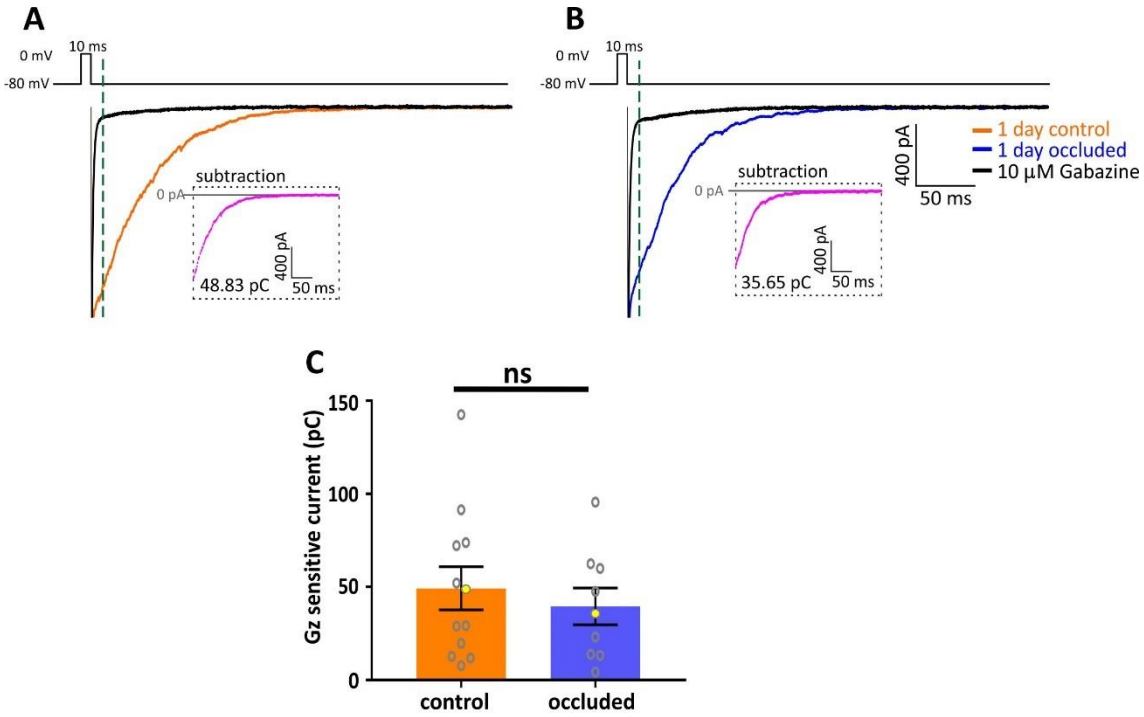

Figure 5.8: Auto-inhibition after 1 day of unilateral naris occlusion

A-B: Example traces of auto-evoked inhibition following a 10 ms depolarisation from -80 mV to 0 mV in a (A) 1 day control and (B) 1 day occluded DAT-tdTomato neuron before and after blocking with gabazine. Traces were analysed 10 ms after the end of the voltage step, indicated by the dashed line. **Insets**: gabazine-subtracted traces.

C: Scatter plot with bar shows the mean ± SEM charge (pC) of the gabazine-sensitive current in 1 day control and 1 day occluded neurons. Open grey circles represent individual cells, yellow circles show the values of the example cells in A-B. t-test; ns: non-significant.

[C (n): 1 day control (12); 1 day occluded (9)].

To further test whether GABA release was being affected after occlusion, I modified the protocol to include a second (paired) 10 ms voltage step with a 50 ms inter-stimulus interval. Due to the short inter-stimulus interval, the first voltage step response from the paired protocol was not analysed. Therefore, the response from the single voltage step protocol was compared to the second voltage step response from the paired protocol (**Figure 5.9A-B**). In the control condition, the paired response was significantly smaller than the single response (mean ± SEM: control single, 64.68 ± 14.55 pC, n = 8; control paired, 42.89 ± 7.78 pC, n = 8. Paired t-test, $t_{(7)}$ = 3.09, p = 0.018) (**Figure 5.9C**), while there was no difference in this measure in the occluded neurons (mean ± SEM: occluded single, 42.72 ± 10.59 pC, n = 8; occluded paired, 37.64 ± 8.48 pC, n = 8. Paired t-test, $t_{(7)}$ = 1.01, p = 0.35) (**Figure 5.9D**). This might suggest that there is minor paired-pulse depression of the auto-evoked inhibition in control neurons that is no longer present after 1 day of occlusion. However, a direct comparison of the paired-pulse ratio, calculated as the paired response/single response, was not significantly different between treatment groups (mean ± SEM: control, 0.75 ± 0.07, n = 8; occluded, 0.97 ± 0.13, n = 8. t-test, $t_{(14)}$ = 1.54, p = 0.15) (**Figure 5.9E**). These results suggest that presynaptic processes involved in GABA release from these neurons may be slightly affected after occlusion.

5.2.6 Comparison of auto-evoked inhibition in AIS-positive and AIS-negative olfactory bulb dopaminergic neuron populations

I have shown that I can record $GABA_A$-mediated auto-inhibition in monophasic dopaminergic neurons. As these neurons likely lack an axon and as anaxonic olfactory bulb dopaminergic neurons have previously been shown to make dendrodendritic connections (Kiyokage et al., 2017), this auto-inhibition is likely due to the release of GABA from their dendrites which subsequently binds to their dendritic $GABA_A$ receptors. However, there is another subpopulation of dopaminergic neuron in the olfactory bulb that possesses an axon and it is unknown whether these neurons can also release neurotransmitter from their dendrites. With established protocols in place to measure auto-evoked inhibition in olfactory bulb dopaminergic neurons, I, therefore, asked whether I could observe auto-evoked inhibition in axon-bearing dopaminergic neurons.

Despite axonic dopaminergic neurons being underrepresented in the $DAT^{IRES cre}$ mouse line, work from my lab has shown that there is still a proportion of these neurons that are labelled (Galliano et al., 2018). These neurons have a larger soma in comparison to the monophasic neurons and are located at the border of the glomerular layer and external plexiform layer. I used

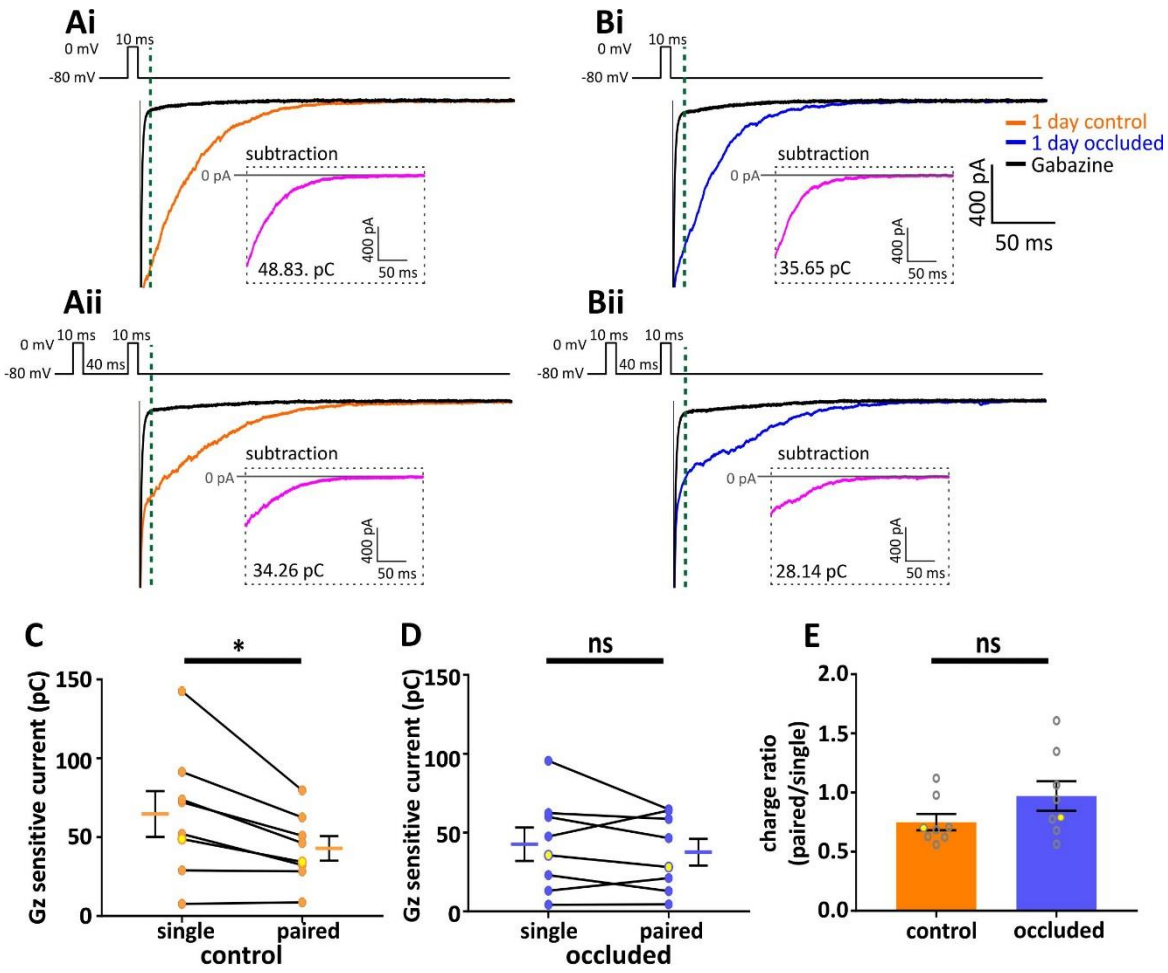

Figure 5.9: Paired-pulse depression may be affected by 1 day of occlusion

A-B: Example traces of auto-evoked inhibition following a (i) single or (ii) paired (50 ms inter-stimulus interval) 10 ms depolarisation from -80 mV to 0 mV in a (A) 1 day control and (B) 1 day occluded DAT-tdTomato neuron before and after blocking with gabazine. Traces were analysed 10 ms after the end of the voltage step, indicated by the dashed line. **Insets**: gabazine-subtracted traces.

C-D: Comparison of the auto-evoked inhibition charge (pC) following either a single or paired 10 ms voltage step in (C) control and (D) occluded cells. Circles represent individual cells, line plots show mean ± SEM, and yellow circles show the values of the example cells in A-B.C; Paired t-test, *p<0.05; ns: non-significant.

E: Scatter plot with bar comparing the charge ratio (paired/single 10 ms response) in control and occluded cells. Open grey circles represent individual cells, yellow circles show the values of the example cells in A-B, bar shows mean ± SEM. t-test, ns: non-significant.

[C-E (n): 1 day control (8); 1 day occluded (8)].

non-somatic action potential generation as a functional indicator for the presence of an axon (Chand et al., 2015; Galliano et al., 2018). In current clamp, I recorded action potentials fired to threshold 10 ms somatic current injection and assessed their spike waveform with phase plane plots. Using a caesium-based intracellular solution resulted in a slow repolarisation of the action potential due to the blocking of potassium channels (**Figure 5.10Ai, Bi**). However, the initial, rising component of the spike waveform, which is driven by sodium channels, appeared grossly normal. Importantly, I was able to differentiate two distinct action potential waveforms under these recording conditions. In phase plane plots a smooth, monophasic plot is indicative of an action potential initiated at the soma (**Figure 5.10Aii**). In contrast, neurons that initiate an action potential away from the soma, almost always at the AIS (Shu et al., 2007), display a biphasic or "double-bumped" phase plane plot waveform (**Figure 5.10Bii**). Neurons were, therefore, categorised as monophasic or biphasic, likely corresponding to the absence or presence of an AIS, respectively.

As I have previously shown, auto-inhibition in monophasic DAT-tdTomato neurons can be evoked by a depolarising voltage step from -80 mV to 0 mV for 10 ms, producing a gabazine-sensitive inward current. As there were no significant differences between control and occluded monophasic DAT-tdTomato neurons, these results were combined for comparison between cell types. I initially used this protocol in biphasic DAT-tdTomato neurons to study auto-evoked inhibition in these cells (**Figure 5.10C-D**). Despite this protocol evoking a prominent auto-inhibition response in monophasic neurons, this was not observed for biphasic neurons. On average, the auto-evoked inhibition response was virtually absent in this subpopulation. Monophasic neurons had a significantly larger gabazine-sensitive current compared to biphasic neurons (mean ± SEM: monophasic, 42.69 ± 5.78 pC, n = 33; biphasic, 3.8 ± 2.8 pC, n = 9. Mann-Whitney U = 19, p < 0.0001) (**Figure 5.10E**).

Biphasic neurons did produce a tail current in response to the auto-inhibition protocol; however, this was mostly insensitive to gabazine. This gabazine-insensitive current was significantly larger in biphasic neurons compared to monophasic neurons (mean ± SEM: monophasic, 5.07 ± 0.81 pC, n = 33; biphasic, 20.03 ± 3.71 pC, n = 9. Mann-Whitney U = 43, p = 0.0007) (**Figure 5.10F**). In 31 of 33 (94%) DAT-tdTomato neurons classified as monophasic, the gabazine-sensitive current was bigger than the gabazine-insensitive current. However, the opposite was found in 8 of 9 (89%) biphasic neurons (**Figure 5.10G**).

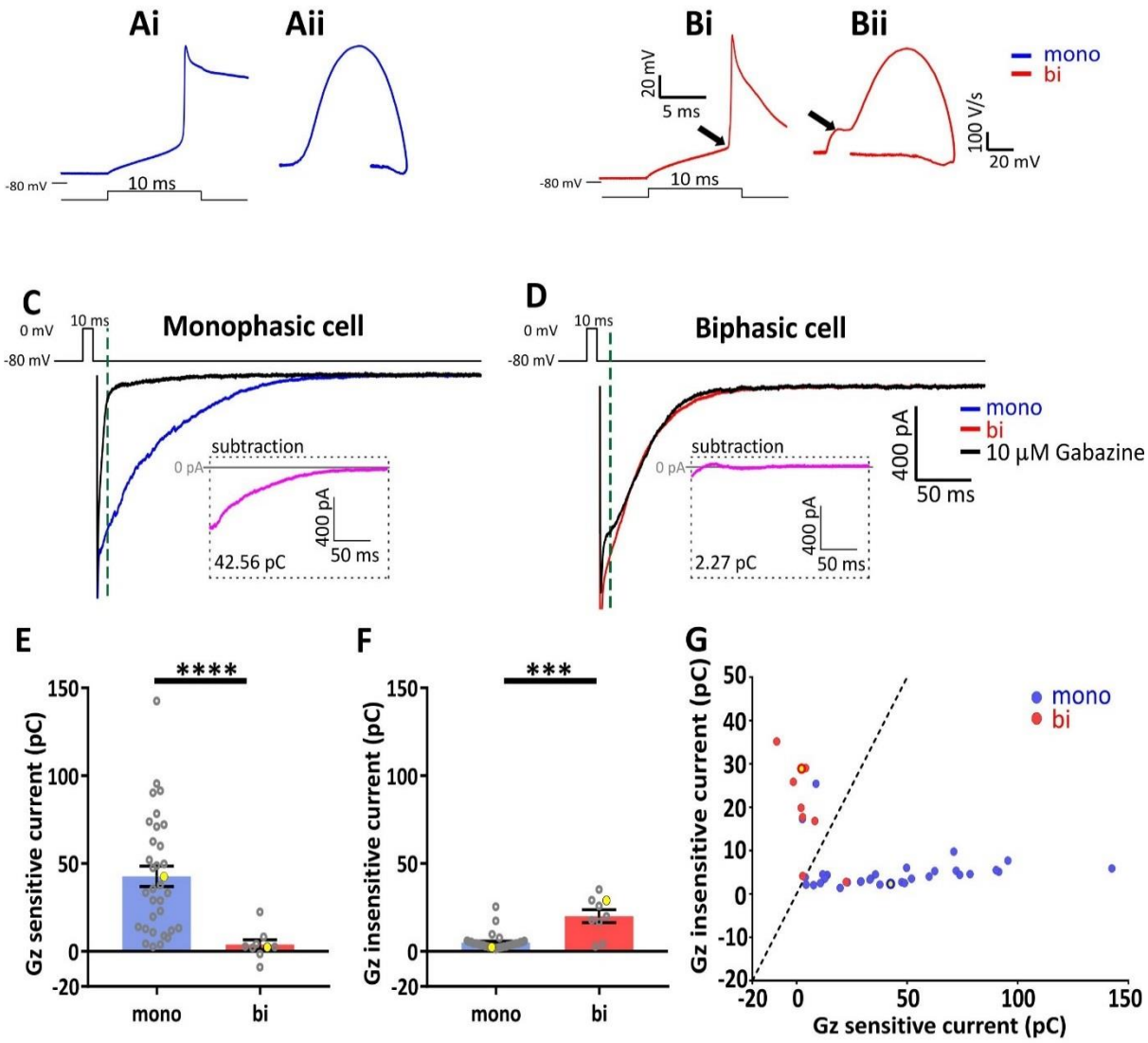

Figure 5.10: Comparing auto-evoked inhibition in monophasic and biphasic DAT-tdTomato neurons.

A-B: Example current-clamp traces of single action potentials fired by (A) monophasic and (B) biphasic cells. (i) Action potentials fired to threshold 10 ms somatic current injection. (ii) Phase plane plots of the spikes shown in (i). Arrow points to the AIS-dependent first action potential phase. Note: slow repolarisation of action potentials due to caesium-based internal solution.

C-D: Example traces of auto-evoked inhibition following a 10 ms depolarisation from -80 mV to 0 mV in the (C) monophasic and (D) biphasic cells shown in A-B before and after blocking with gabazine. Traces were analysed 10 ms after the end of the voltage step, indicated by the dashed line. **Insets**: gabazine-subtracted traces.

E-F: Scatter plot with bar shows the mean ± SEM charge (pC) of the (E) gabazine-sensitive current and (F) gabazine-insensitive current in monophasic and biphasic neurons. Open grey circles represent individual cells, yellow circles show the values of the example cells in A-B. Mann-Whitney test, ****p<0.0001; ***p<0.001.

G: Scatter plot of the gabazine-sensitive current versus the gabazine-insensitive current of monophasic (blue) and biphasic (red) cells. Circles represent individual cells and yellow circles show the values of the example cells in C-D. The dashed line represents unity.

[E-F (n): monophasic (33); biphasic (9)].

If biphasic neurons do not have $GABA_A$-mediated auto-inhibition it may be due to these cells not having these receptors. However, recording spontaneous postsynaptic potentials before and after gabazine demonstrated that both populations had $GABA_A$ receptors (**Figure 5.11**). Using a high chloride internal solution and blocking glutamatergic synaptic events, spontaneous inhibitory postsynaptic potentials (sIPSPs) were recorded as inward events at -80 mV. These recordings were done without TTX to increase the likelihood of seeing events, due to the low frequency of mIPSCs (see Figure 5.4C). In every monophasic (n = 45) and biphasic (n = 11) neuron GABAergic events could be observed.

I next asked whether there were differences in the passive properties of monophasic and biphasic neurons that could account for the small or absent auto-evoked inhibition seen in the latter cell type. The passive properties were assessed in voltage clamp using a -10 mV voltage step from a holding voltage of -60 mV. There were no cell type differences in the holding current (I_{HOLD}) (mean ± SEM: monophasic, -11.04 ± 2.87 pA, n = 45; biphasic, -1.29 ± 9.9 pA, n = 11. Mann-Whitney U = 162, p = 0.07), series resistance (R_S) (mean ± SEM: monophasic, 13.72 ± 0.4 MΩ, n = 33; biphasic, 12.97 ± 0.84 MΩ, n = 11. t-test, $t_{(54)}$ = 0.82, p = 0.42), or membrane capacitance (C_M) (mean ± SEM: monophasic, 41.57 ± 1.35 MΩ, n = 45; biphasic, 46.08 ± 4.8 MΩ, n = 11. Mann-Whitney U = 215, p = 0.50) (**Figure 5.12A-C**). Biphasic neurons did; however, have significantly lower input resistance (R_I) compared to monophasic neurons (mean ± SEM: monophasic, 683.8 ± 47.11 MΩ, n = 45; biphasic, 324 ± 31.93 MΩ, n = 11. t-test, $t_{(54)}$ = 3.7, p = 0.0005) (**Figure 5.12D**).

R_I is indicative of total leak channel number in a cell's membrane, with current leak increasing as R_I decreases. The ability to depolarise a neuron sufficiently to evoke neurotransmitter release with the auto-inhibition protocol could be affected by high current leak. If this were the case, then the lower R_I in biphasic neurons could indicate that the voltage step was not evoking GABA release. However, R_I was found to not be significantly correlated with auto-evoked inhibition response charge in either cell type (linear regression analysis, monophasic, R^2 = 0.07, p = 0.17, n = 33; biphasic R^2 = 0.006, p = 0.84, n = 9) (**Figure 5.12E**). The non-significant trends were negative, indicating that lower R_I may actually produce increased auto-evoked inhibition. In fact, the scatter plot demonstrated that there were several monophasic neurons with lower R_I than some biphasic neurons, but with the largest recorded auto-evoked inhibition responses. Therefore, the dissimilarity in the response to the auto-evoked inhibition protocol cannot be explained by differences in the passive properties of monophasic and biphasic neurons

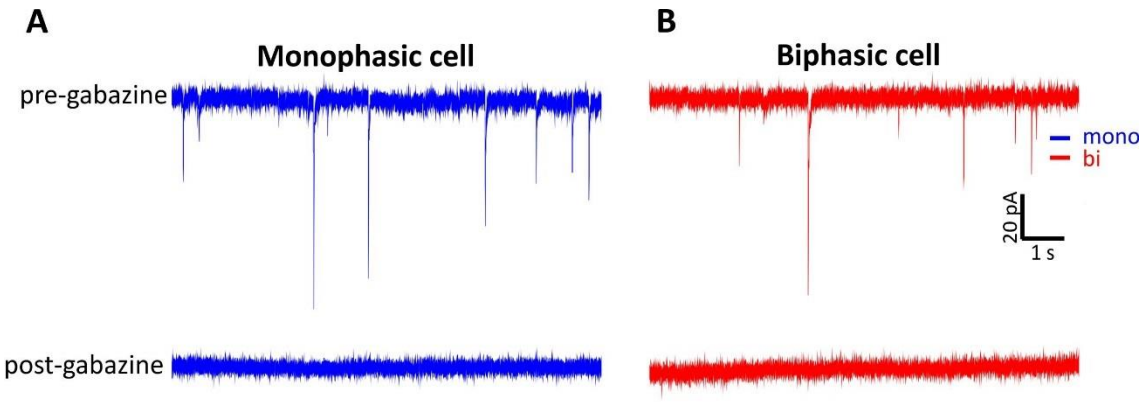

Figure 5.11: Both monophasic and biphasic neurons have $GABA_A$ receptors

A-B: Example traces of spontaneous inhibitory postynaptic potentials recorded at -80 mV in (A) monophasic and (B) biphasic DAT-tdTomato neurons before and after blocking with 10 µM gabazine.

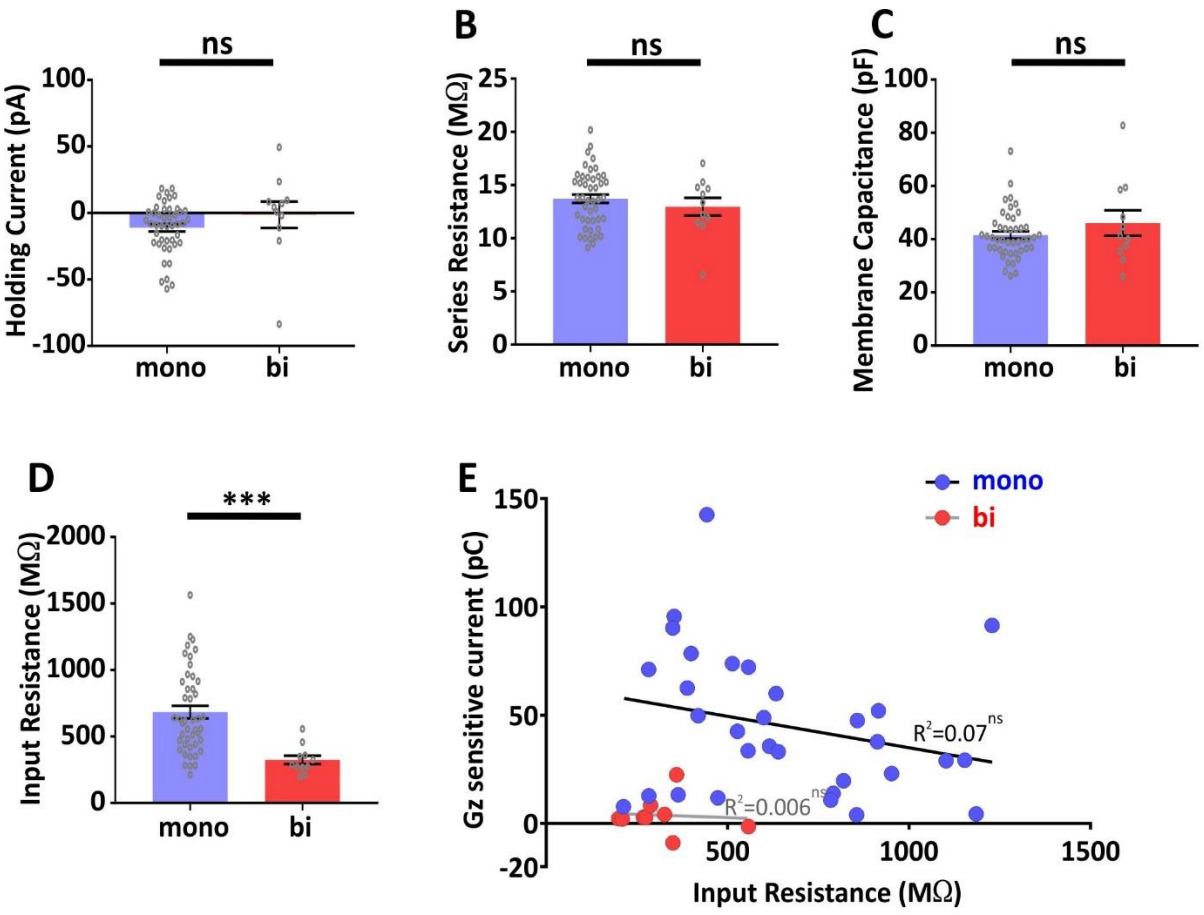

Figure 5.12: Passive properties of monophasic and biphasic neurons

A-D: Scatter plot with bar comparing the (A) holding current (pA), (B) series resistance (MΩ), (C) membrane capacitance (pF) and (D) input resistance (MΩ) in monophasic and biphasic cells. Open grey circles represent individual cells, bar shows mean ± SEM. A. Mann-Whitney test, ns: non-significant. B-D; t-test, *** $p<0.001$; ns: non-significant.

E: Scatter plot of input resistance (MΩ) versus the auto-evoked inhibition response (pC) after a 10 ms depolarisation in monophasic and biphasic cells. Each circle represents one cell. Lines shows linear regression analysis for both cell types and the R^2, ns: non-significant.

[A-D (n): monophasic (45); biphasic (11)]. [E (n): monophasic (33); biphasic (9)].

5.2.7 Enhancing the auto-evoked inhibition response

The presence of $GABA_A$ receptors on biphasic DAT-tdTomato neurons and no effect of passive properties suggests that if these neurons do release GABA from their dendrites, the auto-inhibition protocol should be able to evoke a response. However, one possibility is that a single 10 ms voltage step is not sufficient to induce neurotransmitter release in AIS-positive olfactory bulb dopaminergic neurons with more broadly ramified dendrites (Galliano et al., 2018). Smith and Jahr (2002) found that auto-inhibition in periglomerular neurons have prolonged and delayed GABA release due to the slow sequestration of calcium. If calcium influx into biphasic DAT-tdTomato neuron dendrites is not large enough following brief somatic depolarisation, it could explain why auto-evoked inhibition was not observed in biphasic neurons. I, therefore, investigated whether I could enhance GABA release to evoke an auto-inhibition response.

The first approach I attempted was a paired-pulse protocol by injecting a second 10 ms voltage step 50 ms after the start of the first (**Figure 5.13A-B**). If only a fraction of vesicles are released during the first pulse, a subsequent pulse can produce a transient increase in vesicular release due to an accumulation of residual calcium at the presynapse. Previous work has found that auto-evoked inhibition can show paired-pulse facilitation (Bouhours et al., 2011). As shown above, the gabazine-sensitive response in monophasic neurons showed a significant paired-pulse depression (mean ± SEM: single response, 45.57 ± 7.82 pC, n = 21; paired response, 34.87 ± 4.9 pC, n = 21. Paired t-test $t_{(20)} = 2.82$, $p = 0.01$) (**Figure 5.13C**). Biphasic neurons did not show paired-pulse facilitation, in fact, the paired auto-evoked response was even smaller (mean ± SEM: single response, 5.4 ± 2.61 pC, n = 8; paired response, 1.51 ± 2.91 pC, n = 8. Wilcoxon matched-pairs signed rank test $W = -28$, $p = 0.06$) (**Figure 5.13D**). There was; however, a small increase in the charge of the gabazine-insensitive current in both cell types, which reached significance in monophasic neurons (mean ± SEM: monophasic single response, 5.5 ± 1.22 pC, n = 21; monophasic paired response, 7.2 ± 1.58 pC, n = 21. Wilcoxon matched-pairs signed rank test $W = 171$, $p = 0.002$. Biphasic single response, 18.13 ± 3.32 pC, n = 8; biphasic paired response, 20.67 ± 3.87 pC, n = 8. Paired t-test $t_{(7)} = 1.49$, $p = 0.18$) (**Figure 5.13E-F**). These results show that I could not evoke a larger auto-inhibition response in biphasic DAT-tdTomato neurons using a paired-pulse protocol.

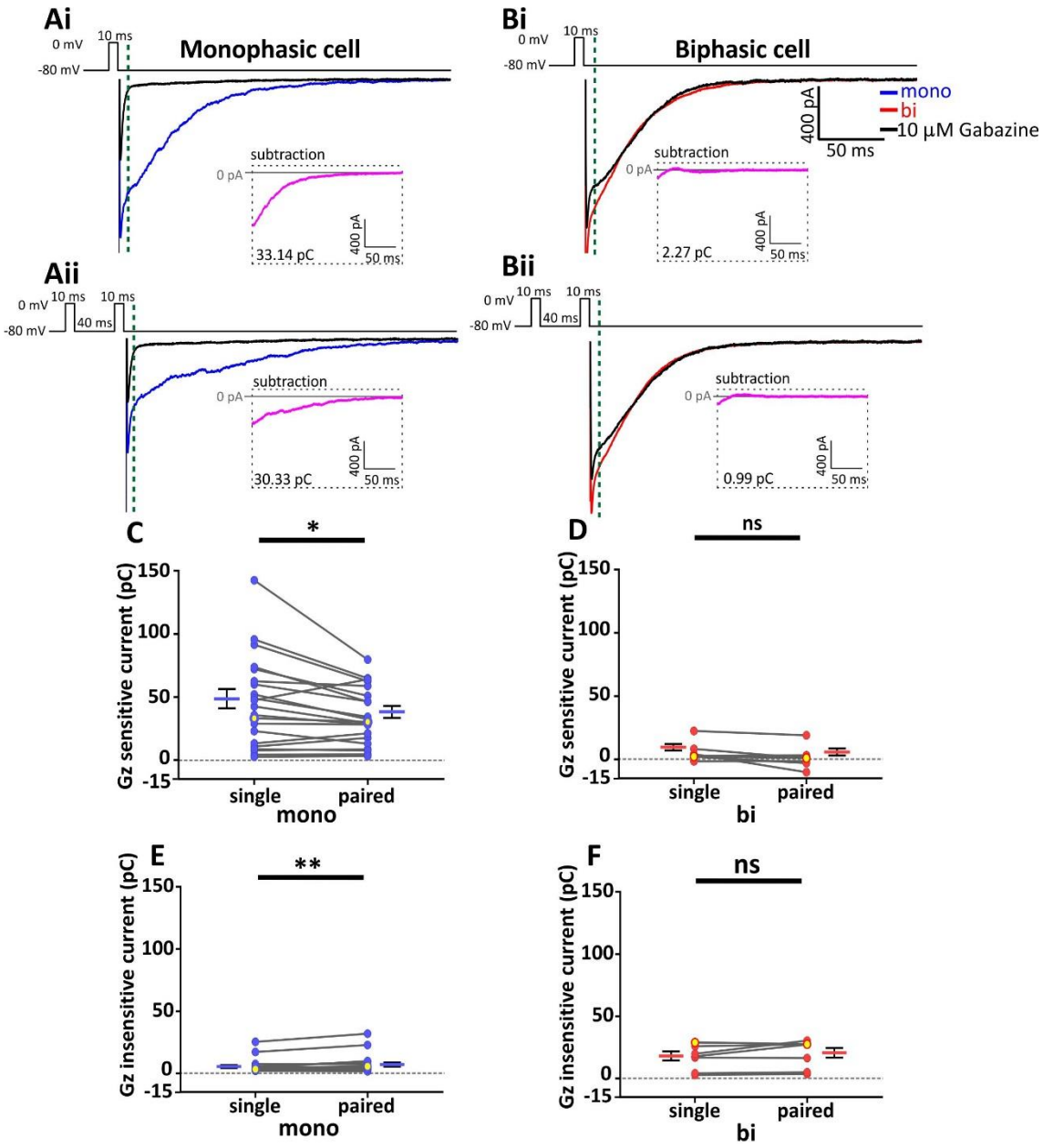

Figure 5.13: Paired-pulse stimulation does not facilitate the auto-evoked inhibition response

A-B: Example traces of auto-evoked inhibition following a (i) single or (ii) paired (50 ms inter-stimulus interval) 10 ms depolarisation from -80 mV to 0 mV in a (A) monophasic and (B) biphasic cell before and after blocking with gabazine. Traces were analysed 10 ms after the end of the voltage step, indicated by the dashed line. **Insets**: gabazine-subtracted traces.

C-F: Comparison of the (C-D) gabazine-sensitive current (pC) and (E-F) gabazine-sinsensitive current (pC) following either a single or paired 10 ms voltage step in monophasic and biphasic cells. Circles represent individual cells, line plots show mean ± SEM, and yellow circles show the values of the example cells in A-B. C, F; Paired t-test, * $p < 0.05$, ns: non-significant. D, F; Wilcoxon matched-pairs signed rank test, ** $p < 0.01$, ns: non-significant.

[C-F (n): monophasic (21); biphasic (8)].

Previous work has shown that increasing the duration of the depolarising voltage step evoked auto-inhibition currents in periglomerular neurons that were larger and more prolonged (Murphy et al., 2005; Smith and Jahr, 2002). To try to uncover auto-evoked inhibition response in biphasic DAT-tdTomato neurons, the single voltage step was, therefore, increased from 10 ms to 100 ms. The gabazine-sensitive charge was calculated from the same timepoint (110 ms) after the start of both pulses (**Figure 5.14A-B**). This is to take into account the fact that the largest part of the auto-evoked inhibition happens within the first 100 ms and, for the longer-duration depolarisation stimulus, would be occurring during the longer voltage step. In every monophasic neuron there was an increase in the charge of the gabazine-sensitive current after the 100 ms voltage step compared to the shorter pulse (mean ± SEM: 10 ms response, 7.67 ± 1.66 pC, n = 20; 100 ms response, 55.28 ± 7.54 pC, n = 20. Wilcoxon matched-pairs signed rank test W = 210, p < 0.0001) (**Figure 5.14C**). This reliable prolonged release of GABA was not found in biphasic neurons, with some cells showing a smaller response after 100ms (mean ± SEM: 10 ms response, 0.26 ± 0.21 pC, n = 7; 100 ms response, 7.75 ± 7.51 pC, n = 7. Wilcoxon matched-pairs signed rank test W = 14, p = 0.30) (**Figure 5.14D**). Again, there was a significantly larger gabazine-insensitive tail current in biphasic neurons compared to monophasic neurons (mean ± SEM: monophasic, 24.04 ± 6.94 pC, n = 20; biphasic, 94.96 ± 17.92 pC, n = 7. Mann-Whitney U = 16, p = 0.002) (**Figure 5.14E**). Interestingly, the tail current after the 100 ms voltage step was approximately 5 times larger than the tail current after the 10 ms protocol (compare Figures 5.10F and 5.14E).

Therefore, there is no evidence for auto-evoked inhibition in biphasic neurons under baseline conditions, even when applying stimulation protocols that maximises the response in the monophasic DAT-tdTomato neurons and in other neurons (Bouhours et al., 2011; Smith and Jahr, 2002). If auto-evoked inhibition is present in these biphasic DAT-tdTomato neurons, its properties are not the same as those seen in monophasic neurons.

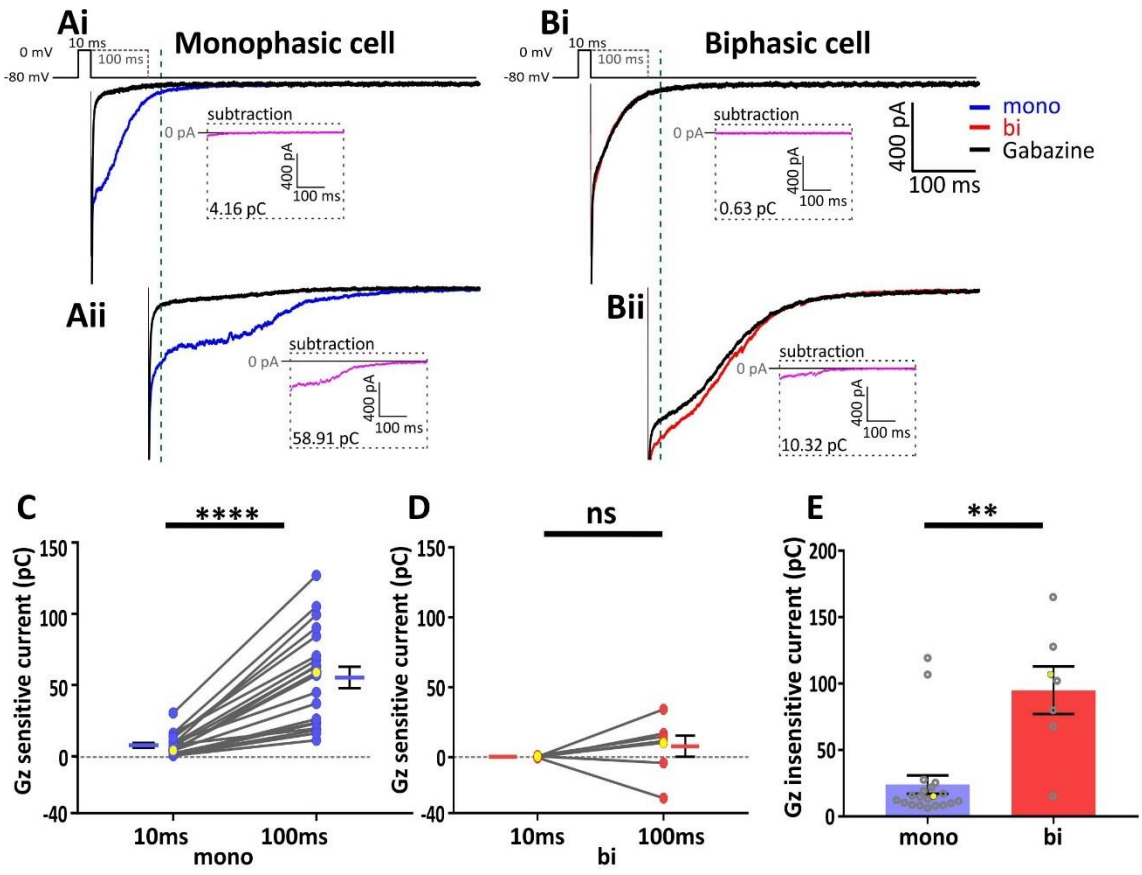

Figure 5.14: Longer depolarisation reliably increases the auto-evoked inhibition response only in monophasic neurons

A-B: Example traces of auto-evoked inhibition following a (i) 10 ms or (ii) 100 ms depolarisation from -80 mV to 0 mV in a (A) monophasic and (B) biphasic cell before and after blocking with gabazine. Both voltage steps were compared by analysing from the same time after stimulus start, indicated by the dashed line. **Insets**: gabazine-subtracted traces.

C-D: Comparison of the analysed auto-evoked inhibition charge (pC) following either a 10 ms or 100 ms voltage step. Circles represent individual cells, line plots show mean ± SEM, and yellow circles show the values of the example cells in A-B. Wilcoxon signed-rank test, ****p<0.0001; ns: non-significant.

E: Scatter plot with bar comparing the gabazine-insensitive current following 100 ms depolarisation in monophasic and biphasic cells. Open grey circles represent individual cells, yellow circles show the values of the example cells in A-B, bar shows mean ± SEM. Mann-Whitney test, **p<0.01.

[C-E (n): monophasic (20); biphasic (7)].

5.2.8 Pharmacological enhancement of the auto-evoked response

Calcium influx through voltage-gated calcium channels is required for the release of GABA in periglomerular neurons (Smith and Jahr, 2002). P/Q-type calcium channels are necessary for dendritic GABA release from these neurons, though L-type calcium channels are not (Murphy et al., 2005). Curiously, the application of the L-type calcium channel agonist, Bay K 8644 has been shown to lead to an increase in the auto-inhibition current, even though blocking this channel does not affect the current (Murphy et al., 2005). It has been suggested that the calcium influx through the facilitated L-type channels supports the release of GABA, I investigated whether the $GABA_A$-dependent auto-inhibition current in dopaminergic neurons could also be pharmacologically increased by the application of 5 µM Bay K 8644 (**Figure 5.15A-B**). A baseline auto-evoked inhibition response was recorded and the drug washed-in. The resulting Bay K response was significantly larger than baseline in monophasic neurons, as has been previously shown for the dendritic release of GABA in periglomerular neurons in general (mean ± SEM: baseline response, 46.55 ± 18.14 pC, n = 6; Bay K response, 79.74 ± 24.55 pC, n = 6. Paired t-test $t_{(5)}$ = 3.71, p = 0.01) (**Figure 5.15C**). Interestingly, the Bay K response in biphasic neurons was also significantly increased compared to baseline (mean ± SEM: baseline response, -0.93 ± 4.07 pC, n = 3; Bay K response, 34.44 ± 6.13 pC, n = 3. Paired t-test $t_{(2)}$ = 8.9, p = 0.01) (**Figure 5.15D**). This result has given the strongest indication that, at least under certain conditions of pharmacologically elevated calcium influx, biphasic neurons can show auto-evoked inhibition through the release of GABA binding to their $GABA_A$ receptors.

5.2.9 Calcium influx is required for the biphasic tail current

One of the most striking results from the experiments studying auto-evoked inhibition was the gabazine-insensitive tail current that was predominately present in biphasic neurons. This indicates a functional difference between the two dopaminergic subpopulations in the olfactory bulb and possibly reflects differences in expression or biophysical properties of particular ion channels between the two cell types. It is unclear what is driving this response; however, depolarisation is required. In gabazine, holding a biphasic neuron at 0 mV for 30 seconds and then hyperpolarising to -80 mV did not produce a tail current (**Figure 5.16**). Therefore, the tail current is not a hyperpolarisation-activated current. During the voltage step for the auto-evoked inhibition protocols there is calcium influx through voltage-gated calcium channels, which is required for the dendritic release of GABA (Murphy et al., 2005; Smith and Jahr, 2002). To determine whether the tail current is calcium-dependent, I recorded a baseline response after

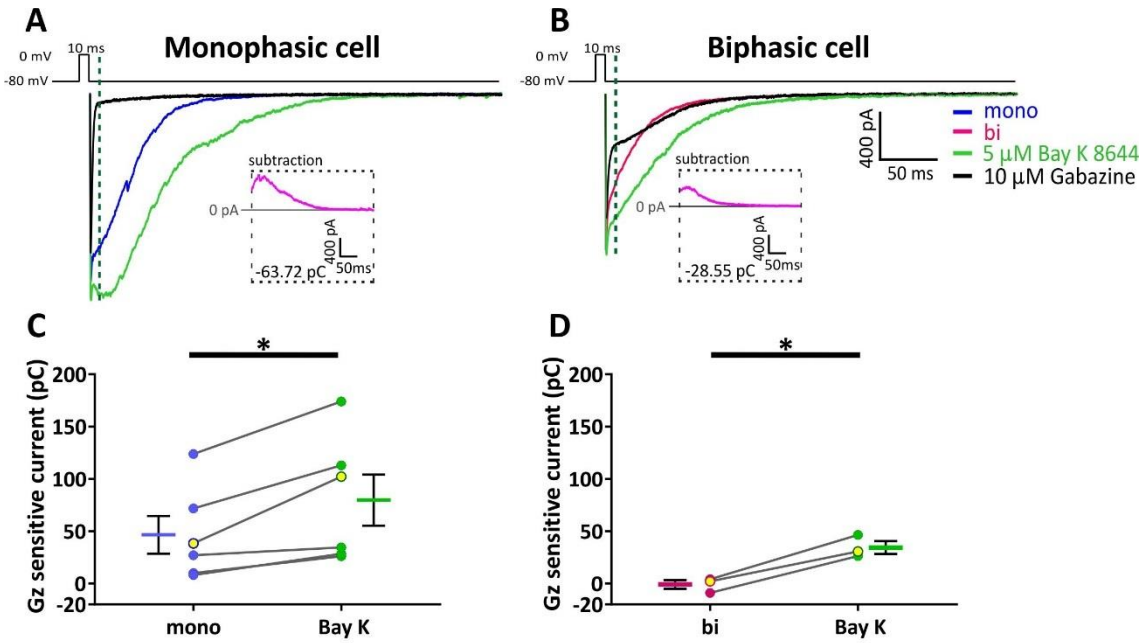

Figure 5.15: Bay K 8644 enhances the auto-evoked inhibition response

A-B: Example traces of auto-evoked inhibition following a 10ms depolarisation from -80 mV to 0 mV in a (A) monophasic and (B) biphasic cell before and after the addition of Bay K and blocking with gabazine. **Insets**: traces show the baseline response subtracted from the Bay K response.

C-D: Comparison of the auto-evoked inhibition charge (pC) following a 10 ms voltage step before and after the addition of Bay K in (C) monophasic or (D) biphasic cells. Circles represent individual cells, line plots show mean ± SEM and yellow circles show the values of the example cells in A-B. Paired t-test, *$p < 0.05$.

[C-D (n): monophasic (6); biphasic (3)].

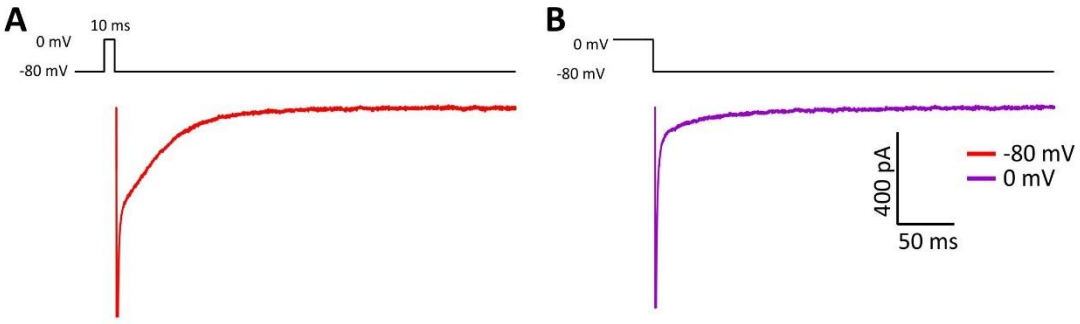

Figure 5.16: Depolarisation is required for the tail current in biphasic neurons

A-B: Example traces of the gabazine-insensitive tail current in a biphasic DAT-tdTomato neuron after (A) 10 ms voltage step from -80 mV to 0 mV and (B) holding neuron at 0 mV and hyperpolarising to -80 mV.

a single 10 ms voltage step and then added the general calcium channel blocker, cadmium (200 μM) (**Figure 5.17A-B**).

In both monophasic and biphasic neurons, the addition of cadmium resulted in the complete block of the tail current following the 10 ms voltage step (cadmium sensitive current: mean ± SEM: monophasic, 49.82 ± 9.27 pC, *n* = 5; biphasic, 24.1 ± 6.69 pC, *n* = 2) (**Figure 5.17C**). Comparing the tail currents of monophasic and biphasic neurons revealed that 99.7% and 86.1% had been blocked by cadmium, respectively (**Figure 5.17D**). Based on these results, the large gabazine-insensitive tail current in biphasic olfactory bulb DAT-tdTomato neurons is dependent on calcium influx driven by phasic depolarisation of the neuron.

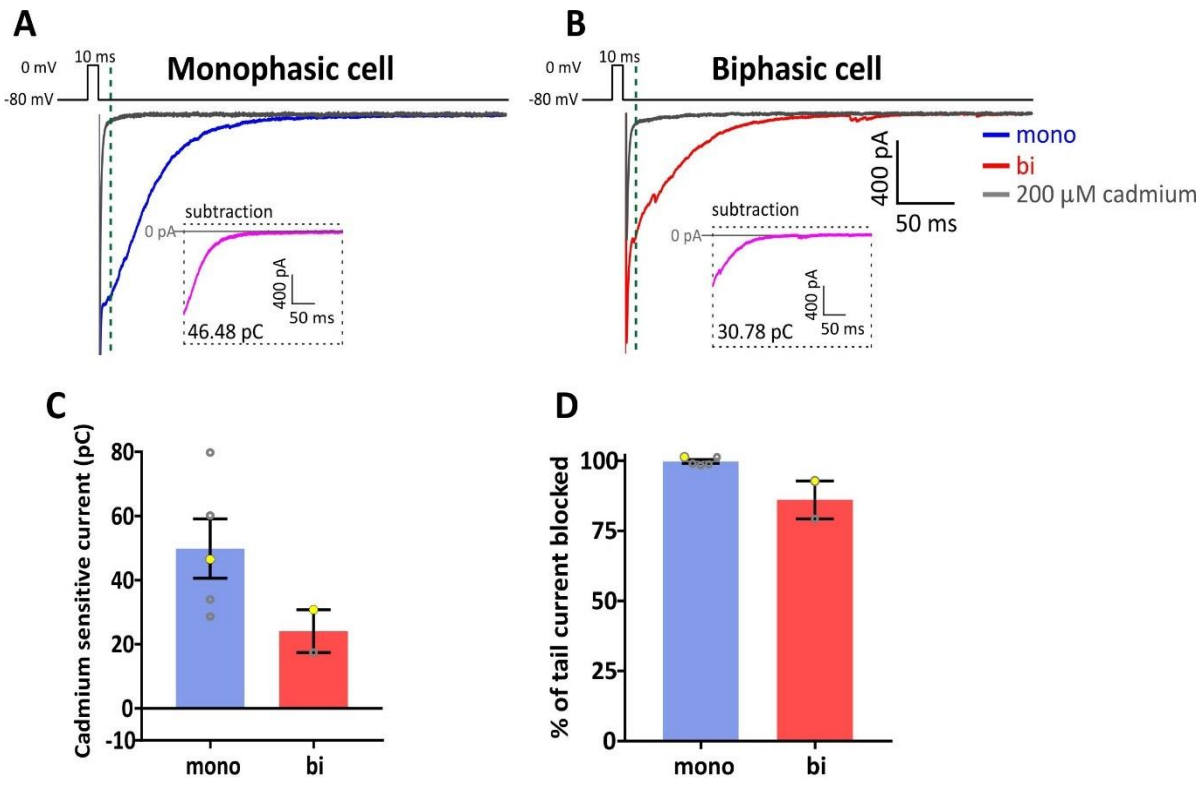

Figure 5.17: The biphasic tail current is calcium-dependent

A-B: Example traces of auto-evoked inhibition following a 10 ms depolarisation from -80 mV to 0 mV in a (A) monophasic and (B) biphasic cell before and after blocking with cadmium. Traces were analysed 10 ms after the end of the voltage step, indicated by the dashed line. **Insets**: cadmium-subtracted traces.

C-D: Scatter plot with bar shows the mean ± SEM (C) charge (pC) of the cadmium-sensitive current and (D) the percentage of the tail current charge blocked in monophasic and biphasic neurons after adding cadmium. Open grey circles represent individual cells, yellow circles show the values of the example cells in A-B.

[C-D (n): monophasic (5); biphasic (2)].

5.3 Discussion

In this chapter, I investigated excitatory and inhibitory synaptic input onto the anaxonic subpopulation of dopaminergic neurons in the olfactory bulb in response to 1 or 3 days of unilateral naris occlusion. I characterised dendritic release of GABA in these neurons and found that after 1 day of occlusion, occluded neurons have a slightly reduced paired-pulse depression compared to controls. I also found that biphasic DAT-tdTomato neurons can only show auto-evoked inhibition by pharmacologically enhancing calcium influx and have a calcium-dependent tail current not present in the majority of monophasic DAT-tdTomato neurons.

5.3.1 Strengthening of excitatory inputs after unilateral naris occlusion

I found that odour deprivation induces changes to excitatory input onto monophasic olfactory bulb DAT-tdTomato neurons. After 3 days of unilateral naris occlusion there is a significant increase in the charge of AMPA-mediated mEPSCs, supporting the results of Tyler et al. (2007) in the rat olfactory bulb that found an increase in the amplitude of mEPSCs in external tufted cells and glomerular layer GABAergic interneurons after 3 days of occlusion. Tyler et al. (2007) found that this increase was due to the strengthening of AMPA receptors on the postsynapse. Initial work studying synaptic scaling concentrated on changes to the amplitude of mEPSCs (Turrigiano et al., 1998); however, I found this was only slightly increased following occlusion. This indicates that studying charge transfer may be a more sensitive approach to investigating mEPSCs as it is less affected by dendritic filtering (Han and Stevens, 2009) and is a more direct measure of the total AMPA response.

It is interesting that there was a significant increase in the occurrence of very large events in occluded neurons measured by both amplitude and charge. This suggests that there is a potentiation of certain excitatory synapses in response to occlusion. This was supported by the finding that there did not appear to be a multiplicative increase in the amplitude or charge of mEPSCs events, despite the distribution of scaled events from occluded neurons being nearly indistinguishable from control events. There is evidence that synaptic scaling can be global, acting on all of a neuron's excitatory synapses (Turrigiano et al., 1998), or local, acting on individual or small groups of synapses (Sutton et al., 2006). Synaptic scaling may preferentially increase the number of AMPA receptors or rapidly affect the composition or conductance of AMPA receptors at the largest synapses (Thiagarajan et al., 2005), which could explain the increase observed following occlusion. However, it is not clear whether this is a feature of all large excitatory synapses in the neuron or whether there are specific inputs being strengthened.

It could also be possible that larger synapses are potentiated first and smaller synapses take longer to increase in size.

The functional properties of neurons are largely determined by the expression and biophysical properties of receptors and voltage and calcium-gated ion channels. Protein synthesis and changes in protein trafficking are important for the induction of synaptic scaling of excitatory and inhibitory inputs by increasing or decreasing the density of AMPA and $GABA_A$ receptors at the postsynapse (Kilman et al., 2002; Rannals and Kapur, 2011; Wierenga et al., 2005). There may also be activity-dependent changes to specific subunits or the subunit composition of receptors and channels, which can alter their kinetics and conductance (Angulo et al., 1997; Goel et al., 2011; Hyun et al., 2013).

Based on EM and electrophysiological research it is clear that olfactory bulb dopaminergic neurons receive excitatory input from OSNs, external tufted cells, bulbar projection neurons and cortical feedback inputs (Boyd et al., 2012; Kiyokage et al., 2017; Toida et al., 2000). I cannot, therefore, conclude whether specific excitatory inputs are becoming stronger. Proximal excitatory inputs have been suggested to be primarily coming from non-OSN inputs (Kiyokage et al., 2017), so this might reflect selective potentiation of input from the cortical feedback inputs, dendrites of external tufted cells and/or bulbar projection neurons. Another possibility is that distal OSN inputs are, in fact, the largest inputs to these neurons. Stimulating OSNs, cortical feedback inputs and excitatory bulbar neurons and recording the evoked EPSC in connected dopaminergic neurons would give a more detailed description for how specific excitatory synapses may have been affected by unilateral naris occlusion.

5.3.2 GABA release may be affected by occlusion

Studying auto-evoked inhibition in control and 1 day occluded neurons demonstrated that there was no significant difference. However, there was a difference in paired-pulse depression, showing that occluded neurons had smaller paired-pulse depression. As auto-evoked responses are variable between neurons, more data is needed to confirm whether this small difference is a real phenotype. As recording mIPSCs showed $GABA_A$ receptors were not affected by 1 or 3 day occlusion, this suggests that there may be changes in vesicle release in occluded neurons. Increased paired-pulse depression is generally believed to represent enhanced transmitter release (Zucker and Regehr, 2002). However, my data was based on depolarisation-evoked responses, which would have longer activation of voltage-gated calcium channels as opposed to action potential-evoked responses. As vesicle release is dependent on calcium, decreased paired-pulse depression could represent a change in calcium dynamics, for example, increased

residual calcium after the first pulse. However, without proper characterisation of release probability and calcium dynamics in these neurons, it is not possible to determine whether release probability has been affected. This could be done by studying calcium dynamics at presynaptic sites using calcium imaging (Murphy et al., 2005). Recording unitary IPSCs between monophasic DAT-tdTomato and monosynaptically connected neurons in different concentrations of extracellular divalent cations (Ca^{2+} and Mg^{2+}) could be used to estimate release probability (Kraushaar and Jonas, 2000).

5.3.3 How might the synaptic and intrinsic changes interact?

The prediction from these synaptic results would be that these neurons are more sensitive to excitatory input, which would increase their excitation and potentially increase intraglomerular inhibition. However, mitral cells have been found to be more sensitive to sensory input following odour deprivation, suggesting that inhibition is reduced (Philpot et al., 1997; Wilson and Sullivan, 1995). Considering the results presented in Chapter 3, olfactory bulb dopaminergic neurons would have decreased synthesis and release of dopamine. Monophasic dopaminergic neurons may also have a small decrease in release of GABA, reflected in reduced paired-pulse depression. In light of the results of Chapter 4 showing that the sag potential and medium AHP are increased by unilateral naris occlusion, particularly after 3 days, it is interesting to consider how these intrinsic changes may relate to the mE/IPSC results.

As discussed in Chapter 4, increased expression of HCN channels and the channels that may underlie the medium AHP at dendrites have been shown to attenuate excitatory and inhibitory inputs by shunting EPSCs (Angelo et al., 2007; Faber et al., 2005; Magee, 1998; Shah et al., 2011). The increased dendritic suppression of postsynaptic currents (PSCs) associated with upregulation of these channels appears to contradict my results; 3 day occlusion was associated with an increase in the amplitude and charge of mEPSCs. However, it is likely that the channels conducting I_h and medium AHP are being blocked when recording PSCs. A caesium-based internal solution was used for the synaptic recordings to block potassium channels. Intra and extracellular caesium have been shown to block potassium channels and HCN channels (Bohannon and Hablitz, 2018; Cecchi et al., 1987; Yu et al., 2004). Therefore, the shunting effect of these channels could be blocked. If enhanced I_h and medium AHP are affecting mE/IPSC, there would be expected to be a decrease in these responses under physiological conditions. If this is the case, it can be assumed that unilateral naris occlusion has increased the number or conductance of AMPA receptors, particularly at very large synapses, while $GABA_A$ receptors have not been affected. As the responses through these receptors can be shunted by I_h and channels

mediating medium AHP, it suggests that $GABA_A$-inhibitory inputs will be more strongly suppressed than AMPA-excitatory inputs after 3 days of occlusion.

The location of HCN channels in olfactory bulb dopaminergic neurons is believed to be highest at dendrites (Pignatelli et al., 2013). In other neurons, including mitral cells, distal dendrites have the greatest density of HCN channels (Angelo and Margrie, 2011; Berger et al., 2001; Magee, 1998). If the same distribution of HCN channels is present in olfactory bulb dopaminergic neurons, it would suggest that OSN inputs to the distal dendrites could be particularly attenuated by dendritic filtering and active HCN channels, unless the large mEPSC responses observed are from OSN-inputs. In contrast, the proximal dendritic inputs that are driven by local bulbar excitatory neurons would be less affected. Further work should investigate the distribution of these channels on olfactory bulb dopaminergic neurons and use more physiological intracellular solution to study the effect of HCN and SK or Kv7 channels on mE/IPSCs in control and occluded neurons.

If these neurons are adapting to reduced sensory input by decreasing their output and, potentially, reducing their excitation, why would there be potentiation of mEPSC responses? One possibility is increasing mEPSC responses may be a generic postsynaptic process affecting all resident neurons in the glomerular layer. Another possibility is that glomerular layer GABAergic interneurons need to retain excitation to provide some level of glomerular inhibition to prevent unrestrained excitation and maintain odour processing abilities, particularly in cases of strong and/or repetitive input.

5.3.4 Dendritic release of GABA

Monophasic DAT-tdTomato neurons had a clear inward current following step depolarisation in voltage-clamp that was blocked by gabazine. This current resembled the auto-evoked inhibition response previously described for glomerular layer interneurons: it showed current noise that indicates asynchronous release, the response was increased by longer duration depolarisation, it is also calcium dependent and can be increased by activating L-type calcium channels (Maher and Westbrook, 2008; Murphy et al., 2005; Smith and Jahr, 2002). The mean charge (pC) of the auto-evoked response was much larger (~50 pC) than that previously shown for olfactory bulb dopaminergic neurons (~4.5 pC) (Maher and Westbrook, 2008). It is possible that the different holding potentials in the two studies (-80 mV in this thesis and -60 mV in the published study) increased the driving force of chloride through the open $GABA_A$ receptors, enhancing the recorded charge. Maher and Westbrook (2008) also patched dopaminergic neurons that were

labelled by *Th*, which could be a more heterogeneous population than neurons labelled by the *Dat* promoter (Chapter 3).

Holding monophasic neurons at depolarised somatic potentials did not affect the auto-inhibition response. In cerebellar interneurons, the P/Q type of calcium channels are primarily responsible for enhanced GABA release following subthreshold somatic depolarisation (Bouhours et al., 2011). While these are high-threshold voltage-gated calcium channels, they appear to be activated at low-thresholds in these neurons to facilitate the auto-inhibition response. However, in monophasic DAT-tdTomato olfactory bulb neurons the subthreshold depolarisation may not have been sufficient to activate these channels. Therefore, it did not raise the calcium concentration, which could have increased the auto-evoked inhibition response. There is also the possibility that depolarisation of dendrites in electrotonically compact monophasic dopaminergic neurons is more effective than the depolarisation of, presumably, more distant and electrically isolated terminals in cerebellar axons. Therefore, there may be a ceiling effect whereby there is maximum release following standard depolarisation. However, release can be augmented by activation of L-type calcium channels, which are not normally required for release in glomerular layer GABAergic interneurons (Murphy et al., 2005).

Studying auto-evoked inhibition in DAT-tdTomato neurons allowed an investigation of whether dendritic release of GABA was a feature shared by both monophasic and biphasic olfactory bulb dopaminergic neurons. Whether biphasic DAT-tdTomato neurons have dendritic release is still unclear, this subpopulation does not show evidence for auto-evoked inhibition under standard conditions. Injecting a second pulse shortly after the first did not evoke paired-pulse facilitation, which has previously been shown for auto-evoked inhibition in cerebellar Purkinje neurons (Bouhours et al., 2011). A striking difference between the two dopaminergic subpopulations is biphasic neurons failing to increase auto-evoked inhibition in response to longer depolarisation. In monophasic neurons this reliably evoked an extended auto-inhibition response in every neuron. However, biphasic neurons did not show this increase, with some neurons even having a smaller gabazine-sensitive response compared to the shorter pulse. The only demonstration of auto-evoked inhibition was by pharmacologically increasing calcium influx to facilitate neurotransmitter release. However, this response was still smaller than the baseline response of monophasic neurons in standard conditions. While this suggests that auto-evoked inhibition can be present under specific recording conditions in biphasic neurons, it does not prove dendritic release of neurotransmitter. It would be assumed that the longer 100 ms depolarisation would also have generated a large calcium response to facilitate release. One possibility could be that Bay K is increasing GABA release in other glomerular layer interneurons,

which could be facilitated by depolarisation through gap junctions. It has been reported that dopaminergic neurons have gap junctions (Banerjee et al., 2015). Repeating the Bay K experiment in the presence of gap junction blockers could demonstrate whether this is happening.

Previous EM work did not find evidence for the dendrites of large dopaminergic neurons forming presynaptic connections (Liberia et al., 2012). However, this was done in the rat olfactory bulb and was based on TH-expressing neurons located deep in the external plexiform layer. However, axonic dopaminergic neurons are generally located at the border of the glomerular layer and the external plexiform layer (Galliano et al., 2018). As the $DAT^{IRES cre}$ mouse underrepresents the axon-bearing population it has to be asked why this happens and whether the minority of axonic dopaminergic neurons labelled in this mouse are different to the rest of population. Further work should investigate the presence of presynaptic markers specifically at the dendrites of these neurons, by using EM or Cre-dependent viruses to label synaptophysin or bassoon. If biphasic neurons have dendritic release, there is the question of why auto-evoked inhibition is very different from the monophasic subpopulation. Perhaps there is a difference in the distribution of $GABA_A$ receptors and presynaptic release sites on their dendrites or there was not sufficient calcium influx during the depolarisation protocols to evoke release. To confirm that the auto-evoked inhibition protocols are sufficiently depolarising the dendrites, it could be possible to measure calcium influx by filling the neurons with calcium-sensitive dyes (Kisfali et al., 2013). This could then be combined with recordings in Bay K to understand whether there are increased dendritic calcium levels that may explain the Bay K-mediated auto-evoked inhibition.

If biphasic neurons do not have dendritic release, there is a possibility that the observed auto-evoked inhibition in the presence of Bay K is due to axonal release of neurotransmitter and activation of $GABA_A$ receptors on the axon (Bouhours et al., 2011). However, it would be assumed that axonal auto-evoked inhibition would be observed following longer duration depolarisation. In order to substantiate this claim $GABA_A$ receptors would need to be present on the axons of these neurons, which has not been demonstrated for these neurons. There would also need to be some preservation of axonal terminals during the preparation of acute slices. If the axon of these neurons can be filled with Alexa dye, it could be possible to follow the axon and use a picospritzer to apply small puffs of GABA at a sufficient distance away from the soma and dendrites and record $GABA_A$-mediated responses. Another possibility is the presence of autapses, where a neuron forms axonal synapses onto itself. Again, this assumes that autapses are present on these neurons and had not been damaged during acute slicing.

5.3.5 Functional difference between monophasic and biphasic olfactory bulb dopaminergic neurons

The presence of the gabazine-insensitive current indicated a striking functional difference between the two subpopulations, with the majority of biphasic neurons displaying a clear inward current following the depolarisation protocols. Previous work has suggested that the functional properties of both subpopulations are largely similar, except there is an average increase in the excitability of biphasic neurons (Galliano et al., 2018). However, there was not total segregation of the gabazine-insensitive current based on the monophasic and biphasic classification and this raises the question of whether classifying by action potential waveform can lead to misclassifications. Neurons that do display a monophasic waveform could still be axon-bearing dopaminergic neurons in situations where the axon is located very distal to the recording pipette or the axon was severed during the acute slice preparation. An explanation for anaxonic neuron appearing biphasic is more difficult to explain. If an action potential is generated in a dendrite, it may appear biphasic, particularly if the pipette is located at a distance from the initiation site. Work by Kosaka et al. (2008) has also described the presence of dendritic "hot spots" on olfactory bulb neurons, including neurons in the glomerular layer. These "hot spots" are small dendritic regions that display AIS-characteristics, such as a high density of sodium channels. As such, an anaxonic neuron could be classified as biphasic by the opening of these sodium channels during spike initiation. However, the presence of these "hot spots" has not been described on the dendrites of olfactory bulb dopaminergic neurons.

Without specific markers to distinguish the two subpopulations, the monophasic and biphasic classification is the most accurate method for identifying these neurons by electrophysiology, although verification of this is missing and requires recovery of neurons after patching and performance of immunohistochemistry for axonal markers. Future work to identify the channel(s) underlying the gabazine-insensitive current should be followed by an investigation into their expression in olfactory bulb dopaminergic neurons. The results presented here can be used to narrow the potential targets. It is clear that this tail current is dependent on calcium and depolarisation. Therefore, this could be a tail current from a voltage-gated calcium channel (VGCC). The presence of caesium in the intracellular recording solution can block potassium channels; however, it has been shown that hyperpolarised voltage potentials can unblock calcium-activated potassium channels (Cecchi et al., 1987). Holding at 0 mV and hyperpolarising the neuron did not evoke a tail current; however, it is unknown what the intracellular calcium levels are after holding at 0 mV for ~30 seconds, though it would be expected to be high. These calcium-activated potassium channels include BK, IK and SK channels (Vergara et al., 1998). The

BK channel controls the fast AHP (Storm, 1987); however, this is not different between monophasic and biphasic olfactory bulb dopaminergic neurons (Galliano et al., 2018). The SK channel has been implicated in the medium AHP (Bond et al., 2004; Stackman et al., 2002) and the IK channel in the slow AHP (King et al., 2015). As discussed in Chapter 4, the monophasic subpopulation may have SK channels, though this needs further investigation. I also did not find evidence for the slow AHP; however, further work is needed to confirm this and whether biphasic neurons have this current. Another potential candidate are calcium-activated chloride channels, which are known to be present in OSNs (Stephan et al., 2009); however, their expression in the neurons of the olfactory bulb is not known.

It is also possible that there could be differences in the biophysical properties of the channels, for example, different subunits or channel kinetics that could generate this gabazine-insensitive tail current. An ongoing project in my lab is to investigate the single-cell transcriptome of olfactory bulb dopaminergic neurons, which could identify markers of the two subpopulations and potential candidates that regulate this tail current. Follow-up targeted pharmacology experiments based on these results could then begin to identify the tail current.

5.3.6 Implications for the role of dopaminergic neurons in the olfactory bulb

A fundamental question about the two subpopulations of olfactory bulb dopaminergic neurons is what the function is for having one subpopulation with an axon and another without. Both subpopulations possess dendrites that ramify within glomeruli. If both subpopulations have dendritic release, then they both engage in intraglomerular inhibition. However, whether both subpopulations make connections with the same neuronal populations within a glomerulus is not fully known. However, if the biphasic subpopulation does not have dendritic release, then there is a marked difference in the function of the two subpopulations. This would indicate that monophasic dopaminergic neurons engage in local, mostly intraglomerular, inhibition, whereas biphasic dopaminergic neurons would be exclusively involved in lateral, interglomerular inhibition.

Axonic olfactory bulb dopaminergic neuron are unlikely to be receiving direct OSN input as neurons defined as short-axon cells have been shown to only receive sensory input through external tufted cells and are not believed to be involved in presynaptic inhibition of OSN terminals (Hayar et al., 2004b; Kiyokage et al., 2010; McGann et al., 2005). These neurons also have broadly ramifying dendrites and contact multiple glomeruli (Galliano et al., 2018; Kiyokage et al., 2010). As odours evoke a spatial map of activated glomeruli across the olfactory bulb surface, these neurons are best placed to sample the incoming activity. If a glomerulus is strongly

activated, so too will its associated axonic dopaminergic neurons. Rather than inhibiting this response, these neurons can then signal and silence other glomeruli by inhibiting either external tufted cells or mitral/tufted cells (Banerjee et al., 2015; Liu et al., 2016; Whitesell et al., 2013). Odour sensory maps are also formed by the temporal activation of glomeruli (Spors and Grinvald, 2002). As GABA and dopamine release in olfactory bulb dopaminergic neurons is temporally distinct, they can drive interglomerular inhibition and then excitation responses in external tufted cells (Liu et al., 2013). Therefore, these cells may also be involved in shaping the temporal pattern of odour maps.

If axonic olfactory bulb dopaminergic neurons do have dendritic release; however, further work is needed to understand what role this is playing in intra and interglomerular inhibition and what are the postsynaptic targets of their dendrites. EM work would be needed to identify the postsynaptic targets of both subpopulations. It is has also been posited that GABA release in the compact neuropil of glomeruli diffuses and activates GABA receptors via spillover (Murphy et al., 2005; Smith and Jahr, 2002). Based on the differences observed in auto-evoked inhibition, axonic dopaminergic neurons would likely only have a minimal contribution to intraglomerular inhibition compared to the anaxonic subpopulation. It is possible that the function of smaller and more difficult to evoke auto-inhibition could reflect a need for dendritic release under specific circumstances, for example, strong stimulation. This would suggest that intraglomerular inhibition from axonic olfactory bulb dopaminergic neurons would have a different role in odour processing.

Chapter Six – General Discussion

6.1 Thesis summary

The work presented in this thesis was aimed at understanding experience-dependent plasticity in monophasic dopaminergic neurons in the DAT^{IREScre} mouse olfactory bulb. Of note, I described how odour deprivation induces activity-dependent changes in protein expression as quickly as 1 day after unilateral naris occlusion in this cell type. I used whole-cell electrophysiology in acute slices to characterise intrinsic and synaptic plasticity changes and found that functional changes are slower to emerge. While there are trends for changes in the sag potential, medium AHP and miniature excitatory postsynaptic currents changing after 1 day of occlusion, by 3 days these properties had significantly increased. In **Table 6.1** I summarise the results of significant changes in monophasic DAT-tdTomato olfactory bulb neurons after 1 and 3 days of occlusion compared to their respective controls.

I also investigated dendritic release of GABA in both subpopulations of dopaminergic neurons in the mouse olfactory bulb by studying $GABA_A$-mediated auto-inhibition currents in DAT-tdTomato neurons. I found that monophasic, presumed AIS-negative, DAT-tdTomato neurons have a clearly identifiable auto-inhibition response; however, biphasic, presumed AIS-positive, DAT-tdTomato neurons only show this response after enhancing L-type calcium channels. I also identified a calcium-dependent current primarily present in biphasic DAT-tdTomato neurons. These results indicate a striking functional difference between both subpopulations of olfactory bulb dopaminergic neurons, with implications for their roles in odour processing in the olfactory bulb.

In this final section, I will discuss using olfactory bulb dopaminergic neurons and unilateral naris occlusion as a model to study experience-dependent plasticity. I will also explore how the different forms of plasticity that I identified may affect the neuron, what these changes might mean for odour processing in the olfactory bulb. Finally, I will end with some suggestions for future directions based on this work.

	1 day occluded	3 day occluded
cFos expression	↓	↓
TH expression	↓	⇓
DDC expression	↓	–
Sag potential	–	↑
Rebound spike at current step offset	↑	⇑
Medium afterhyperpolarisation (peak)	–	↑
Medium afterhyperpolarisation (area)	–	↑
mEPSC charge	–	↑
mEPSC large events	–	↑

Table 6.1 Summary of results
↓ (decrease) ⇓ (further decrease) ↑ (increase) ⇑ (further increase) - (no change)

6.2 Monophasic olfactory bulb DAT^{IREScre} neurons as a model system

As discussed in Chapter 3, the DAT^{IREScre} mouse has advantages and disadvantages for the study of olfactory bulb dopaminergic neurons. The majority of olfactory bulb TH-positive neurons expressed tdTomato when this line is crossed with a tdTomato reporter mouse. Both subpopulations of olfactory bulb dopaminergic neurons are labelled; however, the axonic subpopulation are underrepresented though still present (Chapter 5 and (Galliano et al., 2018)). While there is off-target expression in a subpopulation of calretinin glomerular layer interneuron, these neurons can be identified by immunohistochemistry, electrophysiology and, to an extent, morphology and tdTomato intensity (see Figure 3.5).

Based on the birthdating results presented, it is clear that there is a range in the maturational age of monophasic DAT-tdTomato neurons that have been studied during this project. The minimum age of a DAT-tdTomato neuron in the P28 olfactory bulb is ~14 days old (see Figure 3.7). While neurons this young are a very small proportion of the total population, it is clear that

a sizeable proportion of DAT-tdTomato neurons were generated postnatally. However, the general population labelled by DDC and TH appear to have a wider age range, with a greater proportion generated postnatally than DAT-tdTomato neurons (see Figure 3.8). As immature neurons can express *Th* without significant TH translation (Baker et al., 2001) and DDC may be detectable prior to TH, it is likely that mice expressing a fluorescent label under the control of a *Th* or *Ddc* promoter would label more immature neurons than the $DAT^{IRES\mathit{cre}}$ mouse.

Adult neurogenesis is believed to endow newborn neurons with heightened plasticity compared to the more mature population. It is, therefore, unclear whether the experience-dependent plasticity observed following unilateral naris occlusion affects immature monophasic DAT-tdTomato neurons more than those that are more mature. An ongoing project in my lab is to investigate this very question by using viral technology to specifically label adult generated dopaminergic neurons in the olfactory bulb and study their plasticity in response to sensory manipulations compared to more mature monophasic dopaminergic neurons.

An important question is whether there is a better approach available to study olfactory bulb dopaminergic neurons in live tissue. However, the decision ultimately depends on the research question. Unless specific markers are identified that can distinguish the two subtypes, all currently available transgenic mice will label both dopaminergic subpopulations, with associated maturational heterogeneity. Anaxonic dopaminergic neurons can be specifically studied by viral injection postnatally, which can also give temporal specificity. However, the number of labelled neurons will likely be low and the virus would need to be specific for labelling dopaminergic neurons. If calretinin neurons only express *Dat* during early development, labelling these non-dopaminergic neurons can be avoided by using an inducible Cre mouse and switching on Cre later in development. However, there will still be maturational heterogeneity in the labelled neurons, unless mature neurons do not continue expressing *Dat*.

6.3 Odour deprivation by unilateral naris occlusion

Unilateral naris occlusion by insertion of a small plug is a simple and reliable method to induce odour deprivation and experience-dependent plasticity (Cheetham et al., 2016; Cummings et al., 1997; Kass et al., 2013). There is a history of using sensory deprivation in rodents to investigate how sensory systems can adapt to changes in the environment, including monocular deprivation and whisker trimming. While monocular deprivation requires surgery, unilateral naris occlusion using a plug has the advantage of being a quick and simple technique. The manipulation also does not need to be repeated, while whisker trimming often needs to be repeated every 2-3

days (Li et al., 2009). As naris occlusion is essentially a blocked nose, like can happen with a common cold, this manipulation is physiologically relevant or at least relevantly pathophysiological. In addition, olfactory sensory neurons (OSNs) can be naturally damaged or lost due to exposure to toxins, infections or trauma. Therefore, unilateral naris occlusion allows an understanding of how the olfactory bulb can change and adapt to the loss of sensory input under naturally-relevant circumstances and how it responds when input is restored.

I have shown that the activity of DAT-tdTomato neurons is reduced after only 1 day of naris occlusion and there is a detectable decrease in the expression of TH, 1 day earlier than previously described (Young Cho et al., 1996). While there may not be striking functional changes in these neurons after 1 day of occlusion, there are clear synaptic and intrinsic plasticity modifications after 3 days. This work adds to previous studies demonstrating that olfactory bulb dopaminergic neurons have experience-dependent plasticity and supports employing the DAT$^{IRES\textit{cre}}$ mouse as a model to study plasticity.

There are caveats that may be associated with unilateral naris occlusion. The olfactory bulb is known to be innervated by cortical neurons and it is unknown whether these inputs have been affected by 1 or 3 days of unilateral naris occlusion. It is possible that the occluded bulb is receiving feedback input from cortical regions activated by sensory input to the open bulb. The expression of cFos has been found to increase in occluded bulbs in response to odour presentation (Jin et al., 1996). Therefore, there may not be total silencing in the deprived bulb. However, this is likely reflecting what would happen in non-experimental conditions, as cortical input is an established property of the olfactory bulb. Complete silencing is not needed to investigate plasticity and is likely more natural if activity is decreased rather than completely silenced.

There is also the issue of the most appropriate control to use. Many studies use the olfactory bulb contralateral to the occluded naris as a control. While this is an attractive approach as it is a within animal control, it assumes that this olfactory bulb represents a “normal” condition. However, this manipulation forces the open side to carry more airflow and over long periods of time (>6 weeks) has been shown to result in the loss of OSNs and hypertrophy of the olfactory epithelium (Maruniak et al., 1989, 1990). Other potential controls are naïve mice that had no manipulation or sham mice. However, there may be subtle effects associated with the occlusion procedure that have been revealed using sham controls (Chapter 4 & (Kass et al., 2013). There is unlikely to be a perfect control for odour deprivation. Some studies address these concerns by using combinations of controls, for example contralateral control and naïve (Grier et al., 2016)

or both bulbs from occluded and sham animals (Kass et al., 2013). However, there are ethical and practical concerns about the number of groups and animals a study needs. There should be careful consideration of the control(s) to be used in unilateral naris occlusion experiments.

6.4 Experience-dependent plasticity of monophasic olfactory bulb dopaminergic neurons

Many forms of experience-dependent plasticity can be viewed as a compensatory mechanism that acts to stabilise neuron and circuit activity, particularly in response to long-term changes to activity. The balance between excitation and inhibition is believed to be crucial for maintaining network stability. As such, following activity deprivation this balance would be expected to shift to increase excitation and decrease inhibition in response to reduced input. The olfactory bulb would, therefore, be adapting to be able to respond to any remaining incoming input or to input following the onset of recovery. One mechanism that olfactory bulb dopaminergic neurons employ to reduce their output is by decreasing the synthesis of dopamine, as quickly as 1 day after unilateral naris occlusion. Dopamine release has been shown to have an inhibitory role on OSN input to the olfactory bulb, therefore, there would be predicted to be reduced intraglomerular inhibition associated with this form of plasticity (Vaaga et al., 2017). However, dopamine may also produce a rebound excitatory response in distant external tufted cells, which is believed to increase their activity and release, exciting mitral cells and glomerular layer GABAergic interneurons (Liu et al., 2013). Therefore, reduced interglomerular dopamine release could prolong external tufted cell inactivity, resulting in decreased intraglomerular inhibition and enhancing mitral cell sensitivity to OSN input. It is also unclear what is happening to the quantal release of dopamine when synthesis rates of the transmitter are lowered. There may be reduced dopamine molecules per dopamine vesicle, which would result in a consistent reduction in the release of dopamine. However, if vesicles are being filled as normal from a diminished overall pool of cytoplasmic dopamine, there may be fewer available dopamine vesicles, which would result in an initial period of unchanged release, followed by a period of depleted available vesicles. Both scenarios would affect the postsynaptic targets, but the latter would be use-dependent.

Neurons can also adapt to less activity by strengthening excitatory synapses or weakening inhibitory synapses to receive more input. I found that odour deprivation increased both the amplitude and charge of mEPSCs in olfactory bulb dopaminergic neurons, supporting the evidence of increased mEPSC amplitude in external tufted cells and glomerular layer GABAergic interneurons after occlusion in the rat olfactory bulb (Tyler et al., 2007). Therefore, monophasic

olfactory bulb dopaminergic neurons would be expected to have a greater excitatory response, suggesting that they would be more excitable. This is counterintuitive to the idea of compensatory plasticity. However, intrinsic excitability controls how this input is translated to output and may offer an explanation for how inhibitory output is reduced.

I observed distinct increases in the sag potential and medium AHP after 3 days of naris occlusion, which are known to affect neuronal excitability. However, there were no significant accompanying differences in the firing properties of these neurons. As discussed in Chapter 4, these functional changes could be affecting firing under more physiological conditions or attenuating synaptic input at dendrites. The currents regulating the sag potential and medium AHP have previously been shown to be modified in an activity-dependent manner. Activity deprivation in organotypic slice cultures of rat cerebellum increases I_h and decreases the excitability of the GABAergic, cerebellar Purkinje cells (Shim et al., 2016). Increased activity can decrease I_h, resulting in increased excitability of entorhinal cortical neurons (Shah et al., 2004). However, these changes can be cell type-dependent, with activity-deprivation in the rat barrel cortex associated with a decrease in HCN channel density and increased excitability in pyramidal neurons (Breton and Stuart, 2009). Learning can reduce the medium AHP and increase the excitability of pyramidal neurons in the hippocampus and basolateral amygdala (Motanis et al., 2014; Oh, 2010). In the olfactory bulb, repeated odour exposure produces a reduction in the AHP of mitral cells, while blocking synaptic activity increases the AHP (Duménieu et al., 2015). The results of this thesis further support the plasticity of I_h and medium AHP.

As discussed in Chapters 4 and 5, the intrinsic plasticity changes could attenuate excitatory and inhibitory responses in monophasic olfactory bulb dopaminergic neurons by shunting. Active HCN channels and the channels that may regulate the medium AHP have all been found to reduce postsynaptic potentials (Berger et al., 2001; Faber et al., 2005; Magee, 1999; Ngo-Anh et al., 2005). These changes could potentially increase the shunting of postsynaptic currents, reducing synaptic-driven excitability. However, mEPSCs may be potentiated as a mechanism to retain a level of excitation in these neurons to ensure glomerular layer inhibition under certain circumstances. Nevertheless, it is unclear whether this is happening in monophasic olfactory bulb DAT-tdTomato neurons after occlusion as these channels are likely to be blocked by the caesium internals used to study synaptic properties. Further work would be required to understand the effect that increased I_h and medium AHP are having on input and intrinsic excitability.

Studying dendritic release of GABA following 1 day of occlusion found that there was a trend for less release and decreased paired-pulse depression (see Figure 5.8–5.9), which is unlikely to be due to changes in $GABA_A$ receptors (see Figure 5.4). This could reflect changes in GABA release, which could be mediated by changes in calcium dynamics at release sites or release probability. It is possible to directly measure calcium dynamics (Chen et al., 2013; Jensen et al., 2017), GABA release (Looger et al., 2018) and dopamine release (Patriarchi et al., 2018) using sensors that enable high spatiotemporal measurements of neurotransmitter release.

These results have provided important insights into the activity-dependent plasticity of monophasic olfactory bulb DAT-tdTomato neurons following odour deprivation. In particular, they highlight the importance of studying plasticity mechanisms in isolation as many of these processes could potentially interact and be obscured. It would be expected that these experience-dependent changes would affect odour processing in the olfactory bulb.

6.5 Implications for olfactory processing

Research has found that olfactory bulb dopaminergic neurons are important regulators of intraglomerular inhibition (Vaaga et al., 2017). Based on the results in Chapter 5, this is likely to be specific to the monophasic, presumed anaxonic subpopulation, because the biphasic, presumed axonic, subpopulation did not demonstrate auto-evoked inhibition that indicates dendritic release of GABA. Therefore, experience-dependent plasticity in these neurons would be assumed to affect odour processing in the olfactory bulb, especially intraglomerular inhibition. The finding that TH expression is significantly downregulated in DAT-tdTomato neurons following occlusion suggests that the ability to synthesise dopamine has been affected. Reduced dopamine would affect the phasic and tonic inhibition of glomeruli, which would have implications for odour processing.

Given the role of dopamine in modulating neurotransmitter release at OSN terminals, it is likely that the strength of presynaptic inhibition through D_2 receptors would be reduced by the plastic changes accompanying short-term occlusion. Dopamine receptors are also expressed throughout glomeruli and this neurotransmitter plays an important role in the excitability of glomerular layer neurons and the transmission of sensory input from OSN terminals to the bulbar projections neurons (Gutièrrez-Mecinas et al., 2005; Vaaga et al., 2017). Activation of olfactory bulb dopaminergic neurons that express channelrhodopsin significantly decreases OSN input to mitral cells and external tufted cells (Vaaga et al., 2017). Therefore, reduced dopamine-mediated inhibition would be expected to increase OSN-evoked responses. Indeed,

in the rat olfactory bulb, long-term (>1 month) odour deprivation increases the sensitivity and activity of mitral and tufted cells in response to odour stimulation (Wilson and Sullivan, 1995). Moreover, these authors were able to replicate this result by blocking D_2 receptors.

It would be interesting to investigate the functional diversity between dopaminergic neurons, particularly after odour deprivation. Previous work studying mitral cells has found that there is a high level of diversity in their sag potential (Angelo and Margrie, 2011). However, mitral cells belonging to the same glomerular circuit show stereotypic sag potential and I_h current (Angelo and Margrie, 2011). Interestingly, in a mouse expressing only a single odorant receptor, the interglomerular differences are diminished. However, mitral cells associated with the same glomerulus still remain more similar (Angelo et al., 2012). Therefore, sensory input and local connectivity contributes to regulating sag diversity. Firing of mitral cells between populations is also heterogenous and is regulated by AHP (Duménieu et al., 2015; Padmanabhan and Urban, 2010). Whether interglomerular interneurons also show this functional diversity is unknown. Future work should investigate functional diversity of monophasic DAT-tdTomato neurons by patching neurons around a glomerulus and confirm association with the same glomerulus by stimulating OSN inputs or studying dendritic morphology and glomerulus innervation, either live with Alexa dye in the intracellular solution or post-hoc with immunohistochemistry for biocytin. If there is intraglomerular homogeneity in functional properties, this should be followed by an investigation of monophasic DAT-tdTomato neurons and mitral cells affiliated with the same glomerulus. This could reveal how specific activity-dependent changes are affecting glomerular output.

It is unclear how the pacemaker activity of monophasic DAT-tdTomato neurons has been affected, if at all, by occlusion. The expression of the neuronal activity marker, cFos, is significantly downregulated in olfactory bulb DAT-tdTomato neurons after odour deprivation and it has been shown that calcium influx following membrane depolarisation can induce cFos expression (Sheng et al., 1990). Therefore, pacemaker activity could induce cFos expression, suggesting that this activity could have been inhibited by odour deprivation. Dopaminergic neurons in other regions of the brain can retain rhythmic firing even in the absence of synaptic inputs (Feigenspan et al., 1998; Hainsworth et al., 1991). Acutely dissociated olfactory bulb dopaminergic neurons have increased pacemaker activity compared to slice recordings, suggesting it can be regulated under more physiological conditions (Pignatelli et al., 2005). Pharmacologically blocking glutamatergic and GABAergic input has been found to occasionally inhibit rhythmic firing (Pignatelli et al., 2005). It remains to be seen whether *in vivo* inhibition of OSN input affects the pacemaker activity of olfactory bulb dopaminergic neurons and tonic

inhibition of the glomerular layer. If tonic inhibition has been reduced, this could increase OSN input and excitation of glomerular layer neurons.

While inhibition is decreased, odour deprivation has been shown to increase the expression of glutamatergic synapse proteins in glomeruli and increase excitatory synaptic input to glomerular layer interneurons (Chapter 5 and (Tyler et al., 2007)). Overall, the glomerular layer is adapting to reduced synaptic input by increasing its excitation. This is making the olfactory bulb more sensitive to odour input, as previously described following odour deprivation (Guthrie et al., 1991; Rodríguez et al., 2013; Wilson and Sullivan, 1995). There is also the question of what effect these experience-dependent changes would have on interglomerular inhibition. Downregulation of TH expression is a feature of all olfactory bulb dopaminergic populations. In addition, work from my lab has shown that the biphasic population has a shorter axon initial segment (AIS) and decreased excitability following 1 day of occlusion *in vivo* or TTX treatment *in vitro* (Galliano et al., *in preparation*; Chand et al., 2015). Therefore, the inhibition-excitation of external tufted cells by the axonic subpopulation will be affected (Liu et al., 2013). This could affect signal-to-noise enhancement by lateral inhibition and the temporal dynamics of glomerular activity, which are important for odour discrimination (Kass et al., 2015). Odour deprivation and reduced dopamine have both been implicated in reducing odour discrimination (Escanilla et al., 2009; Rodríguez et al., 2013; Wilson and Sullivan, 1995). Therefore, the glomerular layer may be adapting to unilateral naris occlusion by increasing sensitivity of the olfactory bulb to odour input, at the expense of discriminability. However, behavioural studies would be required to understand how odour detection and odour discrimination may be affected following unilateral naris occlusion.

6.6 Future directions

The work presented in this thesis can form the basis of a number of future experiments and areas of research. While discussing the findings in the results chapters and this discussion chapter I have indicated many results that require further investigation and characterisation. In particular, the consequences of increased sag potential and medium AHP on activity and whether the very weak auto-evoked inhibition response in biphasic DAT-tdTomato neurons is dendritic GABA release. Additionally, there are many other questions that I feel are particularly worth pursuing.

6.6.1 Plasticity in both olfactory bulb dopaminergic populations

Work from my lab has investigated experience-dependent plasticity in monophasic and biphasic dopaminergic neurons after 1 day of unilateral naris occlusion and found that both populations have a trend for decreased excitability (Elisa Galliano, *in preparation*). I built on this work by exclusively studying the monophasic population after different periods of odour deprivation and studying functional properties not previously investigated, specifically the sag potential and medium AHP. Based on the results presented in this thesis, future work should investigate whether the biphasic subpopulation also demonstrates activity-dependent plasticity in these properties. This would determine whether these changes are a general adaptation response in olfactory bulb dopaminergic neurons to odour deprivation or specific to the monophasic population.

My lab has identified differences in odorant responses between these two subpopulations. The biphasic dopaminergic neurons have a weaker response, but for certain types of long-latency response are more broadly tuned to odour stimuli compared to the monophasic neurons (Galliano et al., 2018). If occlusion is reducing glomerular layer inhibition, which could increase OSN input, there should be an investigation of whether odorant responses in both olfactory bulb dopaminergic subpopulations have also been affected. Additionally, there have been other forms of activity-dependent plasticity identified in glomerular layer interneurons, with some associated with dopaminergic neurons, including gene expression, epigenetic modifications and dendritic plasticity (Banerjee et al., 2013; Bovetti et al., 2013; Mizrahi, 2007; Wang et al., 2017). It would be interesting to study and compare these in the different subpopulations of olfactory bulb dopaminergic neuron. Sparse labelling of the two subpopulations (Galliano et al., 2018), coupled with naris occlusion could allow an investigation of dendritic and also axonal plasticity. Ongoing work in my lab is investigating the epigenome and transcriptome of DAT-tdTomato neurons on a single-cell level following occlusion (Marcela Lipovsek), providing crucial information on how these neurons are regulating activity-dependent plasticity on a genetic level.

6.6.2 Different occlusion durations

The effects of unilateral naris occlusion in this study are dependent on the duration of the manipulation. It would be interesting to understand how olfactory bulb dopaminergic neurons respond to longer periods of odour deprivation. Previous studies have found that the decrease in TH expression stabilises around 21 to 30 days after naris occlusion (Bastien-Dionne et al., 2010; Young Cho et al., 1996). Therefore, it would be expected that continued occlusion would

reduce TH expression further in DAT-tdTomato neurons. However, it is not clear what would be the effect on the electrophysiological functional properties of these neurons. Previous work has shown that the firing rate of certain inhibitory neurons in the visual cortex recovers to baseline after 1 day of monocular deprivation, while other inhibitory populations do not recover their activity (Barnes et al., 2015; Hengen et al., 2013). Additionally, there may be a recovery at a population-level; however, individual cells can still show considerable variability (Slomowitz et al., 2015). As the survival of olfactory bulb dopaminergic neurons may be reduced by odour deprivation (Grier et al., 2016; Sawada et al., 2011), it would be sensible to not extend the duration of occlusion too long. An initial investigation could study the effect of ~1 week of occlusion to determine whether the observed plasticity changes were stable compared to 3 days of occlusion or if they had increased further or recovered to baseline.

Activity-dependent plasticity in the olfactory bulb can also occur on a rapid timescale, with relocation of dendritic spines within minutes following mitral cell activity (Breton-Provencher et al., 2016). Within a few minutes of unilateral naris occlusion, there is a decrease in spontaneous activity of mitral cells and their activity was no longer locked to the respiration cycle (Philpot et al., 1997). Additionally, a few minutes after reopening the closed naris there was an increase in mitral cell activity above baseline (Philpot et al., 1997). Therefore, there may be forms of plasticity induced rapidly following changes in odour input.

6.6.3 Alternative sensory manipulations

In this thesis I investigated how reducing activity by odour deprivation affected anaxonic olfactory bulb dopaminergic neurons. However, activity can be changed in the olfactory bulb using different approaches such as odour enrichment, odour learning, fear-conditioning or mating. Given the importance of sensory input to regulate the activity of olfactory bulb dopaminergic neurons, it would be interesting to investigate the experience-dependent plasticity of this neuron population in response to other sensory manipulations. TH expression can be increased by enhancing activity in *in vitro* cell cultures of olfactory bulb dopaminergic neurons and *in vivo* after mating (Chand et al., 2015; Serguera et al., 2008). Previous work has investigated odour enrichment *in vivo* and found that it increases the number of newborn neurons in the glomerular layer of the olfactory bulb, in particular the dopaminergic population (Bonzano et al., 2014). Therefore, olfactory bulb dopaminergic neurons can show bidirectional plasticity dependent on experience.

While unilateral naris occlusion is a reliable manipulation for reducing activity across the deprived bulb, an equivalent bulb-wide increase in activity is more difficult to achieve. This is

due to odorant receptors having different binding affinities, dependent on odorant identity and concentration. Unpublished work from my lab has found that mice exposed to four different odour pairs that are changed every two hours and then presented altogether overnight significantly increased cFos and TH expression in olfactory bulb dopaminergic neurons (Elisa Galliano). This could, therefore, be one approach to increase activity, with the caveat that increased sensory input would be variable across glomeruli. A more reliable approach could be to enhance activity in particular glomeruli. For example, the odorant receptor that responds to acetophenone (M72) has been genetically labelled in a transgenic mouse, allowing targeted investigation of a specific glomerulus (Geramita and Urban, 2016).

It would be assumed that increasing the activity of olfactory bulb dopaminergic neurons would enhance intraglomerular and interglomerular inhibition. This could act in the short-term as a gain control mechanism to reduce response saturation and maintain odour identity detection. But what would be the longer-term experience-dependent changes to the functional properties of olfactory bulb dopaminergic neurons? It would be interesting to investigate whether there is a bidirectional effect on the plasticity changes I have identified. Early studies of synaptic scaling found that increased activity reduces the amplitude of mEPSCs (Turrigiano et al., 1998). The I_h and medium AHP also show bidirectional changes in response to activity. Therefore, many of the effects that I observed could go both ways depending on sensory input. Alternatively, there could be completely different responses to elevated versus reduced activity.

6.6.4 Odour processing after restoring sensory input

After identifying experience-dependent plasticity in monophasic olfactory bulb dopaminergic neurons the most obvious question is what these changes are doing to the function of the olfactory bulb. Studying the effect of dopaminergic plasticity on odour processing can be done using *ex vivo* and *in vivo* approaches. By crossing the $DAT^{IRES\mathit{cre}}$ mouse to a Cre-dependent channelrhodopsin mouse, it would be possible to directly activate dopaminergic neurons in acute slices while electrically stimulating OSN fibres and recording the evoked response from bulbar projection neurons (Vaaga et al., 2017). Combining this *ex vivo* approach with pharmacological manipulation of dopamine and GABA receptors would give insight into the intraglomerular inhibition capability of dopaminergic neurons after occlusion. *In vivo* experiments could be used to further understand the effect of unilateral naris occlusion on olfactory bulb dopaminergic neurons. In particular, characterising the activity of DAT-tdTomato by performing targeted *in vivo* extracellular recordings while stimulating OSNs expressing channelrhodopsin or removing the nasal plug and presenting odour stimuli. Using this

characterisation of their activity, it could be possible to evoke this activity *in vivo* using a DAT-channelrhodopsin mouse. By combining this with presentation of odour stimuli and extracellular single-unit recordings of bulbar projections neurons, it could be possible to understand how *in vivo* bulbar output has been affected by the plasticity in DAT-positive neurons.

6.7 Final comment

Several decades of work into plasticity have described the remarkable ways that the brain can change and adapt to experiences. With the work presented in this thesis I have, hopefully, contributed to this field and furthered our understanding of olfactory bulb dopaminergic neurons for future research.

References

Adam, Y., and Mizrahi, A. (2011). Long-term imaging reveals dynamic changes in the neuronal composition of the glomerular layer. Journal of Neuroscience *31*, 7967–7973.

Agoston, Z., Heine, P., Brill, M.S., Grebbin, B.M., Hau, A.-C., Kallenborn-Gerhardt, W., Schramm, J., Götz, M., and Schulte, D. (2014). Meis2 is a Pax6 co-factor in neurogenesis and dopaminergic periglomerular fate specification in the adult olfactory bulb. Development *141*, 28–38.

Aizenman, C.D., and Linden, D.J. (2000). Rapid, synaptically driven increases in the intrinsic excitability ofcerebellar deep nuclear neurons. Nature Neuroscience *3*, 109–111.

Allen, Z.J., Waclaw, R.R., Colbert, M.C., and Campbell, K. (2007). Molecular identity of olfactory bulb interneurons: transcriptional codes of periglomerular neuron subtypes. Journal of Molecular Histology *38*, 517–525.

Alonso, M., Viollet, C., Gabellec, M.-M., Meas-Yedid, V., Olivo-Marin, J.-C., and Lledo, P.-M. (2006). Olfactory Discrimination Learning Increases the Survival of Adult-Born Neurons in the Olfactory Bulb. Journal of Neuroscience *26*, 10508–10513.

Andrade, R., Foehring, R.C., and Tzingounis, A. V (2012). The calcium-activated slow AHP: cutting through the Gordian knot. Frontiers in Cellular Neuroscience *6*, 47.

Angelo, K., and Margrie, T.W. (2011). Population diversity and function of hyperpolarization-activated current in olfactory bulb mitral cells. Scientific Reports *1*, 50.

Angelo, K., London, M., Christensen, S.R., and Hausser, M. (2007). Local and Global Effects of Ih Distribution in Dendrites of Mammalian Neurons. Journal of Neuroscience *27*, 8643–8653.

Angelo, K., Rancz, E.A., Pimentel, D., Hundahl, C., Hannibal, J., Fleischmann, A., Pichler, B., and Margrie, T.W. (2012). A biophysical signature of network affiliation and sensory processing in mitral cells. Nature *488*, 375–378.

Angulo, M.C., Lambolez, B., Audinat, E., Hestrin, S., and Rossier, J. (1997). Subunit composition, kinetic, and permeation properties of AMPA receptors in single neocortical nonpyramidal cells. Journal of Neuroscience *17*, 6685–6696.

Antal, M., Eyre, M., Finklea, B., and Nusser, Z. (2006). External tufted cells in the main olfactory bulb form two distinct subpopulations. European Journal of Neuroscience *24*, 1124–1136.

Aroniadou-Anderjaska, V., Zhou, F.-M., Priest, C.A., Ennis, M., and Shipley, M.T. (2000). Tonic and Synaptically Evoked Presynaptic Inhibition of Sensory Input to the Rat Olfactory Bulb Via GABA B Heteroreceptors. Journal of Neurophysiology *84*, 1194–1203.

Arruda-Carvalho, M., Akers, K.G., Guskjolen, A., Sakaguchi, M., Josselyn, S.A., and Frankland, P.W. (2014). Posttraining Ablation of Adult-Generated Olfactory Granule Cells Degrades Odor-Reward Memories. Journal of Neuroscience *34*, 15793–15803.

Aumann, T.D., Egan, K., Lim, J., Boon, W.C., Bye, C.R., Chua, H.K., Baban, N., Parish, C.L., Bobrovskaya, L., Dickson, P., et al. (2011). Neuronal activity regulates expression of tyrosine hydroxylase in adult mouse substantia nigra pars compacta neurons. Journal of Neurochemistry *116*, 646–658.

Aungst, J.L., Heyward, P.M., Puche, A.C., Karnup, S. V., Hayar, A., Szabo, G., and Shipley, M.T. (2003). Centre–surround inhibition among olfactory bulb glomeruli. Nature *426*, 623–629.

Bäckman, C.M., Malik, N., Zhang, Y., Shan, L., Grinberg, A., Hoffer, B.J., Westphal, H., and Tomac, A.C. (2006). Characterization of a mouse strain expressing Cre recombinase from the 3′ untranslated region of the dopamine transporter locus. Genesis *44*, 383–390.

Bagley, J., LaRocca, G., Jimenez, D.A., and Urban, N.N. (2007). Adult neurogenesis and specific replacement of interneuron subtypes in the mouse main olfactory bulb. BMC Neuroscience *8*, 92.

Bakalyar, H.A., and Reed, R.R. (1990). Identification of a specialized adenylyl cyclase that may mediate odorant detection. Science *250*, 1403–1406.

Baker, H. (1990). Unilateral, neonatal olfactory deprivation alters tyrosine hydroxylase expression but not aromatic amino acid decarboxylase or GABA immunoreactivity. Neuroscience *36*, 761–771.

Baker, H., Kawano, T., Margolis, F.L., and Joh, T.H. (1983). Transneuronal regulation of tyrosine hydroxylase expression in olfactory bulb of mouse and rat. Journal of Neuroscience *3*, 69–78.

Baker, H., Morel, K., Stone, D.M., and Maruniak, J.A. (1993). Adult naris closure profoundly reduces tyrosine hydroxylase expression in mouse olfactory bulb. Brain Research *614*, 109–116.

Baker, H., Liu, N., Chun, H.S., Saino, S., Berlin, R., Volpe, B., and Son, J.H. (2001). Phenotypic differentiation during migration of dopaminergic progenitor cells to the olfactory bulb. Journal of Neuroscience *21*, 8505–8513.

Balu, R., Pressler, R.T., and Strowbridge, B.W. (2007). Multiple Modes of Synaptic Excitation of Olfactory Bulb Granule Cells. Journal of Neuroscience *27*, 5621–5632.

Banerjee, A., Marbach, F., Anselmi, F., Gupta, P., Li, B., and Correspondence, D.F.A. (2015). An Interglomerular Circuit Gates Glomerular Output and Implements Gain Control in the Mouse Olfactory Bulb. Neuron *87*, 193–207.

Banerjee, K., Akiba, Y., Baker, H., and Cave, J.W. (2013). Epigenetic control of neurotransmitter expression in olfactory bulb interneurons. International Journal of Developmental Neuroscience *31*, 415–423.

Baranauskas, G., Mukovskiy, A., Wolf, F., and Volgushev, M. (2010). The determinants of the onset dynamics of action potentials in a computational model. Neuroscience *167*, 1070–1090.

Barber, C.N., and Coppola, D.M. (2015). Compensatory plasticity in the olfactory epithelium: age, timing, and reversibility. Journal of Neurophysiology *114*, 2023–2032.

Barnes, S.J., Sammons, R.P., Jacobsen, R.I., Mackie, J., Keller, G.B., and Keck, T. (2015). Subnetwork-Specific Homeostatic Plasticity in Mouse Visual Cortex In Vivo. Neuron *86*, 1290–1303.

Barnes, S.J., Franzoni, E., Jacobsen, R.I., Clopath, C., Keller, G.B., and Keck Correspondence, T. (2017). Deprivation-Induced Homeostatic Spine Scaling In Vivo Is Localized to Dendritic Branches that Have Undergone Recent Spine Loss. Neuron *96*, 871–882.

Bartley, A.F., Huang, Z.J., Huber, K.M., and Gibson, J.R. (2008). Differential Activity-Dependent, Homeostatic Plasticity of Two Neocortical Inhibitory Circuits. Journal of Neurophysiology *100*, 1983–1994.

Bastien-Dionne, P.-O., David, L.S., Parent, A., and Saghatelyan, A. (2010). Role of sensory activity on chemospecific populations of interneurons in the adult olfactory bulb. The Journal of Comparative Neurology *518*, 1847–1861.

Batista-Brito, R., Close, J., Machold, R., and Fishell, G. (2008). The distinct temporal origins of olfactory bulb interneuron subtypes. Journal of Neuroscience *28*, 3966–3975.

Becherer, U., and Rettig, J. (2006). Vesicle pools, docking, priming, and release. Cell and Tissue Research *326*, 393–407.

Belnoue, L., Grosjean, N., Abrous, D.N., and Koehl, M. (2011). A Critical Time Window for the Recruitment of Bulbar Newborn Neurons by Olfactory Discrimination Learning. Journal of Neuroscience *31*, 1010–1016.

Benson, T.E., Ryugo, D.K., Hinds, J.W., and Murthy, V.N. (1984). Effects of sensory deprivation on the developing mouse olfactory system: a light and electron microscopic, morphometric analysis. Journal of Neuroscience *4*, 638–653.

Bepari, A.K., Watanabe, K., Yamaguchi, M., Tamamaki, N., and Hirohide, T. (2012). Visualization of odor-induced neuronal activity by immediate early gene expression. BMC Neuroscience *13*, 140.

Berger, T., Larkum, M.E., and Lüscher, H.-R. (2001). High I_h Channel Density in the Distal Apical Dendrite of Layer V Pyramidal Cells Increases Bidirectional Attenuation of EPSPs. Journal of Neurophysiology *85*, 855–868.

Bi, G.Q., and Poo, M.M. (1998). Synaptic modifications in cultured hippocampal neurons: dependence on spike timing, synaptic strength, and postsynaptic cell type. Journal of Neuroscience *18*, 10464–10472.

Biel, M., Wahl-Schott, C., Michalakis, S., and Zong, X. (2009). Hyperpolarization-Activated Cation Channels: From Genes to Function. Physiological Reviews *89*, 847–885.

Björklund, A., and Dunnett, S.B. (2007). Dopamine neuron systems in the brain: an update. Trends in Neurosciences *30*, 194–202.

Björklund, A., and Lindvall, O. (1975). Dopamine in dendrites of substantia nigra neurons: suggestions for a role in dendritic terminals. Brain Research *83*, 531–537.

Bliss, T. V, and Lømo, T. (1973). Long-lasting potentiation of synaptic transmission in the dentate area of the anaesthetized rabbit following stimulation of the perforant path. The Journal of Physiology *232*, 331–356.

Bohannon, A.S., and Hablitz, J.J. (2018). Developmental Changes in HCN Channel Modulation of Neocortical Layer 1 Interneurons. Frontiers in Cellular Neuroscience *12*, 20.

Bolding, K.A., and Franks, K.M. (2018). Recurrent cortical circuits implement concentration-invariant odor coding. Science *361*, eaat6904.

Bond, C.T., Herson, P.S., Strassmaier, T., Hammond, R., Stackman, R., Maylie, J., and Adelman, J.P. (2004). Small Conductance Ca2+-Activated K+ Channel Knock-Out Mice Reveal the Identity of Calcium-Dependent Afterhyperpolarization Currents. Journal of Neuroscience *24*, 5301–5306.

Bonzano, S., Bovetti, S., Fasolo, A., Peretto, P., and De Marchis, S. (2014). Odour enrichment increases adult-born dopaminergic neurons in the mouse olfactory bulb. European Journal of Neuroscience *40*, 3450–3457.

Borin, M., Fogli Iseppe, A., Pignatelli, A., and Belluzzi, O. (2014). Inward rectifier potassium (Kir) current in dopaminergic periglomerular neurons of the mouse olfactory bulb. Frontiers in Cellular Neuroscience *8*, 223.

Borisovska, M., Bensen, A.L., Chong, G., and Westbrook, G.L. (2013). Distinct modes of dopamine and GABA release in a dual transmitter neuron. Journal of Neuroscience *33*, 1790–1796.

Bouhours, B., Trigo, F.F., and Marty, A. (2011). Somatic depolarization enhances GABA release in cerebellar interneurons via a calcium/protein kinase C pathway. Journal of Neuroscience *31*, 5804–5815.

Bovetti, S., Veyrac, A., Peretto, P., Fasolo, A., and De Marchis, S. (2009). Olfactory Enrichment Influences Adult Neurogenesis Modulating GAD67 and Plasticity-Related Molecules Expression in Newborn Cells of the Olfactory Bulb. PLoS ONE *4*, e6359.

Bovetti, S., Bonzano, S., Garzotto, D., Giannelli, S.G., Iannielli, A., Armentano, M., Studer, M., and De Marchis, S. (2013). COUP-TFI controls activity-dependent tyrosine hydroxylase expression in adult dopaminergic olfactory bulb interneurons. Development *140*, 4850–4859.

Boyd, A.M., Sturgill, J.F., Poo, C., and Isaacson, J.S. (2012). Cortical feedback control of olfactory bulb circuits. Neuron *76*, 1161–1174.

Breton-Provencher, V., Lemasson, M., Peralta, M.R., and Saghatelyan, A. (2009). Interneurons Produced in Adulthood Are Required for the Normal Functioning of the Olfactory Bulb Network and for the Execution of Selected Olfactory Behaviors. Journal of Neuroscience *29*, 15245–15257.

Breton-Provencher, V., Bakhshetyan, K., Hardy, D., Bammann, R.R., Cavarretta, F., Snapyan, M., Côté, D., Migliore, M., and Saghatelyan, A. (2016). Principal cell activity induces spine relocation of adult-born interneurons in the olfactory bulb. Nature Communications *7*, 12659.

Breton, J.-D., and Stuart, G.J. (2009). Loss of sensory input increases the intrinsic excitability of layer 5 pyramidal neurons in rat barrel cortex. The Journal of Physiology *587*, 5107–5119.

Brill, J., Shao, Z., Puche, A.C., Wachowiak, M., and Shipley, M.T. (2016). Serotonin increases synaptic activity in olfactory bulb glomeruli. Journal of Neurophysiology *115*, 1208–1219.

Brill, M.S., Snapyan, M., Wohlfrom, H., Ninkovic, J., Jawerka, M., Mastick, G.S., Ashery-Padan, R., Saghatelyan, A., Berninger, B., and Gotz, M. (2008). A Dlx2- and Pax6-Dependent Transcriptional Code for Periglomerular Neuron Specification in the Adult Olfactory Bulb. Journal of Neuroscience *28*, 6439–6452.

Briñón, J.G., Crespo, C., Weruaga, E., Martínez-Guijarro, F.J., Aijón, J., and Alonso, J.R. (2001). Bilateral olfactory deprivation reveals a selective noradrenergic regulatory input to the olfactory bulb. Neuroscience *102*, 1–10.

Buck, L., and Axel, R. (1991). A Novel Multigene Family May Encode Odorant Receptors: A Molecular Basis for Odor Recognition. Cell *65*, 175–187.

Buhl, E.H., Han, Z.S., Lorinczi, Z., Stezhka, V. V., Karnup, S. V., and Somogyi, P. (1994). Physiological properties of anatomically identified axo-axonic cells in the rat hippocampus. Journal of Neurophysiology *71*, 1289–1307.

Burton, S.D., and Urban, N.N. (2014). Greater excitability and firing irregularity of tufted cells underlies distinct afferent-evoked activity of olfactory bulb mitral and tufted cells. The Journal of Physiology *592*, 2097–2118.

Burton, S.D., LaRocca, G., Liu, A., Cheetham, C.E.J., and Urban, N.N. (2017). Olfactory Bulb Deep Short-Axon Cells Mediate Widespread Inhibition of Tufted Cell Apical Dendrites. Journal of Neuroscience *37*, 1117–1138.

Bywalez, W.G., Ona-Jodar, T., Lukas, M., Ninkovic, J., and Egger, V. (2016). Dendritic Arborization Patterns of Small Juxtaglomerular Cell Subtypes within the Rodent Olfactory Bulb. Frontiers in Neuroanatomy *10*, 127.

Carlson, G.C., Shipley, M.T., and Keller, A. (2000). Long-lasting depolarizations in mitral cells of the rat olfactory bulb. Journal of Neuroscience *20*, 2011–2021.

Castillo, P.E. (2012). Presynaptic LTP and LTD of Excitatory and Inhibitory Synapses. Cold Spring Harbor Perspectives in Biology *4*, a005728–a005728.

Castillo, P.E., Carleton, A., Vincent, J.D., and Lledo, P.M. (1999). Multiple and opposing roles of cholinergic transmission in the main olfactory bulb. Journal of Neuroscience *19*, 9180–9191.

Cauthron, J.L., and Stripling, J.S. (2014). Long-term plasticity in the regulation of olfactory bulb activity by centrifugal fibers from piriform cortex. Journal of Neuroscience *34*, 9677–9687.

Cave, J.W., and Baker, H. (2009). Dopamine systems in the forebrain. Advances in Experimental Medicine and Biology *651*, 15–35.

Cave, J.W., Akiba, Y., Banerjee, K., Bhosle, S., Berlin, R., and Baker, H. (2010). Differential regulation of dopaminergic gene expression by Er81. Journal of Neuroscience *30*, 4717–4724.

Cecchi, X., Wolff, D., Alvarez, O., and Latorre, R. (1987). Mechanisms of Cs+ blockade in a Ca2+-activated K+ channel from smooth muscle. Biophysical Journal *52*, 707–716.

Chand, A.N., Galliano, E., Chesters, R.A., and Grubb, M.S. (2015). A distinct subtype of dopaminergic interneuron displays inverted structural plasticity at the axon initial segment. Journal of Neuroscience *35*, 1573–1590.

Chang, M.C., Park, J.M., Pelkey, K.A., Grabenstatter, H.L., Xu, D., Linden, D.J., Sutula, T.P., McBain, C.J., and Worley, P.F. (2010). Narp regulates homeostatic scaling of excitatory synapses on parvalbumin-expressing interneurons. Nature Neuroscience *13*, 1090–1097.

Cheetham, C.E.J., Park, U., and Belluscio, L. (2016). Rapid and continuous activity-dependent plasticity of olfactory sensory input. Nature Communications *7*, 10729.

Chen, W.R., and Shepherd, G.M. (2005). The olfactory glomerulus: A cortical module with specific functions. Journal of Neurocytology *34*, 353–360.

Chen, L., Xie, Z., Turkson, S., and Zhuang, X. (2015). A53T Human -Synuclein Overexpression in Transgenic Mice Induces Pervasive Mitochondria Macroautophagy Defects Preceding Dopamine Neuron Degeneration. Journal of Neuroscience *35*, 890–905.

Chen, T.-W., Wardill, T.J., Sun, Y., Pulver, S.R., Renninger, S.L., Baohan, A., Schreiter, E.R., Kerr, R.A., Orger, M.B., Jayaraman, V., et al. (2013). Ultrasensitive fluorescent proteins for imaging neuronal activity. Nature *499*, 295–300.

Chittajallu, R., Craig, M.T., McFarland, A., Yuan, X., Gerfen, S., Tricoire, L., Erkkila, B., Barron, S.C., Lopez, C.M., Liang, B.J., et al. (2013). Dual origins of functionally distinct O-LM interneurons revealed by differential 5-HT(3A)R expression. Nature Neuroscience *16*, 1598–1607.

Chotibut, T., Apple, D.M., Jefferis, R., and Salvatore, M.F. (2012). Dopamine Transporter Loss in 6-OHDA Parkinson's Model Is Unmet by Parallel Reduction in Dopamine Uptake. PLoS ONE *7*, e52322.

Christie, J.M., Bark, C., Hormuzdi, S.G., Helbig, I., Monyer, H., and Westbrook, G.L. (2005). Connexin36 mediates spike synchrony in olfactory bulb glomeruli. Neuron *46*, 761–772.

Chuhma, N., Zhang, H., Masson, J., Zhuang, X., Sulzer, D., Hen, R., and Rayport, S. (2004). Dopamine neurons mediate a fast excitatory signal via their glutamatergic synapses. Journal of Neuroscience *24*, 972–981.

Cigola, E., Volpe, B.T., Lee, J.W., Franzen, L., and Baker, H. (1998). Tyrosine hydroxylase expression in primary cultures of olfactory bulb: role of L-type calcium channels. Journal of Neuroscience *18*, 7638–7649.

Clowney, E.J., LeGros, M.A., Mosley, C.P., Clowney, F.G., Markenskoff-Papadimitriou, E.C., Myllys, M., Barnea, G., Larabell, C.A., and Lomvardas, S. (2012). Nuclear Aggregation of Olfactory Receptor Genes Governs Their Monogenic Expression. Cell *151*, 724–737.

Cockerham, R., Liu, S., Cachope, R., Kiyokage, E., Cheer, J.F., Shipley, M.T., and Puche, A.C. (2016). Subsecond Regulation of Synaptically Released Dopamine by COMT in the Olfactory Bulb. Journal of Neuroscience *36*, 7779–7785.

Collingridge, G.L., Peineau, S., Howland, J.G., and Wang, Y.T. (2010). Long-term depression in the CNS. Nature Reviews Neuroscience *11*, 459–473.

Coopersmith, R., Weihmuller, F.B., Kirstein, C.L., Marshall, J.F., and Leon, M. (1991). Extracellular dopamine increases in the neonatal olfactory bulb during odor preference training. Brain Research *564*, 149–153.

Cope, D.W., Hughes, S.W., and Crunelli, V. (2005). GABAA receptor-mediated tonic inhibition in thalamic neurons. Journal of Neuroscience *25*, 11553–11563.

Coppola, D.M. (2012). Studies of Olfactory System Neural Plasticity: The Contribution of the Unilateral Naris Occlusion Technique. Neural Plasticity *2012*, 1–14.

Cragg, S.J., Nicholson, C., Kume-Kick, J., Tao, L., and Rice, M.E. (2001). Dopamine-Mediated Volume Transmission in Midbrain Is Regulated by Distinct Extracellular Geometry and Uptake. Journal of Neurophysiology *85*, 1761–1771.

Crespo, C., Liberia, T., Blasco-Ibáñez, J.M., Nácher, J., and Varea, E. (2013). The Circuits of the Olfactory Bulb. The Exception as a Rule. The Anatomical Record *296*, 1401–1412.

Cummings, D.M., and Belluscio, L. (2010). Continuous Neural Plasticity in the Olfactory Intrabulbar Circuitry. Journal of Neuroscience *30*, 9172–9180.

Cummings, D.M., Henning, H.E., and Brunjes, P.C. (1997). Olfactory bulb recovery after early sensory deprivation. Journal of Neuroscience *17*, 7433–7440.

Davison, I.G., and Katz, L.C. (2007). Sparse and Selective Odor Coding by Mitral/Tufted Neurons in the Main Olfactory Bulb. Journal of Neuroscience *27*, 2091–2101.

Dehorter, N., Ciceri, G., Bartolini, G., Lim, L., del Pino, I., and Marín, O. (2015). Tuning of fast-spiking interneuron properties by an activity-dependent transcriptional switch. Science *349*, 1216–1220.

Desai, N.S., Rutherford, L.C., and Turrigiano, G.G. (1999a). Plasticity in the intrinsic excitability of cortical pyramidal neurons. Nature Neuroscience *2*, 515–520.

Desai, N.S., Rutherford, L.C., and Turrigiano, G.G. (1999b). BDNF regulates the intrinsic excitability of cortical neurons. Learning & Memory *6*, 284–291.

Desai, N.S., Cudmore, R.H., Nelson, S.B., and Turrigiano, G.G. (2002). Critical periods for experience-dependent synaptic scaling in visual cortex. Nature Neuroscience *5*, 783–789.

Dhallan, R.S., Yau, K.-W., Schrader, K.A., and Reed, R.R. (1990). Primary structure and functional expression of a cyclic nucleotide-activated channel from olfactory neurons. Nature *347*, 184–187.

Dietz, S.B., and Murthy, V.N. (2005). Contrasting short-term plasticity at two sides of the mitral-granule reciprocal synapse in the mammalian olfactory bulb. The Journal of Physiology *569*, 475–488.

Dudek, S.M., and Bear, M.F. (1992). Homosynaptic long-term depression in area CA1 of hippocampus and effects of N-methyl-D-aspartate receptor blockade. Proceedings of the National Academy of Sciences *89*, 4363–4367.

Duménieu, M., Fourcaud-Trocmé, N., Garcia, S., and Kuczewski, N. (2015). Afterhyperpolarization (AHP) regulates the frequency and timing of action potentials in the mitral cells of the olfactory bulb: role of olfactory experience. Physiological Reports *3*, e12344.

Dunkley, P.R., Bobrovskaya, L., Graham, M.E., Von Nagy-Felsobuki, E.I., and Dickson, P.W. (2004). Tyrosine hydroxylase phosphorylation: regulation and consequences. Journal of Neurochemistry *91*, 1025–1043.

Echegoyen, J., Neu, A., Graber, K.D., and Soltesz, I. (2007). Homeostatic Plasticity Studied Using In Vivo Hippocampal Activity-Blockade: Synaptic Scaling, Intrinsic Plasticity and Age-Dependence. PLoS ONE *2*, e700.

Eckmeier, D., and Shea, S.D. (2014). Noradrenergic plasticity of olfactory sensory neuron inputs to the main olfactory bulb. Journal of Neuroscience *34*, 15234–15243.

Ennis, M., Linster, C., Aroniadou-Anderjaska, V., Ciombor, K., and Shipley, M.T. (1998). Glutamate and synaptic plasticity at mammalian primary olfactory synapses. Annals of the New York Academy of Sciences *855*, 457–466.

Ennis, M., Zhou, F.-M., Ciombor, K.J., Aroniadou-Anderjaska, V., Hayar, A., Borrelli, E., Zimmer, L.A., Margolis, F., and Shipley, M.T. (2001). Dopamine D2 Receptor–Mediated Presynaptic Inhibition of Olfactory Nerve Terminals. Journal of Neurophysiology *86*, 2986–2997.

Escanilla, O., Yuhas, C., Marzan, D., and Linster, C. (2009). Dopaminergic modulation of olfactory bulb processing affects odor discrimination learning in rats. Behavioral Neuroscience *123*, 828–833.

Evans, M.D., Dumitrescu, A.S., Kruijssen, D.L.H., Taylor, S.E., and Grubb, M.S. (2015). Rapid Modulation of Axon Initial Segment Length Influences Repetitive Spike Firing. Cell Reports *13*, 1233–1245.

Eyre, M.D., Antal, M., and Nusser, Z. (2008). Distinct Deep Short-Axon Cell Subtypes of the Main Olfactory Bulb Provide Novel Intrabulbar and Extrabulbar GABAergic Connections. Journal of Neuroscience *28*, 8217–8229.

Faber, E.S.L., Delaney, A.J., and Sah, P. (2005). SK channels regulate excitatory synaptic transmission and plasticity in the lateral amygdala. Nature Neuroscience *8*, 635–641.

Farbman, A.I., Brunjes, P.C., Rentfro, L., Michas, J., and Ritz, S. (1988). The effect of unilateral naris occlusion on cell dynamics in the developing rat olfactory epithelium. Journal of Neuroscience *8*, 3290–3295.

Feigenspan, A., Gustincich, S., Bean, B.P., and Raviola, E. (1998). Spontaneous activity of solitary dopaminergic cells of the retina. Journal of Neuroscience *18*, 6776–6789.

Fiszman, M.L., Zuddas, A., Masana, M.I., Barker, J.L., and di Porzio, U. (1991). Dopamine synthesis precedes dopamine uptake in embryonic rat mesencephalic neurons. Journal of Neurochemistry *56*, 392–399.

Fogli Iseppe, A., Pignatelli, A., and Belluzzi, O. (2016). Calretinin-Periglomerular Interneurons in Mice Olfactory Bulb: Cells of Few Words. Frontiers in Cellular Neuroscience *10*, 231.

Foster, K.A., Kreitzer, A.C., and Regehr, W.G. (2002). Interaction of Postsynaptic Receptor Saturation with Presynaptic Mechanisms Produces a Reliable Synapse. Neuron *36*, 1115–1126.

Fukunaga, I., Berning, M., Kollo, M., Schmaltz, A., and Schaefer, A.T. (2012). Two distinct channels of olfactory bulb output. Neuron *75*, 320–329.

Galliano, E., Franzoni, E., Breton, M., Chand, A.N., Byrne, D.J., Murthy, V.N., and Grubb, M.S. (2018). Embryonic and postnatal neurogenesis produce functionally distinct subclasses of dopaminergic neuron. ELife *7*, e32373.

Gao, Y., and Strowbridge, B.W. (2009). Long-term plasticity of excitatory inputs to granule cells in the rat olfactory bulb. Nature Neuroscience *12*, 731–733.

Geramita, M., and Urban, N.N. (2016). Postnatal Odor Exposure Increases the Strength of Interglomerular Lateral Inhibition onto Olfactory Bulb Tufted Cells. Journal of Neuroscience *36*, 12321–12327.

Geramita, M., and Urban, N.N. (2017). Differences in Glomerular-Layer-Mediated Feedforward Inhibition onto Mitral and Tufted Cells Lead to Distinct Modes of Intensity Coding. Journal of Neuroscience *37*, 1428–1438.

Geramita, M.A., Burton, S.D., and Urban, N.N. (2016). Distinct lateral inhibitory circuits drive parallel processing of sensory information in the mammalian olfactory bulb. ELife *5*, e16039.

Gibson, J.R., Bartley, A.F., and Huber, K.M. (2006). Role for the Subthreshold Currents I_{Leak} and I_{H} in the Homeostatic Control of Excitability in Neocortical Somatostatin-Positive Inhibitory Neurons. Journal of Neurophysiology *96*, 420–432.

Gire, D.H., Franks, K.M., Zak, J.D., Tanaka, K.F., Whitesell, J.D., Mulligan, A.A., Hen, R., and Schoppa, N.E. (2012). Mitral cells in the olfactory bulb are mainly excited through a multistep signaling path. Journal of Neuroscience *32*, 2964–2975.

Giros, B., Jaber, M., Jones, S.R., Wightman, R.M., and Caron, M.G. (1996). Hyperlocomotion and indifference to cocaine and amphetamine in mice lacking the dopamine transporter. Nature *379*, 606–612.

Goel, A., Xu, L.W., Snyder, K.P., Song, L., Goenaga-Vazquez, Y., Megill, A., Takamiya, K., Huganir, R.L., and Lee, H.-K. (2011). Phosphorylation of AMPA Receptors Is Required for Sensory Deprivation-Induced Homeostatic Synaptic Plasticity. PLoS ONE *6*, e18264.

Gómez, C., Briñón, J.G., Colado, M.I., Orio, L., Vidal, M., Barbado, M.V., and Alonso, J.R. (2006). Differential effects of unilateral olfactory deprivation on noradrenergic and cholinergic systems in the main olfactory bulb of the rat. Neuroscience *141*, 2117–2128.

Gómez, C., Briñón, J.G., Orio, L., Colado, M.I., Lawrence, A.J., Zhou, F.C., Vidal, M., Barbado, M. V., and Alonso, J.R. (2007). Changes in the serotonergic system in the main olfactory bulb of rats unilaterally deprived from birth to adulthood. Journal of Neurochemistry *100*, 924–938.

Grace, A.A., and Bunney, B.S. (1983). Intracellular and extracellular electrophysiology of nigral dopaminergic neurons—1. Identification and characterization. Neuroscience *10*, 301–315.

Grace, A.A., and Onn, S.P. (1989). Morphology and electrophysiological properties of immunocytochemically identified rat dopamine neurons recorded in vitro. Journal of Neuroscience *9*, 3463–3481.

Gracia-Llanes, F.J., Crespo, C., Blasco-Ibáñez, J.M., Nacher, J., Varea, E., Rovira-Esteban, L., and Martínez-Guijarro, F.J. (2010). GABAergic basal forebrain afferents innervate selectively GABAergic targets in the main olfactory bulb. Neuroscience *170*, 913–922.

Greer, C.A. (1987). Golgi analyses of dendritic organization among denervated olfactory bulb granule cells. The Journal of Comparative Neurology *257*, 442–452.

Grier, B.D., Belluscio, L., and Cheetham, C.E.J. (2016). Olfactory Sensory Activity Modulates Microglial-Neuronal Interactions during Dopaminergic Cell Loss in the Olfactory Bulb. Frontiers in Cellular Neuroscience *10*, 178.

Grosmaitre, X., Santarelli, L.C., Tan, J., Luo, M., and Ma, M. (2007). Dual functions of mammalian olfactory sensory neurons as odor detectors and mechanical sensors. Nature Neuroscience *10*, 348–354.

Grubb, M.S., and Burrone, J. (2010). Activity-dependent relocation of the axon initial segment fine-tunes neuronal excitability. Nature *465*, 1070–1074.

Grubb, M.S., Nissant, A., Murray, K., and Lledo, P.-M. (2008). Functional Maturation of the First Synapse in Olfaction: Development and Adult Neurogenesis. Journal of Neuroscience *28*, 2919–2932.

Gschwend, O., Abraham, N.M., Lagier, S., Begnaud, F., Rodriguez, I., and Carleton, A. (2015). Neuronal pattern separation in the olfactory bulb improves odor discrimination learning. Nature Neuroscience *18*, 1474–1482.

Gu, N., Vervaeke, K., Hu, H., and Storm, J.F. (2005). Kv7/KCNQ/M and HCN/h, but not KCa2/SK channels, contribute to the somatic medium after-hyperpolarization and excitability control in CA1 hippocampal pyramidal cells. The Journal of Physiology *566*, 689–715.

Guan, D., Armstrong, W.E., and Foehring, R.C. (2015). Electrophysiological properties of genetically identified subtypes of layer 5 neocortical pyramidal neurons: Ca^{2+} dependence and differential modulation by norepinephrine. Journal of Neurophysiology *113*, 2014–2032.

Guthrie, K.M., Pullara, J.M., Marshall, J.F., and Leon, M. (1991). Olfactory deprivation increases dopamine D2 receptor density in the rat olfactory bulb. Synapse *8*, 61–70.

Gutièrrez-Mecinas, M., Crespo, C., Blasco-Ibáñez, J.M., Gracia-Llanes, F.J., Marqués-Marí, A.I., Nácher, J., Varea, E., and Martínez-Guijarro, F.J. (2005). Distribution of D2 dopamine receptor in the olfactory glomeruli of the rat olfactory bulb. European Journal of Neuroscience *22*, 1357–1367.

Habecker, B.A., Klein, M.G., Sundgren, N.C., Li, W., and Woodward, W.R. (2002). Developmental regulation of neurotransmitter phenotype through tetrahydrobiopterin. Journal of Neuroscience *22*, 9445–9452.

Hack, M.A., Saghatelyan, A., de Chevigny, A., Pfeifer, A., Ashery-Padan, R., Lledo, P.-M., and Götz, M. (2005). Neuronal fate determinants of adult olfactory bulb neurogenesis. Nature Neuroscience *8*, 865–872.

Hadjiconstantinou, M., Wemlinger, T.A., Sylvia, C.P., Hubble, J.P., and Neff, N.H. (1993). Aromatic L-amino acid decarboxylase activity of mouse striatum is modulated via dopamine receptors. Journal of Neurochemistry *60*, 2175–2180.

Hainsworth, A.H., Röper, J., Kapoor, R., and Ashcroft, F.M. (1991). Identification and electrophysiology of isolated pars compacta neurons from guinea-pig substantia nigra. Neuroscience *43*, 81–93.

Halász, N., Johansson, O., Hökfelt, T., Ljungdahl, A., and Goldstein, M. (1981). Immunohistochemical identification of two types of dopamine neuron in the rat olfactory bulb as seen by serial sectioning. Journal of Neurocytology *10*, 251–259.

Halliwell, J. V, and Adams, P.R. (1982). Voltage-clamp analysis of muscarinic excitation in hippocampal neurons. Brain Research *250*, 71–92.

Han, E.B., and Stevens, C.F. (2009). Development regulates a switch between post- and presynaptic strengthening in response to activity deprivation. Proceedings of the National Academy of Sciences *106*, 10817–10822.

Van Harreveld, A., and Fifkova, E. (1975). Swelling of dendritic spines in the fascia dentata after stimulation of the perforant fibers as a mechanism of post-tetanic potentiation. Experimental Neurology *49*, 736–749.

Hartman, K.N., Pal, S.K., Burrone, J., and Murthy, V.N. (2006). Activity-dependent regulation of inhibitory synaptic transmission in hippocampal neurons. Nature Neuroscience *9*, 642–649.

Haug, T., and Storm, J.F. (2000). Protein Kinase A Mediates the Modulation of the Slow Ca^{2+}-Dependent K^{+} Current, I_{sAHP}, by the Neuropeptides CRF, VIP, and CGRP in Hippocampal Pyramidal Neurons. Journal of Neurophysiology *83*, 2071–2079.

Hayar, A., Karnup, S., Shipley, M.T., and Ennis, M. (2004a). Olfactory Bulb Glomeruli: External Tufted Cells Intrinsically Burst at Theta Frequency and Are Entrained by Patterned Olfactory Input. Journal of Neuroscience *24*, 1190–1199.

Hayar, A., Karnup, S., Ennis, M., and Shipley, M.T. (2004b). External tufted cells: a major excitatory element that coordinates glomerular activity. Journal of Neuroscience *24*, 6676–6685.

Hayar, A., Shipley, M.T., and Ennis, M. (2005). Olfactory bulb external tufted cells are synchronized by multiple intraglomerular mechanisms. Journal of Neuroscience *25*, 8197–8208.

He, J., Tian, H., Lee, A.C., and Ma, M. (2012). Postnatal experience modulates functional properties of mouse olfactory sensory neurons. European Journal of Neuroscience *36*, 2452–2460.

Hebb, D.O. (1949). The Organization of Behavior; A Neuropsychological Theory (New York: Wiley).

Hengen, K.B., Lambo, M.E., Van Hooser, S.D., Katz, D.B., and Turrigiano, G.G. (2013). Firing rate homeostasis in visual cortex of freely behaving rodents. Neuron *80*, 335–342.

Hengen, K.B., Torrado Pacheco, A., McGregor, J.N., Van Hooser, S.D., and Turrigiano, G.G. (2016). Neuronal Firing Rate Homeostasis Is Inhibited by Sleep and Promoted by Wake. Cell *165*, 180–191.

Hinds, J.W. (1968). Autoradiographic study of histogenesis in the mouse olfactory bulb I. Time of origin of neurons and neuroglia. The Journal of Comparative Neurology *134*, 287–304.

Hirasawa, H., Betensky, R.A., and Raviola, E. (2012). Corelease of dopamine and GABA by a retinal dopaminergic neuron. Journal of Neuroscience *32*, 13281–13291.

Holl, A.-M. (2018). Survival of mature mouse olfactory sensory neurons labeled genetically perinatally.

Molecular and Cellular Neuroscience *88*, 258–269.

Honnuraiah, S., and Narayanan, R. (2013). A Calcium-Dependent Plasticity Rule for HCN Channels Maintains Activity Homeostasis and Stable Synaptic Learning. PLoS ONE *8*, e55590.

Hsia, A.Y., Vincent, J.-D., and Lledo, P.-M. (1999). Dopamine Depresses Synaptic Inputs Into the Olfactory Bulb. Journal of Neurophysiology *82*, 1082–1085.

Hu, H., Vervaeke, K., and Storm, J.F. (2002). Two forms of electrical resonance at theta frequencies, generated by M-current, h-current and persistent Na^+ current in rat hippocampal pyramidal cells. The Journal of Physiology *545*, 783–805.

Huang, L., Ung, K., Garcia, I., Quast, K.B., Cordiner, K., Saggau, P., and Arenkiel, B.R. (2016). Task Learning Promotes Plasticity of Interneuron Connectivity Maps in the Olfactory Bulb. Journal of Neuroscience *36*, 8856–8871.

Huang, Z., Walker, M.C., and Shah, M.M. (2009). Loss of dendritic HCN1 subunits enhances cortical excitability and epileptogenesis. Journal of Neuroscience *29*, 10979–10988.

Huisman, E., Uylings, H.B.M., and Hoogland, P. V. (2004). A 100% increase of dopaminergic cells in the olfactory bulb may explain hyposmia in Parkinson's disease. Movement Disorders *19*, 687–692.

Huisman, E., Uylings, H.B.M., and Hoogland, P. V. (2008). Gender-related changes in increase of dopaminergic neurons in the olfactory bulb of Parkinson's disease patients. Movement Disorders *23*, 1407–1413.

Hyun, J.H., Eom, K., Lee, K.-H., Ho, W.-K., and Lee, S.-H. (2013). Activity-dependent downregulation of D-type K^+ channel subunit Kv1.2 in rat hippocampal CA3 pyramidal neurons. The Journal of Physiology *591*, 5525–5540.

Imayoshi, I., Sakamoto, M., Ohtsuka, T., Takao, K., Miyakawa, T., Yamaguchi, M., Mori, K., Ikeda, T., Itohara, S., and Kageyama, R. (2008). Roles of continuous neurogenesis in the structural and functional integrity of the adult forebrain. Nature Neuroscience *11*, 1153–1161.

Inoue, T., Ota, M., Ogawa, M., Mikoshiba, K., and Aruga, J. (2007). Zic1 and Zic3 Regulate Medial Forebrain Development through Expansion of Neuronal Progenitors. Journal of Neuroscience *27*, 5461–5473.

Iravani, M.M., Muscat, R., and Kruk, Z.L. (1996). Comparison of somatodendritic and axon terminal dopamine release in the ventral tegmental area and the nucleus accumbens. Neuroscience *70*, 1025–1037.

Isaacson, J.S., and Strowbridge, B.W. (1998). Olfactory reciprocal synapses: dendritic signaling in the CNS. Neuron *20*, 749–761.

Ito, M., and Kano, M. (1982). Long-lasting depression of parallel fiber-Purkinje cell transmission induced by conjunctive stimulation of parallel fibers and climbing fibers in the cerebellar cortex. Neuroscience Letters *33*, 253–258.

Jaffe, E.H., Marty, A., Schulte, A., and Chow, R.H. (1998). Extrasynaptic vesicular transmitter release from the somata of substantia nigra neurons in rat midbrain slices. Journal of Neuroscience *18*, 3548–3553.

Jensen, T.P., Zheng, K., Tyurikova, O., Reynolds, J.P., and Rusakov, D.A. (2017). Monitoring single-synapse glutamate release and presynaptic calcium concentration in organised brain tissue. Cell Calcium *64*, 102–108.

Jin, B.K., Franzen, L., and Baker, H. (1996). Regulation of c-Fos mRNA and fos protein expression in olfactory bulbs from unilaterally odor-deprived adult mice. International Journal of Developmental Neuroscience *14*, 971–982.

Jones, S.L., To, M.-S., and Stuart, G.J. (2017). Dendritic small conductance calcium-activated potassium channels activated by action potentials suppress EPSPs and gate spike-timing dependent synaptic plasticity. ELife *6*, e30333.

Kaneko, H., Putzier, I., Frings, S., Kaupp, U.B., and Gensch, T. (2004). Chloride Accumulation in Mammalian Olfactory Sensory Neurons. Journal of Neuroscience *24*, 7931–7938.

Karmarkar, U.R., and Buonomano, D. V. (2006). Different forms of homeostatic plasticity are engaged with distinct temporal profiles. European Journal of Neuroscience *23*, 1575–1584.

Kasowski, H.J., Kim, H., and Greer, C.A. (1999). Compartmental organization of the olfactory bulb glomerulus. The Journal of Comparative Neurology *407*, 261–274.

Kass, M.D., Pottackal, J., Turkel, D.J., and McGann, J.P. (2013). Changes in the neural representation of odorants after olfactory deprivation in the adult mouse olfactory bulb. Chemical Senses *38*, 77–89.

Kass, M.D., Guang, S.A., Moberly, A.H., and McGann, J.P. (2015). Changes in Olfactory Sensory Neuron Physiology and Olfactory Perceptual Learning After Odorant Exposure in Adult Mice. Chemical Senses *41*, 123–133.

Kato, Y., Kaneko, N., Sawada, M., Ito, K., Arakawa, S., Murakami, S., and Sawamoto, K. (2012). A Subtype-Specific Critical Period for Neurogenesis in the Postnatal Development of Mouse Olfactory Glomeruli. PLoS ONE *7*, e48431.

Katz, B., and Miledi, R. (1968). The role of calcium in neuromuscular facilitation. The Journal of Physiology *195*, 481–492.

Kawano, T., and Margolis, F.L. (1982). Transsynaptic regulation of olfactory bulb catecholamines in mice and rats. Journal of Neurochemistry *39*, 342–348.

Kay, L.M., and Sherman, S.M. (2007). An argument for an olfactory thalamus. Trends in Neurosciences *30*, 47–53.

Kay, L.M., Beshel, J., Brea, J., Martin, C., Rojas-Líbano, D., and Kopell, N. (2009). Olfactory oscillations: the what, how and what for. Trends in Neurosciences *32*, 207–214.

Keck, T., Scheuss, V., Jacobsen, R.I., Wierenga, C.J., Eysel, U.T., Bonhoeffer, T., and Hübener, M. (2011). Loss of Sensory Input Causes Rapid Structural Changes of Inhibitory Neurons in Adult Mouse Visual Cortex. Neuron *71*, 869–882.

Keck, T., Keller, G.B., Jacobsen, R.I., Eysel, U.T., Bonhoeffer, T., and Hü Bener, M. (2013). Synaptic Scaling and Homeostatic Plasticity in the Mouse Visual Cortex In Vivo. Neuron *80*, 327–334.

Kelsch, W., Mosley, C.P., Lin, C.-W., and Lois, C. (2007). Distinct Mammalian Precursors Are Committed to Generate Neurons with Defined Dendritic Projection Patterns. PLoS Biology *5*, e300.

Kelsch, W., Lin, C.-W., Mosley, C.P., and Lois, C. (2009). A critical period for activity-dependent synaptic development during olfactory bulb adult neurogenesis. Journal of Neuroscience *29*, 11852–11858.

Kilman, V., van Rossum, M.C.W., and Turrigiano, G.G. (2002). Activity deprivation reduces miniature IPSC amplitude by decreasing the number of postsynaptic GABA(A) receptors clustered at neocortical synapses. Journal of Neuroscience *22*, 1328–1337.

Kim, J., and Alger, B.E. (2010). Reduction in endocannabinoid tone is a homeostatic mechanism for specific inhibitory synapses. Nature Neuroscience *13*, 592–600.

Kim, J., Tsien, R.W., and Alger, B.E. (2012). An Improved Test for Detecting Multiplicative Homeostatic Synaptic Scaling. PLoS ONE *7*, e37364.

Kimm, T., Khaliq, Z.M., and Bean, B.P. (2015). Differential Regulation of Action Potential Shape and Burst-Frequency Firing by BK and Kv2 Channels in Substantia Nigra Dopaminergic Neurons. Journal of Neuroscience *35*, 16404–16417.

King, B., Rizwan, A.P., Asmara, H., Heath, N.C., Engbers, J.D.T., Dykstra, S., Bartoletti, T.M., Hameed, S., Zamponi, G.W., and Turner, R.W. (2015). IKCa Channels Are a Critical Determinant of the Slow AHP in CA1 Pyramidal Neurons. Cell Reports *11*, 175–182.

Kisfali, M., Lőrincz, T., and Vizi, E.S. (2013). Comparison of Ca^{2+} transients and $[Ca^{2+}]_i$ in the dendrites and boutons of non-fast-spiking GABAergic hippocampal interneurons using two-photon laser microscopy and high- and low-affinity dyes. The Journal of Physiology *591*, 5541–5553.

Kiyokage, E., Pan, Y.-Z., Shao, Z., Kobayashi, K., Szabo, G., Yanagawa, Y., Obata, K., Okano, H., Toida, K., Puche, A.C., et al. (2010). Molecular Identity of Periglomerular and Short Axon Cells. Journal of Neuroscience *30*, 1185–1196.

Kiyokage, E., Kobayashi, K., and Toida, K. (2017). Spatial distribution of synapses on tyrosine hydroxylase-expressing juxtaglomerular cells in the mouse olfactory glomerulus. Journal of Comparative Neurology *525*, 1059–1074.

Kosaka, K., and Kosaka, T. (2007). Chemical properties of type 1 and type 2 periglomerular cells in the mouse olfactory bulb are different from those in the rat olfactory bulb. Brain Research *1167*, 42–55.

Kosaka, T., and Kosaka, K. (2005). Intraglomerular dendritic link connected by gap junctions and chemical synapses in the mouse main olfactory bulb: Electron microscopic serial section analyses. Neuroscience *131*, 611–625.

Kosaka, T., and Kosaka, K. (2008). Tyrosine hydroxylase-positive GABAergic juxtaglomerular neurons are the main source of the interglomerular connections in the mouse main olfactory bulb. Neuroscience Research *60*, 349–354.

Kosaka, T., and Kosaka, K. (2009). Two types of tyrosine hydroxylase positive GABAergic juxtaglomerular neurons in the mouse main olfactory bulb are different in their time of origin. Neuroscience Research *64*, 436–441.

Kosaka, K., Aika, Y., Toida, K., Heizmann, C.W., Hunziker, W., Jacobowitz, D.M., Nagatsu, I., Streit, P., Visser, T.J., and Kosaka, T. (1995). Chemically defined neuron groups and their subpopulations in the glomerular layer of the rat main olfactory bulb. Neuroscience Research *23*, 73–88.

Kosaka, K., Toida, K., Margolis, F.L., and Kosaka, T. (1997). Chemically defined neuron groups and their subpopulations in the glomerular layer of the rat main olfactory bulb--II. Prominent differences in the intraglomerular dendritic arborization and their relationship to olfactory nerve terminals. Neuroscience *76*, 775–786.

Kosaka, T., Hataguchi, Y., Hama, K., Nagatsu, I., and WU, J.Y. (1985). Coexistence of immunoreactivities for glutamate decarboxylase and tyrosine hydroxylase in some neurons in the periglomerular region of the rat main olfactory bulb: possible coexistence of gamma-aminobutyric acid (GABA) and dopamine. Brain Research *343*, 166–171.

Kosaka, T., Kosaka, K., Hama, K., Wu, J.-Y., and Nagatsu, I. (1987). Differential effect of functional olfactory deprivation on the GABAergic and catecholaminergic traits in the rat main olfactory bulb. Brain Research *413*, 197–203.

Kosaka, T., Deans, M.R., Paul, D.L., and Kosaka, K. (2005). Neuronal gap junctions in the mouse main olfactory bulb: Morphological analyses on transgenic mice. Neuroscience *134*, 757–769.

Kosaka, T., Komada, M., and Kosaka, K. (2008). Sodium channel cluster, βIV-spectrin and ankyrinG positive “hot spots” on dendritic segments of parvalbumin-containing neurons and some other neurons in the mouse and rat main olfactory bulbs. Neuroscience Research *62*, 176–186.

Kraushaar, U., and Jonas, P. (2000). Efficacy and stability of quantal GABA release at a hippocampal interneuron-principal neuron synapse. Journal of Neuroscience *20*, 5594–5607.

Kruzich, P.J., and Grandy, D.K. (2004). Dopamine D2 receptors mediate two-odor discrimination and reversal learning in C57BL/6 mice. BMC Neuroscience *5*, 12.

Kuba, H., Oichi, Y., and Ohmori, H. (2010). Presynaptic activity regulates Na+ channel distribution at the axon initial segment. Nature *465*, 1075–1078.

Kuba, H., Yamada, R., Ishiguro, G., and Adachi, R. (2015). Redistribution of Kv1 and Kv7 enhances neuronal excitability during structural axon initial segment plasticity. Nature Communications *6*, 8815.

Kuhlman, S.J., Olivas, N.D., Tring, E., Ikrar, T., Xu, X., and Trachtenberg, J.T. (2013). A disinhibitory microcircuit initiates critical-period plasticity in the visual cortex. Nature *501*, 543–546.

Laaris, N., Puche, A., and Ennis, M. (2007). Complementary postsynaptic activity patterns elicited in olfactory bulb by stimulation of mitral/tufted and centrifugal fiber inputs to granule cells. Journal of Neurophysiology *97*, 296–306.

Lammel, S., Steinberg, E.E., Földy, C., Wall, N.R., Beier, K., Luo, L., and Malenka, R.C. (2015). Diversity of Transgenic Mouse Models for Selective Targeting of Midbrain Dopamine Neurons. Neuron *85*, 429–438.

Lau, C.G., and Murthy, V.N. (2012). Activity-Dependent Regulation of Inhibition via GAD67. Journal of Neuroscience *32*, 8521–8531.

Lazarini, F., Gabellec, M.-M., Moigneu, C., de Chaumont, F., Olivo-Marin, J.-C., and Lledo, P.-M. (2014).

Adult Neurogenesis Restores Dopaminergic Neuronal Loss in the Olfactory Bulb. Journal of Neuroscience *34*, 14430–14442.

Lepousez, G., Nissant, A., Bryant, A.K., Gheusi, G., Greer, C.A., and Lledo, P.-M. (2014). Olfactory learning promotes input-specific synaptic plasticity in adult-born neurons. Proceedings of the National Academy of Sciences *111*, 13984–13989.

Levy, W.B., and Steward, O. (1983). Temporal contiguity requirements for long-term associative potentiation/depression in the hippocampus. Neuroscience *8*, 791–797.

Lewis, A.S., Schwartz, E., Chan, C.S., Noam, Y., Shin, M., Wadman, W.J., Surmeier, D.J., Baram, T.Z., Macdonald, R.L., and Chetkovich, D.M. (2009). Alternatively spliced isoforms of TRIP8b differentially control h channel trafficking and function. Journal of Neuroscience *29*, 6250–6265.

Li, C., Lu, Q., Huang, P., Fu, T., Li, C., Guo, L., and Xu, X. (2015). Activity-dependent downregulation of M-Type (Kv7) K+ channels surface expression requires the activation of iGluRs/Ca2+/PKC signaling pathway in hippocampal neuron. Neuropharmacology *95*, 154–167.

Li, P., Rudolph, U., and Huntsman, M.M. (2009). Long-term sensory deprivation selectively rearranges functional inhibitory circuits in mouse barrel cortex. Proceedings of the National Academy of Sciences *106*, 12156–12161.

Liberia, T., Blasco-Ibáñez, J.M., Nácher, J., Varea, E., Zwafink, V., and Crespo, C. (2012). Characterization of a population of tyrosine hydroxylase-containing interneurons in the external plexiform layer of the rat olfactory bulb. Neuroscience *217*, 140–153.

Linster, C., Nai, Q., and Ennis, M. (2011). Nonlinear effects of noradrenergic modulation of olfactory bulb function in adult rodents. Journal of Neurophysiology *105*, 1432–1443.

Liu, W.-L., and Shipley, M.T. (1994). Intrabulbar associational system in the rat olfactory bulb comprises cholecystokinin-containing tufted cells that synapse onto the dendrites of GABAergic granule cells. The Journal of Comparative Neurology *346*, 541–558.

Liu, S., Plachez, C., Shao, Z., Puche, A., and Shipley, M.T. (2013). Olfactory bulb short axon cell release of GABA and dopamine produces a temporally biphasic inhibition-excitation response in external tufted cells. Journal of Neuroscience *33*, 2916–2926.

Liu, S., Puche, A.C., and Shipley, M.T. (2016). The Interglomerular Circuit Potently Inhibits Olfactory Bulb Output Neurons by Both Direct and Indirect Pathways. Journal of Neuroscience *36*, 9604–9617.

Livneh, Y., and Mizrahi, A. (2011). Long-term changes in the morphology and synaptic distributions of adult-born neurons. The Journal of Comparative Neurology *519*, 2212–2224.

Livneh, Y., Adam, Y., and Mizrahi, A. (2014). Odor Processing by Adult-Born Neurons. Neuron *81*, 1097–1110.

Lledo, P.-M., Alonso, M., and Grubb, M.S. (2006). Adult neurogenesis and functional plasticity in neuronal circuits. Nature Reviews Neuroscience *7*, 179–193.

Lodovichi, C., Belluscio, L., and Katz, L.C. (2003). Functional Topography of Connections Linking Mirror-Symmetric Maps in the Mouse Olfactory Bulb. Neuron *38*, 265–276.

Looger, L.L., Marvin, J.S., Shimoda, Y., Magloire, V., Leite, M., Kawashima, T., Jensen, T.P., Knott, E.L., Novak, O., Podgorski, K., et al. (2018). A genetically encoded fluorescent sensor for in vivo imaging of GABA. BioRxiv 322578.

Ludwig, A., Zong, X., Jeglitsch, M., Hofmann, F., and Biel, M. (1998). A family of hyperpolarization-activated mammalian cation channels. Nature *393*, 587–591.

Luo, R., Partridge, J.G., and Vicini, S. (2013). Distinct roles of synaptic and extrasynaptic GABAAreceptors in striatal inhibition dynamics. Frontiers in Neural Circuits *7*, 186.

Luskin, M.B. (1993). Restricted proliferation and migration of postnatally generated neurons derived from the forebrain subventricular zone. Neuron *11*, 173–189.

Lyons, D.B., Allen, W.E., Goh, T., Tsai, L., Barnea, G., and Lomvardas, S. (2013). An epigenetic trap stabilizes singular olfactory receptor expression. Cell *154*, 325–336.

Ma, L., Qiu, Q., Gradwohl, S., Scott, A., Yu, E.Q., Alexander, R., Wiegraebe, W., and Yu, C.R. (2012a).

Distributed representation of chemical features and tunotopic organization of glomeruli in the mouse olfactory bulb. Proceedings of the National Academy of Sciences *109*, 5481–5486.

Ma, T.-F., Zhao, X.-L., Cai, L., Zhang, N., Ren, S.-Q., Ji, F., Tian, T., and Lu, W. (2012b). Regulation of Spike Timing-Dependent Plasticity of Olfactory Inputs in Mitral Cells in the Rat Olfactory Bulb. PLoS ONE *7*, e35001.

Maffei, A., and Turrigiano, G.G. (2008). Multiple modes of network homeostasis in visual cortical layer 2/3. Journal of Neuroscience *28*, 4377–4384.

Maffei, A., Nelson, S.B., and Turrigiano, G.G. (2004). Selective reconfiguration of layer 4 visual cortical circuitry by visual deprivation. Nature Neuroscience *7*, 1353–1359.

Magavi, S.S.P., Mitchell, B.D., Szentirmai, O., Carter, B.S., and Macklis, J.D. (2005). Adult-born and preexisting olfactory granule neurons undergo distinct experience-dependent modifications of their olfactory responses in vivo. Journal of Neuroscience *25*, 10729–10739.

Magee, J.C. (1998). Dendritic hyperpolarization-activated currents modify the integrative properties of hippocampal CA1 pyramidal neurons. Journal of Neuroscience *18*, 7613–7624.

Magee, J.C. (1999). Erratum: Dendritic Ih normalizes temporal summation in hippocampal CA1 neurons. Nature Neuroscience *2*, 848–848.

Maher, B.J., and Westbrook, G.L. (2008). Co-Transmission of Dopamine and GABA in Periglomerular Cells. Journal of Neurophysiology *99*, 1559–1564.

Malnic, B., Hirono, J., Sato, T., and Buck, L.B. (1999). Combinatorial receptor codes for odors. Cell *96*, 713–723.

Mandairon, N., Jourdan, F., and Didier, A. (2003). Deprivation of sensory inputs to the olfactory bulb up-regulates cell death and proliferation in the subventricular zone of adult mice. Neuroscience *119*, 507–516.

Margrie, T.W., Sakmann, B., and Urban, N.N. (2001). Action potential propagation in mitral cell lateral dendrites is decremental and controls recurrent and lateral inhibition in the mammalian olfactory bulb. Proceedings of the National Academy of Sciences *98*, 319–324.

Markram, H., Lübke, J., Frotscher, M., and Sakmann, B. (1997). Regulation of synaptic efficacy by coincidence of postsynaptic APs and EPSPs. Science *275*, 213–215.

Marks, C.A., Cheng, K., Cummings, D.M., and Belluscio, L. (2006). Activity-Dependent Plasticity in the Olfactory Intrabulbar Map. Journal of Neuroscience *26*, 11257–11266.

Maruniak, J.A., Lin, P.J., and Henegar, J.R. (1989). Effects of unilateral naris closure on the olfactory epithelia of adult mice. Brain Research *490*, 212–218.

Maruniak, J.A., Henegar, J.R., and Sweeney, T.P. (1990). Effects of long-term unilateral naris closure on the olfactory epithelia of adult mice. Brain Research *526*, 65–72.

Matiašová, A., Ševc, J., Mikeš, J., Jendželovský, R., Daxnerová, Z., and Fedoročko, P. (2014). Flow cytometric determination of 5-bromo-2'-deoxyuridine pharmacokinetics in blood serum after intraperitoneal administration to rats and mice. Histochemistry and Cell Biology *142*, 703–712.

Matsuzaki, M., Ellis-Davies, G.C., Nemoto, T., Miyashita, Y., Iino, M., and Kasai, H. (2001). Dendritic spine geometry is critical for AMPA receptor expression in hippocampal CA1 pyramidal neurons. Nature Neuroscience *4*, 1086–1092.

Matthews, E.A., Weible, A.P., Shah, S., and Disterhoft, J.F. (2008). The BK-mediated fAHP is modulated by learning a hippocampus-dependent task. Proceedings of the National Academy of Sciences *105*, 15154–15159.

McClelland, S., Flynn, C., Dubé, C., Richichi, C., Zha, Q., Ghestem, A., Esclapez, M., Bernard, C., and Baram, T.Z. (2011). Neuron-restrictive silencer factor-mediated hyperpolarization-activated cyclic nucleotide gated channelopathy in experimental temporal lobe epilepsy. Annals of Neurology *70*, 454–465.

McGann, J.P., Pírez, N., Gainey, M.A., Muratore, C., Elias, A.S., and Wachowiak, M. (2005). Odorant Representations Are Modulated by Intra- but Not Interglomerular Presynaptic Inhibition of Olfactory Sensory Neurons. Neuron *48*, 1039–1053.

McLean, J.H., and Shipley, M.T. (1988). Postmitotic, postmigrational expression of tyrosine hydroxylase in olfactory bulb dopaminergic neurons. Journal of Neuroscience *8*, 3658–3669.

Mitsumoto, Y., Mori, A., Ohashi, S., Nakai, M., and Moriizumi, T. (2005). Differential effects of 1-methyl-4-phenyl-1,2,3,6-tetrahydropyridine in the olfactory bulb and the striatum in mice. Neuroscience Research *51*, 111–115.

Mizrahi, A. (2007). Dendritic development and plasticity of adult-born neurons in the mouse olfactory bulb. Nature Neuroscience *10*, 444–452.

Mizrahi, A., Lu, J., Irving, R., Feng, G., and Katz, L.C. (2006). In vivo imaging of juxtaglomerular neuron turnover in the mouse olfactory bulb. Proceedings of the National Academy of Sciences *103*, 1912–1917.

Mombaerts, P., Wang, F., Dulac, C., Chao, S.K., Nemes, A., Mendelsohn, M., Edmondson, J., and Axel, R. (1996). Visualizing an Olfactory Sensory Map. Cell *87*, 675–686.

Moreno, M.M., Linster, C., Escanilla, O., Sacquet, J., Didier, A., and Mandairon, N. (2009). Olfactory perceptual learning requires adult neurogenesis. Proceedings of the National Academy of Sciences *106*, 17980–17985.

Mori, K., Takahashi, Y.K., Igarashi, K.M., and Yamaguchi, M. (2006). Maps of Odorant Molecular Features in the Mammalian Olfactory Bulb. Physiological Reviews *86*, 409–433.

Morón, J.A., Brockington, A., Wise, R.A., Rocha, B.A., and Hope, B.T. (2002). Dopamine uptake through the norepinephrine transporter in brain regions with low levels of the dopamine transporter: evidence from knock-out mouse lines. Journal of Neuroscience *22*, 389–395.

Motanis, H., Maroun, M., and Barkai, E. (2014). Learning-Induced Bidirectional Plasticity of Intrinsic Neuronal Excitability Reflects the Valence of the Outcome. Cerebral Cortex *24*, 1075–1087.

Mundiñano, I.-C., Caballero, M.-C., Ordóñez, C., Hernandez, M., DiCaudo, C., Marcilla, I., Erro, M.-E., Tuñon, M.-T., and Luquin, M.-R. (2011). Increased dopaminergic cells and protein aggregates in the olfactory bulb of patients with neurodegenerative disorders. Acta Neuropathologica *122*, 61–74.

Murphy, G.J., Glickfeld, L.L., Balsen, Z., and Isaacson, J.S. (2004). Sensory neuron signaling to the brain: properties of transmitter release from olfactory nerve terminals. Journal of Neuroscience *24*, 3023–3030.

Murphy, G.J., Darcy, D.P., and Isaacson, J.S. (2005). Intraglomerular inhibition: signaling mechanisms of an olfactory microcircuit. Nature Neuroscience *8*, 354–364.

Mutoh, H., Yuan, Q., and Knöpfel, T. (2005). Long-term depression at olfactory nerve synapses. Journal of Neuroscience *25*, 4252–4259.

Nadi, N.S., Head, R., Grillo, M., Hempstead, J., Grannot-Reisfeld, N., and Margolis, F.L. (1981). Chemical deafferentation of the olfactory bulb: plasticity of the levels of tyrosine hydroxylase, dopamine and norepinephrine. Brain Research *213*, 365–377.

Nagayama, S., Takahashi, Y.K., Yoshihara, Y., and Mori, K. (2004). Mitral and Tufted Cells Differ in the Decoding Manner of Odor Maps in the Rat Olfactory Bulb. Journal of Neurophysiology *91*, 2532–2540.

Najac, M., De Saint Jan, D., Reguero, L., Grandes, P., and Charpak, S. (2011). Monosynaptic and Polysynaptic Feed-Forward Inputs to Mitral Cells from Olfactory Sensory Neurons. Journal of Neuroscience *31*, 8722–8729.

Najac, M., Sanz Diez, A., Kumar, A., Benito, N., Charpak, S., and De Saint Jan, D. (2015). Intraglomerular Lateral Inhibition Promotes Spike Timing Variability in Principal Neurons of the Olfactory Bulb. Journal of Neuroscience *35*, 4319–4331.

Nakamura, T., and Gold, G.H. (1987). A cyclic nucleotide-gated conductance in olfactory receptor cilia. Nature *325*, 442–444.

Nataraj, K., Le Roux, N., Nahmani, M., Lefort, S., and Turrigiano, G. (2010). Visual Deprivation Suppresses L5 Pyramidal Neuron Excitability by Preventing the Induction of Intrinsic Plasticity. Neuron *68*, 750–762.

Negus, V. (1959). Comparative Anatomy and Physiology of the Nose and Paranasal Sinuses. Postgraduate

Medical Journal *35*, 364–364.

Neuhoff, H., Neu, A., Liss, B., and Roeper, J. (2002). I(h) channels contribute to the different functional properties of identified dopaminergic subpopulations in the midbrain. Journal of Neuroscience *22*, 1290–1302.

Ngo-Anh, T.J., Bloodgood, B.L., Lin, M., Sabatini, B.L., Maylie, J., and Adelman, J.P. (2005). SK channels and NMDA receptors form a Ca2+-mediated feedback loop in dendritic spines. Nature Neuroscience *8*, 642–649.

Nicoll, R.A., and Jahr, C.E. (1982). Self-excitation of olfactory bulb neurones. Nature *296*, 441–444.

Ninkovic, J., Mori, T., and Götz, M. (2007). Distinct modes of neuron addition in adult mouse neurogenesis. Journal of Neuroscience *27*, 10906–10911.

Ninkovic, J., Pinto, L., Petricca, S., Lepier, A., Sun, J., Rieger, M.A., Schroeder, T., Cvekl, A., Favor, J., and Götz, M. (2010). The Transcription Factor Pax6 Regulates Survival of Dopaminergic Olfactory Bulb Neurons via Crystallin αA. Neuron *68*, 682–694.

Nissant, A., Bardy, C., Katagiri, H., Murray, K., and Lledo, P.-M. (2009). Adult neurogenesis promotes synaptic plasticity in the olfactory bulb. Nature Neuroscience *12*, 728–730.

Nusser, Z. (2002). Release-independent short-term facilitation at GABAergic synapses in the olfactory bulb. Neuropharmacology *43*, 573–583.

O'Leary, T., van Rossum, M.C.W., and Wyllie, D.J.A. (2010). Homeostasis of intrinsic excitability in hippocampal neurones: dynamics and mechanism of the response to chronic depolarization. The Journal of Physiology *588*, 157–170.

Oh (2010). Learning and aging related changes in intrinsic neuronal excitability. Frontiers in Aging Neuroscience *2*, 2.

Padmanabhan, K., and Urban, N.N. (2010). Intrinsic biophysical diversity decorrelates neuronal firing while increasing information content. Nature Neuroscience *13*, 1276–1282.

Panzanelli, P., Fritschy, J.M., Yanagawa, Y., Obata, K., and Sassoè-Pognetto, M. (2007). GABAergic phenotype of periglomerular cells in the rodent olfactory bulb. The Journal of Comparative Neurology *502*, 990–1002.

De Paola, V., Holtmaat, A., Knott, G., Song, S., Wilbrecht, L., Caroni, P., and Svoboda, K. (2006). Cell Type-Specific Structural Plasticity of Axonal Branches and Boutons in the Adult Neocortex. Neuron *49*, 861–875.

Parrish-Aungst, S., Shipley, M.T., Erdelyi, F., Szabo, G., and Puche, A.C. (2007). Quantitative analysis of neuronal diversity in the mouse olfactory bulb. The Journal of Comparative Neurology *501*, 825–836.

Parrish-Aungst, S., Kiyokage, E., Szabo, G., Yanagawa, Y., Shipley, M.T., and Puche, A.C. (2011). Sensory experience selectively regulates transmitter synthesis enzymes in interglomerular circuits. Brain Research *1382*, 70–76.

Parsa, P.V., D'Souza, R.D., and Vijayaraghavan, S. (2015). Signaling between periglomerular cells reveals a bimodal role for GABA in modulating glomerular microcircuitry in the olfactory bulb. Proceedings of the National Academy of Sciences *112*, 9478–9483.

Patriarchi, T., Cho, J.R., Merten, K., Howe, M.W., Marley, A., Xiong, W.-H., Folk, R.W., Broussard, G.J., Liang, R., Jang, M.J., et al. (2018). Ultrafast neuronal imaging of dopamine dynamics with designed genetically encoded sensors. Science *360*, eaat4422.

Pedarzani, P., McCutcheon, J.E., Rogge, G., Jensen, B.S., Christophersen, P., Hougaard, C., Strøbaek, D., and Stocker, M. (2005). Specific enhancement of SK channel activity selectively potentiates the afterhyperpolarizing current I(AHP) and modulates the firing properties of hippocampal pyramidal neurons. The Journal of Biological Chemistry *280*, 41404–41411.

Pencea, V., and Luskin, M.B. (2003). Prenatal development of the rodent rostral migratory stream. The Journal of Comparative Neurology *463*, 402–418.

Perrone-Capano, C., Tino, A., and di Porzio, U. (1994). Target cells modulate dopamine transporter gene expression during brain development. Neuroreport *5*, 1145–1148.

Petreanu, L., and Alvarez-Buylla, A. (2002). Maturation and death of adult-born olfactory bulb granule neurons: role of olfaction. Journal of Neuroscience *22*, 6106–6113.

Philpot, B.D., Foster, T.C., and Brunjes, P.C. (1997). Mitral/tufted cell activity is attenuated and becomes uncoupled from respiration following naris closure. Journal of Neurobiology *33*, 374–386.

Pignatelli, A., Kobayashi, K., Okano, H., and Belluzzi, O. (2005). Functional properties of dopaminergic neurones in the mouse olfactory bulb. The Journal of Physiology *564*, 501–514.

Pignatelli, A., Ackman, J.B., Vigetti, D., Beltrami, A.P., Zucchini, S., and Belluzzi, O. (2009). A potential reservoir of immature dopaminergic replacement neurons in the adult mammalian olfactory bulb. Pflügers Archiv - European Journal of Physiolpinchogy *457*, 899–915.

Pignatelli, A., Borin, M., Fogli Iseppe, A., Gambardella, C., and Belluzzi, O. (2013). The h-Current in Periglomerular Dopaminergic Neurons of the Mouse Olfactory Bulb. PLoS ONE *8*, e56571.

Pinching, A.J., and Powell, T.P.S. (1971a). The neuron types of the glomerular layer of the olfactory bulb. Journal of Cell Science *9*, 305–345.

Pinching, A.J., and Powell, T.P.S. (1971b). The neuropil of the glomeruli of the olfactory bulb. Journal of Cell Science *9*, 347.

Pinching, A.J., and Powell, T.P.S. (1971c). The neuropil of the periglomerular region of the olfactory bulb. Journal of Cell Science *9*, 379.

Pirez, N., and Wachowiak, M. (2008). In Vivo Modulation of Sensory Input to the Olfactory Bulb by Tonic and Activity-Dependent Presynaptic Inhibition of Receptor Neurons. Journal of Neuroscience *28*, 6360–6371.

Platel, J.-C., Angelova, A., Bugeon, S., Ganay, T., Chudotvorova, I., Deloulme, J.-C., Beclin, C., Tiveron, M.-C., Core, N., and Cremer, H. (2018). Neuronal integration in the adult olfactory bulb is a non-selective addition process. BioRxiv 289009.

Ponti, G., Obernier, K., Guinto, C., Jose, L., Bonfanti, L., and Alvarez-Buylla, A. (2013). Cell cycle and lineage progression of neural progenitors in the ventricular-subventricular zones of adult mice. Proceedings of the National Academy of Sciences *110*, E1045-54.

Puche, A.C., and Shipley, M.T. (1999). Odor-induced, activity-dependent transneuronal gene induction in vitro: mediation by NMDA receptors. Journal of Neuroscience *19*, 1359–1370.

Puopolo, M., Bean, B.P., and Raviola, E. (2005). Spontaneous Activity of Isolated Dopaminergic Periglomerular Cells of the Main Olfactory Bulb. Journal of Neurophysiology *94*, 3618–3627.

Quast, K.B., Ung, K., Froudarakis, E., Huang, L., Herman, I., Addison, A.P., Ortiz-Guzman, J., Cordiner, K., Saggau, P., Tolias, A.S., et al. (2017). Developmental broadening of inhibitory sensory maps. Nature Neuroscience *20*, 189–199.

Rall, W., Shepherd, G.M., Reese, T.S., and Brightman, M.W. (1966). Dendrodendritic synaptic pathway for inhibition in the olfactory bulb. Experimental Neurology *14*, 44–56.

Rannals, M.D., and Kapur, J. (2011). Homeostatic strengthening of inhibitory synapses is mediated by the accumulation of GABA(A) receptors. Journal of Neuroscience *31*, 17701–17712.

Rochefort, C., Gheusi, G., Vincent, J.-D., and Lledo, P.-M. (2002). Enriched odor exposure increases the number of newborn neurons in the adult olfactory bulb and improves odor memory. Journal of Neuroscience *22*, 2679–2689.

Rodriguez-Gil, D.J., Bartel, D.L., Jaspers, A.W., Mobley, A.S., Imamura, F., and Greer, C.A. (2015). Odorant receptors regulate the final glomerular coalescence of olfactory sensory neuron axons. Proceedings of the National Academy of Sciences *112*, 5821–5826.

Rodríguez, F.B., Huerta, R., and Aylwin, M. de la L. (2013). Neural Sensitivity to Odorants in Deprived and Normal Olfactory Bulbs. PLoS ONE *8*, e60745.

Rosenkranz, J.A., and Grace, A.A. (2002). Dopamine-mediated modulation of odour-evoked amygdala potentials during pavlovian conditioning. Nature *417*, 282–287.

Royet, J.P., Souchier, C., Jourdan, F., and Ploye, H. (1988). Morphometric study of the glomerular population in the mouse olfactory bulb: Numerical density and size distribution along the

rostrocaudal axis. The Journal of Comparative Neurology *270*, 559–568.

Rutherford, L.C., Nelson, S.B., and Turrigiano, G.G. (1998). BDNF Has Opposite Effects on the Quantal Amplitude of Pyramidal Neuron and Interneuron Excitatory Synapses. Neuron *21*, 521–530.

Saghatelyan, A., Roux, P., Migliore, M., Rochefort, C., Desmaisons, D., Charneau, P., Shepherd, G.M., and Lledo, P.-M. (2005). Activity-Dependent Adjustments of the Inhibitory Network in the Olfactory Bulb following Early Postnatal Deprivation. Neuron *46*, 103–116.

Sailor, K.A., Valley, M.T., Wiechert, M.T., Riecke, H., Sun, G.J., Adams, W., Dennis, J.C., Sharafi, S., Ming, G., Song, H., et al. (2016). Persistent Structural Plasticity Optimizes Sensory Information Processing in the Olfactory Bulb. Neuron *91*, 384–396.

Saino-Saito, S., Sasaki, H., Volpe, B.T., Kobayashi, K., Berlin, R., and Baker, H. (2004). Differentiation of the dopaminergic phenotype in the olfactory system of neonatal and adult mice. The Journal of Comparative Neurology *479*, 389–398.

De Saint Jan, D., Hirnet, D., Westbrook, G.L., and Charpak, S. (2009). External Tufted Cells Drive the Output of Olfactory Bulb Glomeruli. Journal of Neuroscience *29*, 2043–2052.

Salcedo, E., Tran, T., Ly, X., Lopez, R., Barbica, C., Restrepo, D., and Vijayaraghavan, S. (2011). Activity-dependent changes in cholinergic innervation of the mouse olfactory bulb. PloS One *6*, e25441.

Santini, E., Quirk, G.J., and Porter, J.T. (2008). Fear conditioning and extinction differentially modify the intrinsic excitability of infralimbic neurons. Journal of Neuroscience *28*, 4028–4036.

Saponaro, A., Pauleta, S.R., Cantini, F., Matzapetakis, M., Hammann, C., Donadoni, C., Hu, L., Thiel, G., Banci, L., Santoro, B., et al. (2014). Structural basis for the mutual antagonism of cAMP and TRIP8b in regulating HCN channel function. Proceedings of the National Academy of Sciences *111*, 14577–14582.

Savić, N., Pedarzani, P., and Sciancalepore, M. (2001). Medium Afterhyperpolarization and Firing Pattern Modulation in Interneurons of Stratum Radiatum in the CA3 Hippocampal Region. Journal of Neurophysiology *85*, 1986–1997.

Sawada, M., Kaneko, N., Inada, H., Wake, H., Kato, Y., Yanagawa, Y., Kobayashi, K., Nemoto, T., Nabekura, J., and Sawamoto, K. (2011). Sensory input regulates spatial and subtype-specific patterns of neuronal turnover in the adult olfactory bulb. Journal of Neuroscience *31*, 11587–11596.

Schmidt, L.J., and Strowbridge, B.W. (2014). Modulation of olfactory bulb network activity by serotonin: synchronous inhibition of mitral cells mediated by spatially localized GABAergic microcircuits. Learning & Memory *21*, 406–416.

Schneggenburger, R., Sakaba, T., and Neher, E. (2002). Vesicle pools and short-term synaptic depression: lessons from a large synapse. Trends in Neurosciences *25*, 206–212.

Serguera, C., Triaca, V., Kelly-Barrett, J., Banchaabouchi, M. Al, and Minichiello, L. (2008). Increased dopamine after mating impairs olfaction and prevents odor interference with pregnancy. Nature Neuroscience *11*, 949–956.

Shah, M.M., Anderson, A.E., Leung, V., Lin, X., and Johnston, D. (2004). Seizure-Induced Plasticity of h Channels in Entorhinal Cortical Layer III Pyramidal Neurons. Neuron *44*, 495–508.

Shah, M.M., Migliore, M., and Brown, D.A. (2011). Differential effects of Kv7 (M-) channels on synaptic integration in distinct subcellular compartments of rat hippocampal pyramidal neurons. The Journal of Physiology *589*, 6029–6038.

Shao, Z., Puche, A.C., Kiyokage, E., Szabo, G., and Shipley, M.T. (2009). Two GABAergic Intraglomerular Circuits Differentially Regulate Tonic and Phasic Presynaptic Inhibition of Olfactory Nerve Terminals. Journal of Neurophysiology *101*, 1988–2001.

Shao, Z., Puche, A.C., Liu, S., and Shipley, M.T. (2012). Intraglomerular inhibition shapes the strength and temporal structure of glomerular output. Journal of Neurophysiology *108*, 782–793.

Sheng, M., McFadden, G., and Greenberg, M.E. (1990). Membrane depolarization and calcium induce c-fos transcription via phosphorylation of transcription factor CREB. Neuron *4*, 571–582.

Shim, H.G., Jang, S.-S., Jang, D.C., Jin, Y., Chang, W., Park, J.M., and Kim, S.J. (2016). mGlu 1 receptor mediates homeostatic control of intrinsic excitability through I h in cerebellar Purkinje cells. Journal

of Neurophysiology *115*, 2446–2455.

Shin, M., Brager, D., Jaramillo, T.C., Johnston, D., and Chetkovich, D.M. (2008). Mislocalization of h channel subunits underlies h channelopathy in temporal lobe epilepsy. Neurobiology of Disease *32*, 26–36.

Shinoda, Y., Kamikubo, Y., Egashira, Y., Tominaga-Yoshino, K., and Ogura, A. (2005). Repetition of mGluR-dependent LTD causes slowly developing persistent reduction in synaptic strength accompanied by synapse elimination. Brain Research *1042*, 99–107.

Shipley, M.T., and Adamek, G.D. (1984). The connections of the mouse olfactory bulb: a study using orthograde and retrograde transport of wheat germ agglutinin conjugated to horseradish peroxidase. Brain Research Bulletin *12*, 669–688.

Shipley, M.T., Zimmer, L.A., Ennis, M., and McLean, J.H. (1996). Chapter III The olfactory system. Handbook of Chemical Neuroanatomy *12*, 469–573.

Shu, Y., Duque, A., Yu, Y., Haider, B., and McCormick, D.A. (2007). Properties of Action-Potential Initiation in Neocortical Pyramidal Cells: Evidence From Whole Cell Axon Recordings. Journal of Neurophysiology *97*, 746–760.

Slomowitz, E., Styr, B., Vertkin, I., Milshtein-Parush, H., Nelken, I., Slutsky, M., and Slutsky, I. (2015). Interplay between population firing stability and single neuron dynamics in hippocampal networks. ELife *4*, e04378.

Smith, T.C., and Jahr, C.E. (2002). Self-inhibition of olfactory bulb neurons. Nature Neuroscience *5*, 760–766.

Spors, H., and Grinvald, A. (2002). Spatio-temporal dynamics of odor representations in the mammalian olfactory bulb. Neuron *34*, 301–315.

Stackman, R.W., Hammond, R.S., Linardatos, E., Gerlach, A., Maylie, J., Adelman, J.P., and Tzounopoulos, T. (2002). Small conductance Ca2+-activated K+ channels modulate synaptic plasticity and memory encoding. Journal of Neuroscience *22*, 10163–10171.

Stenman, J., Toresson, H., and Campbell, K. (2003). Identification of two distinct progenitor populations in the lateral ganglionic eminence: implications for striatal and olfactory bulb neurogenesis. Journal of Neuroscience *23*, 167–174.

Stephan, A.B., Shum, E.Y., Hirsh, S., Cygnar, K.D., Reisert, J., and Zhao, H. (2009). ANO2 is the cilial calcium-activated chloride channel that may mediate olfactory amplification. Proceedings of the National Academy of Sciences *106*, 11776–11781.

Stone, D.M., Wessel, T., Joh, T.H., and Baker, H. (1990). Decrease in tyrosine hydroxylase, but not aromatic l-amino acid decarboxylase, messenger RNA in rat olfactory bulb following neonatal, unilateral odor deprivation. Molecular Brain Research *8*, 291–300.

Stone, D.M., Grillo, M., Margolis, F.L., Joh, T.H., and Baker, H. (1991). Differential effect of functional olfactory bulb deafferentation on tyrosine hydroxylase and glutamic acid decarboxylase messenger RNA levels in rodent juxtaglomerular neurons. The Journal of Comparative Neurology *311*, 223–233.

Storm, J.F. (1987). Action potential repolarization and a fast after-hyperpolarization in rat hippocampal pyramidal cells. The Journal of Physiology *385*, 733–759.

Sun, Q.-Q. (2009). Experience-dependent intrinsic plasticity in interneurons of barrel cortex layer IV. Journal of Neurophysiology *102*, 2955–2973.

Surges, R., Brewster, A.L., Bender, R.A., Beck, H., Feuerstein, T.J., and Baram, T.Z. (2006). Regulated expression of HCN channels and cAMP levels shape the properties of the h current in developing rat hippocampus. European Journal of NeuroscienceJournal of Neuroscience *24*, 94–104.

Sutton, M.A., Ito, H.T., Cressy, P., Kempf, C., Woo, J.C., and Schuman, E.M. (2006). Miniature neurotransmission stabilizes synaptic function via tonic suppression of local dendritic protein synthesis. Cell *125*, 785–799.

Tatti, R., Bhaukaurally, K., Gschwend, O., Seal, R.P., Edwards, R.H., Rodriguez, I., and Carleton, A. (2014). A population of glomerular glutamatergic neurons controls sensory information transfer in the mouse olfactory bulb. Nature Communications *5*, 3791.

Tavakoli, A., Schmaltz, A., Schwarz, D., Margrie, T.W., Schaefer, A.T., and Kollo, M. (2018). Quantitative Association of Anatomical and Functional Classes of Olfactory Bulb Neurons. The Journal of Neuroscience *38*, 7204–7220.

Tecuapetla, F., Patel, J.C., Xenias, H., English, D., Tadros, I., Shah, F., Berlin, J., Deisseroth, K., Rice, M.E., Tepper, J.M., et al. (2010). Glutamatergic Signaling by Mesolimbic Dopamine Neurons in the Nucleus Accumbens. Journal of Neuroscience *30*, 7105–7110.

Thiagarajan, T.C., Lindskog, M., and Tsien, R.W. (2005). Adaptation to Synaptic Inactivity in Hippocampal Neurons. Neuron *47*, 725–737.

Tillack, K., Aboutalebi, H., and Kramer, E.R. (2015). An Efficient and Versatile System for Visualization and Genetic Modification of Dopaminergic Neurons in Transgenic Mice. PLoS ONE *10*, e0136203.

Tillerson, J.L., Caudle, W.M., Parent, J.M., Gong, C., Schallert, T., and Miller, G.W. (2006). Olfactory discrimination deficits in mice lacking the dopamine transporter or the D2 dopamine receptor. Behavioural Brain Research *172*, 97–105.

Tobin, V.A., Hashimoto, H., Wacker, D.W., Takayanagi, Y., Langnaese, K., Caquineau, C., Noack, J., Landgraf, R., Onaka, T., Leng, G., et al. (2010). An intrinsic vasopressin system in the olfactory bulb is involved in social recognition. Nature *464*, 413–417.

Toida, K., Kosaka, K., Heizmann, C.W., and Kosaka, T. (1998). Chemically defined neuron groups and their subpopulations in the glomerular layer of the rat main olfactory bulb: III. Structural features of calbindin D28K-immunoreactive neurons. The Journal of Comparative Neurology *392*, 179–198.

Toida, K., Kosaka, K., Aika, Y., and Kosaka, T. (2000). Chemically defined neuron groups and their subpopulations in the glomerular layer of the rat main olfactory bulb--IV. Intraglomerular synapses of tyrosine hydroxylase-immunoreactive neurons. Neuroscience *101*, 11–17.

Trachtenberg, J.T., Chen, B.E., Knott, G.W., Feng, G., Sanes, J.R., Welker, E., and Svoboda, K. (2002). Long-term in vivo imaging of experience-dependent synaptic plasticity in adult cortex. Nature *420*, 788–794.

Treloar, H.B., Feinstein, P., Mombaerts, P., and Greer, C.A. (2002). Specificity of glomerular targeting by olfactory sensory axons. Journal of Neuroscience *22*, 2469–2477.

Tritsch, N.X., Ding, J.B., and Sabatini, B.L. (2012). Dopaminergic neurons inhibit striatal output through non-canonical release of GABA. Nature *490*, 262–266.

Turrigiano, G.G. (2008). The self-tuning neuron: synaptic scaling of excitatory synapses. Cell *135*, 422–435.

Turrigiano, G.G., and Nelson, S.B. (2000). Hebb and homeostasis in neuronal plasticity. Current Opinion in Neurobiology *10*, 358–364.

Turrigiano, G.G., Leslie, K.R., Desai, N.S., Rutherford, L.C., and Nelson, S.B. (1998). Activity-dependent scaling of quantal amplitude in neocortical neurons. Nature *391*, 892–896.

Tyler, W.J., Petzold, G.C., Pal, S.K., and Murthy, V.N. (2007). Experience-dependent modification of primary sensory synapses in the mammalian olfactory bulb. Journal of Neuroscience *27*, 9427–9438.

Tzingounis, A. V, and Nicoll, R.A. (2008). Contribution of KCNQ2 and KCNQ3 to the medium and slow afterhyperpolarization currents. Proceedings of the National Academy of Sciences *105*, 19974–19979.

Vaaga, C.E., and Westbrook, G.L. (2016). Parallel processing of afferent olfactory sensory information. The Journal of Physiology *594*, 6715–6732.

Vaaga, C.E., and Westbrook, G.L. (2017). Distinct temporal filters in mitral cells and external tufted cells of the olfactory bulb. The Journal of Physiology *595*, 6349–6362.

Vaaga, C.E., Yorgason, J.T., Williams, J.T., and Westbrook, G.L. (2017). Presynaptic gain control by endogenous cotransmission of dopamine and GABA in the olfactory bulb. Journal of Neurophysiology *117*, 1163–1170.

Vandecasteele, M., Deniau, J.-M., and Venance, L. (2011). Spike frequency adaptation is developmentally regulated in substantia nigra pars compacta dopaminergic neurons. Neuroscience *192*, 1–10.

Vergaño-Vera, E., Yusta-Boyo, M.J., de Castro, F., Bernad, A., de Pablo, F., and Vicario-Abejón, C. (2006). Generation of GABAergic and dopaminergic interneurons from endogenous embryonic olfactory bulb precursor cells. Development *133*, 4367–4379.

Vergara, C., Latorre, R., Marrion, N. V, and Adelman, J.P. (1998). Calcium-activated potassium channels. Current Opinion in Neurobiology *8*, 321–329.

Vinje, W.E., and Gallant, J.L. (2000). Sparse coding and decorrelation in primary visual cortex during natural vision. Science *287*, 1273–1276.

Volgushev, M., Malyshev, A., Balaban, P., Chistiakova, M., Volgushev, S., and Wolf, F. (2008). Onset Dynamics of Action Potentials in Rat Neocortical Neurons and Identified Snail Neurons: Quantification of the Difference. PLoS ONE *3*, e1962.

Vučinić, D., Cohen, L.B., and Kosmidis, E.K. (2006). Interglomerular Center-Surround Inhibition Shapes Odorant-Evoked Input to the Mouse Olfactory Bulb In Vivo. Journal of Neurophysiology *95*, 1881–1887.

Wachowiak, M., and Cohen, L.B. (2001). Representation of odorants by receptor neuron input to the mouse olfactory bulb. Neuron *32*, 723–735.

Wallace, J.L., Wienisch, M., and Murthy, V.N. (2017). Development and Refinement of Functional Properties of Adult-Born Neurons. Neuron *96*, 883–896.e7.

Wang, K., Mateos-Aparicio, P., Hönigsperger, C., Raghuram, V., Wu, W.W., Ridder, M.C., Sah, P., Maylie, J., Storm, J.F., and Adelman, J.P. (2016). IK1 channels do not contribute to the slow afterhyperpolarization in pyramidal neurons. ELife *5*, e11206.

Wang, M., Ramos, B.P., Paspalas, C.D., Shu, Y., Simen, A., Duque, A., Vijayraghavan, S., Brennan, A., Dudley, A., Nou, E., et al. (2007). α2A-Adrenoceptors Strengthen Working Memory Networks by Inhibiting cAMP-HCN Channel Signaling in Prefrontal Cortex. Cell *129*, 397–410.

Wang, M., Cai, E., Fujiwara, N., Fones, L., Brown, E., Yanagawa, Y., and Cave, J.W. (2017). Odorant Sensory Input Modulates DNA Secondary Structure Formation and Heterogeneous Ribonucleoprotein Recruitment on the Tyrosine Hydroxylase and Glutamic Acid Decarboxylase 1 Promoters in the Olfactory Bulb. Journal of Neuroscience *37*, 4778–4789.

Wang, W., Zhang, K., Yan, S., Li, A., Hu, X., Zhang, L., and Liu, C. (2011). Enhancement of apamin-sensitive medium afterhyperpolarization current by anandamide and its role in excitability control in cultured hippocampal neurons. Neuropharmacology *60*, 901–909.

Wayment, H.K., Schenk, J.O., and Sorg, B.A. (2001). Characterization of extracellular dopamine clearance in the medial prefrontal cortex: role of monoamine uptake and monoamine oxidase inhibition. Journal of Neuroscience *21*, 35–44.

van Welie, I., van Hooft, J.A., and Wadman, W.J. (2004). Homeostatic scaling of neuronal excitability by synaptic modulation of somatic hyperpolarization-activated Ih channels. Proceedings of the National Academy of Sciences *101*, 5123–5128.

Wesson, D.W., Carey, R.M., Verhagen, J. V, and Wachowiak, M. (2008). Rapid Encoding and Perception of Novel Odors in the Rat. PLoS Biology *6*, e82.

Whitesell, J.D., Sorensen, K.A., Jarvie, B.C., Hentges, S.T., and Schoppa, N.E. (2013). Interglomerular lateral inhibition targeted on external tufted cells in the olfactory bulb. Journal of Neuroscience *33*, 1552–1563.

Whitman, M.C., and Greer, C.A. (2007). Adult-generated neurons exhibit diverse developmental fates. Developmental Neurobiology *67*, 1079–1093.

Wierenga, C.J., Ibata, K., and Turrigiano, G.G. (2005). Postsynaptic Expression of Homeostatic Plasticity at Neocortical Synapses. Journal of Neuroscience *25*, 2895–2905.

Wilson, D.A., and Sullivan, R.M. (1995). The D2 Antagonist Spiperone Mimics the Effects Deprivation on Mitral/Tufted Cell Odor Response of Olfactory Patterns. Journal of Neuroscience *15*, 5574–5581.

Wilson, G.W., and Garthwaite, J. (2010). Hyperpolarization-activated ion channels as targets for nitric oxide signalling in deep cerebellar nuclei. European Journal of Neuroscience *31*, 1935–1945.

Wilson, T.J., and Kola, I. (2001). The LoxP/CRE System and Genome Modification. In Gene Knockout

Protocols, (New Jersey: Humana Press), pp. 83–94.

Wu, X.-S., Xue, L., Mohan, R., Paradiso, K., Gillis, K.D., and Wu, L.-G. (2007). The Origin of Quantal Size Variation: Vesicular Glutamate Concentration Plays a Significant Role. Journal of Neuroscience *27*, 3046–3056.

Yaksi, E., Judkewitz, B., and Friedrich, R.W. (2007). Topological Reorganization of Odor Representations in the Olfactory Bulb. PLoS Biology *5*, e178.

Yamada, M., Onodera, M., Mizuno, Y., and Mochizuki, H. (2004). Neurogenesis in olfactory bulb identified by retroviral labeling in normal and 1-methyl-4-phenyl-1,2,3,6-tetrahydropyridine-treated adult mice. Neuroscience *124*, 173–181.

Yamaguchi, M., and Mori, K. (2005). Critical period for sensory experience-dependent survival of newly generated granule cells in the adult mouse olfactory bulb. Proceedings of the National Academy of Sciences *102*, 9697–9702.

Young, K.M., Fogarty, M., Kessaris, N., and Richardson, W.D. (2007). Subventricular Zone Stem Cells Are Heterogeneous with Respect to Their Embryonic Origins and Neurogenic Fates in the Adult Olfactory Bulb. Journal of Neuroscience *27*, 8286–8296.

Young Cho, J., Min, N., Franzen, L., and Harriet Baker, A. (1996). Rapid Down-Regulation of Tyrosine Hydroxylase Expression in the Olfactory Bulb of Naris-Occluded Adult Rats. The Journal of Comparative Neurology *369264*, 276.

Yu, X., Duan, K.-L., Shang, C.-F., Yu, H.-G., and Zhou, Z. (2004). Calcium influx through hyperpolarization-activated cation channels (I(h) channels) contributes to activity-evoked neuronal secretion. Proceedings of the National Academy of Sciences *101*, 1051–1056.

Yuan, Q. (2009). Theta bursts in the olfactory nerve paired with beta-adrenoceptor activation induce calcium elevation in mitral cells: a mechanism for odor preference learning in the neonate rat. Learning & Memory *16*, 676–681.

Zha, Q., Brewster, A.L., Richichi, C., Bender, R.A., and Baram, T.Z. (2008). Activity-dependent heteromerization of the hyperpolarization-activated, cyclic-nucleotide gated (HCN) channels: role of N-linked glycosylation. Journal of Neurochemistry *105*, 68–77.

Zhang, X., and Firestein, S. (2002). The olfactory receptor gene superfamily of the mouse. Nature Neuroscience *5*, 124–133.

Zhao, C., Dreosti, E., and Lagnado, L. (2011). Homeostatic synaptic plasticity through changes in presynaptic calcium influx. Journal of Neuroscience *31*, 7492–7496.

Zhou, W., Lee, Y.M., Guy, V.C., and Freed, C.R. (2009). Embryonic Stem Cells with GFP Knocked into the Dopamine Transporter Yield Purified Dopamine Neurons in vitro and from Knock-in Mice. Stem Cells *27*, 2952–2961.

Zhu, M.-Y., Juorio, A. V., Alick Paterson, I., and Boulton, A.A. (1993). Regulation of striatal aromatic L-amino acid decarboxylase: Effects of blockade or activation of dopamine receptors. European Journal of Pharmacology *238*, 157–164.

Zhuang, X., Masson, J., Gingrich, J.A., Rayport, S., and Hen, R. (2005). Targeted gene expression in dopamine and serotonin neurons of the mouse brain. Journal of Neuroscience Methods *143*, 27–32.

Zong, X., Krause, S., Chen, C.-C., Krüger, J., Gruner, C., Cao-Ehlker, X., Fenske, S., Wahl-Schott, C., and Biel, M. (2012). Regulation of hyperpolarization-activated cyclic nucleotide-gated (HCN) channel activity by cCMP. The Journal of Biological Chemistry *287*, 26506–26512.

Zucker, R.S., and Regehr, W.G. (2002). Short-Term Synaptic Plasticity. Annual Review of Physiology *64*, 355–405.